

EFFECTS OF TYPES OF VEHICLES AND MANEUVERS ON VEHICLE KINEMATICS DURING STEERING-INDUCED SOIL-TRIP ROLLOVERS

Taewung Kim
Varun Bollapragada
Jason Kerrigan
Jeff Crandall

University of Virginia Center for Applied Biomechanics
USA

Mark Clauser

Toyota Motor Engineering & Manufacturing North America, Inc.
USA

Paper Number 13-0050

ABSTRACT

Controlled rollover test methods have been developed where touchdown conditions of the vehicle are specified as test inputs. Rollover crash touchdown parameters can vary widely due to variations in road surface and topography, maneuvers, and vehicles. While vehicular accident reconstruction teams have performed steering induced rollover tests and reported on touchdown conditions in the literature, such kinematic parameters are only available for an extremely limited set of conditions and vehicles. Furthermore, information about the sensitivity of touchdown conditions to changes in vehicle and maneuvers is missing from the literature. Thus, the goals of this study were threefold: to develop and validate two vehicle models in ADAMSTM, use them to simulate common types of steering-induced soil-trip rollovers, and to evaluate how differences in maneuvers and vehicle type affect vehicle kinematics at touchdown.

First, vehicle inertia measurement tests, suspension tests, tire tests, bushing tests, and driving tests, including double lane change, J-turn, and fishhook, were performed using a sedan and a pickup truck. Next, vehicle models for each vehicle were built and validated with the experimental data. A straight highway was modeled following road design guidelines and a soil-tire interaction model was implemented. Analysis of NASS-CDS cases showed that rollover accidents occurred as a result of the vehicle leaving the roadway and either attempting to drive back onto the road (corrective) or continuing to steer from the road (non-corrective). Then specific

cases exemplifying the corrective and non-corrective maneuvers were reconstructed with the two vehicle models to determine baseline driver inputs. Lastly, 120 Monte Carlo simulations were performed to compare vehicle kinematics and touchdown conditions of the two types of vehicles and maneuvers.

The two vehicle models showed good correlations with the static and dynamic test data. The median values of roll rates of the sedan were 290 deg/sec and 380 deg/sec in corrective and non-corrective maneuvers, respectively. The pickup truck showed lower roll rates in the same maneuvers (210 and 250 deg/sec, respectively). Touchdown roll angles were higher in the sedan (120 and 190 degrees) than in the pickup (103 and 104 degrees) and higher in the non-corrective maneuver for both vehicles. Vertical speeds at touchdown were about 2.6 m/s higher in the non-corrective maneuver than in the corrective maneuver.

The vehicle models were validated with results from component tests, static tests, and dynamic tests but no steering-induced rollover test data were available to validate the vehicle models. Subsequent to this study, steering-induced rollover tests will be performed to validate the models further and the soil model will be validated by testing the soil at the test site.

Despite these limitations, the methodology and results presented provide for the best available means to determine touchdown parameters for use in controlled rollover crash testing. The data presented show a substantial difference in touchdown conditions with respect to types of vehicles and maneuvers. Therefore, when a

rollover test is performed, the test conditions should be carefully selected depending on types of vehicles or maneuvers to generate realistic outcome.

INTRODUCTION

Rollover accidents accounted for 35.5 percents of all occupant fatalities in 2008 in the United States [1]. Although there has been a lot of research to investigate injury mechanisms and mitigate injuries during rollover accidents, a standardized dynamic rollover test method has not been developed. One of the reasons is because it requires much more information to fully define states of a vehicle and an occupant when the vehicle touches down to ground than any other crash modes.

Therefore, identifying vehicle kinematics from pre-ballistic to touchdown conditions is a crucial step to investigate rollover accidents because it can be used to determine touchdown conditions of a vehicle and an occupant for rollover testing and further computer-aided engineering studies. Many rollover test devices have been proposed. To conduct a rollover test, initial conditions of a test vehicle should be chosen carefully to consider realistic rollover scenarios. However, there exist many questions such as dependency of touchdown conditions of vehicles and occupants on the types of vehicles and types of maneuvers. It is, however, not suitable to obtain these kinds of information by conducting steering induced rollover tests due to the varieties of possible rollover scenarios, costs, and safety issues.

There were studies that simulated rollover scenarios by using simplified vehicle models but those models were not validated to various dynamic maneuvering tests [10-11] or focused on rollover sensing so there was little considerations on steering induced trip rollovers which turned out to be one of the common types of rollover accidents [12].

NASS-CDS database has been investigated and it was found that the one of the common rollover scenarios were a steering induced soil-trip rollover. Two types of vehicle models, a sedan and a pick-up truck, were considered in this study to see the effects of vehicle types on touchdown parameters during rollover crashes. The two vehicles were built and validated to static and dynamic tests. Two target maneuvers from NASS-CDS cases were reconstructed to determine

baseline driver's inputs and initial speeds of vehicles. Lastly, Monte Carlo simulations were carried out based on the identified baseline driver's input and initial speed of vehicle to compare touchdown conditions of the two different types of vehicles and maneuvers.

METHODOLOGY

Vehicle Testing

Suspension modeling A sedan and a pick-up truck vehicle models have been developed for rollover simulations. The models have been developed by using mainly 3D measurement data and limited CAD data. The sedan model has a Mcpherson type and a multi-link type suspensions as the front and rear-ends, respectively. The pickup truck model has a double wishbone type and leaf springs with solid axle suspensions at the front and rear-ends, respectively. The leaf spring of the pickup truck model was modeled by using a three-link and nonlinear bushings [2].

Bushing component test Component tests for bushing have been conducted at Axle™ (MI, USA) to reduce the number of parameters to be tuned in the vehicle models. The bushings which are near control arms and leaf spring of the suspensions were tested in a static mode and the test data were directly used to model non-linear bushings (Figure 1).



Figure 1. An example of bushing test

Inertial properties and kinematics and compliance test Inertial properties of both vehicles were measured (Table 1) and kinematics and compliance tests were performed at SEA™ (OH, USA) to validate the suspension models under static conditions such as ride test, roll test, lateral compliance test, and steering compliance test.

Driving test Driving tests of the sedan and the pickup have been performed at TRC™ (OH, USA) to generate data for validation of the two models under dynamic loading conditions. Driving test modes include constant radius turn, single lane change, double lane change, J-turn, and slalom (Table 2). It should be mentioned that the driver's inputs were not the standardized forms such as ISO double lane change [15]. The driving tests were performed under high speeds and aggressive steering inputs to induce loss of control of the test vehicles, in-order to mimic the conditions of soil trip rollover accidents. Since the roll behavior of the vehicles were one of the main interests of these tests string potentiometers were installed near each strut to measure suspension deflection (Figure 2). In addition, vehicle's linear acceleration, linear velocity, angular velocity, wheel speeds, throttle input, and brake pressure were measured by using Differential GPS (DGPS), inertial sensors, and Controller Area Network (CAN) during the tests.

Table 1.
Mass properties of two vehicles

	Sedan	Pickup	unit
cg height (h_{cg})	559	742	mm
track width (t)	1580	1725	mm
SSF ($=t/(2h_{cg})$)	1.41	1.16	
mass	1460	2440	kg
I_{xx}	563	1130	kgm^2
I_{yy}	2550	6770	kgm^2
I_{zz}	2810	7154	kgm^2
I_{xz}	62.4	-231	kgm^2

Table 2.
Driving test matrix

Test maneuver	Speed for sedan [km/h]	Speed for pickup [km/h]
100 feet circle	0-56	0-53
Single lane change	80-113	80-113
Double lane change	80-129	80-129
Slalom	121	113-121
J-turn w/ or w/o brake	121	121

Vehicle Model Validation

To run a simulation for model validation, longitudinal speed and steering wheel angle collected during the tests were used as inputs for the vehicle models. In most cases the longitudinal speed of the vehicle model followed to the test data. (Figure 6 (b)).

The vehicle models were validated with respect to static suspension tests by adjusting locations of joints and properties of bushings that were not tested. Since inertial properties of the fully

instrumented test vehicles with a test driver were not available the inertial properties including the location of center of mass and I_{xx} , I_{yy} , I_{zz} , and I_{xz} were matched to the test results without instrumentation or a driver. Then, masses of driver and instrumentation equipment were added in corresponding locations.



Figure 2. String potentiometers installed along damper and DGPS installed at the center of vehicle

Then, the two vehicle models were validated by using the driving test data and selected results were represented in the result section.

Soil Model

To model soil-to-tire interaction, a semi-empirical soil model was considered [3]. This model assumes rigid wheel and is based on Bekker's method [4] to predict sinkage depth of a tire. Then, bulldozing force was calculated by using the area of the side wall of a tire sunk into the soil and Mohr-Coulomb failure criterion. Soil parameters measured from a mud-like soil (Table 3) were used in the simulations [5]. This soil was chosen because it generates high bulldozing force enough to roll over a vehicle but it would be interesting to check how different soils change touchdown parameters.

Table 3.
Soil properties [5]

Terrain	Heavy clay
Moisture content [%]	25
k_c [kN/m^{n+1}]	12.70
k_ϕ [kN/m^{n+2}]	1555.95
c [kPa]	68.95
ϕ [deg]	28°

Road Model

The two lane highway has been modeled in ADAMS (Figure 3) following roadway design

guidelines and AASHTO's Green Book [6-8]. For the paved area, which includes lanes and shoulders, friction coefficient of 0.95 has been used. For the rest of the area friction coefficient of 0.6 has been used. The recommended slope of shoulder wedge, recovery, and median is between 6 to 1 and 4 to 1, so 6 to 1 has been used. The soil model was engaged when the wheel center moved outside of the paved area during the simulations.

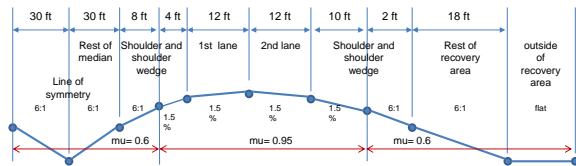


Figure 3. Cross section of two-lane highway model

Target Maneuvers

Several rollover cases from NASS-CDS database were investigated to determine target maneuvers. Among single vehicle rollover cases many soil trip rollovers were observed and two common patterns could be found. The two patterns were determined as target maneuvers and these were reconstructed by using the two vehicle models by adjusting driver's inputs (Figure 8 and Figure 9). These were used as baseline driver's inputs for subsequent Monte Carlo simulations.

Monte Carlo Simulation

Monte Carlo method is widely used to estimate the distributions of outputs of nonlinear systems under given variations of inputs. As the number of simulations increases the estimated mean values approaches to the population faster than deterministic design of experiment when the dimension of design space is large [13].

Vehicular rollover is a highly non-linear phenomenon, and slight change in driver's input can change vehicle kinematics drastically. Therefore, comparing the touchdown conditions by using only two simulation results is not reliable. Therefore, Monte Carlo simulations were performed by imposing variations in the parameters that were used to define baseline driver's inputs to consider variations in touchdown conditions of the target maneuvers. Then, the effect of types of maneuvers and vehicles on touchdown conditions were examined by comparing the median values of touchdown conditions.

RESULTS

Validation of Vehicle Model

The two vehicle models were first validated to static test data and some of results were shown in Figure 4 and Figure 5. Then, the inertial properties were validated as mentioned earlier. The two vehicle models validated to the static test data and inertial measurements showed good correlations with driving test data under various maneuvers such as double lane change, slalom, and J-turn. There were slight modifications on bushing properties and joint locations of steering systems to improve the correlation. Comparisons of the results of a double lane change test of the sedan and a slalom test of the pickup truck were depicted in Figure 6 and Figure 7, respectively. It should be noted that the vehicle models showed similar roll motion to the test vehicles as well as yaw motion (Figure 6 and Figure 7).

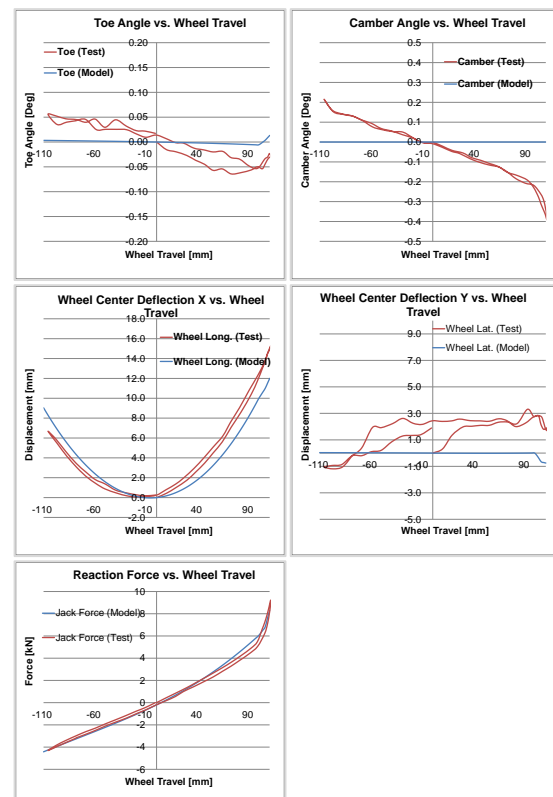


Figure 4. Comparison of ride behaviors of rear suspension of pickup truck

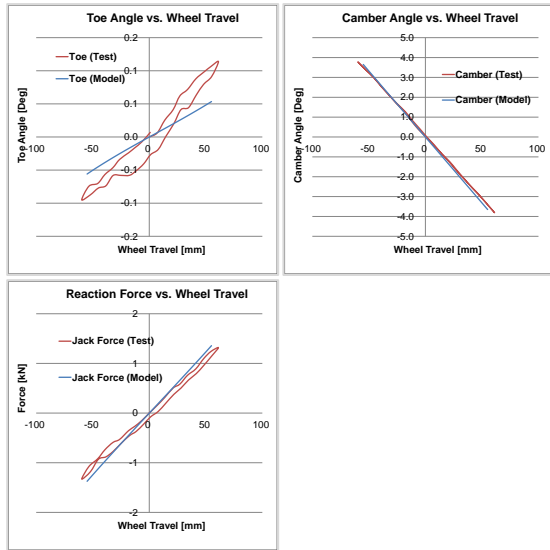
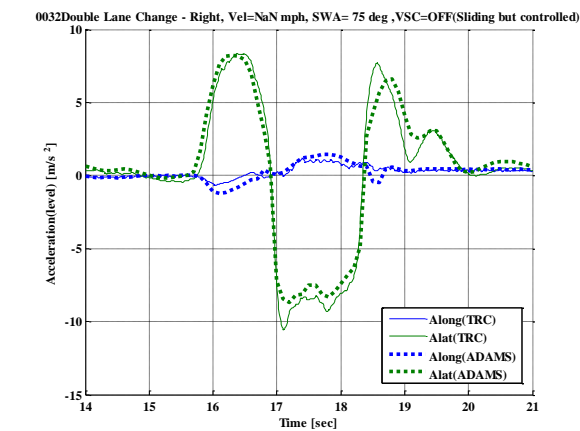
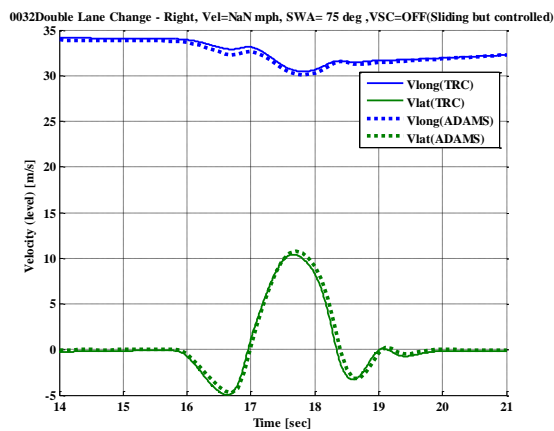


Figure 5. Comparison of roll behaviors of front suspension of pickup truck

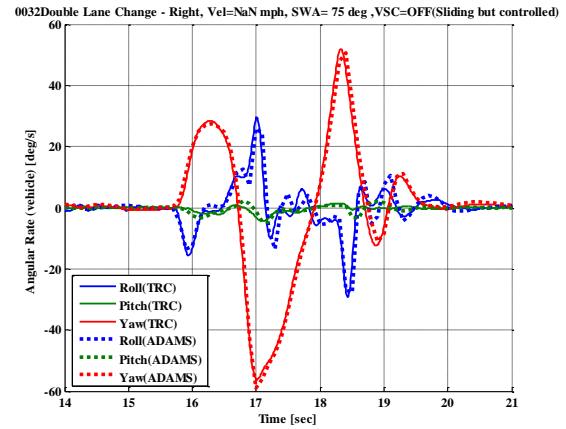


(a) Longitudinal and lateral accelerations

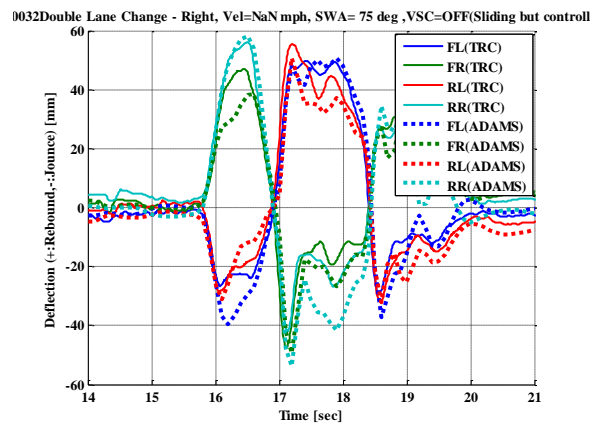


(b) Longitudinal and lateral speeds

Figure 6. Comparison of test data and simulation results of double lane change of sedan (cont'd)

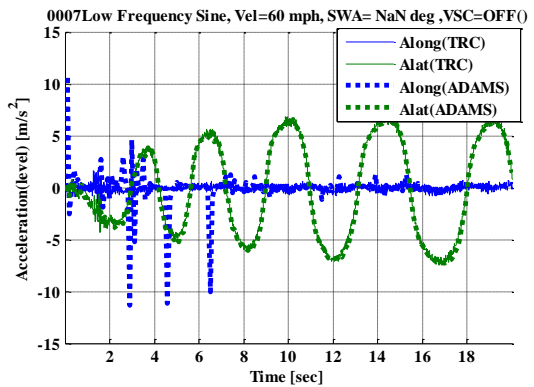


(c) Angular rates



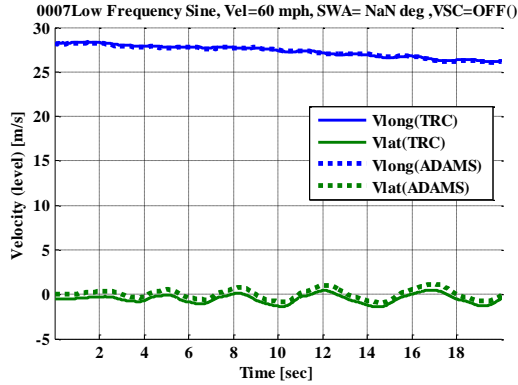
(d) suspension deflection amounts

Figure 6. Comparison of test data and simulation results of double lane change of sedan

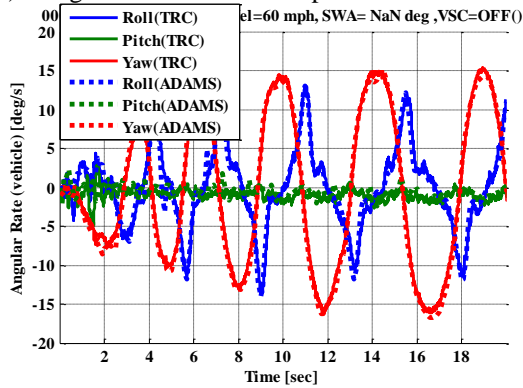


(a) Longitudinal and lateral accelerations

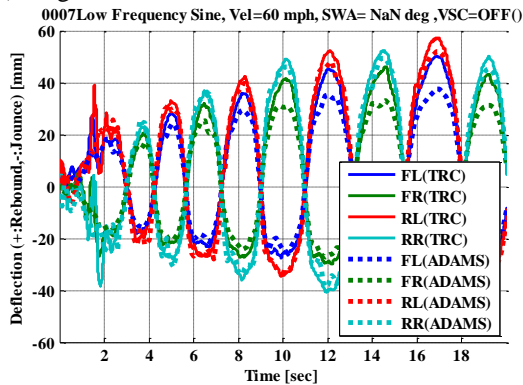
Figure 7. Comparison of test data and simulation results (Pickup truck, slalom) (cont'd)



(b) Longitudinal and lateral speeds



(c) Angular rates



(d) suspension deflection amounts

Figure 7. Comparison of test data and simulation results (Pickup truck, slalom)

Baseline Simulation

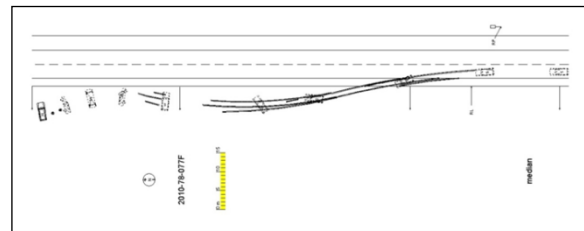
Two target maneuvers were selected from NASS-CDS database (Figure 8 and Figure 9). The case vehicles, which rolled over due to soil tripping force, usually went off the road and either changed its yawing direction (corrective maneuver) or not (non-corrective maneuver). It should be mentioned that the terms, corrective and non-corrective, are only based on the trajectories of vehicles in this study. There can be various kinds of driver's inputs that result in the similar vehicle trajectories

and rollovers but there was limited information on NASS-CDS database about driver's steering and brake input. So, we have chosen to use the simplest forms of steering input time histories. To reconstruct the corrective maneuver case the fishhook-like driver's input (Figure 8 (d)) was used and to reconstruct the non-corrective maneuver case the J-turn-like driver's input (Figure 9 (d)) was used. Since many skid marks were observed on scene diagrams, a step brake input was considered and applied with major steering inputs.

The baseline driver's inputs (Table 4) that resulted in similar vehicle trajectories and rollovers to target maneuvers were identified by performing multiple simulations with changing parameters for driver's input time histories (Figure 8 (d) and Figure 9 (d)).

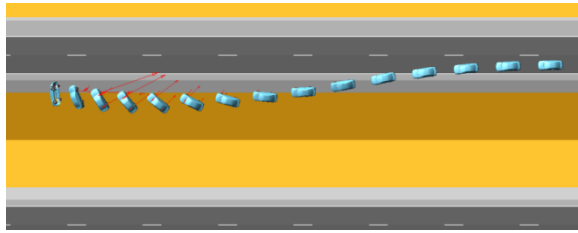
Table 4. Input parameters used in the baseline simulations

Corrective maneuver	Sedan	Pickup truck
Initial speed [mi/h]	74	64
SWA1 [deg]	-34	-52
SWR1 [deg/s]	-23	-42
DT1 [sec]	0.4	0.32
SWA2 [deg]	130	130
SWR2 [deg/s]	400	431
Brake [g]	0.3	0.3
Non-corrective maneuver	Sedan	Pickup truck
Initial speed [mi/h]	84	74
SWA1 [deg]	155	191
SWR1 [deg/s]	131	516
Brake [g]	0.3	0.25

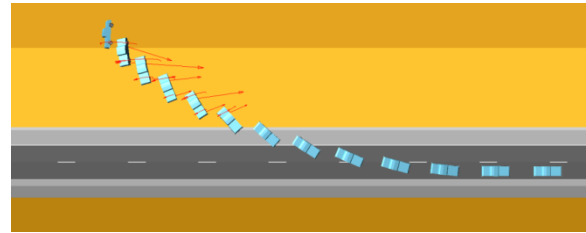


(a) NASS-CDS scene diagram

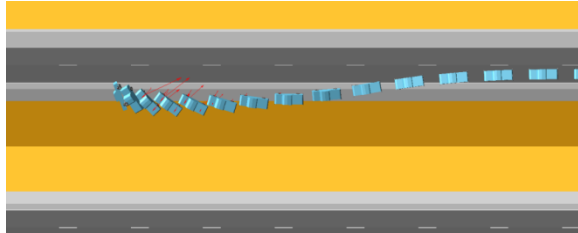
Figure 8. Baseline simulation results for corrective maneuvers (cont'd)



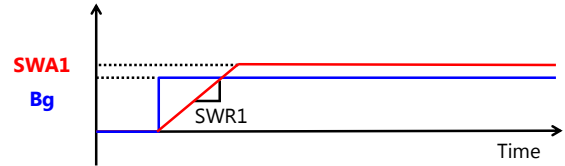
(b) Reconstructed case by the sedan model



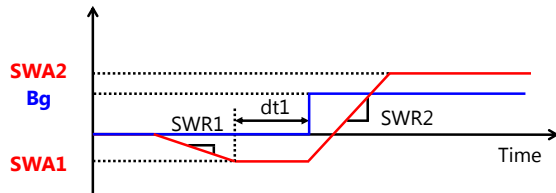
(c) Reconstructed case by Pickup truck model



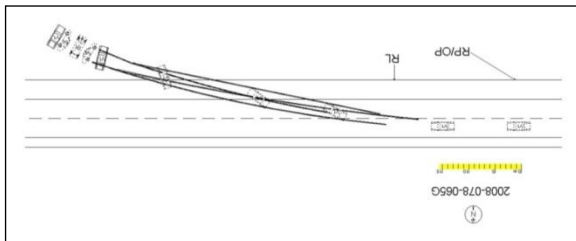
(c) Reconstructed case by the pickup model



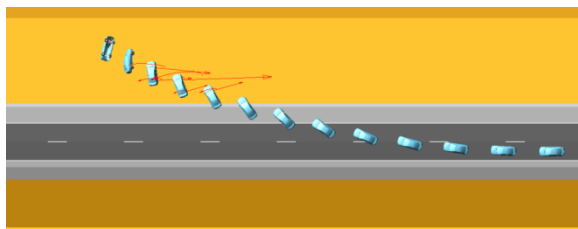
(d) Driver's input for non-corrective maneuvers
Figure 9. Baseline simulation results for non-corrective maneuvers



(d) Driver's input for corrective maneuvers
Figure 8. Baseline simulation results for corrective maneuvers



(a) NASS-CDS scene diagram



(b) Reconstructed case by sedan model
Figure 9. Baseline simulation results for non-corrective maneuvers (cont'd)

Touchdown Parameters

The functional forms for driver's input (Figure 8 (d) and Figure 9 (d)) for the baseline simulations were used and certain amounts of variations were imposed on each parameter following Gaussian distribution (Table 6). Thirty cases of rollover simulations were run for each target maneuver and vehicle type and the distributions of touchdown conditions were obtained (Figure 10). The sign conventions for touchdown parameters were summarized in Table 5.

Table 5.

Sign conventions for touchdown parameters

Parameters	Description
Roll Rate	(+): passenger side leading rollover
Roll Angle	0 deg < roll angle < 180 deg: passenger side touchdown first
Pitch Angle	(+): touchdown rear-side of vehicle first
Side Slip Angle	0 deg < side slip angle < 180 deg: passenger side tripping

The convergence of the analysis results should be checked by increasing the number of simulations but 30 simulations per each case were used due to the limit of time. Further detailed analysis by using Monte Carlo simulation will be conducted in the future research.

Table 6.

Distributions for sampling driver's inputs

Corrective maneuver	Sedan	Pickup truck
Initial Speed [mi/h]	$N(75, 10^2)$	$N(75, 10^2)$
SWA1 [deg]	$N(-35, 5^2)$	$N(-40, 6^2)$
SWR1 [deg/s]	$N(-35, 5^2)$	$N(-40, 6^2)$
DT1 [sec]	$N(0.45, 0.15^2)$	$N(0.5, 0.075^2)$

SWA2 [deg]	N(130,30 ²)	N(120,18 ²)
SWR2 [deg/s]	N(-400,100 ²)	N(-475,71.3 ²)
Brake [g]	N(0.3,0.1 ²)	N(0.3,0.1 ²)
Non-corrective maneuver	Sedan	Pickup truck
Initial Speed [mi/h]	N(75,10 ²)	N(75,7.5 ²)
SWA1 [deg]	N(155,45 ²)	N(200,20 ²)
SWR1 [deg/s]	N(135,45 ²)	N(530,53 ²)
Brake [g]	N(0.3,0.1 ²)	N(0.25,0.1 ²)

For corrective maneuver, there were 15 and 8 rollover cases of sedan and pickup truck, respectively. Most of the distributions were not Gaussian or unimodal distributions due to the high dimensions of the design space and nonlinearities of vehicle model and road shape so boxplots were used to represent the results. For non-corrective maneuver, there were 13 and 19 rollover cases of sedan and pickup truck, respectively. Most of the distributions of touchdown parameters were not Gaussian or unimodal distributions like the corrective maneuver due to the same reasons mentioned previously.

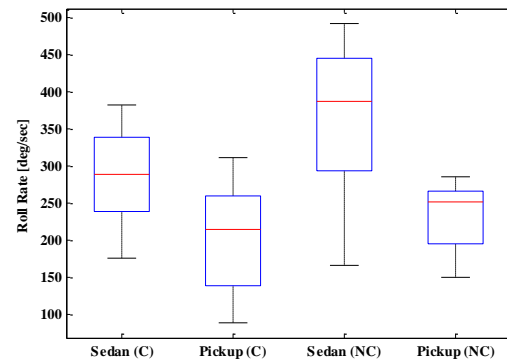
The median values of roll rates of the sedan were around 290 *deg/sec* and 380 *deg/sec* in corrective and non-corrective maneuvers, respectively. The pickup truck showed lower roll rates in the same types of maneuvers (210 and 250 *deg/sec*, respectively) than those of the sedan. Both vehicles showed higher median values of roll rates in the non-corrective maneuver than those in the corrective maneuver.

The median values of roll angles at touchdown were higher in the sedan (120 *degrees* in corrective maneuvers and 190 *degrees* in non-corrective maneuvers) than in the pickup (around 103 and 104 *degrees*). The different roll angles at touchdown between the two vehicle types suggest that different countermeasures may be needed to protect occupants in different types of vehicles.

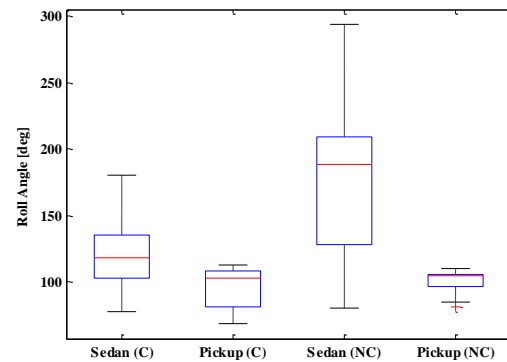
The median values of the drop speeds, which is known to be one of the most influential factors in structural responses of a vehicle during rollover [9], were 1.9 *m/s* and 2.3 *m/s* higher in the non-corrective maneuver (sedan: 2.4 *m/s* and pickup: 2.8 *m/s*) than those in the corrective maneuver (sedan: 0.47 *m/s* and pickup: 0.48 *m/s*) for the sedan and the pickup truck, respectively. This is because the vehicles tended to roll over while going down the slope in non-corrective maneuvers but roll over while going up or along the slope in corrective maneuvers. The higher drop speed can cause more structural deformation during vehicle-to-ground interaction. For the same reason, the

signs of median values of pitch angles were different between corrective and non-corrective maneuvers (Figure 10 (d)).

The side slip angle is angle between the longitudinal and traveling directions of a vehicle in vehicle dynamics [14]. In this study, the angle between the projected forward direction of the vehicle on level ground and the direction of tangential velocity of the vehicle was defined as a side slip angle at touchdown. The larger magnitude of this angle means that the vehicle was traveling in more laterally than longitudinally. Since the sedan is more agile than the pickup truck the magnitude of the median values of side slip angles of the sedan were higher than those of the pickup truck (Figure 10 (f)).

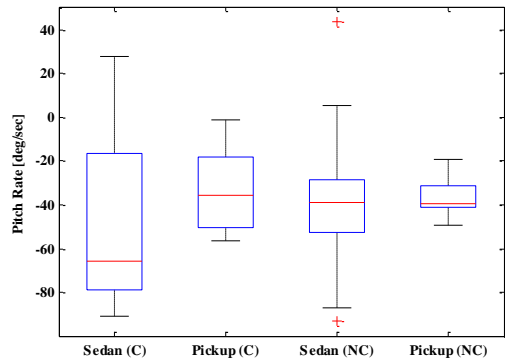


(a) Roll rates at touchdown

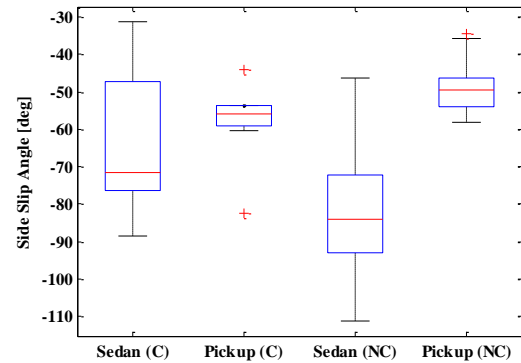


(b) Roll angle at touchdown

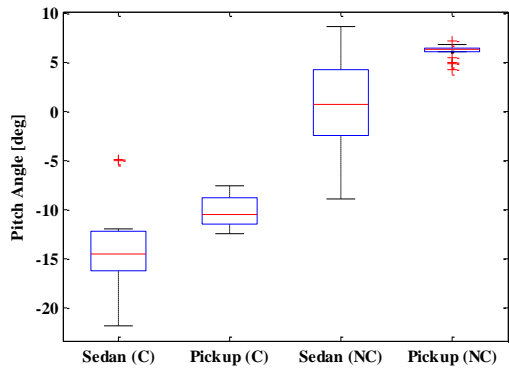
Figure 10. Distribution of touchdown parameters (cont'd)



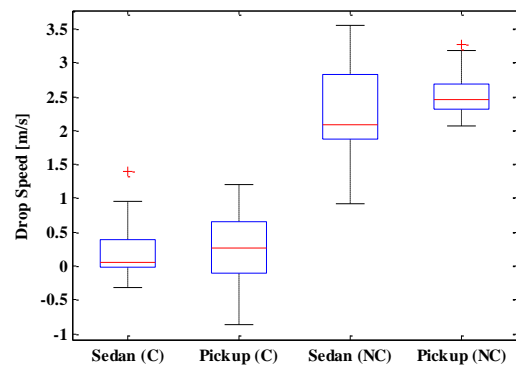
(c) Pitch rate at touchdown



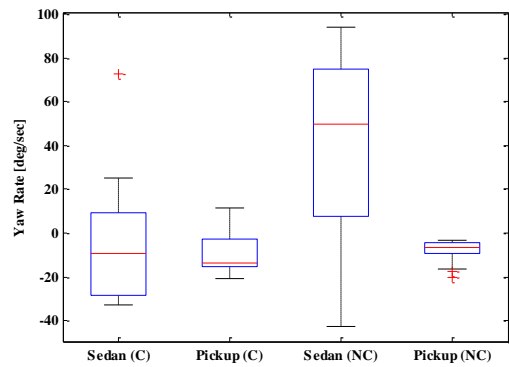
(f) Side slip angle at touchdown



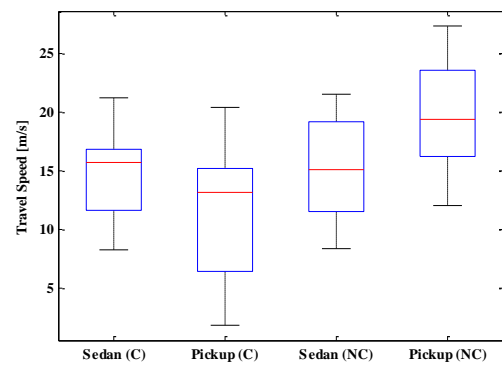
(d) Pitch angle at touchdown



(g) Drop speed at touchdown



(e) Yaw rate at touchdown



(h) Tangential speed at touchdown

Figure 10. Distribution of touchdown parameters (cont'd)

Figure 10. Distribution of touchdown parameters

DISCUSSION

The two vehicle models built in this study showed good correlations with the static and dynamic test data.

Most distributions of the touchdown parameters were not Gaussian-like or unimodal distributions. It seems that the number of simulations was insufficient

compared to the level of complexity of the rollover phenomenon because the distributions of touchdown parameters did not show any typical distributions. The result, however, suggested clear differences in some of the touchdown parameters with respect to the types of maneuvers and types of vehicles.

The non-corrective maneuvers resulted in higher roll rates, roll angle, and drop speed at touchdown than those of corrective maneuvers regardless of the considered types of vehicles. The roll angles at touchdown in the non-corrective rollover case tended to larger than those of the corrective rollover case due to the longer airborne phase and higher roll rates. The roll angles of the pickup truck were around 100 *degrees*, which implies touchdown on ground on the side of the vehicle rather than roof area.

The drop speeds were a lot lower in corrective maneuver than those of the non-corrective maneuver because of the travel direction of the vehicles with respect to the slope. The vehicle tended to roll over toward uphill or along the level direction of the slope in corrective maneuvers but the vehicle tended to roll over toward downhill in non-corrective maneuvers. This implies that there could be larger deformation during rollovers induced by non-corrective maneuvers because the drop speed is one of the significant factors that affect the vehicle deformation [9].

The pickup truck showed lower roll rates and roll angles in the both maneuvers than those of the sedan. The different roll angles at touchdown between the two vehicle types suggest that different countermeasures may be needed to protect occupants in different types of vehicles. Interestingly, the median values of drop speeds of the two vehicles were similar to each other in contrast to the differenced in roll behavior.

Another thing, which should be noted, is that in many cases the vehicle touched down on slope due to the road geometry (Figure 3). Many dynamic rollover tests are performed on flat ground and the effect of the geometry of ground should be evaluated to justify the test conditions.

Despite the detailed validations performed on the vehicle models, no steering-induced rollover test data were available to validate the vehicle and soil models. Subsequent to this study, steering-induced rollover tests will be performed to validate the models further. Especially, the soil model should be validated by testing the soil at the test site.

The vehicle kinematics time histories generated through this study can be used for occupant simulations for injury risk assessment during rollover accidents which includes pre-ballistic, ballistic, and until the touchdown. This would be meaningful because vehicle kinematics during pre-ballistic and ballistic phases could affect the location of occupants at the times of countermeasure activation and touchdown. After the touchdown finite element model should be incorporated to consider vehicle deformation after touchdown.

CONCLUSION

Despite these limitations, the methodology and results presented provide for the best available means to determine touchdown parameters for use in controlled rollover crash testing. The data presented show a substantial difference in touchdown conditions with respect to types of vehicles and maneuvers.

Therefore, when a rollover test is performed, the test conditions should be carefully selected depending on types of vehicles or maneuvers to generate realistic outcome.

Especially, the different drop speed suggests that the vehicle will deform more during rollover accidents initiated from non-corrective maneuvers. In addition, different touchdown roll angles imply that different countermeasures for a rollover accident may necessary for different types of vehicles.

ACKNOWLEDGEMENT

The Toyota Collaborative Safety Research Center provided both technical and financial support via Cooperative Agreement No. PO#NAFAC-0000124579. Note that the views in expressed this paper are those of the authors and not of the sponsors.

REFERENCES

- [1] NHTSA Traffic Safety Facts 2008, Early Edition
- [2] P. Jayakumar, J. Alanoly, and R. Johnson. 2005. "Three-Link Leaf-Spring Model for Road Loads" Society of Automotive Engineers, Warrendale, PA, SAE Paper 2005-01-0625
- [3] Chi-Ying Liang, R. Wade Allen, Theodore J. Rosenthal and Jeffrey P. Chrstos. 2004. "Tire Modeling for Off-Road Vehicle Simulation"

- Society of Automotive Engineers, Warrendale, PA, SAE Paper 2004-01-2058
- [4] Bekker, M. G. 1969. "Introduction to terrain-vehicle systems" University of Michigan Press, Ann Arbor, 1969
- [5] Wong, J. Y. 1978. "Theory of Ground Vehicle" John Wiley & Sons, New York, 1978
- [6] Road Design Manual. 2004. Delaware Department of Transportation
- [7] Roadway Design Guidelines. 2007. Arizona Department of Transportation Roadway Engineering Group
- [8] A Policy on Geometric Design of Highways and Streets. 2004. American Association of State Highway and Transportation Officials
- [9] Daniel P. Parent, Jason R. Kerrigan & Jeff R. Crandall (2011): Comprehensive computational rollover sensitivity study, Part 1: influence of vehicle pre-crash parameters on crash kinematics and roof crush, International Journal of Crashworthiness, 16:6, 633-644
- [10] Madana Gopal, Ken Baron, and Minoo Shah. 2004. "Simulation and Testing of a Suite of Field Relevant Rollovers" Society of Automotive Engineers, Warrendale, PA, SAE Paper 2004-01-0335
- [11] Terry D. Day. 2005. "Simulation of Tire Interaction with Curbs and Irregular Terrain", Engineering Dynamics Corporation, HVE White Papers, Library Ref. WP-2005-6.
- [12] David C. Viano and Chantal S. Parenteau. 2004. "Rollover Crash Sensing and Safety Overview" Society of Automotive Engineers, Warrendale, PA, SAE Paper 2004-01-0342
- [13] George S. Fishman. 2011. "Monte Carlo: Concepts, Algorithms, and Applications", New York, NY: Springer.
- [14] Thomas D. Gillespie. 1992. "Fundamentals of Vehicle Dynamics" Society of Automotive Engineers
- [15] ISO 3888-1:1999 Passenger cars – Test track for a severe manoeuvre – Part 1: Double lane-change

PASSENGER VEHICLE STRUCTURAL RESPONSE IN A DYNAMIC ROLLOVER TEST

Garrett A. Mattos

Raphael H. Grzebieta

Mike R. Bambach

Andrew S. McIntosh

Transport and Road Safety (TARS) Research

University of New South Wales

Australia

Paper Number 13-0067

ABSTRACT

The structural performance of a vehicle has been shown to be associated with the likelihood of sustaining serious injury in passenger vehicle rollover crashes. With increasing interest in implementing interior safety features, such as side curtain airbags, to mitigate injury during rollover it is important to understand the response of the vehicle structure onto which many of these devices are attached. Further, research is ongoing to determine the feasibility of using a dynamic rollover test device, such as the Jordan Rollover System (JRS), to accurately assess a vehicle's ability to protect occupants in rollover crashes. This research requires an understanding of the performance of the tests performed on such a system. The objective of this paper is to investigate the response of the vehicle structure, as tested on the JRS, with specific focus on the relationship between the dynamic and residual roof intrusion. This paper will also investigate the kinematic response of the vehicle and how it is related to roof performance and test conditions.

INTRODUCTION

The structural performance (maximum/residual roof intrusion and intrusion speed) of a vehicle in dynamic rollover and quasi-static roof strength tests has been shown to be significantly associated with its real world rollover injury rate [1-3]. Differences in vehicle kinematics during dolly rollover tests have been observed for the same vehicle shape with different roof strengths [4, 5]. The Jordan Rollover System (JRS) is currently the test device of choice in an effort to assess the viability of a dynamic rollover test for use in compliance and/or vehicle performance rating tests [6]. In this effort it is important to understand how vehicles perform on the system as well as how the test conditions affect that performance.

METHODS

Dynamic rollover tests of forty-eight passenger vehicles conducted over the past 5 years on the Jordan Rollover System (JRS) at the Center for Injury Research (CFIR) were used to study various measures of vehicle structural and kinematic

performance. The test data was provided to the authors by the CFIR.

The JRS, Figure 1, is a dynamic rollover test device that has been proven to provide a repeatable and valid representation of the interaction between the roadbed and roof of the vehicle during a lateral tripped rollover [7-10]. The JRS suspends a vehicle, which is free to spin about its longitudinal axis, above a track with a moving roadbed. The vehicle can be positioned with predetermined pitch, yaw, and drop height. At the start of the test the vehicle is rotated at a prescribed angular velocity and is dropped to impact the moving roadbed at the designated roll and pitch angle. The terms near and far are used to describe the side of the vehicle that impacts the road first and last, respectively.

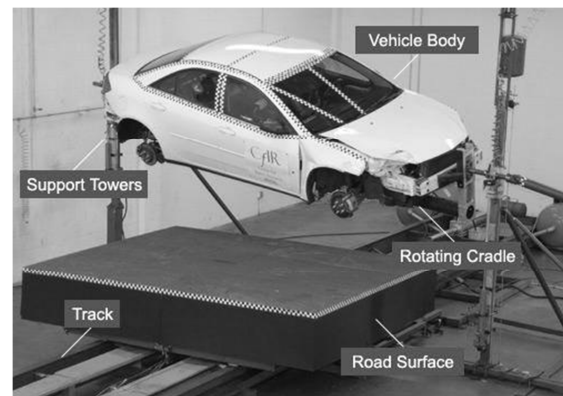


Figure 1. Jordan rollover system.

The JRS measures roadbed speed, vertical and lateral road loads, vehicle angular velocity, and vehicle vertical motion at the front and rear towers. With this information the energy of the entire system can be tracked throughout each test using the basic equations for potential and kinetic energy of rigid body motion. The energy tracked throughout the event includes the kinetic energy in the moving roadbed, which represents the translation of a vehicle in a real world rollover.

The mass of the roadbed was maintained at 1633 kg for each JRS test, therefore the initial kinetic energy in the road was approximately equal for all tests. The propulsion system pulls the roadbed throughout the entire event, including during impact. The increase in kinetic energy, due to the

sustained propulsion, is calculated from a calibration (no-impact) run for each test (Figure 2). During the impact test the roadbed slows, but not as much as it would have if the propulsion had not been sustained. The increase in kinetic energy, calculated from the calibration run, is deducted from the measured kinetic energy during the impact test to produce an adjusted profile. The adjusted data was used in all energy calculations.

The roadbed approaches the impact zone on rollers but throughout impact it slides along lubricated skids during which time the roadbed slows due to friction. The amount of energy dissipated by friction during impact was estimated using the known coefficient of kinetic friction and the measured normal force on the road.

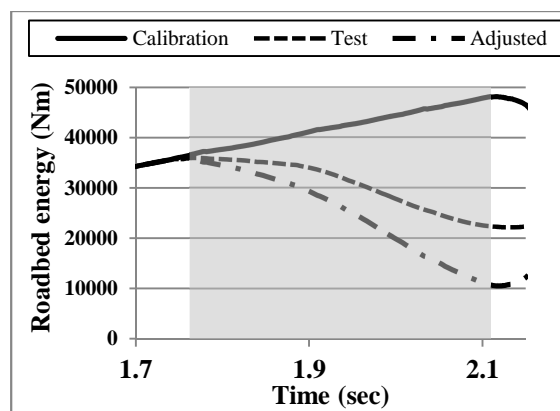


Figure 2. Roadbed energy profile for calibration test, impact test and adjusted result. Grey band indicates duration of vehicle to road impact.

The potential, vertical kinetic and rotational (roll and pitch) kinetic energy of each vehicle was calculated for the entire event. The potential energy of the vehicle was calculated using the distance between the CG of the vehicle and the roadbed, thus a vehicle in direct contact with the roadbed would have a non-zero potential energy. All rotational energy calculations were made assuming the rotation occurred about the appropriate axis passing through the centre of gravity and that the moments of inertia were constant. The sign convention used for the pitch motion, rotation about the lateral centre of gravity, is described in Figure 3. For an inverted vehicle the pitch is taken to be zero when horizontal and increases as the front moves nearer to the ground.

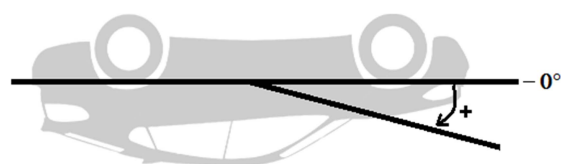


Figure 3. Pitch sign convention.

String potentiometers were used to measure the dynamic movement of the interior of the vehicle roof, relative to the approximate longitudinal centre of gravity (roll axis), at the top of each A-pillar, top of the far side B-pillar, and at the roof header approximately 200 mm inboard of the roof rail as shown in Figure 4. String potentiometers have been used in other dynamic rollover tests to measure dynamic roof movement [11, 12] and proved to provide accurate results. All test data was filtered at SAE channel frequency class 60, but the roof displacement data was further smoothed using a regularization method prior to being differentiated to obtain velocity and acceleration [13, 14]. This was done to reduce the amount of noise that is inherently amplified during numerical differentiation. The terms end of test (EOT) and residual will be used interchangeably throughout this paper to describe the amount of intrusion that is remaining at the end of the test. Roof intrusion is a decrease in the distance between the roof and the chassis. Peak dynamic intrusion is defined as the peak intrusion that occurs during an impact and is not necessarily the same as maximum intrusion which is the maximum amount of intrusion that occurred over a collection of impacts. For instance in a single roll event, where there is only 1 roof impact, the peak dynamic intrusion will be equal to the maximum intrusion. However in a two roll event with two roof impacts the maximum intrusion will be equal to the amount of residual intrusion from the first impact plus the peak dynamic intrusion from the second impact.

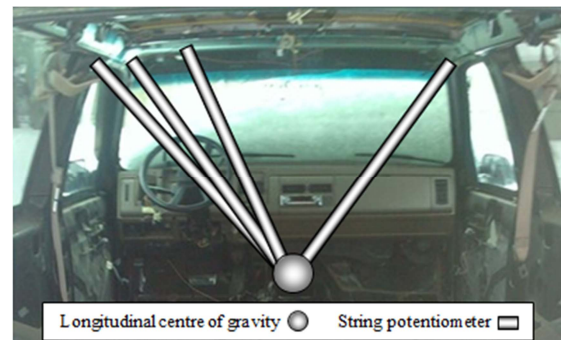


Figure 4. String potentiometer locations.

Two sections of results are presented below. The first, comprising roof intrusion data for all 48 vehicles, includes tests performed at a wide range of initial protocols. The second section, comprising vehicle kinematic and energy data for 21 vehicles, includes sequential tests performed at protocols A and B described in Table 1. The two differences between protocols A and B are the initial pitch angles and the fact that vehicles tested at protocol B had previously been tested once at protocol A.

Table 1.
Initial test conditions

Pitch (A/B)	5° / 10°
Yaw	10°
Roll rate	180°/sec
Impact roll angle	145°
Road speed	6.7 m/s
Drop height	10.2 cm

The duration of the rollover event is defined as the time between first roof to ground impact and the time at which the vehicle is no longer in contact with the roadbed surface.

RESULTS

Roof Performance

The relationship between the maximum intrusion and the end of test intrusion was consistent for all vehicles, initial conditions, numbers of roof impacts and roof measurement locations. The scatter plot in Figure 5 was generated using 230 far side roof measurements from 83 various protocol JRS tests of 48 different vehicles. Equation 1, derived from the best fit line ($R^2 = 0.96$) of the aggregated data, estimates the maximum amount of roof intrusion sustained during the event, y , from the known residual intrusion, x , as measured in centimetres. Occasionally the far side header experienced slight outward tenting during the near side impact which resulted in an overall negative residual intrusion value.

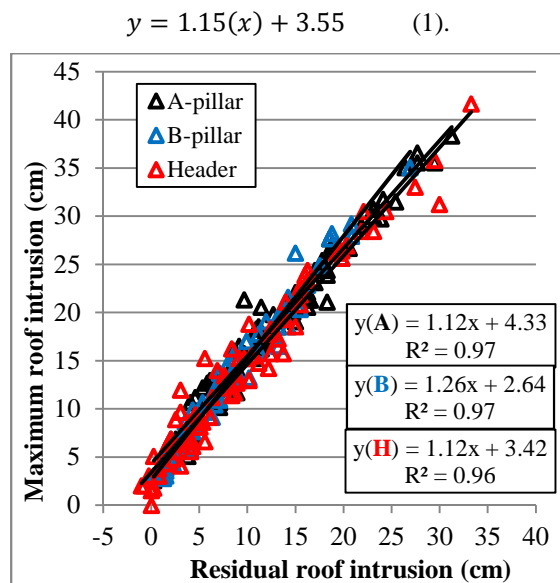


Figure 5. Residual roof intrusion vs. maximum intrusion by measurement location.

Similar results were obtained in inverted drop tests conducted by Batzer et al. [15] (Figure 6) and in curb trip tests [12]. The amount of maximum roof intrusion estimated by Equation 1 and the amount estimated by the inverted drop test data varied less than 5 cm over 40 cm of residual intrusion.

There was a moderate relationship between the peak speed at which the roof intruded during a roof to ground impact and the amount of dynamic intrusion that occurred, Figure 7.

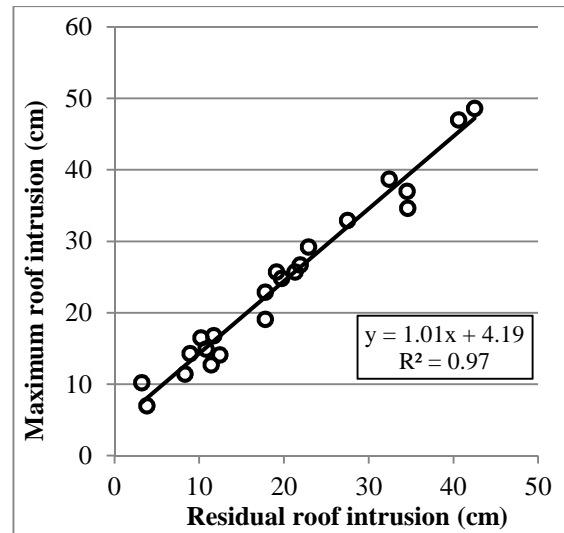


Figure 6. Residual roof intrusion vs. maximum roof intrusion in inverted drop tests after Batzer et al. [15]. Measurements taken at far side A-pillar, perpendicular to impact surface.

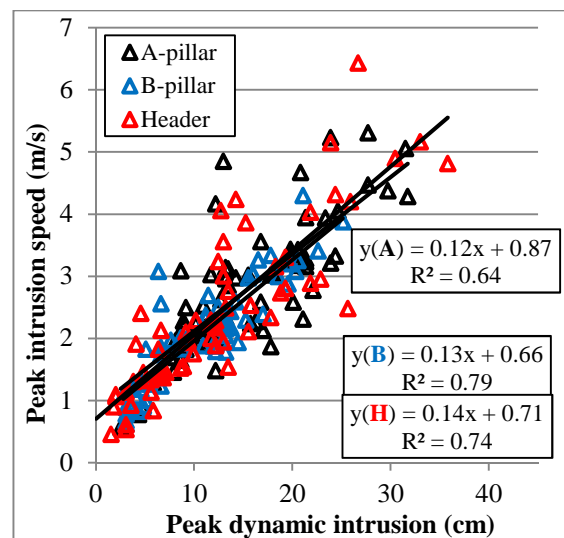


Figure 7. Peak dynamic roof intrusion vs. peak intrusion speed.

In general the peak acceleration of the intruding roof increased with increased peak dynamic intrusion, but the relationship was weak (Figure 8).

The peak acceleration was more closely related to the peak speed of roof intrusion, Figure 9. The relationships between all parameters in Figures 5-9 was strongest for measurements taken at the far side B-pillar.

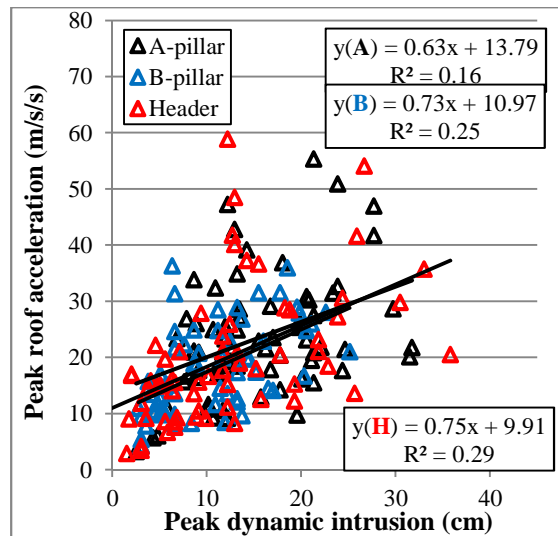


Figure 8. Peak dynamic roof intrusion vs. peak roof intrusion acceleration.

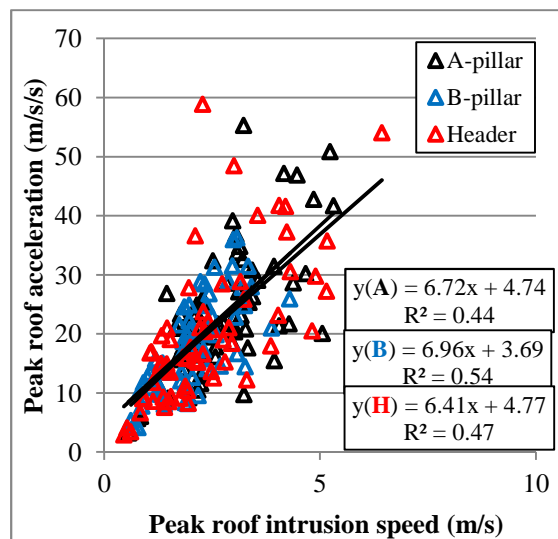


Figure 9. Peak roof intrusion speed vs. peak roof intrusion acceleration

Vehicle Kinematics

The following results were obtained solely from tests conducted at protocols A and/or B. These tests were performed sequentially; therefore all vehicles tested at protocol B had previously been tested once at protocol A.

The total duration of impact varied between vehicles. It ranged from 0.389 to 0.294 seconds with an average of 0.347 seconds for test protocol

A. For test protocol B the duration of impact ranged from 0.404 to 0.272 seconds with an average of 0.333 seconds. On average the far side impact lasted 66.4 % longer than the near side impact for test protocol A and 33.6 % longer for test protocol B.

Two pitching modes were observed for vehicles tested at protocol A. The first mode, illustrated in Figure 10, consisted of the pitch generally increasing during the event until an impact between the road and far side front fender caused the pitch to stabilise. One example of the general vertical motion of the front and rear of the vehicle throughout the impact for the first pitching mode is shown in Figure 11. For this mode of pitching the front dropped at a constant rate as the rear remained at a fairly constant height. At far side impact the front continued to drop while the rear rose rapidly. When the front far side fender contacted the road, at approximately 210-235 degrees, the pitch stabilised as the vertical motion of the front and rear of the vehicle ceased. Contact between the vehicle and the road generally ended between 240 and 250 degrees of roll at which time the vehicles in this mode had pitch angle ranging from 8.7 to 12.4 degrees.

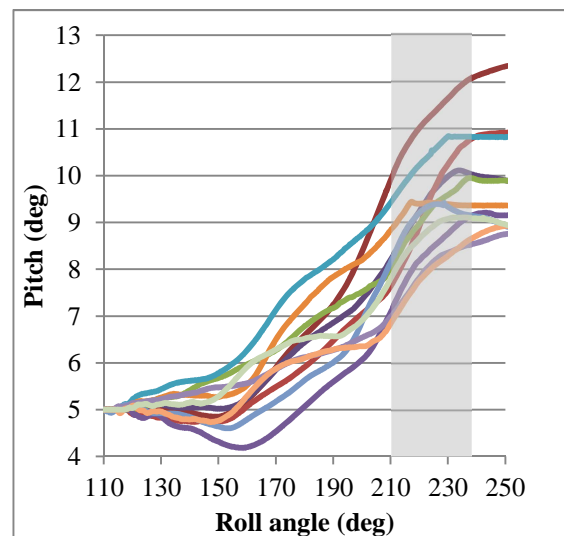


Figure 10. Roll angle vs. pitch for test protocol A. Pitching mode 1. Shaded area represents approximate start of fender contact. Each colour represents a separate test vehicle.

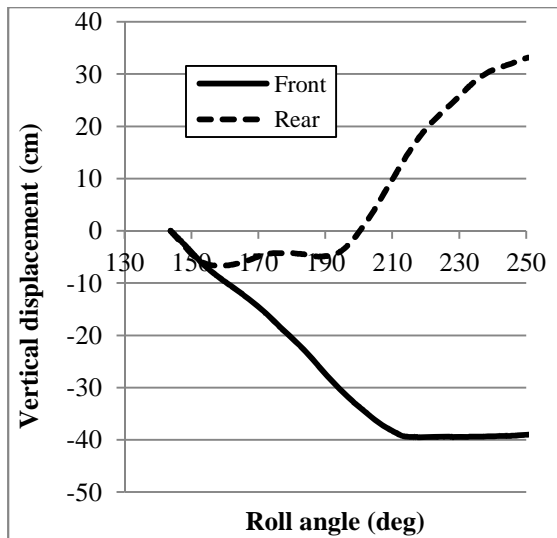


Figure 11. Roll angle vs. vertical displacement of front and rear of the vehicle. Test protocol A. Pitching mode 1.

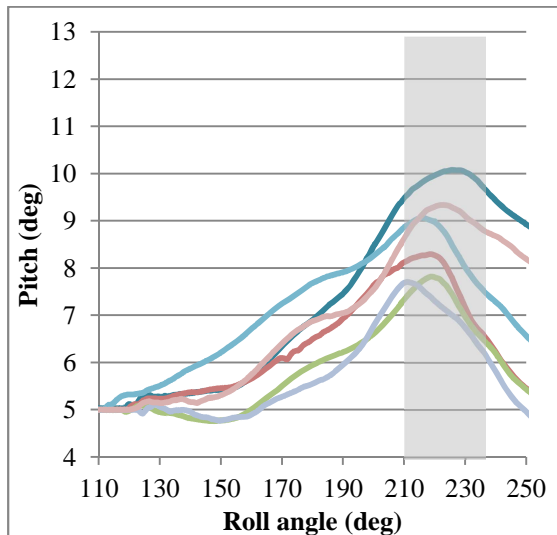


Figure 12. Roll angle vs. pitch for test protocol A. Pitching mode 2. Shaded area represents approximate start of fender contact. Each colour represents a separate test vehicle.

The overall pitch and the general motion of the front and rear of each vehicle in the second mode are shown in Figures 12 and 13 respectively. In this mode the pitch increased, to between 7.6° and 10.1° , up to the point of front far side fender contact at which point the pitch rate changed direction. At the time these vehicles left the roadway they were pitching at approximately -6.1° per quarter turn. The vertical motion at the front and rear of the vehicle was similar to that of mode 1 up until far side roof impact. The impact between the far side of the roof and roadbed caused the rear of the vehicle to slowly move upwards with little effect on the motion of the front of the vehicle.

When the front far side fender contacted the roadbed the vertical motion of the rear of the vehicle was stopped while the front rapidly moved upward resulting in decreasing pitch. The range of pitch angles at far side impact for all vehicles was from 3.4 to 8.1 degrees.

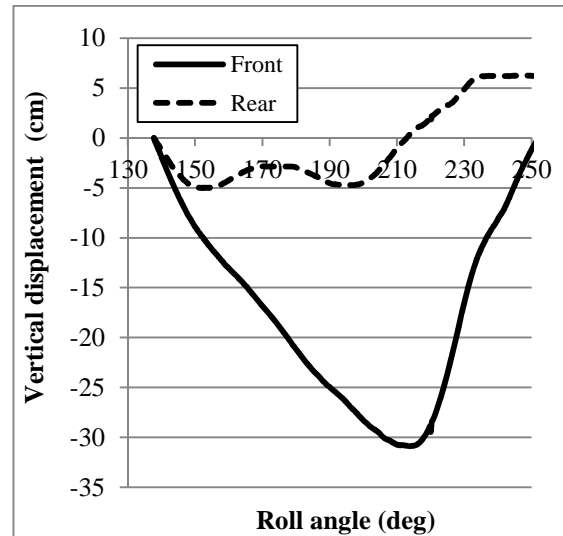


Figure 13. Roll angle vs. vertical displacement of front and rear of the vehicle. Test protocol A. Pitching mode 2.

For vehicles tested at protocol B the pitch response was generally similar, Figure 14. Most vehicles had a slightly increasing or stable pitch from initial impact through the far side roof contact and until front far side fender contact. Fender impact occurred earlier in the roll of test protocol B than test protocol A. The only major differences observed between each vehicle were the pitching motions resulting from far side fender contact. The motions ranged from abrupt changes in pitch, due to combined far side fender and roof contact, to cylindrical-type rolling with minor alterations in pitch angle. The range of pitch angles at far side impact was from 7.8 to 11.9 degrees. The pitch rates at the end of roadbed contact ranged from stable to -8.9° per quarter turn.

Two different modes were identified for the vertical motion at the front and rear of the vehicle. The first mode, Figure 15, was characterised by minimal changes in overall pitch as the front and rear of the vehicle moved in tandem with one another. In the second mode, Figure 16, the front and rear of the vehicles generally fell together until far side roof and front fender impact at which point the front of the vehicle moved rapidly upward while the rear of the vehicle maintained its position.

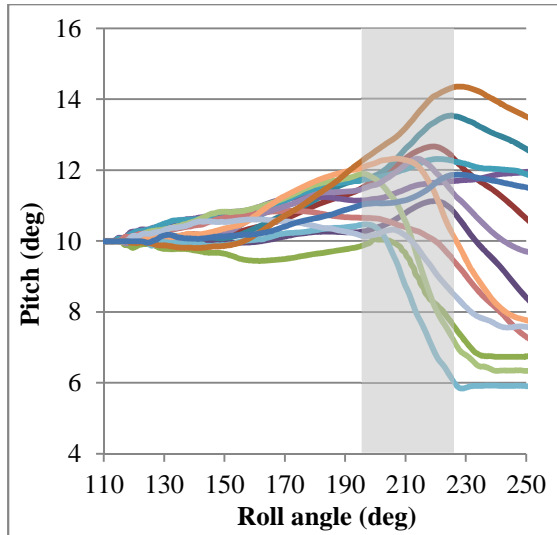


Figure 14. Roll angle vs. pitch for test protocol B. Shaded area represents approximate start of fender contact. Each colour represents a separate test vehicle.

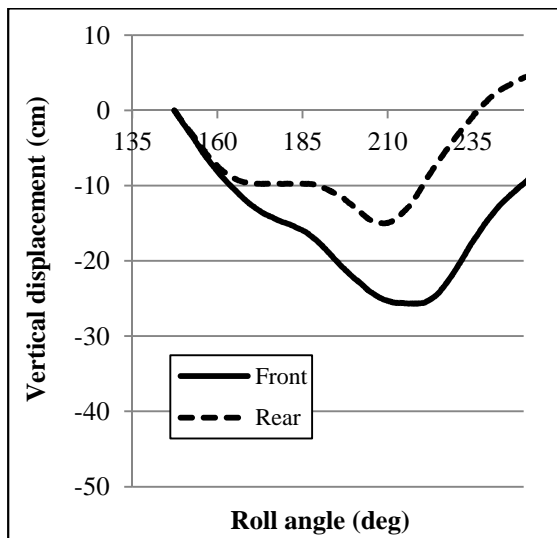


Figure 15. Roll angle vs. vertical displacement of front and rear of vehicle. Test protocol B. Pitching mode 1.

Energy

The energy profiles at three instances in the rollover event for the tests performed at protocols A and B are shown in Figures 17 and 18. In each chart the first column for each vehicle, labelled with the name of the vehicle, describes the energy in the system just prior to initial impact. The second and third columns to the right describe the energy just prior to and just after far side impact, respectively. The difference between the total height of each column indicates the amount of energy dissipated during the event.

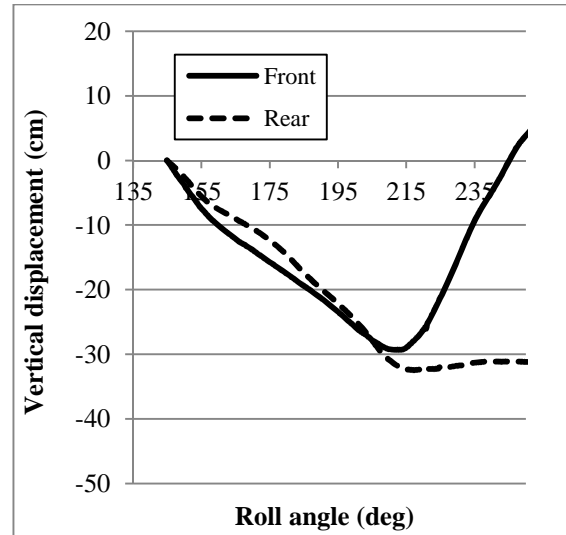


Figure 16. Roll angle vs. vertical displacement of front and rear of vehicle. Test protocol B. Pitching mode 2.

In some tests an increase in total energy was observed to occur during near side impact, e.g. compare the first and second column for the Volkswagen Tiguan in Figure 18. The increase in energy was on the order of 1 % of the total energy and was attributed to roll rate sensor noise.

A net energy loss was recorded for each vehicle during the rollover event. This loss was assumed to be due to the dissipation of energy in the form of friction between the roadbed and skids (calculation described in the methods section) and vehicle deformation. The average amount of energy dissipated during the near and far side impacts was 1.6 % and 19.9 % of the total initial energy for test protocol A, respectively. Of the energy dissipated in the far side impact, between 43.1 % and 84.2 % (average = 55.9 %) was estimated to have been in the form of vehicle deformation. For test protocol B the average amount of energy dissipated during the near and far side impacts was 2.7 % and 22.8% respectively. Of the energy dissipated in the far side impact, between 32.7 % and 75.5 % (average = 50.1 %) was estimated to have been in the form of vehicle deformation. The majority of the remaining energy was estimated to be lost due to friction between the roadbed and skids.

The amount of energy estimated to have been dissipated via far side roof deformation was related to the amount of peak dynamic roof intrusion that occurred during the event, Figure 19. This relationship was not as strong ($R^2=0.35$) for test protocol B.

Figure 17. Energy profile for test protocol A. Note the vertical axis starts at 10,000 Nm.

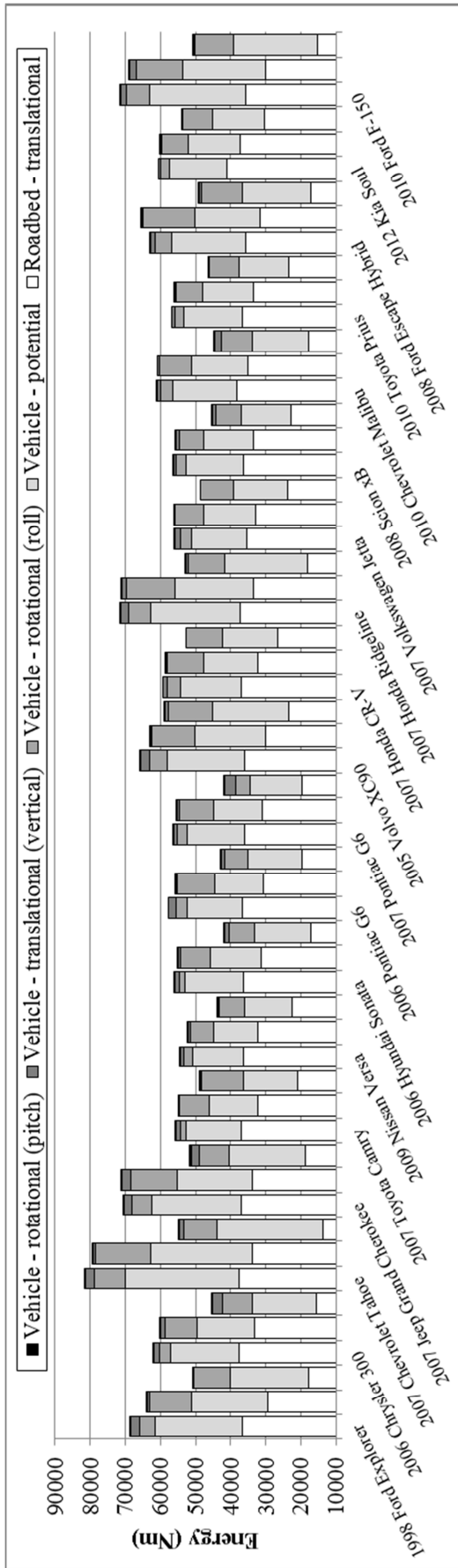
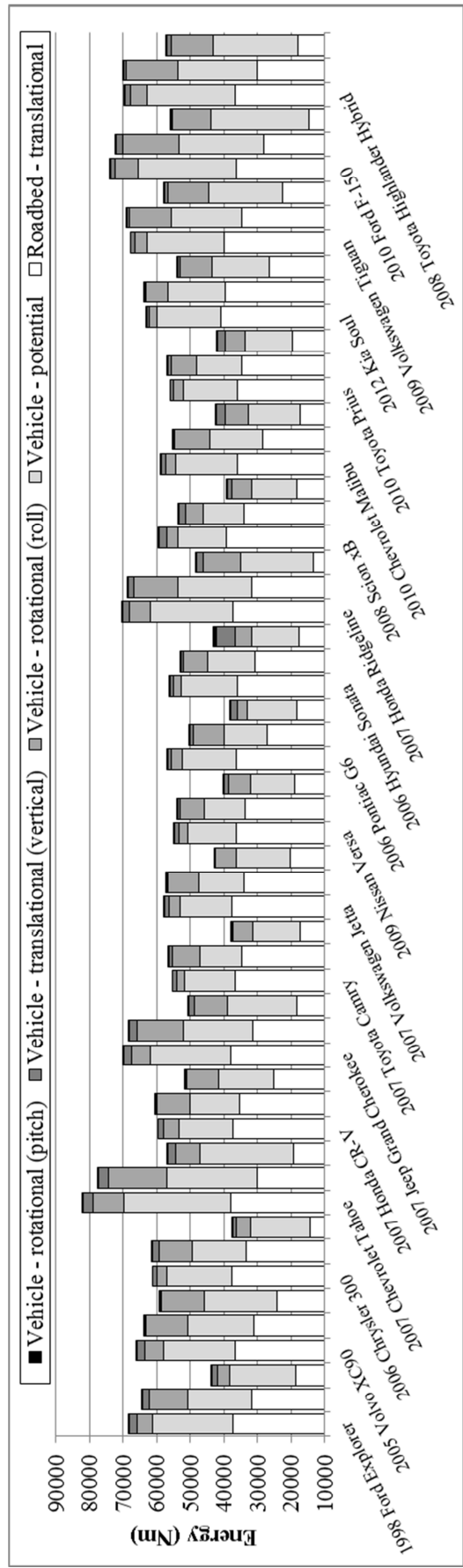


Figure 18. Energy profile for test protocol B. Note the vertical axis starts at 10,000 Nm.



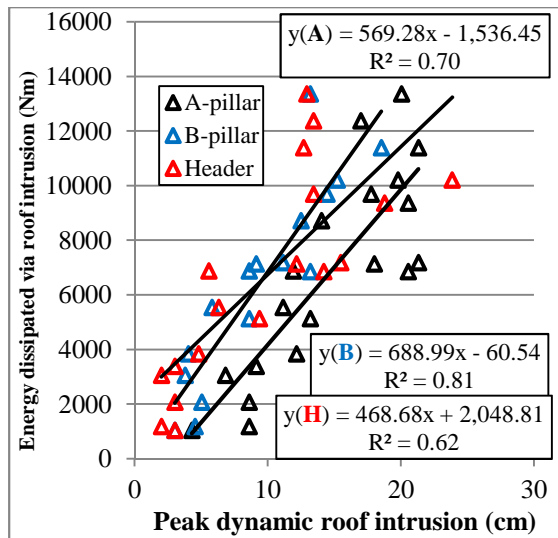


Figure 19. Peak far side dynamic roof intrusion vs. estimated energy dissipated by roof intrusion. Test protocol A.

Table 2 describes the change in energy that occurred throughout the entire event and during near and far side impacts for the three main forms of energy in the system. For each form of energy (roadbed translational, vehicle translational and vehicle rotational) the total range and average per cent change is listed. Overall there was little difference between the transformation of energy in test protocols A and B. The general trend was that the overall translational energy of the roadbed and vehicle decreased while the rotational energy of the vehicle increased. For all vehicles in each test the roadbed slowed during the near and far side impacts. In both test protocols every vehicle lost vertical kinetic and potential energy during near side impact as its vertical motion was slowed due to impact with the road. At far side impact, however, vehicles generally bounced upward causing an increase in the vertical translational energy. On average vehicles tended to end the roll event with less vertical translational energy than they had initially. The near side impact resulted in an increase in rotational energy for every vehicle in every test. For test protocol A the change in a vehicle's rotational energy during far side impact was related to the amount of peak dynamic far side roof deformation, Figure 20. Vehicles with low amounts of intrusion experienced an increase in rotational energy while those with greater amounts of intrusion experienced a decrease in rotational energy. For test protocol B all but one vehicle either maintained or lost rotational energy. There was no relationship between the change in rotational energy and roof intrusion. The amount of energy in the vehicle's pitching motion was less than 1% of the total energy in the system throughout the rollover event.

Table 2. Per cent change in energy for three forms of energy.

	Roadbed translational		Vehicle translational		Vehicle rotational	
	Range	Average	Range	Average	Range	Average
Roll 1	-63.9 – -25.9	-45.1	-17.7 – 2.2	-9.9	6.6 – 271	139.9
Near side	-23.1 – -7.8	-15.5	-18.2 – -7.1	-13.5	90.6 – 261	171.4
Far side	-59.7 – -17.5	-37.6	4.1 – 20.2	5.3	-55.5 – 42.7	-8.9
Roll 2	-64.7 – -32.4	-49.2	-18 – 11.2	-7.3	-23.1 – 288	101.8
Near side	-25.8 – -9.7	-16	-19.6 – -9.3	-14.5	76.2 – 243	158.9
Far side	-58.4 – -23.0	-41.3	-0.1 – 35.3	9.5	-68.9 – 44.4	-23.6

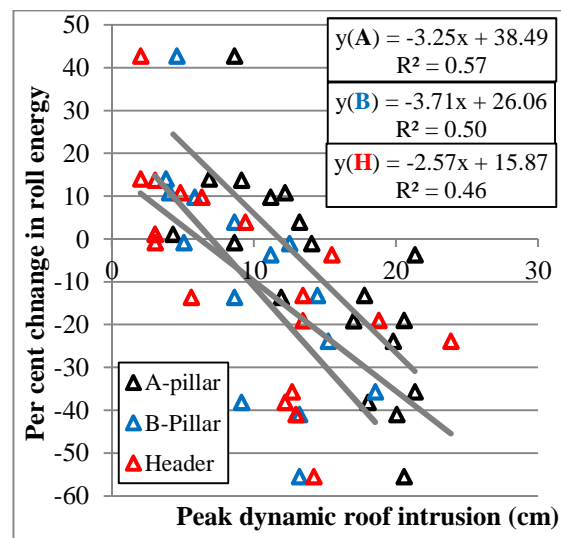


Figure 20. Peak dynamic roof intrusion vs. per cent change in roll energy during far side impact. Test protocol A.

DISCUSSION

Strong relationships were observed between maximum and residual roof intrusion and moderately strong relationships between peak dynamic intrusion and peak intrusion speed. These relationships were always strongest for measurements taken at the far side B-pillar. This is believed to be due to the greater stiffness and alignment of the B-pillar as compared to that of the A-pillar and header. While peak intrusion speed was moderately related to the peak intrusion acceleration, peak dynamic intrusion had a very weak relationship with acceleration. This may be due to the method of calculating speed and acceleration from displacement where a single differentiation step (i.e. between displacement and speed or between speed and acceleration) would maintain any relationship while the two differentiation steps between displacement and acceleration might have amplified enough of the noise to weaken the relationship. Further, differences in roof elasticity and the time at which glazing failed would have an effect on the relationship.

The major difference between the pitching modes observed for protocol A was the effect of far side front fender impact. Vehicles with more volatile pitch (mode 2) had relatively long front bonnets, with respect to their overall length, and a generally lower profile. They also had an average of 52 % more peak dynamic roof intrusion at the A-pillar and 47.6 % more at the B-pillar than vehicles exhibiting behaviour consistent with mode 1. Similarly, the vehicles grouped in the second mode for test protocol B had more severe pitching motion than those in mode 1 and were relatively weaker and longer. The average SWR for mode 2 vehicles was 3.1 compared to 4.3 and they experienced 34.5 % to 70 % more roof intrusion at the A and B pillars, respectively. The vehicles in mode two were an average of 30.5 cm longer than those in mode 1.

The results of the pitching motion highlight the wide range of vehicle kinematics that can occur during the roof impact phase of a rollover due to differences in vehicle shape and roof strength. This difference adds to the complexity of establishing a protocol, considering both vehicle and ATD initial conditions, for a second test.

The energy profiles for all tests had many similarities. The roadbed lost energy throughout the event and the vehicle gained energy in the form of rotational velocity during the near side contact. The increase in roll rate during near side contact was due to the difference in peripheral velocity of the vehicle and translational velocity of the roadbed.

The change in rotational energy during far side impact for test protocol A was dependant on the amount of roof intrusion that occurred. With one exception, the roll rate at far side impact for test protocol B either remained constant or decreased. This was due to the more severe fender contact that occurred with greater pitch angles.

The difference in vehicle performance can be seen in Figures 17 and 18. Vehicles which had low amounts of roof intrusion, such as the Volvo XC90 and Honda CR-V had relatively small amounts of energy lost during near and far side impacts. These vehicles nearly maintained their roll energy through the final impact while the roadbed lost energy gradually. On the other hand vehicles like the Chevrolet Tahoe and the Jeep Grand Cherokee had relatively large losses in energy during the far side impact. The high levels of roof intrusion in these vehicles during the far side impact resulted in great losses in vehicle rotational and roadbed translational energy.

Although the initial conditions of the tests for respective protocols were the same the initial energy was different for each vehicle due to the differences in vehicle size. The amount of initial roll, potential or total energy did not appear to be related to the performance of the roof during the event.

During each test approximately 8-17 % of the total system energy was dissipated via work done deforming the vehicle body. A moderate relationship was found between peak dynamic roof intrusion and energy dissipated via vehicle deformation for test protocol A. The relationship was strong for test protocol A because roof deformation accounted for the majority of vehicle damage. This was not the case for test protocol B in which significant fender to road contact would have resulted in dissipation of energy that would not have been accounted for in roof deformation measurements.

CONCLUSIONS

In tests performed on the JRS at the stated protocols a few relationships were observed. The amount of maximum roof intrusion could be accurately predicted for known amounts of residual roof intrusion using Equation 1. Peak roof intrusion speed is related to, but not fully predicted by, peak dynamic intrusion. Peak roof intrusion speed is moderately related to the peak acceleration of the roof during impact. The resulting pitch motion of a vehicle appears to be related to its geometry and roof performance. The kinetic and potential energy in the roadbed and vehicle could be tracked throughout each JRS test. The amount of energy

dissipated via friction and vehicle deformation could be estimated for each test. For test protocol A the estimated amount of energy dissipated via roof deformation correlated fairly well with the amount of roof intrusion.

ACKNOWLEDGEMENTS

The authors would like to thank the Australian federal government's Australian Research Council for providing funds to carry out this research through the Linkage Projects grants scheme (No: LP110100069). The authors would also like to thank the industry partners for also providing the Partner Organisation funding, namely, the New South Wales state government's Centre for Road Safety, the Victorian state government's 3rd party insurer Transport Accident Commission (TAC), the West Australian (WA) state government's Office of Road Safety at Main Roads WA, the mining company BHP Billiton Ltd, and the US Center for Injury Research (CFIR). CFIR is also gratefully acknowledged for supplying the JRS test data.

REFERENCES

- [1] G.A. Mattos, R. Grzebieta, M. Bambach, and A.S. McIntosh, *Validation of a dynamic rollover test device*, Int. J. Crashworthiness (2013).
- [2] M.L. Brumbelow, E.R. Teoh, D.S. Zuby, and A.T. McCartt, *Roof strength and injury risk in rollover crashes*, Traffic Inj. Prev. 10 (2009), pp. 252-265.
- [3] M.L. Brumbelow and E.R. Teoh, *roof strength and injury risk in rollover crashes of passenger cars*, Traffic Inj. Prev. 10 (2009), pp. 584-592.
- [4] K.F. Orlowski, R.T. Bundorf, and E.A. Moffatt, *Rollover crash tests - the influence of roof strength on injury mechanics*, 1985, Society of Automotive Engineers: Warrendale, PA. p. 181-203.
- [5] G.S. Bahling, R.T. Bundorf, G.S. Kaspzyk, E.A. Moffatt, K.F. Orlowski, and J.E. Stocke, *Rollover and drop tests - The influence of roof strength on injury mechanics using belted dummies*, in Stapp Car Crash Conference 1990, Society of Automotive Engineers: Warrendale, PA. p. 101-112.
- [6] R. Grzebieta, M. Bambach, A. McIntosh, K. Digges, S. Job, D. Friedman, K. Simmons, E.C. Chirwa, R. Zou, and F.A. Pintar, *The dynamic rollover protection (DROP) research program*, Proc. 8th International Crashworthiness Conference, Milan, Italy, 2012.
- [7] J. Bish, J. Caplinger, D. Friedman, A. Jordan, and C. Nash, *Repeatability of a dynamic rollover test system*, Proc. International Crashworthiness Conference Kyoto, Japan, 2008.
- [8] E.C. Chirwa, R.R. Stephenson, S.A. Batzer, and R.H. Grzebieta, *Review of the Jordan Rollover System (JRS) vis-a-vis other dynamic crash test devices*, Int. J. Crashworthiness 15 (2010), pp. 553-569.
- [9] A. Jordan and J. Bish, *Repeatability testing of a dynamic rollover test fixture*, Proc. 19th International technical Conference on the Enhanced Safety of Vehicles, Washington, DC, 2005.
- [10] J.R. Kerrigan, A. Jordan, D. Parent, Q. Zhang, J. Funk, N.J. Dennis, B. Overby, J. Bolton, and J. Crandall, *Design of a dynamic rollover test system*, SAE International Journal of Passenger Cars - Mechanical Systems 4 (2011), pp. 870-903.
- [11] G. Rains and M.A. Van Voorhis, *Quasi static and dynamic roof crush testing*, 1998, NHTSA, Vehicle Research and Test Center: Washington D.C.
- [12] S.W. Harvin, B.M. O'Brien-Mitchell, A.R. Dwoinen, C.A. Nassoioy, D.F. Motowski, A.G. Melocchi, H. Lu, and M.V. Peace, *Evaluation of Dynamic Roof Deformation in Rollover Crash Tests*, SAE International Journal of Passenger Cars - Mechanical Systems 4 (2011), pp. 807-829.
- [13] J.J. Stickel, *Data smoothing and numerical differentiation by a regularization method*, Computers & Chemical Engineering 34 (2010), pp. 467-475.
- [14] P.H.C. Eilers, *A Perfect Smoother*, Analytical Chemistry 75 (2003), pp. 3631-3636.
- [15] S.A. Batzer and R.M. Hooker, *Dynamic roof crush intrusion in inverted drop testing*, Proc. 19th ESV Conference, Washington, D.C. , 2005.

REPLICATING REAL WORLD ROLLOVER CRASH INJURIES

Raphael Grzebieta

Mike Bambach

Andrew McIntosh

Garrett Mattos

Keith Simmons

George Rechner

Transport and Road Safety (TARS) Research, University of New South Wales
Australia

Kennerly Digges

The George Washington University, National Crash Analysis Center
USA

Paper Number 13-0098

ABSTRACT

This paper details the injuries occurring in real world trip-over only rollover crashes, for seat belted and contained occupants, and assesses whether these injuries can be replicated using a Jordan Rollover System (JRS) crash test rig recently installed at Crashlab in Sydney. This research forms part of the Dynamic Rollover Occupant Protection (DROP) project funded by the Australian Research Council and industry collaborators to develop a dynamic rollover crash test protocol that can assess a vehicle's rollover crashworthiness. Australian National Coroners Information System (NCIS) fatality data and US NASS-CDS serious injury data of seat belted occupants involved in single vehicle pure rollover crashes ranging over the period of 2000 to 2010, were investigated. AIS3+ head and thorax injuries and AIS2+ spinal injuries were analysed to determine rollover injury characteristics and to determine possible test conditions under which they occur. Publically available dynamic rollover crash tests carried out by other researchers were also analysed to determine their capability of replicating these real world injuries.

Serious head injuries (SHI), serious neck/spine injuries (SSI) and serious thorax injuries (STI) were found to be distributed in roughly equal proportions, most occurring independently of each other, indicating different injury causal mechanisms. A significant portion of these injuries occurred where there was minimal or no roof crush involvement. Investigations of other researcher's crash test results show dynamic rollover crash test rigs, crash test protocols and anthropomorphic test devices (ATD) have not, in general, been able to replicate ATD loadings consistent with these real world injuries repeatedly in a manner similar to frontal or side impact crash test protocols. The dynamic test conditions, measurement systems (possible ATD) and criteria required to consistently replicate vehicle damage and a particular injury

mode (SHI, STI and SSI) using the JRS are discussed.

It was concluded that to date it appears that current test protocols are not capable of consistently replicating the injuries identified in real world rollover crashes. Addressing roof crush alone via quasi-static testing will not mitigate all real world rollover injuries in typical trip-over only rollover crashes. A more advanced dynamic rollover crash test protocol must be developed that is more representative of the real world crashes and be capable of consistently replicating SHI, STI and SSI. It may be possible using the JRS test rig albeit the rig may need to be modified to tolerate much heavier impacts and a suitable rollover ATD may need to be developed. Until such time that the real world injuries observed in strong roof vehicles can be replicated repeatedly in a realistic manner, research on the development of an appropriate crash test protocol and ATD will need to continue.

INTRODUCTION

This is a summary of a paper which first appeared in the proceedings of the International Crashworthiness Conference ICRASH 2012 held in Milan Italy titled "The Dynamic Rollover Protection (DROP) Research Program" [1]. Readers are directed to the full paper for a more comprehensive discussion of the issues presented here.

A little more more than half of the single vehicle crash fatalities in Australia occur in passenger cars. Of these, about a quarter to one third of the occupants killed is in a vehicle that rolls over ($n \approx 150$ fatalities per annum). Furthermore, rollover crashes account for: 12% of all Australian road fatalities; around 35% of all occupant fatalities occurring in a single vehicle crash injury event; around 17% of Australian spinal injuries; and are now greater in number than fatalities occurring in frontal or side impact vehicle crashes [2, 3].

Elsewhere, one in every three vehicle occupant lives lost in the USA is attributed to vehicle rollover crashes (around 10,000 fatalities), whereas around 10% of road users are killed in such crashes in Europe.

Australians have a very high seatbelt wearing rate ranging from 95% to 97% [4, 5]. Nevertheless, it appears around 60% of occupants killed in a rollover crash were found not wearing a seat belt [2, 3]. This has contributed to the Australia Federal and State governments to consider seat belt interlocks in their National Road Safety Strategy [6]. In regards to crash severity, Fréchède et al [2] found that around 83% of Australian rollover crashes occurred within two or less full rollovers (eight ¼ turns). Earlier studies of US crash data by Digges and Eigen [7] also revealed that around 90% of seriously injured non-ejected seat belted occupants occurred in two or less full rolls.

A number of studies to date have found a positive relationship between the amount of roof crush, roof strength and the likelihood of serious injury in rollover crashes [2, 3, 8-16]. However, the forty year debate on this issue still continues to this day. For example, Funk et al, Moffat and Padmanaban, Padmanaban et al, [17-19] and others continue to opine that there is no significant relationship between vehicle roof strength and injuries occurring in rollover crashes. One of the confounding factors in some analyses has been the inclusion of serious injuries to all body areas in an analysis, rather than injuries to specific regions. While there might not be a relationship between serious thoracic injury (STI) and roof crush, a relationship exists between serious neck injury and roof crush. Recent studies by Bambach et al, Mattos et al and Funk et al [15-17, 20] of contained and restrained occupants involved in single vehicle pure rollover crashes that occurred in the United States indicate that serious injuries to the thorax, head and spine can still occur even when there is little or no roof crush, highlighting the need to improve occupant safety systems.

While a strong roof with an SWR of 4 or more reduces the risk to almost zero in terms of a seat belted occupant being killed in rollovers that are representative of two roll or less pure rollover trip-over crash on relatively flat terrain, serious injuries can still occur [3]. It is not entirely clear how these injuries arise but they appear to be occurring from some form of impact with the interior due to velocity differentials. So far, replicating the real world injuries both in simulations and crash tests has been sporadic and inconsistent. Batzer [21] discussed some of the issues concerning experimental observations of sporadic injurious

loading and relationship to real world crashes for different rollover test rigs.

The Dynamic Rollover Occupant Protection (DROP) research program, funded by the Australian Research Council via an industry linkage partnership, aims to establish which combination of vehicle rollover crash severity, roll kinematics, biomechanical injury criteria, and crash test dummy, best replicate the major proportion of rollover fatalities and serious injuries occurring to seat belted and restrained occupants in a typical 2 roll or less pure trip-over rollover crash over relatively flat terrain. The project industry partner organisations include BHP Billiton, Centre for Road Safety at Transport for NSW, the Transport Accident Commission, the Office of Road Safety at Main Road Western Australia and the US Center for Injury Research. Research centres involved in the project are TARS UNSW, Neuroscience Research Laboratories at the Medical College of Wisconsin, BAARG at University of Bolton, NCAC at George Washington University, and School of Biomedical Engineering and Sciences at Virginia Tech.

The outcomes of this three to four year research program will be an understanding of those factors most important for regulators, industry and consumer groups to consider when developing a dynamic rollover crashworthiness compliance or consumer rating crash test protocol. The DROP team will then determine which vehicle components (roof strength, roof geometry, restraint systems, air curtains, etc.), or combination thereof, provide the most effective, practical, and cost efficient rollover injury mitigation strategies for regulators, industry and consumers to consider and adopt. As has been seen in frontal and side impact crashworthiness, relevant dynamic crash tests with a focus on occupant protection bring many public benefits in terms of injury reduction and improvements in vehicle crashworthiness.

This paper presents the research program and progress on some of the sub tasks from the DROP program. In particular, investigations of how head, chest or thorax fatal injuries that occur to restrained and contained occupants are to be replicated for a reasonable severity rollover crash, will be outlined. The advanced UNSW version of the Jordan Rollover System (JRS), recently built and installed at Sydney Roads and Maritime Services Crashlab test facility is also described in a sister paper [22]. The JRS can carry out rollover crash tests for parametric studies where different aspects of the roll event can be precisely isolated and the results compared to analysis and computer simulations.

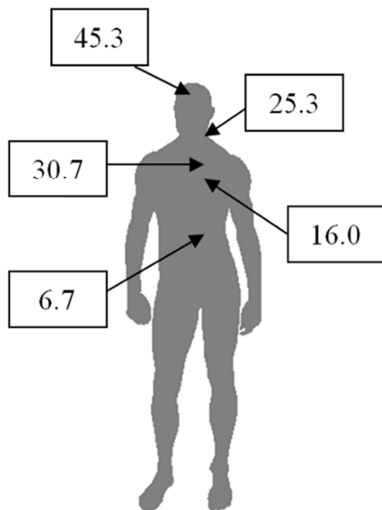


Figure 1. Percentage distribution of cause of death established from Australian NCIS data (after Fréchéde et al [2]).

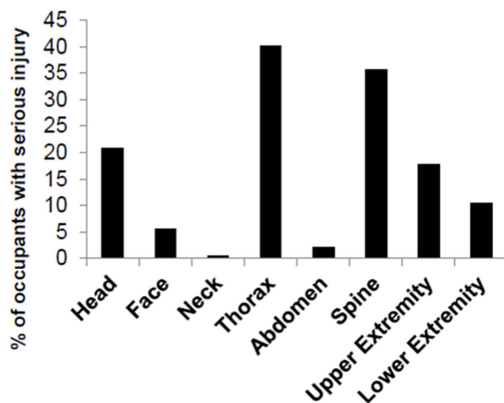


Figure 2. US NASS-CDS serious injury data (after Mattos et al [15]).

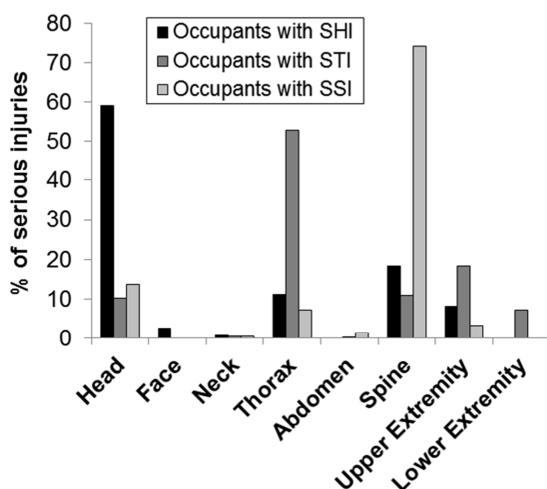


Figure 3. Distribution of occupants with serious injuries AIS 3+ by body region for contained, restrained occupants greater than 16 years old in pure, trip-over rollovers (after Mattos et al [15]).

TAXONOMY OF ROLLOVER INJURIES

Figure 1 shows results of recent studies by Fréchéde et al [2] of Australian National Coroners Information System fatality data between 2000 and 2007 of 474 rollover cases, and Figures 2 and 3 show results of analyses from Bambach et al [16, 20] and Mattos et al [15] of US National Automotive Sampling System – Crashworthiness Data System (NASS-CDS) serious injury data of contained and restrained occupants involved in single vehicle pure rollover crashes ranging from 2000 to 2010 (n=1009 unweighted) for pure trip-over rollovers.

The injury distributions indicate that serious head, neck/spine and thorax injuries appear to be distributed in roughly similar proportions. Furthermore, Mattos et al [15] have determined from their study of AIS 3+ injuries in NASS-CDS data over the period of 2000 to 2010, that the majority of serious head injuries (SHI) appear to occur independently to serious thorax injuries (STI) and serious spine injuries (SSI) (Figure 3). Around 70 % of occupants with SHI had neither a SSI nor STI. Also, 85% of occupants with STI had neither SHI nor SSI. Further, 82% of occupants with SSI had neither SHI nor STI.

The fact that a large portion of head and neck injuries usually occur independently of one another, and possibly have different mechanisms, was first noted by Friedman and Friedman [23] in 1998 and then confirmed by Atkinson et al. [24], Hu et al. [25] and more recently by Funk et al [17].

This fact has assisted the DROP team to decouple the SHI, STI and SSI and treat them as separate mechanisms in terms of research approach.

DROP RESEARCH PROGRAM

The Dynamic Rollover Occupant Protection (DROP) research program was developed as a result of successful research grant submitted to the Australian federal government's Australian Research Council's (ARC) Linkage Project grants scheme (No: LP110100069). As a result of the analyses carried of the NCIS and NASS-CDS data (Figures 1 to 3), the DROP program research has now focussed on replicating each of the thorax, head and spinal injuries observed in real word data as separate sub-tasks. Figure 4 shows a flow diagram of the process.

Currently finite element simulation is being used to determine how the injuries occur in vehicles for specific NASS-CDS cases. Work on replicating thorax injuries for selected cases has already commenced and preliminary results are being

presented in another sister paper by Digges et al [26]. Work has also begun on simulating selected head injury cases. Once the injury mechanism and precise rollover conditions have been established, a computer simulation that models the UNSW JRS, vehicle and occupant represented by a suitable Anthropomorphic Test Dummy (ATD) will be carried out to assess whether the injury mechanism can be consistently replicated using the JRS. The protocol conditions used to apply the biomechanical impact loads that would likely result in any particular SHI, STI or SSI, will be noted. Biomechanical ATD and cadaver tests will be carried out if required to address research gaps regarding the ATD.

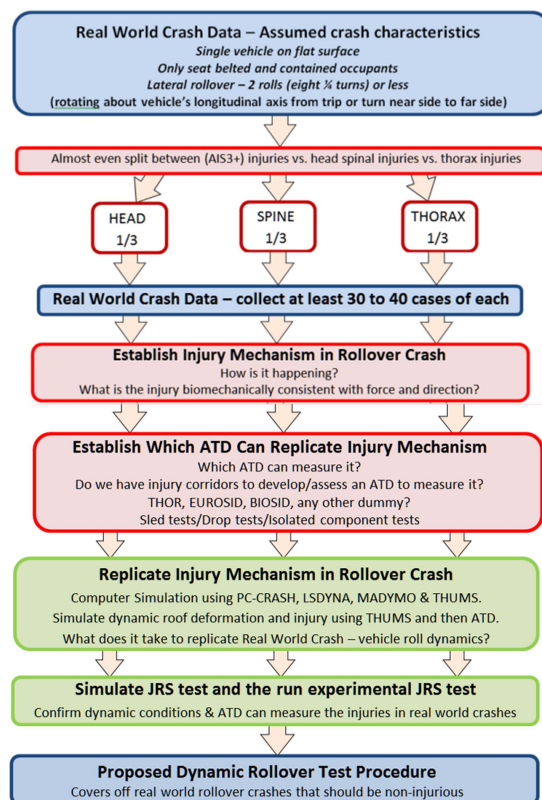


Figure 4. Dynamic Rollover Protection (DROP) program.

The starting point of the analyses replicating real world rollover crash injuries, is that all occupants are assumed to be abiding by the law in accordance with the safe system principles [6], i.e. occupants are all wearing a three point seat belt, travelling within the speed limit, and through no fault of their own are suddenly involved in a crash (e.g. swerving away from an errant oncoming vehicle). It follows that the law abiding driver (and other occupants in that vehicle) wearing an appropriately fitted restraint, should not die or be seriously injured as a result of the crash event. Presently some manufacturers have not been able to ensure occupants will not suffer permanent injury in

rollover crashes of reasonable severity, i.e. two or less rolls over relatively flat terrain, mainly as a result of all the uncertainties in regards to understanding and replicating real world rollover crash injury mechanisms.

The second starting point for the DROP research program is to assume the vehicle's roof has an SWR that is rated 'good' by the US Insurance Institute of Highway Safety [27], i.e. SWR is equal to or greater than 4. Roof strength plays an essential part in the rollover crashworthiness design of vehicles. Limiting intrusion into the occupant compartment during a crash is critical in order to provide sufficient space for the occupant restraint systems to function and assist with occupant ride down decelerations. Analyses to date indicate when the roof structure is strong and the occupants are restrained by a three point seat belt, deaths and a large majority of the injuries in single vehicle rollover crashes are eliminated [3, 8, 9, 27, 28]. To mitigate those injuries which occur for roofs where $SWR \geq 4$ in a reasonable severity two roll or less crash on relatively flat terrain, the team will consider injury cases where there is no obvious roof deformation over the occupant as a proxy that roof crush was likely not causal to the injuries imparted to the occupants.

Replicating injuries that occur in vehicles where $SWR \geq 4$ presents a considerable challenge to the DROP researchers. None of the tests carried out to date in either the JRS or the Malibu II test series reported by Friedman and Grzebieta [29] and Bahling et al [30] have generated the accelerations of a magnitude that would indicate potential injuries as observed in some real world cases in terms of head and thorax injuries where there is little or no roof crush above the occupant. For example, to assess if the Hybrid III crash test dummies are capable of replicating injuries from real world rollover cases in simulated dynamic rollover crash tests, thirty-three head impacts, 15 for the near and 18 for the far side Hybrid III test dummies, were analysed from the Malibu II data FMVSS 208 dolly rollover tests and 26 impacts were analysed in the US Center for Injury Research (CFIR) JRS series of tests for all cases of roof deformation [28]. Analysis of the data found the maximum HIC_{36} was 268 from all JRS tests and 400 from all Malibu II roll-caged vehicle tests. Unfortunately chest injury data was not measured but it is assumed the accelerations would be low [29, 30].

Thus it appears the current test protocols using the FMVSS 208 dolly rollover test and the CFIR JRS and Hybrid III crash tests dummies have not been capable of consistently measuring observed real world head and thorax injuries. Batzer [21]

provides some arguments as to why this may be occurring. It needs to be pointed out though, that the CFIR JRS tests and protocol have been entirely focused on demonstrating how the lower neck and associated spinal cord injury occurs and has shown some experimental correlation with roof crush [10, 29, 31-33]. Considering that head, spine and thorax injuries appear in the majority to occur independently, it is not surprising that the CFIR JRS tests, dummy and protocol do not replicate head and thorax injury. However, the main issue is that any dynamic testing using the JRS and Hybrid III crash test dummy adopting the current test protocols as proposed in Friedman and Grzebieta [29], will likely not be capable of replicating the injuries identified in vehicles with $SWR \geq 4$. Thus a new test protocol must be developed that is more representative of real world crashes where head and thorax injuries occur.

It is worth noting that papers reporting on the Controlled Impact Rollover System (CRIS) indicate the CRIS rig is capable of producing head loads in ATDs that would be fatal to humans. However, Batzer [21] points out that the super-elevation of the vehicle's centre of gravity by more than a metre by the CRIS is not representative of uncomplicated ground level rollovers. Moreover, the trajectory of the vehicle, stripping of the inside lining, and the pre-positioning of the dummy orientation of the ATD with tethers, and release of the vehicle such that it impacts the roof directly over the occupant, has been tuned to demonstrate a diving injury impact event. Neither the wheels nor side opposite to the impact side contact the ground when the vehicle is released prior to head strike. As a result, the input to the head and neck of the dummy is very large and when viewed in totality appears unrealistic [21, 34]. Nevertheless, Friedman and Hutchinson have shown that the same loading can be replicated using the JRS [35]. It thus appears that the rollover kinematics induced by the test rig attempting to replicate the real world trip event and associated serious injuries is also a critical component to assessing the rollover crashworthiness of a vehicle.

Another issue regarding trying to replicate head and thorax injuries that typically occur in real world crashes concern the use of Hybrid III test dummies in dynamic rollover tests to assess potential injury risk. Paver et al [36] and Frechede et al [37] have also indicated issues concerning the Hybrid III's overly stiff neck. Anecdotal evidence indicates that the ATD must be capable of articulating the shoulders relative to the lower torso and hip and the neck may need to be more flexible than the current Hybrid III's neck flexibility. This motion is demonstrated in a rollover crash purportedly of a Volvo vehicle just outside Warsaw

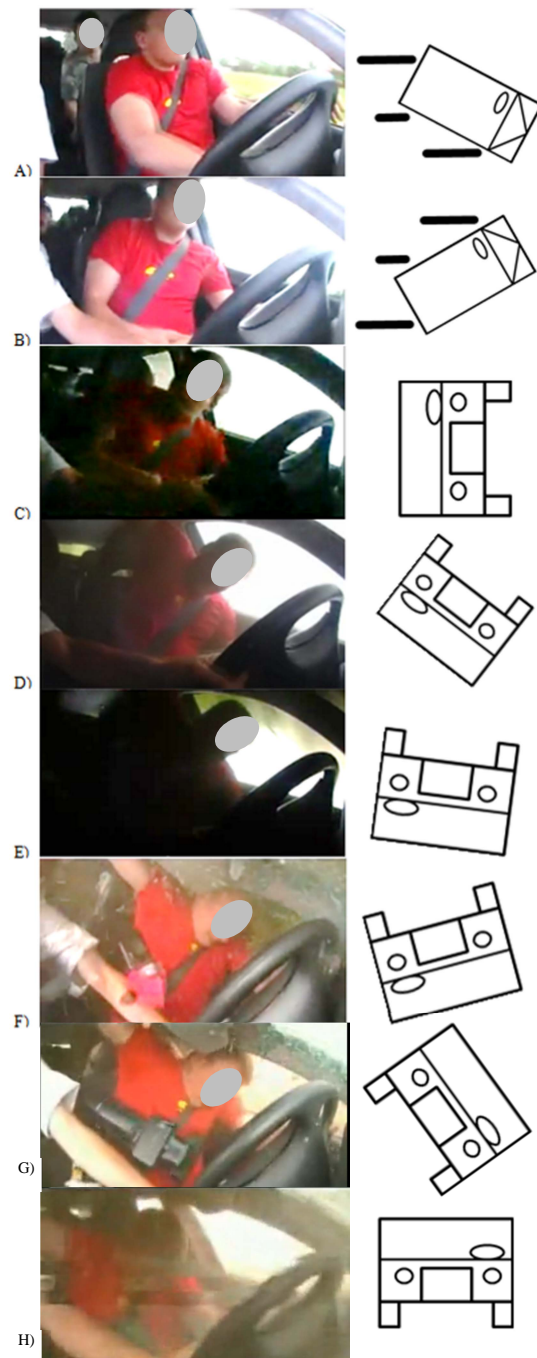


Figure 8. Driver view interior frames from a rollover crash caught on video with figures describing vehicle motion [38].

Poland that was caught on video and posted on YouTube (Figure 8). While detailed information other than what is seen on the video was not available to the Authors, this real world video nevertheless was a useful indicator of some of the possible injury mechanisms the authors are exploring. The following subjective observations are taken from this video.

The frames shown in Figure 8 appear to be an interior video within the vehicle of a pure trip only

rollover consisting of 4 quarter turns [38]. The video from the camera mounted facing the driver, starts with the vehicle being driven down a road. The event begins when the driver swerves and puts the vehicle into a clockwise yaw (A). He then over corrects and the vehicle moves into a counter clockwise yaw (B). The difference in head position between (A) and (B) is worth noting. The driver maintains visual contact of the approaching road on the near side of the vehicle. Also note that the passenger has taken hold of the steering wheel.

In (C) (looking at the front of the vehicle now in frames C to H) we see the vehicle at around 1 quarter turn. The passenger is still gripping the steering wheel. The driver, who is the far side occupant, is being forced towards the window likely as a result of inertial centrifugal force and would have been ejected if not wearing a seat belt and the window was open. The sash part of the seat belt starts to compress into the shoulder. The driver also continues to maintain visual contact with the approaching road through the near side window.

In (D) it appears that the angular acceleration of the vehicle has completely overcome the occupant's muscle strength. The inertial centrifugal force coupled with the opposing force of the seat belt sash restraining the occupant's left shoulder in the vehicle causes his torso, shoulders and head to be tilted towards the window and B-pillar and away from the approaching road. The centrifugal force is so great against the belt restraining the left shoulder that the driver's shoulders are now parallel to the B-pillar. The inboard side of the driver's head is exposed to the roof rail. The seat belt is applying pressure to driver's shoulder and likely the clavicle and the shoulders appear to be tilted parallel to the B-pillar. The pressure applied to the driver's shoulder is evidenced by the embedment of the seat belt into the driver's soft tissue. In (E) we see the driver's head just before it makes contact with the roof rail at approximately 170 degrees of roll. The driver's shoulders are still tilted in line with the B-pillar. The inboard side of the driver's head makes contact with the roof rail in (F) when the vehicle's far side header rail strikes the ground. Note the compression of the seat belt into the shoulder and torso.

As the vehicle rotates back onto its wheels from (G) to (H), the driver is thrown across the vehicle, interacting with the centre console and the seat belt is restraining him from being thrown onto the passenger side, not dissimilar to how an occupant is thrown in a far side impact. This kinematic mode is discussed in detail in the Digges et al sister paper [26].

It is also worth noting that this compression of the seat belt acting on the driver's shoulder, resisting

the inertial centrifugal force, may contribute to or cause clavicle fractures, chest compression with associated rib fractures and possibly lower lumbar spinal injuries in occupants that suffer a torso injury in more severe rollovers. Such injuries have been observed by Bambach et al [20] where they state: *"40% of individuals that received serious thoracic injuries from door impacts in pure rollovers, also received injury to the shoulder region on the same side as the thorax injury. These included shoulder contusions (AIS1), clavicle fractures (AIS2), scapula fractures (AIS2) and acromioclavicular joint dislocations (AIS2). Around half of these injuries were attributed to the seatbelt, with the remainder attributed to contacts with the door or B-pillar."*

This anecdotal evidence from the YouTube video indicates that in order for an ATD to appropriately replicate serious head, thorax and spinal injuries, it will likely require a flexible spine that allows the shoulders to dip and articulate in the manner as observed in Figure 8. With the recent advances and activity in Naturalistic Driver Studies [39] where drivers are observed by cameras, it may be possible to collect further video evidence of occupants during a rollover crash to establish their interactions with vehicle interiors and seat belt restraints and possibly air bags if they fire and stay inflated during a rollover crash.

CONCLUSIONS

The following conclusions can be made from the above:

- Latest investigations of US NASS CDS and Australian NCIS data indicate that serious head, thorax and spine injuries in the majority appear to occur in roughly equal proportions and that they occur more or less independently of each other in terms of injury mechanisms. This indicates that each injury type can be independently researched to establish how they occur in vehicle rollover crashes of reasonable severity, i.e. two rollovers or less on a reasonably flat terrain. Solutions could be explored such as for example, if the roof is sufficiently strong ($SWR \geq 4$) and side air-curtains and airbags are made to fire and maintain inflation during a rollover, this combination could substantially reduce the incidence of both thorax and head injuries. However, the optimum designs for rollover safety systems need to be proven both numerically and experimentally using for example the JRS test rig and a suitably bio-fidelic ATD.
- To date the CFIR JRS tests and test protocols used and proposed have been entirely focused

on demonstrating how lower neck and associated spinal cord injury occur [10, 29, 31, 32, 33]. Test rigs based on the JRS and CRIS rigs appear to be capable of repeatable dynamic testing [29, 34, 35, 40] but these devices still require further analysis to define a range of protocols that best reflect real-world crashes with injuries [21]. Particularly challenging is the capacity of the new UNSW JRS rig's ability to replicate a crash of sufficient severity that characterise the loading conditions where thorax lung contusions and rib fractures are likely to occur.

- The current Hybrid III ATD is not capable of adequately reflecting the movement and impact responses that result in injuries in reasonable severity rollover crashes considered in this paper. It appears that the ATD must be capable of measuring thorax and head injuries similar in nature to that which occurs in side impact crashes, possesses a clavicle and rib structure capable of measuring forces which indicate fracture risk, and have an articulating spine and less stiff neck which results in shoulder and head movement that is reflective of real world human behaviour. In essence a multi directional crash test dummy will likely be required.
- Until such time that the real world injuries observed in strong roof vehicles can be replicated repeatedly in a realistic manner, research on the development of a suitable rollover crash test dummy and appropriate crash test protocol will need to continue.

ACKNOWLEDGEMENTS

The authors would like to thank the Australian federal government's Australian Research Council for providing funds to carry out this research through the Linkage Projects grants scheme (No: LP110100069). The authors would also like to thank the industry partners for also providing the Partner Organisation funding, namely, the New South Wales state government's Centre for Road Safety, the Victorian state government's 3rd party insurer Transport Accident Commission (TAC), the West Australian (WA) state government's Office of Road Safety at Main Roads WA, the mining company BHP Billiton Ltd, and the US Center for Injury Research (CFIR). CFIR is also gratefully acknowledged for supplying the JRS test data and reports.

REFERENCES

- [1] Grzebieta R., Bambach M., McIntosh A.S., Digges K., Job S., Friedman D., Simmons K., Chirwa C., Zou R., Pintar F. and Mattos G.,

(2012). *The Dynamic Rollover Protection (DROP) Research Program*, in Proceedings of the International Crashworthiness Conference ICRASH 2012, July, 18-20, Milan, Italy.

- [2] Fréchède B., McIntosh A., Grzebieta R.H., Bambach M., (2011). *Characteristics of single vehicle rollover fatalities in three Australian states (2000–2007)*, Accident Analysis & Prevention, Vol. 43, Iss. 3, pp. 804-812.
- [3] Young, D., (2010). PhD Thesis, *Protecting Occupants During Passenger Vehicle Rollover Crashes*, Dept. of Civil Engineering, Monash University.
- [4] Fildes, B., Fitzharris, M., Vulcan, A., Koppel, S., (2004). *Benefits of retrofitting seat belt reminder systems to Australian passenger vehicles*. Report for the Australian Transport and Safety Bureau: Monash University Accident Research Centre, Melbourne, Australia.
- [5] Wundersitz, L. N. and Raferty S.J., (2011). *No restraint? Understanding differences in seat belt use between fatal crashes and observational surveys*, Centre for Automotive Safety Research, Uni. of Adelaide, Report No. CASR090, ISBN: 9781921645273.
- [6] Australian Transport Council (ATC), (2011). *National Road Safety Strategy, 2011-2020*.
- [7] Digges K and Eigen A., (2003). *Crash Attributes that Influence the Severity of Rollover Crashes*, Proc. 18th Int. Technical Conference on the Enhanced Safety of Vehicles (ESV), Nagoya, Japan.
- [8] Brumbelow M.L., Teoh E.R., Zuby D.S., and A.T. McCartt, (2009). *Roof strength and injury risk in rollover crashes*, Traffic Inj. Prev. 10, pp. 252-265.
- [9] Brumbelow M.L. and Teoh E.R., (2009). *Roof strength and injury risk in rollover crashes of passenger cars*, Traffic Inj. Prev. 10, pp. 584-592.
- [10] Grzebieta R.H., Bambach M., McIntosh A.S., (2010). *How Stronger Roofs Prevent Diving Injuries In Rollover Crashes*, Proc. 7th Int. Crashworthiness Conf. ICRASH 2010, ed. Chirwa E.C. and S. Kan, Washington DC.
- [11] Grzebieta R.H., Young D., Bambach M., McIntosh A., (2007). *Rollover Crashes: Diving Versus Roof Crush*, Proc. 20th

- International Technical Conference on the Enhanced Safety of Vehicles, Lyon, France.
- [12] Mandell, S.P., Kaufman R., Mack C.D., and Bulger E.M., (2010). *Mortality and injury patterns associated with roof crush in rollover crashes*, Accident Analysis & Prevention, 42 (4): pp. 1326-1331.
- [13] Strashny, A., (2007). *The Role of Vertical Roof Intrusion and Post-Crash Headroom in Predicting Roof Contact Injuries to the Head, Neck, or Face During FMVSS No.216 Rollovers; An Updated Analysis*, DOT, Editor 2007, National Highway Traffic Safety Administration: Washington DC.
- [14] Young D.P. and Grzebieta R.H., (2010). *Vehicle roof strength as it relates to contained occupant injury prevention during rollover crashes*, Proc. Australasian Road Safety Research, Policing and Education Conference, Canberra, Australia.
- [15] Mattos G.A., Grzebieta R.H., Bambach M.R. and McIntosh A.S., (2012). *Head Injuries to Restrained Occupants in Single-Vehicle Rollover Only Crashes*, Traffic Injury Prevention, in press, DOI:10.1080/15389588.2012.722735.
- [16] Bambach M.R., Grzebieta R.H., McIntosh A.S., Mattos G.A., (2012). *Cervical and thoracic spine injury from interactions with vehicle roofs in pure rollover crashes*, Accident Analysis and Prevention, vol. 50, pp.34– 43.
- [17] Funk, J. R., Cormier, J. M., & Manoogian, S. J., (2012). *Comparison of risk factors for cervical spine, head, serious, and fatal injury in rollover crashes*, Accident Analysis & Prevention, 45 (0), 67-74.
- [18] Moffatt E.A. and Padmanaban J., (1995). *The relationship between vehicle roof strength and occupant injury in rollover crash data*, 39th Annual Proceedings - Association for the Advancement of Automotive Medicine, 1995: pp. 245-267.
- [19] Padmanaban J., Moffatt E.A., and Marth D.R., (2005). *Factors influencing the likelihood of fatality and serious/fatal injury in single-vehicle rollover crashes*, New York, NY, ETATS-UNIS: Society of Automotive Engineers.
- [20] Bambach M.R., Grzebieta R.H., McIntosh A.S., (2012). *Thoracic injuries to contained and restrained occupants in single-vehicle pure rollover crashes*, Accident Analysis and Prevention, Volume 50, January 2013, pp. 115-121.
- [21] Batzer S. A., (2011). *Diving Injury Occurrence in Rollover Collisions: A Critical Analysis of Malibu I, Malibu II and CRIS*, Int. J. of Crashworthiness, Vol. 16. No. 2, April, 2011, pp. 219-232.
- [22] Grzebieta R., Jordan A., Jimenez J., Mattos G., Bozzini S., Friedman D., Dal Nevo R., Jackson C., Simmons K., (2013). *Implementation of the UNSW Jordan Rollover System at Sydney's Crashlab Test Facility*, Proc. 23rd International Technical Conference on the Enhanced Safety of Vehicles, Seoul, Korea.
- [23] Friedman, D., Friedman, K., (1998). *Roof crush versus occupant injury from 1998 to 1992 NASS*, Society of Automotive Engineers, Paper No. 980210.
- [24] Atkinson, T., Cooper, J., Patel, B., Atkinson, P., (2004). *Considerations for rollover simulation*, Society of Automotive Engineers, Paper No. 2004-01-0328.
- [25] Hu, J., Chou, C.C., Yang, K.H., King, A.I., (2007). *A weighted logistic regression analysis for predicting the odds of head/face and neck injuries during rollover crashes*, Proc. Assoc. Adv. Automot. Med. 51, 363–379.
- [26] Digges K., Tahan F., Grzebieta R.H., Bambach M., Mattos G., and McIntosh A., (2013). *Crash Damage Patterns Associated With Chest Injuries In Far-Side Rollovers*, Proc. 23rd International Technical Conference on the Enhanced Safety of Vehicles, Seoul, Korea.
- [27] Insurance Institute for Highway Safety, (2010). *First time Institute rates small pickups for rollover protection; only one model rates good in test that assures strength of roof*, News Release, Feb 4, 2010.
- [28] Mattos GA, Grzebieta R, Bambach M, and A. McIntosh, (2013). *Validation of a dynamic rollover test device* International Journal of Crashworthiness, Accepted for publication and in print.
- [29] Friedman D. and Grzebieta R.H., (2009). *A Proposed Rollover and Comprehensive Rating System*, Proc. 21st International Technical

- Conference on the Enhanced Safety of Vehicles, Stuttgart, Germany, Paper Number 09-0515.
- [30] Bahling, G. S., Bundorf, R. T., Kaspzyk, G. S., Moffatt, E. A., Orłowski, K. F., & Stocke, J. E. (1990). *Rollover and drop tests - The influence of roof strength on injury mechanics using belted dummies*, SAE Paper No 902314, Pennsylvania.
- [31] Grzebieta R.H., Young D., McIntosh A., Bambach M., Fréchède B., Tan G., Achilles T., *Rollover Crashworthiness: the final frontier for vehicle passive safety*, Proc. Road Safety Research, Policing and Education Conference, Melbourne, 2007, (also published in Journal of the Australasian College of Road Safety, 19(2), May 2008, pp. 29-38 and corrected reprint in 20(2) May 2009, pp. 46-55).
- [32] Young D., Grzebieta R.H., McIntosh A., Bambach A. & Frechede B., (2007). *Diving vs Roof Intrusion: A Review of Rollover Injury Causation*, International Journal of Crashworthiness, Vol. 12 No. 6 pp. 609–628.
- [33] Grzebieta R.H., Young D., Bambach M., McIntosh A., (2007). *Rollover Crashes: Diving Versus Roof Crush*, Proc. 20th International Technical Conference on the Enhanced Safety of Vehicles, Lyon, France, June 2007.
- [34] Chirwa EC, Stephenson RR, Batzer SA, & Grzebieta R H, (2010). *Review of the Jordan Rollover System (JRS) vis-a-vis other dynamic crash test devices*, International Journal of Crashworthiness, 15(5), 553-569.
- [35] Friedman K and Hutchinson J, (2008). *Review Of Existing Repeatable Vehicle Rollover Dynamic Physical Testing Methods*, Proceedings of IMECE2008 ASME International Mechanical Engineering Congress and Exposition, paper no: IMECE2008-68751, Boston, Massachusetts, USA.
- [36] Paver J, Friedman D, Carlin F, Bish J, Caplinger J and Rohde D, (2008). *Rollover Crash Neck Injury Replication and Injury Potential Assessment*, Proc. International Research Council on Biomechanics of Injury (IRCOBI), Bern Switzerland.
- [37] Fréchède BO, McIntosh AS, Grzebieta RH & Bambach M, (2009). Hybrid III ATD in inverted impacts: influence of impact angle on neck injury risk assessment, Annals of Biomedical Engineering; 37: pp. 1403-1414.
- [38] YouTube, (2009). Roll over in a Volvo Retrieved December 2011, from http://www.youtube.com/watch?v=Gn_xhKT V51Y
- [39] Regan MA, Williamson A, Grzebieta R, Tao L, (2012). *Naturalistic Driving Studies: Literature Review and Planning for the Australian Naturalistic Driving Study*, Proc. Australasian College Of Road Safety Conference, A Safe System: Expanding The Reach, Sydney, August, 2012.
- [40] Bish J., Caplinger J., Friedman D., Jordan A., and Nash C.E., (2005). *Repeatability of a Dynamic Rollover Test System*, Proc. 19th Int. Tech. Conf. Enhanced Safety Vehicles, Washington, USA.

STUDY OF OPTIMAL BODY STRUCTURAL DESIGN FOR COUPE-TYPE VEHICLES IN ROLLOVER EVENTS

Sung Ung, Ryu

Wook, Jin

Safety System Development Team / Hyundai Motor Co.

Young Chul, Shin

Body Durability CAE Team / Hyundai Motor Co.

Ki Soon, Bae

Structure Engineering Design Team 1 / Hyundai Motor Co.

Kwang Bok, Lee

Sheet Metal Development TFT / Hyundai Motor Co.

Korea

Paper Number 13-0173

ABSTRACT

Many types of car crashes can occur on the road. One of the most critical crash types that can happen in the real world is rollover. Unfortunately, analyzing the exact fundamental principle of a rollover incident is difficult and complex. Despite its rise in severity as a serious injury collision, there have been few attempts made to analyze rollover. A stronger vehicle structure corresponds to more efficient protection for the passengers. A two-door coupe or a central pillar-less body vehicle can be subject to more severe conditions in the event of a rollover. Reinforcing the side and roof structure of the body is important to secure safety. This paper presents observations from many case studies and actual tests. Central to this paper is an experimental study on the load redistribution effect. A brief overview is given on analyzing roof crush test results, and the optimal structure is investigated in greater detail.

MOTOR VEHICLE ROLLOVER COLLISION AND ROOF CRUSH TECHNOLOGIES

Rollover crashes make up a relatively small proportion of all collisions around the world, but have a disproportionate share of fatal and serious injuries occurring in rollover crashes. For example, rollovers constitute less than 4% of accidents in the USA each year but almost 36% of all fatalities. Recently, there have been many efforts to protect passengers in rollover. There are three major contributors: (1) electronic stability control (ESC) technology, (2) roof crush strength, and (3) head ejection mitigation. The National Highway Traffic Safety Administration (NHTSA) has created rules for all three elements.

- (1) ESC technology: Apply the brake on each of the four wheels individually to prevent rollover.
- (2) Roof crush strength: Preventing the vehicle structure from collapsing during rollover.

- (3) Head ejection mitigation: Prohibiting the passenger from ejecting out of the car.

The purpose of this paper is to propose the optimal body structural design by assessing the roof crush strength. Roof crush strength will be addressed in this paper with the focus of optimal body structure design. In order to reduce the amount of rollover roof deformation, which is measured as roof deflection or residual headspace, the NHTSA instituted the Federal Motor Vehicle Safety Standard (FMVSS) 216 as a final rule in May 2009, and the Insurance Institute Highway (IIHS) has also adopted their roof crush evaluation as a requirement for the top safety pick (TSP). These two tests are not exactly same but use similar procedures to check if survival space is well enough to mitigate passenger injuries with reasonable roof strength.

ROOF CRUSH SCIENCE

Even though the static roof crush test system has been around for a long time, it is a good tool to evaluate the strength of side and roof structure from the test repeatability and experimental reliability point of view. From a holistic perspective, a brief overview of the general features of the roof crush test system is needed before analysis of the optimal vehicle structure design.

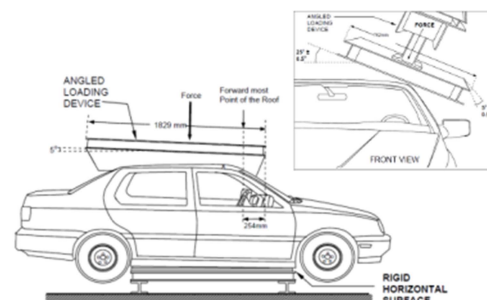


Figure 1. Test device orientation. Source: FMVSS 216.

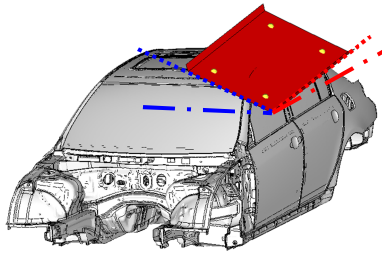


Figure 2. Illustration of roof crush test.

Testing is performed with the test vehicle secured rigidly to eliminate suspension influence. The lower surface of the test platen is aligned with its forward edge 254 mm in front of the forward-most point of the roof, while its longitudinal centerline is parallel with the vehicle's longitudinal centerline and centered either with the initial roof contact point or at the center of the roof contact area. The lower surface of the test platen is oriented at a 5° pitch along its longitudinal axis and 25° roll along its traverse axis (see Figures 1 and 2). A general roof crush plot (force vs. displacement) is shown in Figure 3.

Here, the general plot can be divided into 5 sections describing the behavior of the vehicle structure based on the slope of the stiffness. Each section is split by the amount of travel by the test platen. Even though the test results vary depending on the vehicle type and structure, the general characteristics of each section are as follows:

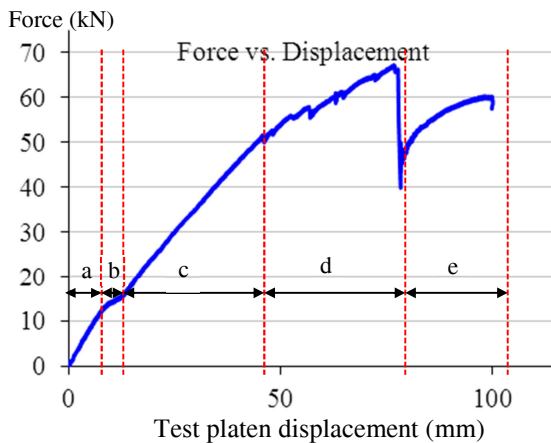


Figure 3. Example of a general plot.

a. Section 0–10 mm

At the beginning of the test, the outer shell and inner reinforced panel of the vehicle are squeezed. As the outer panel is not actually a load-resisting material, the reaction force on the entire testing section is relatively small.

b. Section 10–15 mm

The reinforced panels that constitute the front pillar and upper body structure are crimped. A reaction force appears in the form of a cubic curve through the inflection point of the slope. The deformed shape is shown in Figure 4. Sometimes, this section is difficult to discern. In rare cases, some vehicles do not have this characteristic. On average, vehicles have a range of 1–2 mm. This section is important as a preliminary step for a vehicle to resist a larger reaction.



Figure 4. Compressed shape of inner and outer panels.

c. Section 15–50 mm

This section should sustain a full-scale load. Each upper body member has to distribute the incoming load from the loading device efficiently. They share the task as if they are a single member of the framework. The slope is steep. The reaction force slope, which appears as almost a straight line, is very important to determining the characteristics of the vehicle. Vehicles often have their own unique slope in this section. If two vehicles have the same outward appearance, but different slope characteristics, it can be considered that they have different reinforced member designs.

d. Section 50–80 mm

Upon deflection of the vehicle structure, unlike the previous section each panel and structure behaves in different ways. Each structure is an important element to making the vehicle strong enough to withstand outside loads. The slope gradually becomes gentle.

e. Section over 80 mm

When the windshield glass cracks, many reinforcement members have collapsed. At this point, the maximum reacting load occurs. Although glass is a brittle material, it tends to bear significant loading until it breaks. Figure 5 shows the breaking point of glass.

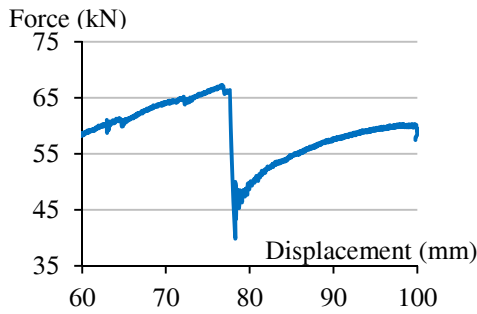


Figure 5. Example of a glass breaking point.

In terms of load dispersion, the most important thing is to determine how to make every different structure component works together as a single member and react with steep slope at section c(50-80mm).

GENERAL VEHICLE STRUCTURE

A vehicle is composed of not only large structures but also many small parts. A good load path design of the vehicle is desired that can efficiently disperse an incoming force in all directions. When rollover occurs, the main elements that withstand the external force are the front roof rail, front pillar, and center pillar. A coupe-type vehicle compared with other vehicle types (sedans, SUVs), has a different design. The center pillar has been pushed reward to allow for access to the back row. The center pillar is located relatively far in the back; in some cases, there is no center pillar to support the roof. An example vehicle is shown in Figure 7.

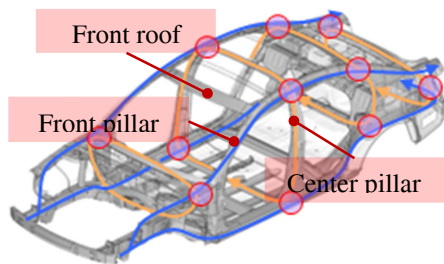


Figure 6. Example of body in white (BIW)



Figure 7. Example of center pillar-less design.

As these kinds of vehicles are vulnerable to outside crash forces and find it difficult to protect passengers, a good design that makes the body stronger is needed. To study the optimal body structural design for coupe-type vehicles, we considered some vehicles that showed a high strength-to-weight ratio (SWR) in

roof crush tests.

STRUCTURAL CONCEPT OF COUPE-TYPE VEHICLES

The goal of this study is to make a stronger vehicle upper body by reducing the number of reinforcement parts and without increasing the overall weight. To do so, it is more important to precisely know which components affect roof crush performance critically..

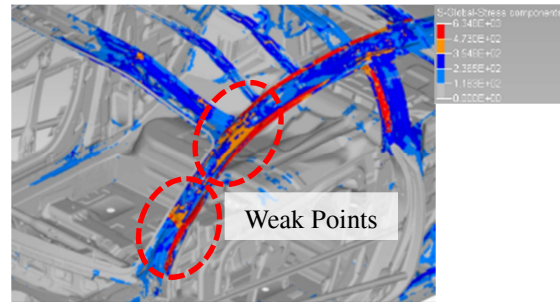


Figure 8. Weak points in roof crush test.

According to CAE analysis, the main parts that take the most of the stress are at the bottom of the front pillar and the connection points of the top of the front pillar and the front roof rail. Figure 8 shows these tendencies. If these parts collapse in the beginning of the test, it is expected not to get a SWR value high enough to sustain adequate vehicle's strain energy of distortion. There have not been many coupe-type vehicles that have been evaluated for strength of their roof and side structure. Thus, a vehicle tested by IIHS for roof strength was chosen to show the difference between strong and weak structures. An example of a well performing vehicle is examined in detail as Figures 9 and 10 show the summary of its roof crush test.

Even though this vehicle does not have a center pillar connecting some side components to the roof structures, the vehicle has body stiffness with a SWR of 5.58.

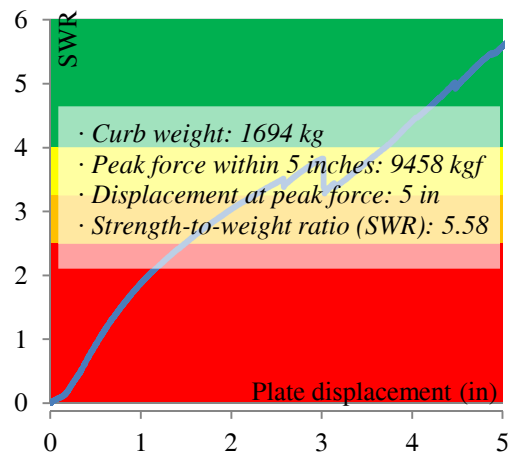


Figure 9. Roof crush result. Source: IIHS, 2010.



Figure10. Post-roof crush test. Source: IIHS, 2010.

This means that the front pillar and connection between the front roof rail and upper side structure contribute more to sustain external force. It can tentatively be concluded that the connectivity between front pillar and roof side structure play an important role in determining the rigidity. Undoubtedly, a better option would be to employ the main parts as simple as possible. It was figured out that this vehicle is composed of a few simple panels and a partially reinforced part. An example design is shown in Figure 11.

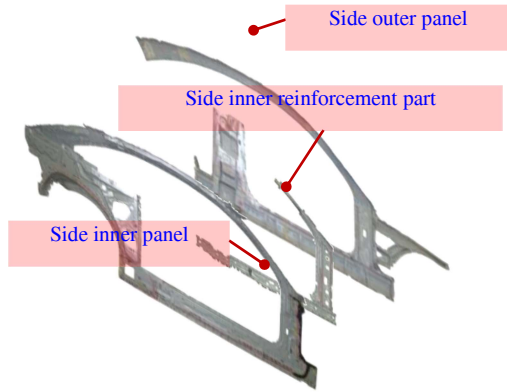


Figure11. Example vehicle with a simple structure.

As shown in Figure 11, the vehicle structure looks very simple at the surface, but the reinforced items are concentrated at load-bearing areas. In other words, the side inner reinforcement part is stronger than the others. To check the quality of the main material, tensile tests and analysis of major chemical components were conducted. The collected specimens for tensile tests of the reinforcement panel were cut into sub-sizes as specified by the American Society for Testing and Materials (ASTM). The specimen is shown in Figure 12.



Figure12. ASTM sub-size specimen.

The engineering stress of these specimens was estimated by using the stress-strain curve (S-S curve) shown in Figure 13.

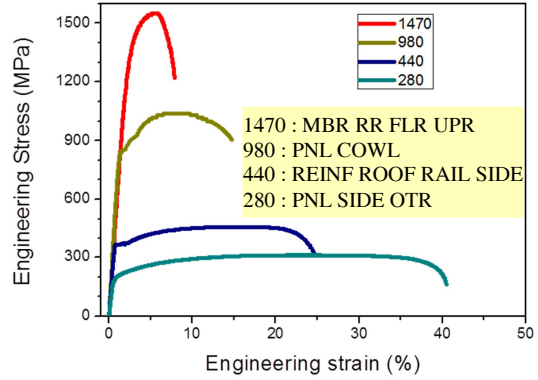


Figure13. Representative stress-strain curve (steel grade).

Also, to verify the quality of material, a chemical analysis was conducted. In addition, the major elements of carbon(C) and sulfur(S) were evaluated with extra measurement for the precision measurement. The main reinforcement is shown in Figure 14.

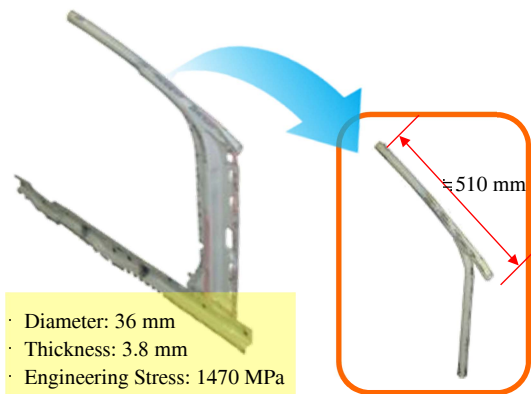


Figure14. Example of side inner main reinforcement.

For reference, Table 1 summarizes the quality of the materials in this vehicle.

Table1
Summary of material quality for vehicle

BIW		
0.7%	6.1%	0.2%
3.8%	10.8%	19.6%
41.4%	17.5%	
Over 60 kgf material: 21%		Average stiffness: 516 MPa

To implement this structural concept into the vehicle,

a coupe-type model with a relatively weak structure in production since 2008 was chosen. This vehicle had a SWR of only 2.8. After remodeling the side structure based on the already mentioned concept, even though the number of side structure components are decreased from six to two parts. The strength of body was increased from SWR of 2.8 to an SWR of 4.2. The total weight of reinforcement was kept almost the same, about 11 kg. Figures 15 and 17 show this concept.

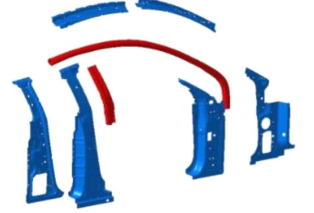
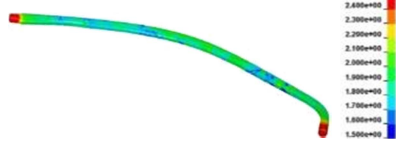
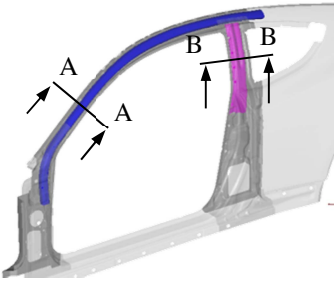
Original side structure design	
-Components: 6 -Weight: 11.7 kg	
Modified side structure design	
- Components: 2 - Weight: 11.8 kg	

Figure 15. The concept of side structure.

The hydro-forming method was used to replace the many parts that made up the side structure with a simple closed pipe. Table 2 presents an illustration and specifications of this component.

Table 2
Main inner reinforcement part with using hydro-forming method

	Reinforcement in the front pillar	
SPEC	$\Phi 48.6 \text{ mm} \times 2.0 \text{ mm thickness} \times 2200 \text{ mm}$ Stiffness: 100 kgf	
APPLICATION		

Because combining the closed pipe made by the hydro-forming method with the inner panel or other parts with the standard spot-welding method was difficult, the one-way spot-welding method should be used. This welding method is shown in Appendix A.

ANALYSIS AND FE MODEL SIMULATION

Nonlinear characteristics are largely divided into three categories: geometric nonlinear characteristics, nonlinear characteristics of materials, and nonlinear behavior due to contact. In the roof crush test, nonlinear finite element analysis was performed because all three attributes are mentioned above. The ABAQUS version 6.9EF computational model was used as the finite element analysis software for the structural response. Figure 16 illustrates the deformation between the base and improved vehicles.

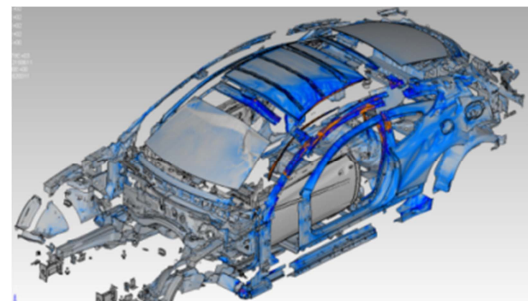
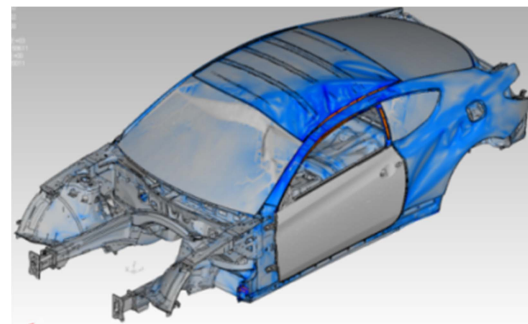
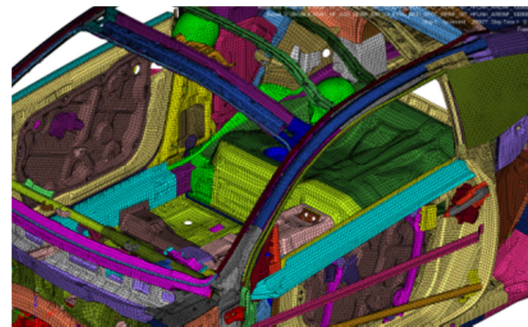


Figure 16. FE model simulation: final deformation at end of test (travel range of loading device was 127 mm).

These simulations showed different structural responses by these vehicles. To compare the deformation of different the simulation results were

captured by the SWR range for each vehicle and are listed in Appendix B. The travel ranges of the loading device results based on SWR are listed in Table 3 and plotted in Figure 17.

Table 3
Test platen displacement based on SWR

	Vehicle		Remarks
	Base vehicle	Improved vehicle	
SWR	Displacement (mm)		
0	0	0	
0.5	10	12	
1.0	23	22	
1.5	43	32	
2.0	71	43	
2.5	100	56	
2.8	122	70	Max
3.0	n/a	72	
3.5	n/a	87	
4.0	n/a	108	
4.2	n/a	124	Max

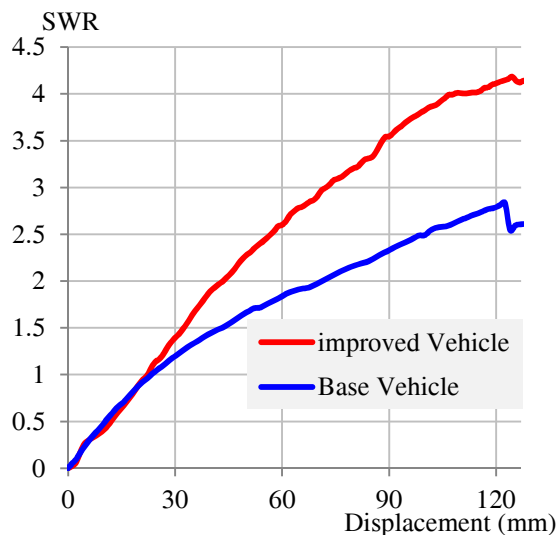


Figure 17. Plot of SWR vs. displacement (displacement is travel range of loading device).

The displacement was measured by the amount of travel range of the loading device. Starting from SWR 0.0 to SWR 1.0, the structural responses of the vehicles were not so different. The amount of deformation does not seem to be a great difference either. But after SWR 1.0, the absolute amount of deformation of each vehicle increases respectively.

At the point of SWR 2.0, the base vehicle needs 127mm of loading device travel. However, the improved vehicle needs only 70mm. In the mean time, the strength of body, as have been noted above, is increased 150% during the testing from SWR 2.8 to SWR 4.2. These results show that if a vehicle has strong enough structure to resist outer load, it is easy

to get a high SWR value in the beginning of roof crush. The earlier to reach the vehicle's maximum roof strength the more the vehicle can secure the occupant's safety compartment. When rollover happens, the amount of occupant's head clearance is an important element to protect occupants. In this extra space area, vehicle can use many high-tech safety gadgets, for example, rollover sensors, side airbags, or multi-link seat belts.

CONCLUSIONS

The conclusions which can be drawn from this study are these:

- 1) A strong A & B pillar ring is the most important component of robust roof strength.
- 2) Components and systems of the vehicle should be well designed to absorb or distribute the energy of roof crush in order to prevent intrusion into the occupant compartment.
- 3) The strength of the inner reinforcement parts in the front pillar is a core element that determines the vehicle's roof stiffness. Each part around the door openings should be well connected as a circular linked structure with the high-density spot welded joint. (Examples – front roof rail, A&B pillar, front header)
- 4) The balance between the front pillar and roof rail is very critical. In other words, overall roof strength will be weak, if relatively some weak points are collapsed. The balance of strength can be determined by the amount of buckling through CAE model.

All of these efforts are to protect occupants preserving space in the event of rollover. To ensure safety, adequate body stiffness is an essential condition in rollover accidents.

There have been many efforts to make new advances in rollover testing modes. The repeatability and reliability are core aspects of in-house modified tests. NHTSA, along with other organizations, makes great efforts to develop new modified rollover protocols. However, a number of problems remain to be explored because rollover accidents occur under many complex conditions, which are difficult to identify as the sole reason. Firstly, the typical main elements that cause a rollover accident should be carefully confirmed. Secondly, a reasonable and trustworthy testing facility that can represent rollover accidents should be constructed using the verified elements. Only after a vehicle's adequate stiffness is secured can other safety equipment be developed step by step. This paper lays the foundation for future work with regard to vehicle strength. Future research will involve the correlation between dynamic

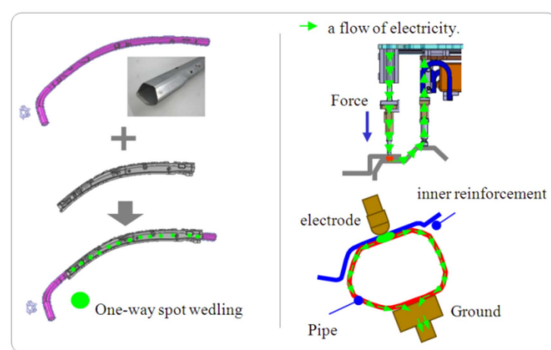
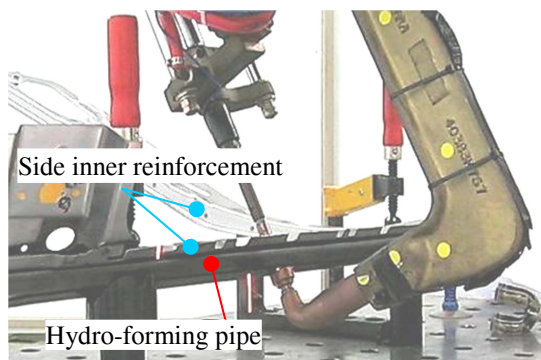
rollover tests and quasi-static roof crush tests in terms of stiffness. The occupant behavior in a vehicle when rollover happens will be a sequential task.

REFERENCES

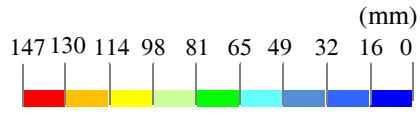
1. Sreekanta Das, Sudip Bhattacharjee and Pratanu Ghosh “Roof Strength Requirement for Vehicles Involved in Rollover Crash” SAE Paper number : 2008-01-0510
2. Samuel P. Mandell, Robert Kaufman, Christopher D. Mack, and Eileen M. Bulger “Mortality and injury patterns associated with roof crush in rollover crashes” Accident Analysis and Prevention Vol. 42, Issue 4, July 2010, Pages 1326–1331
3. Martha W. Bidez, John E. Cochran JR., Dottie King, and Donald S. Burke III “Occupant Dynamics in Rollover Crashes: Influence of Roof Deformation and Seat Belt Performance on Probable Spinal Column Injury” Annals of Biomedical Engineering, Vol. 35, No. 11, November 2007, pages 1973–1988
4. Ruiyi Su, Liangjin Gui and Zijie Fan “Multi-objective optimization for bus body with strength and rollover safety constraints based on surrogate models” Struct Multidisc Optim 2011 44:431–441
5. M.R. Bambach, R.H. Grzebieta, A.S. McIntosh, G.A. Mattos “Cervical and thoracic spine injury from interactions with vehicle roofs in pure rollover crashes” Accident Analysis and Prevention Volume 50, January 2013, Pages 34–43
6. M.D. Freeman, K. Dobbertin, S.S. Kohles, L. Uhrenholt and A. Eriksson “Serious head and neck injury as a predictor of occupant position in fatal rollover crashes” Volume 222, Issues 1–3, 10 October 2012, Pages 228–233
7. Carol Conroy, David B. Hoyt, A. Brent Eastman, Steve Erwin, Sharon Pacyna, Troy Lisa Holbrook, Teresa Vaughan, Michael Sise, Frank Kennedy, Tom Velky "Rollover crashes: Predicting serious injury based on occupant, vehicle, and crash characteristics" Volume 38, Issue 5, September 2006, Pages 835–842
8. Young Rock, Kim. Dae Jun, Song. Hong Lim Choi. “A Study on Load Distribution of Roof Crush Using Section Force Analysis” Hyundai-Kia motors group conference 19th, Paper number : CB-2011-013

APPENDIX A

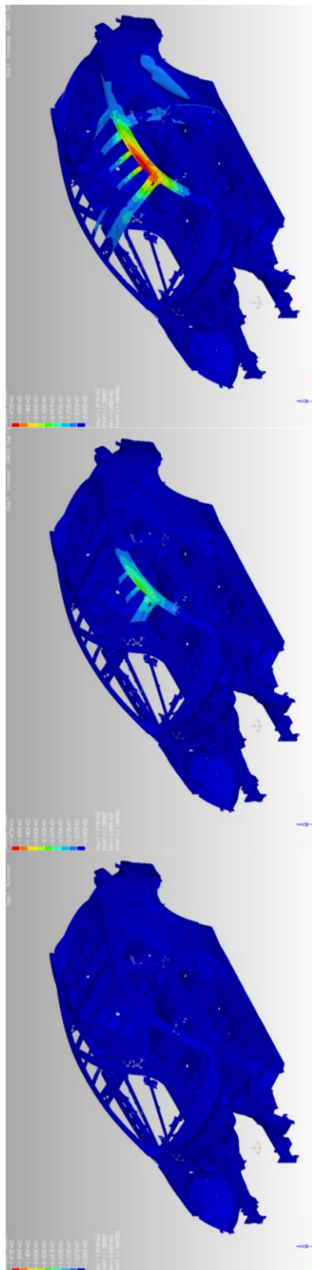
One-way spot welding method



APPENDIX B
 Simulated deformation of base and improved vehicles by SWR



Displacement range from outer surface to inner area

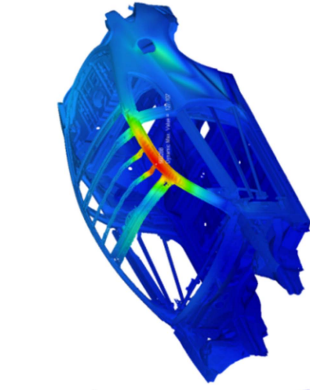


Base vehicle

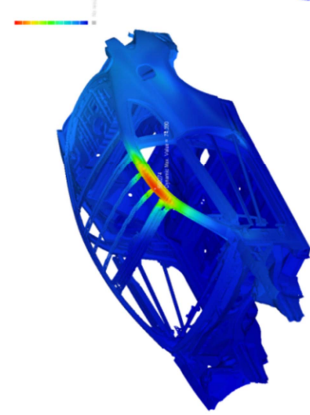
SWR 0.0 @ 0 mm

SWR 2.0 @ 71 mm

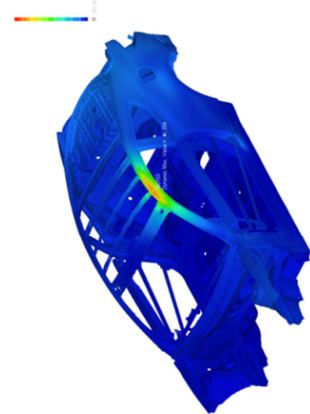
SWR 2.8 @ 122 mm



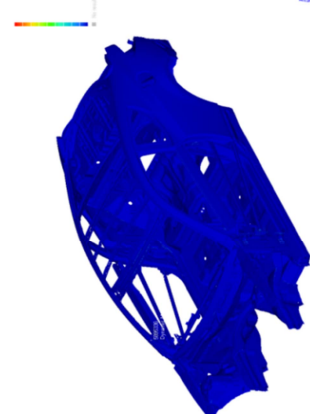
SWR 4.2 @ 124 mm



SWR 2.8 @ 70 mm



SWR 2.0 @ 43 mm



SWR 0.0 @ 0 mm

Improved vehicle

DESIGN OF A DEFORMABLE VEHICLE ROOF STRUCTURE FOR ROLLOVER CRASH TESTING WITH A TEST BUCK

Jacek Toczyski

Institute of Aeronautics and Applied Mechanics, Warsaw University of Technology
Poland

Jason R. Kerrigan

Center for Applied Biomechanics, University of Virginia
United States

Pradeep Mohan

Channabasaveshwara Institute of Technology
India

Jeff R. Crandall

Center for Applied Biomechanics, University of Virginia
United States

Paper Number 13-0203

ABSTRACT

The goal of this study was to determine the detailed design of a greenhouse structure (roof and pillars), such that when it is loaded in a static roof crush test the force-displacement response mimics that of a modern full-size crossover vehicle. This study was carried out using finite element analysis with the goal of identifying a specific design to be fabricated for use with a rollover test buck in dynamic rollover crash testing. A multi-tiered design approach was used consisting first of a simple beam element model, followed by a more complex model meshed with shell and solid elements. A truss-like structure consisting of steel tubing for the pillars, headers and roof rails, connected by steel bars (“plastic joints”) at the intersections was used for the initial design. Individual structure parameters (tubing cross-sections, wall thicknesses, material types, etc.) that did not affect the overall geometry were optimized in repeated simulations of a static roof crush test to ensure that the response of the buck roof matched the response defined by a strength-to-weight ratio of 4.0 for a 2268 kg vehicle. Additionally, different design solutions were examined, e.g. curving the B-pillar, adding a windshield or roof cross beams. The influence of the friction coefficient between the loading platen and the roof was also investigated. Model predictions were validated on component-level by comparing model behavior to three-point bending tests on the plastic joints. The resulting design, including curved B-pillars with additional stiffness elements, was then subjected to a dynamic rollover computer simulation to facilitate qualitative evaluation of the dynamic response in a rollover crash. Further modification of the design may be necessary to improve the response beyond the peak quasi-static test force, but full scale fabrication and testing will be performed first to examine actual

response at these levels before implementing additional changes.

INTRODUCTION

Rollover related deaths are a significant portion of the overall traffic-fatalities in the United States (US). As a result of this problem, rollover crashworthiness (cf. Mohan et al. 2008) as well as injury outcome (cf. Foster et al. 2012) have long been studied by vehicle safety researchers. The National Highway Traffic Safety Administration (NHTSA) has introduced several safety standards aimed at mitigating the effect rollover crashes have on the public health, including mandating stronger roofs (Federal Motor Vehicle Safety Standard (FMVSS) No. 216), electronic stability control (FMVSS No. 126), and ejection mitigation (FMVSS No. 226) (US Department of Transportation 2012). However, currently there is no dynamic rollover test standard for crashworthiness or occupant protection, at least in part, due to the lack of demonstrated biofidelity of crash test dummies and injury metrics in rollover crash tests.

As part of a larger research effort aimed at investigating the crash dummy biofidelity in such tests, the University of Virginia Center for Applied Biomechanics is planning to compare crash test dummy response to post-mortem human surrogate (PMHS) response in multiple series of experimental investigations. To perform some of the analyses, a vehicle-like rollover test buck has been developed. It consists of two major parts: a deformable, replaceable greenhouse (roof and pillars) and a rigid base. The buck has been designed to mimic the geometric and inertial properties of the average of twelve full-size crossover vehicles from the current fleet. The buck will be used in the biofidelity tests for a variety of reasons. Primarily, real vehicle interiors have very complex geometries and complex

material properties. Since such complex structures could feasibly have an effect on occupant kinematics, exact or very similar structures would be necessary to make comparisons between occupant surrogates. Thus, evaluations of dummies modified after initial tests will need to be made with the same structures or a detailed computational model of them. Since such evaluations may be made years after original tests, a simplified buck is used to ensure that replicate structures can be fabricated or simulated easily. Secondly, 3-d optical motion capture systems that have been used to characterize occupant surrogate motion in simulated crash tests (cf. Lessley et al. 2010) require line of sight between off-board cameras and on-board occupant retroreflective markers. Using such a system will provide detailed 3-d kinematics data that can be used to make intricate comparisons between crash test dummies and PMHS. Lastly, unlike real vehicles, a rollover test buck provides a platform for vehicle parameter sensitivity analysis where individual parameters (mass, moment of inertia, seating location, restraint geometry, roof geometry, roof strength, etc.) can be adjusted.

While design of a base structure (that matches the goal geometry and inertial properties) is a relatively easy goal, design of a roof structure with a crushing stiffness that is comparable to real vehicles is more challenging. The use of a replaceable roof buck to evaluate variations in vehicle and occupant parameters has been previously investigated (Jordan et al. 2005). That study concluded that a test buck can be used in rollover crash test studies to examine some characteristics of occupant and vehicle response.

The goal of this study was to determine the detailed design of a greenhouse with large tumblehome angles (ca. 80°), such that when it is loaded in a static roof crush test (similar to the FMVSS No. 216 test) the force-displacement response mimics that of a vehicle with a strength-to-weight ratio (SWR) of 3.9-5.3 (depending on the total buck mass). The study was carried out using finite element analysis to facilitate computationally and monetarily inexpensive evaluations of iterative changes to the design. In studies subsequent to the current one, the resulting buck roof design will be fabricated and tested in static roof crush to evaluate the accuracy of the computational predictions.

BUCK DESIGN

A parametric rollover test buck was developed for use with the Dynamic Rollover Test System (DRoTS) (Kerrigan et al. 2011a) to investigate dummy biofidelity in rollover crash impacts. It was designed to have a rigid base, consisting of all the components below the simulated vehicle belt-line,

and a deformable (and thus replaceable) roof structure, consisting of all the components above the belt line (roof, pillars, headers, cross beams). The base structure (Figure 1) consists of A-, B-, C- and D-pillars, front and rear pillar connections, and removable “doors.”

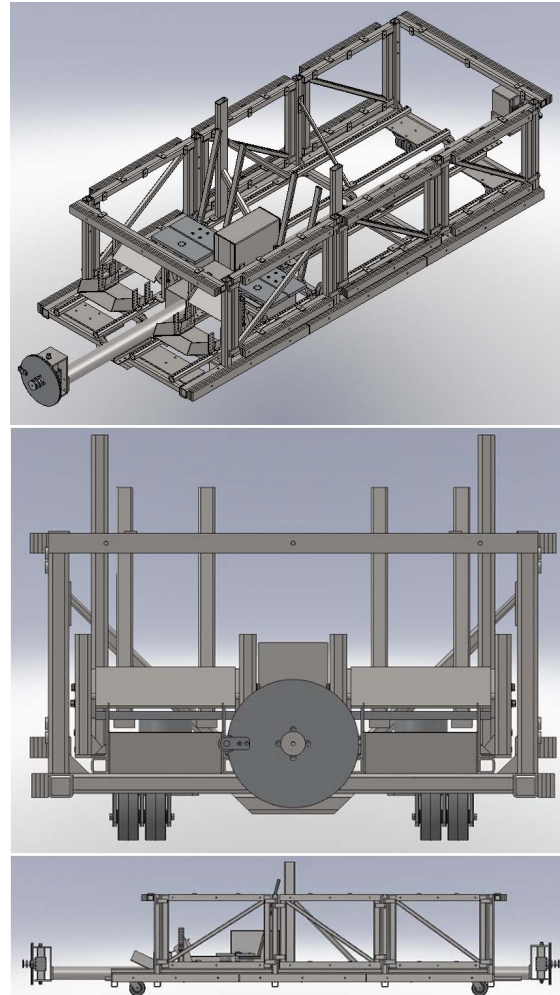


Figure 1. Base structure of rollover test buck: isometric (top), front (middle) and side view (bottom).

The buck was designed to mimic the geometric and inertial properties of twelve late-model full-sized crossover vehicles or mid-sized sport utility vehicles (SUV) from the US fleet, including BMW X5, Ford Explorer, Jeep Grand Cherokee, Kia Sorrento, Volvo XC90 and Volkswagen Touareg. Exterior geometric properties of the vehicles were determined from New Car Assessment Program (NCAP) test reports and they were averaged to specify general dimensions for the buck base (Foltz et al. 2011). The validity of exterior dimensions extracted from the reports was verified by manual measurements made on three of the vehicles. Inertial properties – mass, center of gravity (CG) location, and roll moment of inertia – were either

established or estimated from the literature (Bixel et al. 2010, Heydinger et al. 1999) and consumer marketing materials. Interior geometries of the vehicles, including measurements of the head, leg, shoulder, and hip room in the first and second row seats were determined (also using consumer marketing materials) to vary only minimally across the entire set of considered cars. Maximum coefficient of variation for any measurement was 6%. As a result, detailed measurements were made manually on three of the twelve vehicles, to determine specific interior geometry goals for the buck, including seat to roof / pillar / console / instrument panel distances, overall interior width / height / length, and door opening geometry. Using these geometric definitions, a center console, simple rigid seats, knee bolsters, toe pans and belt D-ring mounting posts were designed to generally match the interior geometry of the vehicles. The occupant seating and restraint hardware can be adjusted in all three dimensions. Most of the buck mass is contained near the CG in a 127 mm diameter solid steel bar. The location of this bar relative to the occupant seating area can be adjusted vertically to simulate variations in the vehicle CG. Additionally, ballast can be added at various locations to adjust the overall mass (1690-2326 kg) and moment of inertia (580-850 kg m²) to achieve the extremes of the distribution from the twelve fleet vehicles.

Examination of the roof geometry data for the considered vehicles showed that the greatest variation was in the shape of the roof. Particularly, the tumblehome angles of the roof structure, and the lateral curvature of the roof seemed to vary widely, with some vehicles having a lower tumblehome angles and curved roofs, and some having fairly flat roofs and steep tumblehome. As a result, two different roof/pillar geometries were determined for the buck to represent variations in the fleet. These two roof geometries varied in a shape parameter, which was defined as the difference between the vehicle CG to roof rail distance (the maximum radius) and the vehicle CG to roof center distance. This parameter estimated the “roundness” of the vehicle with larger values describing a less round shape and smaller values describing a more round shape. The parameter varied across the twelve fleet vehicles from 52 mm to 153 mm (mean: 99 mm, standard deviation: 32 mm). Roof 1 was designed to have a shape parameter of 69 mm (a rounder roof), and Roof 2 was designed to have a shape parameter of 135 mm (a more “boxy” roof). For the purpose of this study, only Roof 2 was considered in the computational analyses, as it will be fabricated and tested first. To determine roof strength or stiffness goal for the buck roof structure, data from Insurance Institute for Highway Safety (IIHS) roof crush testing was

used. Much like the FMVSS No. 216, “Roof crush resistance” test, the IIHS test involves quasi-static loading of the vehicle roof, at a 25 degree roll and 5 degree pitch angle, with a rigid platen. The platen is driven into the vehicle for a distance of 254 mm, and the peak reaction force on the platen generated in the first 127 mm of deformation is normalized by the vehicle weight to determine the strength-to-weight ratio (IIHS 2012). It was assumed that the majority of new vehicles would have strength-to-weight ratios of 4.0 or above, and thus the buck was designed to have a roof with a SWR of 4.0 at its maximum mass (approximately 2268 kg). Data from the IIHS tests were analyzed to determine the general shape of the force-deformation response of the vehicles (Figure 2).

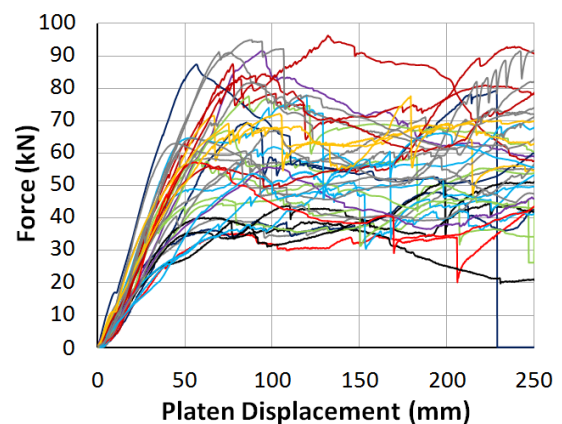


Figure 2. Roof crush force vs. platen displacement for 37 vehicle tests (IIHS 2012).

Based on this data, a goal force-displacement response for the buck roof under quasi-static platen loading at 25 degrees roll and 5 degrees pitch was identified (Figure 3). The goal response should increase approximately linearly from 0 N to the peak force (88.9 kN) over the first 75 mm of deformation, and then remain at an approximately constant force beyond that deformation.

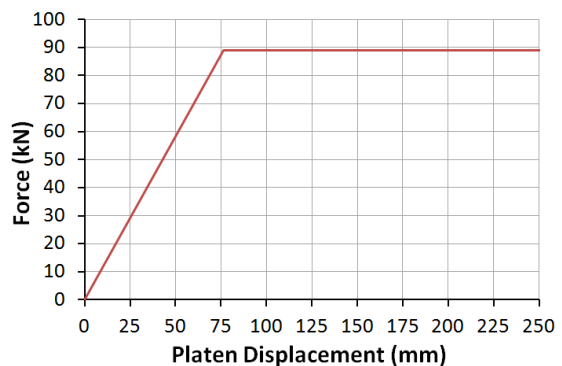


Figure 3. Desired force-deformation response for the roof structure.

METHODS

Initial design

Once the specific geometry of the roof (Roof 2) was determined, a baseline design of the greenhouse structure was created. The design utilized components that could be readily purchased or easily machined. Round tubing was used for the pillars, the roof rails, the windshield header, and connections between the tops of the B-, C- and D-pillars (Figure 4). Additional hat-section beams were used to connect right and left roof rails between the A- and B-, and the B- and C-pillars.

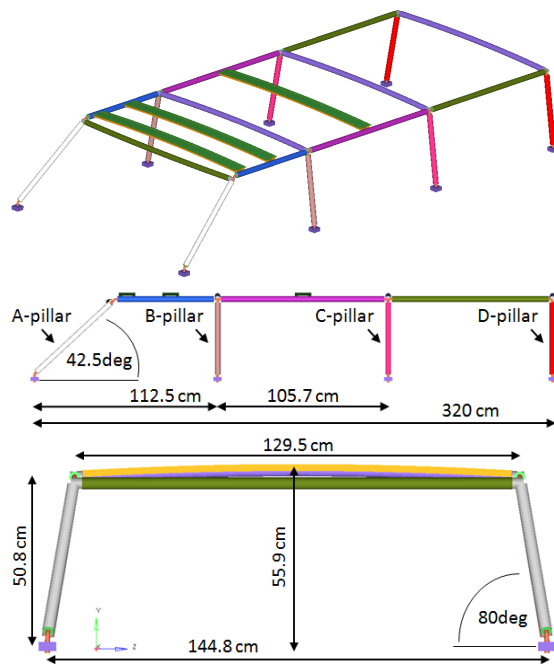


Figure 4. FE model of the initial design of the roof structure.

Plastic joints, consisting of a round bar set into the tube ends (Figures 5 & 6), were used to join tubing at the interfaces between the pillars, roof rails, headers, and additionally at connections between the pillars and the rigid buck base. The joints are made of 1018 low carbon steel, the tubing is manufactured of 1010 or 1020 steel.

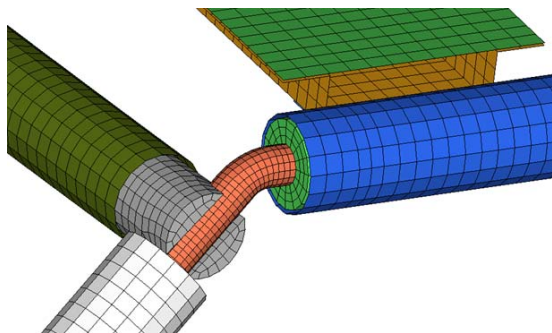


Figure 5. FE Model detail of the A-pillar, windshield header, roof rail intersection.

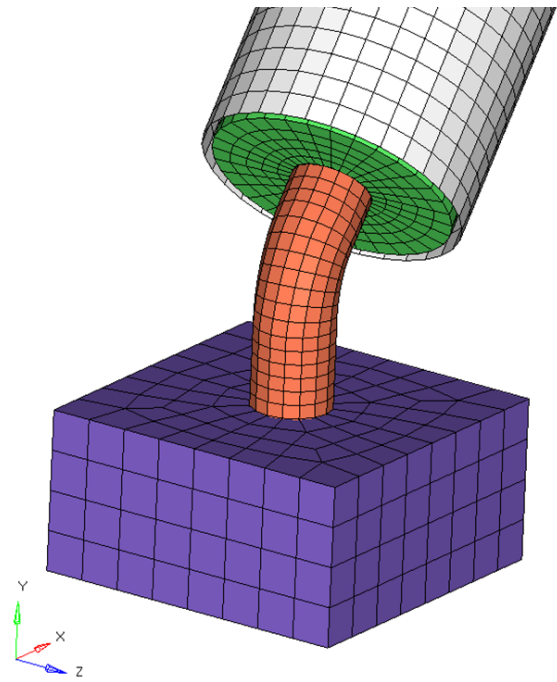


Figure 6. FE Model detail of the A-pillar/beltline interface.

Computational investigation

Each of the plastic joints, tubing and header sections were sized by performing a detailed computational investigation using a commercial implicit finite element (FE) code (Abaqus 6.11-3). A multi-tiered design approach was used consisting first of a simple beam element model (Figure 7), followed by a more complex model meshed with shell (tubes, hat section beams) and solid (plastic joints and inserts) elements. Interfaces between components which are going to be welded in the fabricated structure were modeled using shared nodes (simplified model) or a tied contact (detailed model).

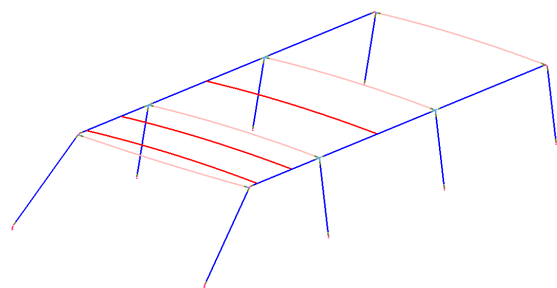


Figure 7. Beam element model of the greenhouse.

Elastic-plastic material models were used to describe the behavior of different steels used for different parts of the roof. The nonlinear stress-strain relationship beyond the yield point was defined as tabular data in the numerical models. The properties were taken from the literature

(Sabih et al. 2012, Padmanabhan et al. 2008, Schaeffer et al. 2007) and validated through three-point bending tests (Figure 8).

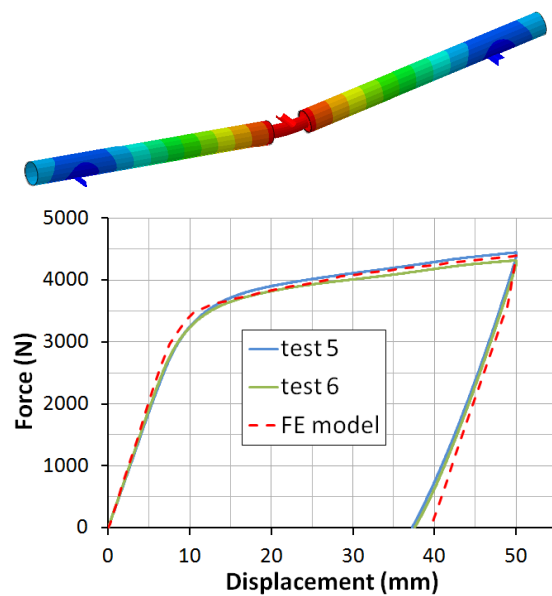


Figure 8. 3-point bending test of a plastic joint buck component: experiment (top), numerical simulation (fringe: resultant displacement; middle) and force vs. displacement comparison (bottom).

Using the FE models, sensitivity studies were carried out to evaluate component sizes, beam curvature and alignment, the number of structural connections and cross beams and the effect of a windshield. For each component of the roof structure cross-sectional shape, dimensions and material properties were assigned. Each parameter was adjusted separately in an iterative fashion. Only the geometry of the individual components was adjusted, and the overall geometry of the greenhouse remained the same. Also, the addition of other structural components was evaluated to determine effects on the overall mechanical behavior.

Most of the simulations were performed with the use of the beam element model (“the simplified model”). The use of the simplified model allowed for keeping the wall clock time of a single

simulation on a reasonable level (between 15 and 30 minutes). When the force-deformation response of the simplified model was satisfactory, it was assessed using the detailed model. Comparisons between the simplified and the detailed model were made with the initial and final design to verify the validity of the simplified model.

Lastly, the final design was evaluated in a dynamic rollover crash computer simulation. To do this, the bases of all the pillars were tied rigidly to a single mass element located at the approximate CG of the entire buck (with the roof added). The mass and inertial properties were chosen from one of the twelve full-sized crossover vehicles used to design the buck ($m = 2002 \text{ kg}$, $I_{xx} = 838.5 \text{ kg m}^2$, $I_{yy} = 3399 \text{ kg m}^2$, $I_{zz} = 3630 \text{ kg m}^2$). The buck was oriented and provided initial velocities (at initial contact) using touchdown parameters (Table 1) extracted from an unpublished deceleration sled test (similar to Kerrigan et al. 2011b) performed on one of the twelve vehicles. Local axes are defined using the Society of Automotive Engineers (SAE) convention for vehicles and global axes are defined to be aligned with the vehicle coordinate system prior to the vehicle’s lateral trip.

Table 1. Touchdown parameters for the dynamic test.

Parameter	Value
Roll Angle (deg)	-181
Pitch Angle (deg)	2.5
Yaw Angle (deg)	7.7
Local X-Angular Velocity (deg/s)	-228
Local Y-Angular Velocity (deg/s)	-8.9
Local Z-Angular Velocity (deg/s)	-23.4
Global X-Velocity (m/s)	0.2
Global Y-Velocity (m/s)	-3.5
Global Z-Velocity (m/s)	2.7

To perform an explicit dynamic rollover simulation the detailed model was converted from ABAQUS 6.11-3 to LS-Dyna V971 R4.2.1.

RESULTS

Evaluation of initial design

In the first loop of numerical simulations the force-displacement response of the greenhouse described in the “Initial design” section was evaluated. Comparison of the detailed and simplified models indicated that the simplified model could provide a relatively accurate response of the full model (Figure 9). While the models showed similar mechanical behavior, the value of a peak force was higher (about 15%) in the beam element model. The “beam” response is also smoother; connections between components were modeled in a very simple way that prevented local effects (e.g.

buckling) from appearing in the global force-deformation response.

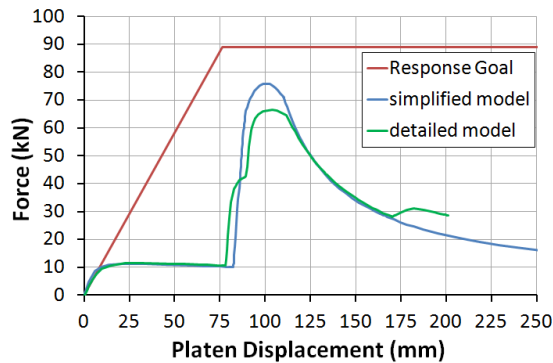


Figure 9. Force-displacement response of initial design.

It was clear that the greenhouse was much too soft over first 80 mm of deformation as well as after 120 mm. Additionally, it was noticed that the response showed a discontinuity around 80 mm of the roof displacement. It was determined that this discontinuity was caused by the platen contacting and loading the B-pillar. The pillar started being compressed and the axial force acting on it became the dominant force acting on the entire structure. It resulted in a very large increase of the crushing force – from 10 kN up to 65-75 kN.

The final deformation of the greenhouse at the end of the numerical analyses showed a “matchbox” effect where the far side pillars were pushed more vertically, and then beyond, whereas the near side pillars were bent inward (Figure 10). No visible plastic deformations in most of the tubes and top cross beams were seen, and only the plastic joints incurred permanent deformations.

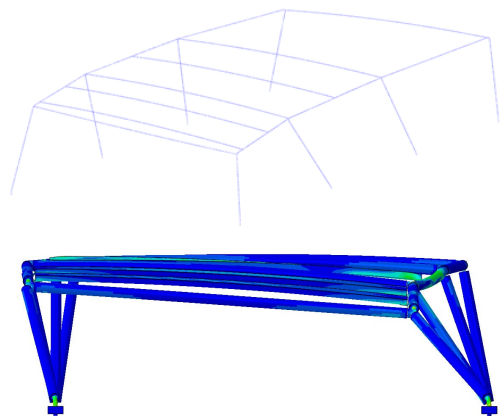


Figure 10. Final deformation of the greenhouse (initial design): isometric view, simplified model (top); front view, detailed model (bottom).

Parametric studies – friction/joint diameter

These initial simulations showed that there was significant sliding between the platen and the tube

structure. To evaluate the influence of the friction between the platen and the roof, a sensitivity study was performed for different values of the friction coefficient. The force-displacement response was heavily dependent on the friction values (Figure 11). The value of a peak force for a friction coefficient of 0.9 was almost eight times higher than for a coefficient of 0.35.

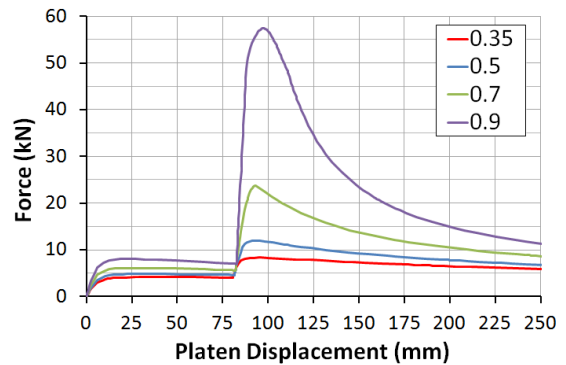


Figure 11. Force-displacement response for different friction coefficients.

Using a friction coefficient of 0.9 the influence of the plastic joint diameter was evaluated in another sensitivity study. As a first step, simulations were performed where every plastic joint in the structure had the same diameter, and diameters readily available for purchase were evaluated (Figure 12). The simulation results showed that there was a slight increase of the force value at the very beginning of the crushing process for the various diameters. After that there was a plateau until the platen came into contact with the B-pillar (~82 mm of platen displacement). The force reached its maximum at 90-100 mm of deformation and then began decreasing nonlinearly. The peak force increased by almost a factor of 2 from a 50% increase in the bar diameter. For the thicker plastic joints numerical instabilities occurred and the analyses terminated due to a not converged solution.

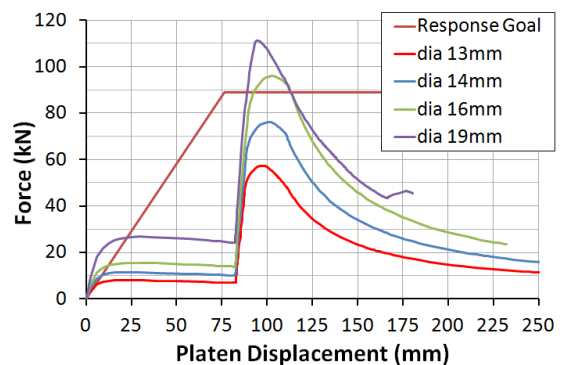


Figure 12. Force-displacement response for different plastic joint diameters.

Improvements in the roof structure

To improve the response of the greenhouse over first 80 mm of platen displacement several different design solutions were proposed and analyzed: curving the B-pillar, adding a windshield, adding cross beams in the roof area or window area between the A- and B-pillars. The windshield was modeled as two steel bars connected in a “cross” orientation between the A-pillar tops and the opposite side A-pillar bases. Cross beams (bars) in the window areas connected the tops of the A-pillars to the bases of the B-pillars. Roof cross beams (bars) were used instead of the hat section beams and they connected the tops of the A-pillars to the tops of the opposite side B-pillars (Figure 13). For each configuration, simulations using the simplified model were performed.

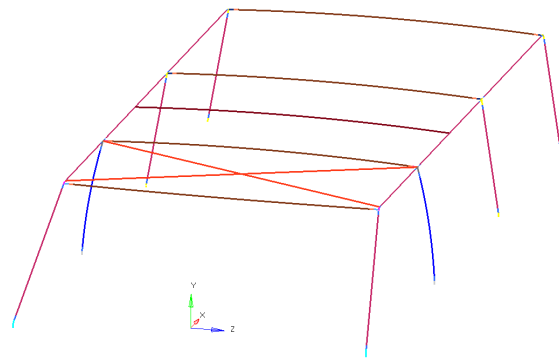


Figure 13. Greenhouse structure with cross beams in the roof area.

Introducing bending to the B-pillar decreased the critical force needed to get the pillar to buckle. Curving it with a 2.26 m radius in the Y-Z plane (SAE vehicle coordinate system reference) of the roof structure reduced the value of a peak force by approximately 45% (Figure 14) and changed the character of the response significantly, especially in the rate of force reduction after the peak force occurred.

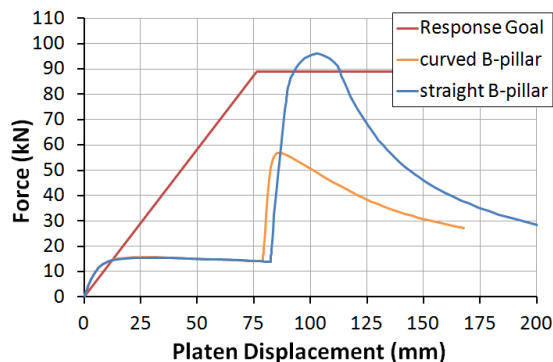


Figure 14. Force-displacement response for straight and curved B-pillar.

The addition of the roof cross beams, the window cross beams, or the windshield cross did not change the global response or the peak force substantially (Figure 15). The addition of the roof cross beams slightly shifted the displacement where the discontinuity occurred. The window cross beams and the simulated windshield increased the initial stiffness and then shifted the discontinuity to a lower (windshield) or higher (window cross beams) deformation level.

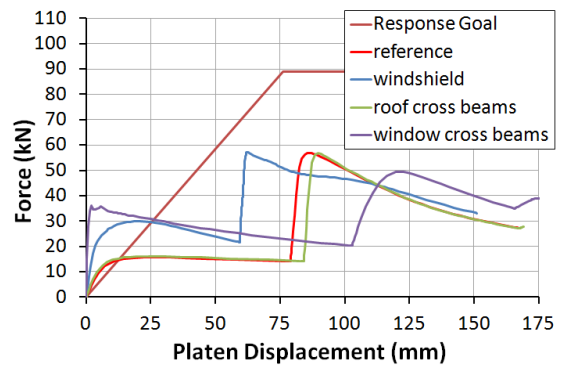


Figure 15. Force-displacement response for analyzed solutions. The reference simulation included the curved B-pillar (Figure 14).

Final design of the Roof 2 structure

Based on the performed simulations a new design of the greenhouse was proposed. In the B-pillar area, two more components were added (Figure 16). The first element was a curved steel tube (outer diameter: 25 mm). The second was a curved steel bar with a 16 mm diameter. Both of the members originated from the base of the B-pillar and rose to the roof rail in the front-row window area. These components were added to increase the stiffness of the overall structure prior to engaging the B-pillar.

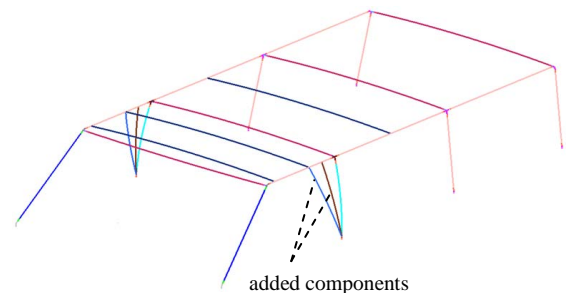


Figure 16. Greenhouse with added components in the B-pillar area.

The force-displacement response of the new design can be divided into several phases (Figure 17). During the first phase (0-30 mm) the platen pushed the A-pillar and the roof rail inwards. After 30 mm of roof displacement the platen hit the first added element (curved steel tube), which caused a large

increase in global stiffness. After about 50 mm of displacement, the next component (steel bar) was engaged, which increased the stiffness again. Similarly, around 70 mm the B-pillar was loaded, which again increased the stiffness. The force reached its maximum value (90 kN) and started decreasing nonlinearly until 160 mm of deformation when the rear edge of the platen contacted the BC-roof rail, which resulted in a small increase of the force. After 235 mm of the roof displacement a significant change in the response was observed when the platen hit the middle section of deformed (bent) added pieces.

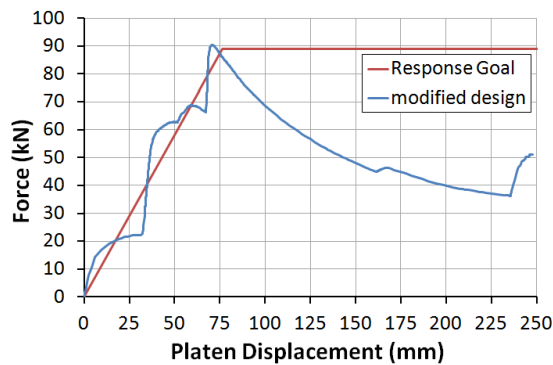


Figure 17. Force-displacement response for the modified design.

The resulting response mimicked that of a vehicle – with a strength-to-weight ratio of 4 – very well over first 75 mm of platen movement. While the response of the roof beyond 75 mm needs to be improved to achieve a constant force goal, the predicted response is not uncommon relative to real vehicles (Figure 2).

To evaluate the response of the considered design the detailed model of it was used. The added components were connected to the AB-rail and the B-pillar through steel C-channels (Figure 18). Detailed connections at each of the joints were implemented to model the fabricated structure as closely as possible.

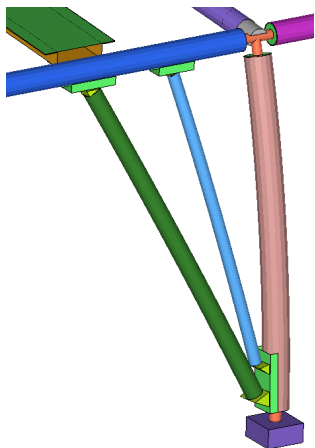


Figure 18. B-pillar area with added components.

The detailed model showed a slightly different response than the simplified model (Figure 19), but overall model response showed agreement in stiffness and peak force. The detailed model showed convergence problems beyond 217 mm of deformation. Structural deformations showed that once the B-pillar and added components began bending, far-side pillar deformations ceased and matchboxing reduced (Figure 20).

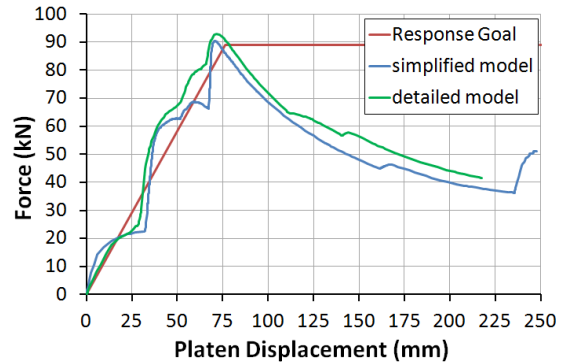


Figure 19. Force-displacement response for the simplified and the detailed model of the modified greenhouse design.

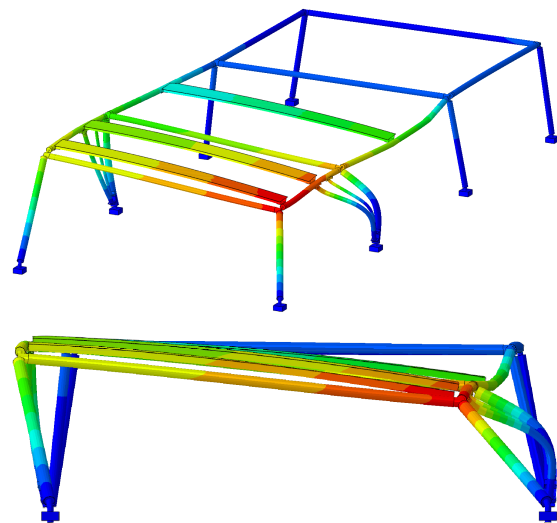


Figure 20. Greenhouse deformation at platen displacement of 217 mm: isometric view (top); front view (bottom).

Dynamic rollover crash simulation

The resulting design was subjected to a dynamic rollover computer simulation to facilitate qualitative evaluation of the dynamic response in a rollover crash (Figure 21). For the simulation, the friction coefficient between the ground and the roof structure was established as 0.4.

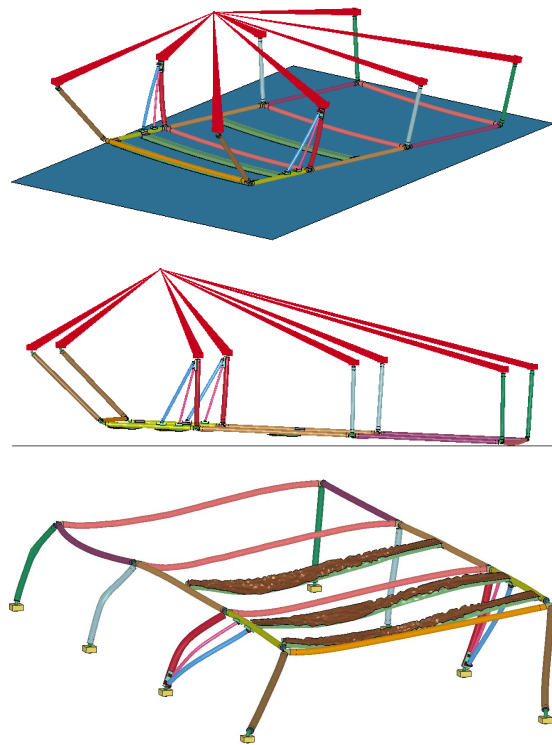


Figure 21. The vehicle at initial contact with the ground: isometric view (top); side view (middle), and final deformation of the roof structure (bottom).

The data (Figure 22) and visualization output showed that the buck, which was initially pitched with the rear end down and the front end up, pitched forward during the simulation to load the trailing-side A-pillar. This occurred since the center of gravity (Figure 21) was located forward of the initial touchdown location, which resulted in a pitching moment generated by the initial rear end contact. Similarly, despite to the initially negative yaw velocity, the buck increased its (positive) yaw angle throughout the simulation due to the initially-high yaw moment that occurred. This yaw moment resulted from the location of the center of gravity relative to the initial contact location and the translational (over the ground) velocity. Lastly the exchange of energy between rotation and translational energy typical in rollover crashes (cf. Funk et al. 2012) was evident in this case also (Figure 23). The roof's contact point initially had a tangential velocity greater than that of the buck CG's translational velocity, and thus, energy was initially transferred from rotation to translation which resulted in a decrease of the angular rate and an increase of the translational velocity. However, when the translational velocity became equal to the tangential velocity, both terms began to decrease.

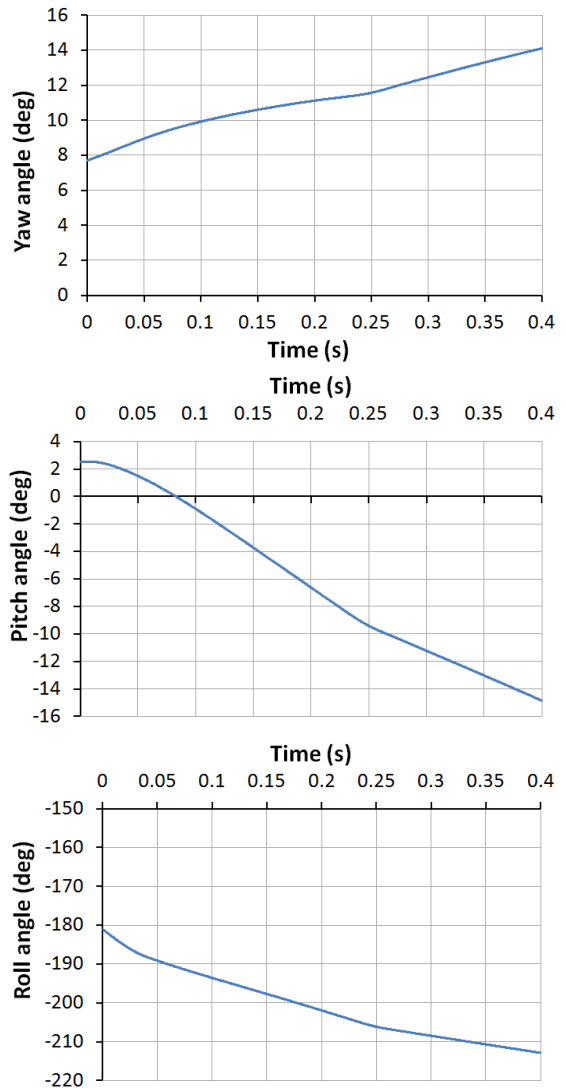


Figure 22. Time histories of the Yaw (top), Pitch (middle) and Roll (bottom) angles.

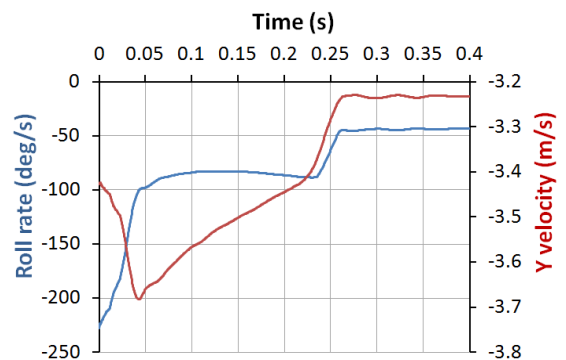


Figure 23. Roll velocity and lateral (Y-axis) translational velocity time histories from the dynamic simulation.

The peak vertical force was 110 kN, which occurred at approximately -187 degrees of roll angle (Figure 24). Previous testing has shown that peak forces between 110 kN and 120 kN between

the vehicle and the ground in a single roof-to-ground rollover crash test are realistic for an SUV (Pontiac Torrent) with a relatively high strength-to-weight ratio (Kerrigan et al. 2013). Ideally, dynamic response data would be compared directly to actual test data for a similarly shaped vehicle with similar inertial properties and roof strength; however, such data could not be identified from the literature.

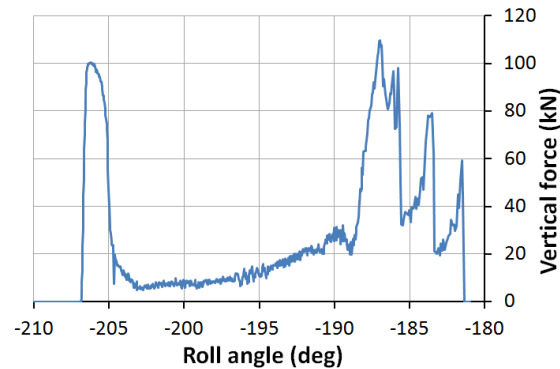


Figure 24. Force-roll angle time history for the buck.

DISCUSSION

Since the buck was designed to simulate the response of real vehicles in a dynamic rollover crash test, using dynamic response targets for the model iterations would have been ideal. However, standardized dynamic test data for a variety of vehicles is not available. As a result, quasi-static roof crush data were used to determine a generally representative response of vehicles in the fleet. While many vehicles show an initially steep increase to the maximum force, followed by a decrease in force over larger deformations in a FMVSS No. 216-like test, the modeling target was designed for a constant force after the peak to generally represent the fleet surveyed (Figure 2). Based on the performed FE simulations the baseline design was modified and converted into a greenhouse that has a force-deformation response that generally matches a real vehicle with a high strength to weight ratio. This was accomplished by modeling off-the-shelf parts and in a way that will make it easily fabricated. The model parameters could now be scaled to create a weaker/stronger model, which still has the same overall geometry. These models could be used to evaluate the effect of roof strength in a dynamic test without changing the critical-to-the-design external dimensions of the structure. It is also worth mentioning that the real value of a friction coefficient between the platen and the roof structure was not determined, but a substantial sensitivity was shown. As a result, until static roof crush testing can be completed, there is no way to

determine how large the difference between the simulation prediction and the test result will be.

CONCLUSION

The goal of this study was to determine a detailed design for a roof structure to be used to perform rollover crash tests with a rollover test buck. Variations in an initial design of the greenhouse and computational analyses yielded a model that has a loading response that is representative of a modern full-size crossover vehicle. Further modification of the design may be necessary to improve the response beyond the peak quasi-static test force, but full scale fabrication and testing will be performed first to examine the actual response at these levels before implementing additional changes. When the final design is fabricated and the model predictions are validated in a real test meeting FMVSS No. 216, the test buck with the greenhouse attached will be used to evaluate dummy biofidelity in future matched PMHS and dummy rollover crash tests. Computational modeling of the more “round” roof structure (with smaller tumblehome angles) is also considered as one of the next steps in this research.

ACKNOWLEDGMENTS

This study was supported in part by the National Highway Traffic Safety Administration (NHTSA) under Cooperative Agreement No. DTNH22-09-H-00247. This study was also supported in part by the European Union in the framework of European Social Fund through the “Didactic Development Program of the Faculty of Power and Aeronautical Engineering of the Warsaw University of Technology.” Views or opinions expressed or implied are those of the authors and are not necessarily representative of the views or opinions of the NHTSA or the Warsaw University of Technology.

REFERENCES

- [1] Bixel, R.A., Heydinger, G.J. and D.A. Guenther. 2010. “Measured vehicle center-of-gravity locations – including NHTSA’s data through 2008 NCAP.” Society of Automotive Engineers (SAE). Paper Number 2010-01-0086. Warrendale, PA
- [2] Foltz, P., Kim, T., Kerrigan, J.R. and J.R. Crandall. 2011. “Vehicle greenhouse shape analysis for design of a parametric test buck for dynamic rollover testing.” In Proceedings of the 22nd International Technical Conference on the Enhanced Safety of Vehicles (ESV) (Washington, D.C., June 13-16)

- [3] Foster, J.B., Kerrigan, J.R., Nightingale, R.W., Funk, J.R., Cormier, J.M., Bose, D., Sochor, M.R., Ridella, S.A., Ash, J.H. and J.R. Crandall. 2012. "Analysis of cervical spine injuries and mechanisms for CIREN rollover crashes." In Proceedings of the 2012 IRCOBI Conference (Dublin, Ireland, Sep 12-14)
- [4] Funk, J., Wirth, J., Bonugli, E., Watson, R. and A. Asay. 2012. "An integrated model of rolling and sliding in rollover crashes." SAE Technical Paper 2012-01-0605. doi: 10.4271/2012-01-0605
- [5] Heydinger, G.J., Bixel, R.A., Garrott, W.R., Pyne, M., Howe, J.G. and D.A. Guenther. 1999. "Measured vehicle inertial parameters – NHTSA's data through November 1998." Society of Automotive Engineers (SAE). Paper Number 1999-01-1336. Warrendale, PA
- [6] Insurance Institute for Highway Safety (IIHS). 2012. Crashworthiness evaluation roof strength test protocol (version II). December 2012. http://www.iihs.org/ratings/protocols/pdf/test_protocol_roof.pdf
- [7] Jordan, A. and J. Bish. 2005. "Repeatability testing of a dynamic rollover test fixture." In Proceedings of the 19th International Technical Conference on the Enhanced Safety of Vehicles (ESV) (Washington, D.C., June 6-9)
- [8] Kerrigan, J.R., Dennis, N.J., Parent, D.P., Pursezov, S., Ash, J.H., Crandall, J.R. and D. Stein. 2011b. "Test system, vehicle and occupant response repeatability evaluation in rollover crash tests: the deceleration rollover sled test." International Journal of Crashworthiness, 16(6): 583-605
- [9] Kerrigan, J.R., Jordan, A., Parent, D., Zhang, Q., Funk, J., Dennis, N.J., Overby, B., Bolton, J. and J.R. Crandall. 2011a. "Design of a dynamic rollover test system." Society of Automotive Engineers (SAE). Paper Number 2011-01-1116. Warrendale, PA
- [10] Kerrigan, J.R., Seppi, J., Lockerby, J., Foltz, P., Overby, B., Bolton, J., Kim, T., Dennis, N.J. and J. Crandall. 2013. "Test methodology and initial results from a Dynamic Rollover Test System." Society of Automotive Engineers (SAE). Paper Number 2013-01-0468. Warrendale, PA.
- [11] Lessley, D., Shaw, G., Parent, D., Arregui-Dalmases, C., Kindig, M., Riley, P., Pursezov, S., Sochor, M., Gochenour, T., Bolton, J., Subit, D., Crandall, J.R., Takayama, S., Ono, K., Kamiji, K. and T. Yasuki. 2010). "Whole-body response to pure lateral impact." Paper Number 2010-22-0014. Stapp Car Crash Journal 54: 289-336
- [12] Mohan, P., Cing-Dao, K. and J. Riley. 2008. "Evaluation of roof strength under multiple loading conditions." In Proceedings of the 2008 International Journal of Crashworthiness Conference (Kyoto, Japan, July 22-25)
- [13] Padmanabhan, R., Oliveira, M.C. and L.F. Menezes. 2008. "Deep drawing of aluminium-steel tailor-welded blanks." Materials and Design 29: 154-160
- [14] Sabih, A. and J.A. Nemes. 2012. "Experimental and finite element simulation study of the adiabatic shear band phenomenon in cold heading process." Journal of Materials Processing Technology 212: 1089-1105
- [15] Schaeffer, L. and A.M.G. Brito. 2007. "FEM numerical simulation and experimental investigation on end-forming of thin-walled tubes using a die." Steel Research International 78, No. 10-11: 789-803
- [16] U.S. Department of Transportation, National Highway Traffic Safety Administration. 2012. Federal Motor Vehicle Safety Standards and Regulations. DOT HS 808 878. <http://www.nhtsa.gov/cars/rules/import/fmvss/index.html>

Evaluation of the dynamic rollover characteristics of trip-over vehicles through multi-body dynamics simulation

Byoungkee Han

Hongik University, Seoul, Korea

Eundok Lee

KATRI, Suwon, Korea

Jungsoo Shim & Jaeho Jung

TUR Engineering Co., Namyang, Korea

ABSTRACT

Despite the high fatality rate due to rollover, this topic little features as a focus of research, when compared to studies on frontal and side collisions. As repeatability issues with the test have meant that there is not yet an established standard for dynamic rollover system that evaluates the safety of rollover of vehicles, the FMVSS 216a Static Roof Crash Resistance is currently applied.

The objective of this paper is to simulate the behavior of crash-test dummies and the deformation of a vehicle body by numerical analysis considering not only bending and torsional modulus, but also the collapse characteristics of main members.

We can find the effect of each member on the SWR of vehicle at the static test (FMVSS 216a), and the effect of SWR on the maximum acceleration value of head. The stiffness of the B-pillar is main member for increasing the SWR value as we know. Next, the A-pillar and center cross member. In terms of the maximum acceleration value of head, this value increases as the SWR of vehicle rises.

We conclude that there exists an appropriate modulus of members in order to decrease the maximum acceleration of head, and particular airbags need to sustain the pressure for about 3.5 sec in order to prevent the ejection of the crash-test dummies.

1. INTRODUCTION

Cars today are more than a means of transporting driver and passenger. They also provide an additional living space. Auto makers, therefore, are faced with a challenge to make cars that can provide not only good traveling performance, but also score well in terms of comfort, aesthetic design and safety. Of these three criteria, safety is particularly significant, as it is directly linked to the seriousness of injury that the driver might sustain in a car accident. In general, a car's safety is dependent on whether its body is designed in such a way that it can minimize the injury of the driver in the event of a frontal crash, side-impact or rear collision. Accordingly, a great deal of research has been devoted to this area, producing technologies that enable the design of highly safe bodies against those types of crashes. In contrast, rollover accidents have not been given as much attention as their proportion of total car accidents is relatively low and, as a consequence, regulations applicable to it are not stringent enough.

The number of fatalities in rollover accidents, however, has been increasing year after year, calling for greater focus. Statistics released in the U.S. show that nearly 250,000 rollover accidents occur every year nationally, claiming over 10,000 lives (35 percent). Rollover accidents in Korea, as in Europe, take up less than one percent of the total accidents, with fatalities from them accounting for around 7 percent of the total. Such a relatively low percentage can be attributed to different road structures and vehicle mix. In 2009, the Insurance Institute for Highway Safety (IIHS) added rollover test results to the criteria for the selection of the Top Safety Pick that already included frontal, side and rear impact

performance in an attempt to help reduce the fatality in rollover accidents. Such a decision is significant in that it suggests the level of fatalities in rollover accidents is simply too high to ignore further.

One of the most common ways to reduce damage from car accidents is adopt active safety technologies that can prevent accidents from happening. Such advanced safety cars and intelligent cars, which have been emerging recently, are those which are equipped with such active safety technologies. Once an accident occurs, what matters is how safe the car's body is. The approach to securing safety in rollover accidents is largely centered on increasing the crush resistance of roofs, which is measured using a static, roof crush resistance test (FMVSS 216). This test, however, has come under severe scrutiny over its effectiveness in protecting occupants in actual rollover accidents. A dolly rollover test (FMVSS 208), which is a dynamic method to measure rollover safety, is often cited as an alternative, but is not widely used because of limited reproducibility.

It is widely agreed that occupant ejection and roof collapse are two major causes of passenger injury or death in rollover accidents as they actually occur on the roads. The National Highway Traffic Safety Administration (NHTSA) is striving to help reduce damage from rollover accidents by raising the minimum strength to weight ratio, which measures roof crush resistance, from 1.5 to 3.0, and requiring the adoption of electronic stability control (see FMVSS 126ESC). The installation of curtain airbags is mandated for selected models to prevent occupant ejection (see FMVSS 226 Ejection Mitigation). In addition, IIHS requires roof crush resistance of SWR=4.0 or higher. Due to this series of regulations, most vehicles launched these days meet the SWR=4.0 requirement and are equipped with various types of airbags.

The purpose of this study is to find out whether improving roof crush resistance is the best way to protect drivers and passengers in rollover accidents. To this end, dynamic rollover simulation is carried out using multi-body dynamics. Many previous papers have examined the behavior of crash-test dummies and external forces applied to the body, but under the assumption that the body is rigid. In this study, in contrast, body modeling takes place based on the bending and torsional rigidity and the collapse properties of key body members, while the

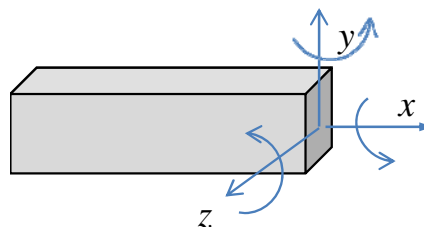
deformation of the body and the behavior of the dummy are observed in a rollover situation. The body is then subjected to a roof crush test (FMVSS 216a) to calculate its SWR. Trip-over, which is the most common type of rollover crash, is selected among others as a parameter for the controlled rollover impact system (CRIS). In order to find out whether vehicles with high SWRs also prove safe in a dynamic rollover test, the acceleration [head injury criteria (HIC) and thorax displacement of the dummy and the displacement of the A-pillar at its top are used.

2. MODELING FOR MULTI-BODY DYNAMICS SIMULATION

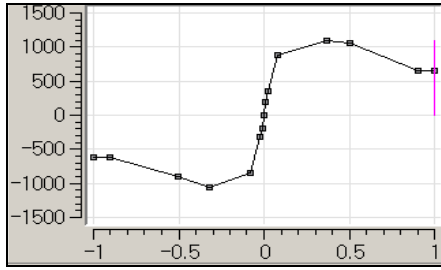
Creating a dynamic interpretation model based on the deformation of the body requires the rigidity properties of key body members to be taken into account. To this end, the bending and torsional rigidity of each pillar (A, B, C and D) and each crossbow (front, center and rear) should be calculated using the finite element method (FEM), whereby the collapse behavior of the members is taken in account.

2.1 Rigidities of member

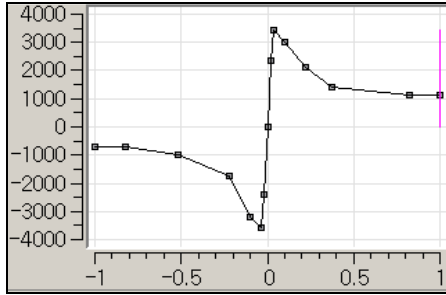
The key members of a car's body are of monocoque structure in the form of a thin tube and show a symptom of collapse beyond the level of maximum load that they can support. Figure 1 (b) through (d) shows examples of member rigidity properties obtained from FEM analysis. A load-deformation diagram is derived based on how the members collapse and applied to the simulation. Notation of axes is as shown in Figure 1 (a): x represents the longitudinal direction of the member; y the inside direction of vehicle; and z the remaining direction, the in-plane direction of vehicle surface.



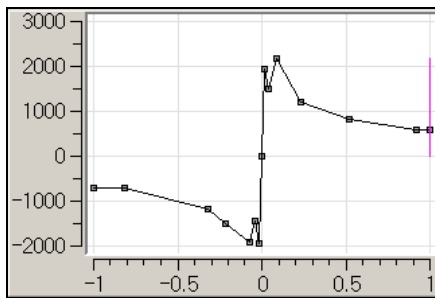
a) Notation of axes



b) Torsion about x axis vs. angle



c) Bending moment about y axis vs. angle



d) Bending moment about z axis vs. angle

Figure 1: Relationship between the bending/torsional moment and the deformed angle

2.2 Derivation of a characteristic curve

The following equations are used to realize the relationship between moment and angle displacement for each member obtained using the finite element method in ADAMS, a dynamic analysis program.

$$\dot{\beta} = \begin{cases} \left(1 - \frac{k \times \beta^n}{T_{MAX}}\right) \times \dot{\theta}, & \beta \times \dot{\theta} > 0 \\ \dot{\theta}, & \beta \times \dot{\theta} \leq 0 \end{cases} \quad (1. a)$$

$$T_{MAX}^* = \begin{cases} 1.0T_{MAX}, & \beta \times \theta > 0 \\ 0.1T_{MAX}, & \beta \times \theta \leq 0 \end{cases} \quad (1. b)$$

Figure 2 shows results from the modeling of A-

and B- pillars' bending rigidity using the equations. It is assumed that spring-back takes place elastically during restoration until the load becomes zero and that one tenth the original load is required for restoration from bending backwards with deformation equal to zero.

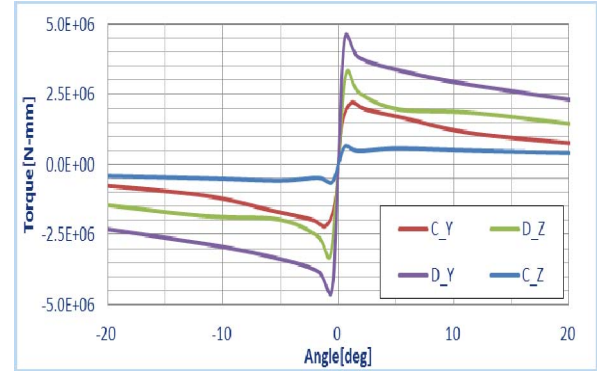


Figure 2 Bending rigidity of A- and B-pillar

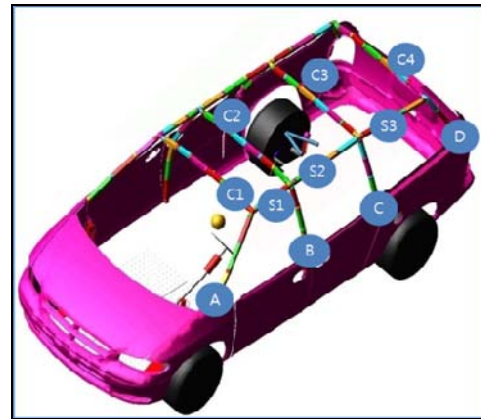


Figure 3 ADAMS Model of vehicle for simulation

The model of vehicle for simulating in ADAMS is consisted of members that consider the deformation of it. Here number of deformable members is 18 as shown in Figure 3. And the number of element of each member is chose to represent well the behavior of member.

3. SIMULATION OF ROOF CRUSH TEST (FMVSS 216)

3.1 Test protocol

Figure 4 shows how the roof crush resistance

testing (FMVSS 216) should be carried out in North America. This protocol requires that vehicles with a gross weight rating of 6000 pounds (2722kg) or less must endure load 1.5 times (SWR x 1.5) as much as their curb weight on their driver's seats and that the displacement of the roofs should be 127mm or lower.

In May 2009, NHTSA announced a tighter standard (FMVSS 216a). The requirement of new protocol (FMVSS 216a) is as follow: vehicles with a gross weight rating of 6000 pounds or less should endure a load three times (SWR x 3.0) as much as their curb weight; vehicles with a gross weight rating of 6000 to 10000 pounds (4536kg) should endure a load 1.5 times as much as their curb weight; head room maintenance is monitored through the use of a head form representing a 50th percentile male seated in the front occupant positions; and the platen force, displacement, and head form contact requirements must be met on both sides of the vehicle's roof structure. This standard must be complied with by all vehicles by 2016.

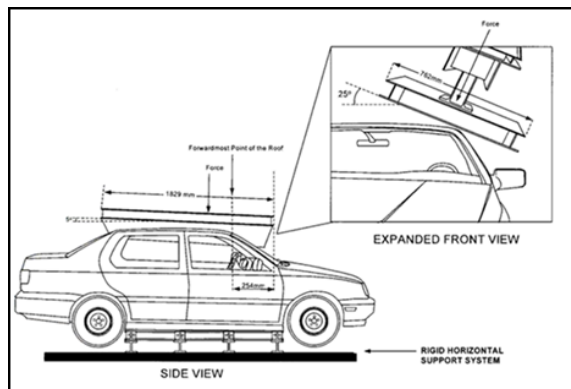


Figure 4 FMVSS 216 roof crush test protocol



Figure 5 Simulation conditions of the new roof crush test (FMVSS 216a)

Figure 5 shows how a simulation to obtain the SWR value (roof crush resistance) should be conducted using ADAMS in accordance with the new standard. The maximum displacement used in this simulation is the old threshold (127mm) for easier interpretation.

3.2 Results of simulation

Results of the simulation show that the loading curve of passenger section (right) is slightly lower than that of the driver section (left). Here the base model had original rigidities of members that were obtained from FEA. The peak load is also similar, but the location is little different. This is because the effect of geometric imperfection due to repeated load is not considered.

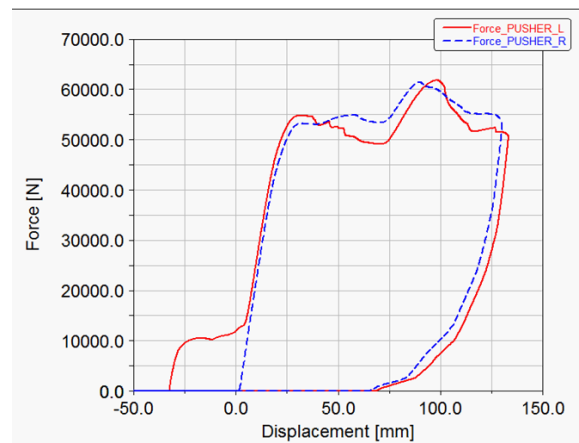
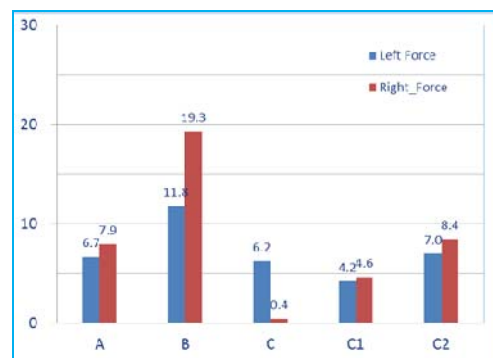
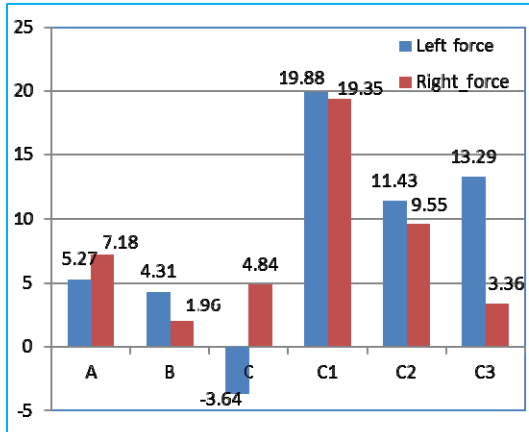


Figure 6 Simulation results of a basic model (FMVSS 216a).



a) FMVSS M216(near side; pitch 10°, yaw 25°, far side; pitch 10°, yaw 40°)



b) FMVSS M216a(both side; pitch 5° , yaw 25°)
Figure 7 Effect of design factors on peak load.

For FMVSS M216, calculation of the effect of key design elements that affect roof crush resistance, including A-, B-, and C- pillar, C1 and C2 roof bow, on peak load reveals that B-pillar has the largest impact, followed by A pillar and C2 roof bow (see Figure 7(a)). It is known that greater rigidity in the B-pillar results in an improved side-impact performance. As anticipated, greater rigidity of each member resulted in higher SWR for the roof. This suggests that SWR increases more effectively when the rigidity of A pillar, B pillar and C2 cross bow increases.

But for FMVSS 216a, quite different results are obtained. The roof bow elements affect seriously roof crush resistance.

4. SIMULATION OF CRIS (Controlled Rollover Impact System)

CRIS is one of the dynamic rollover crush resistance tests and has many benefits including multiple options available for road conditions and initial contact conditions. It however has a major shortcoming: repeatability is very low. Such a shortcoming can be overcome when simulation is used.

4.1 Simulation conditions

Table 1 shows the conditions under which a CRIS test is simulated in ADAMS. The initial contact with the ground is designed to take place at the edge of the near side as shown in Figure 8.

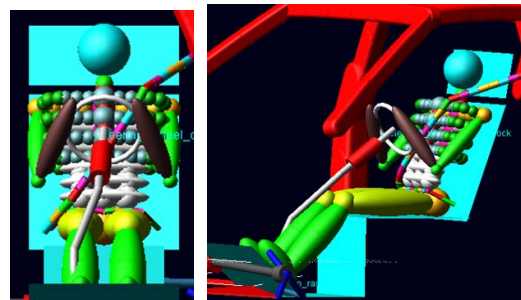
Table 1 Simulation conditions

- Angular velocity: 270deg/s
- Lateral velocity: 8000mm/s
- Weight: 2117kg
- Height of ground to COG of vehicle: 1264mm



Figure 8 Location of initial contact with the ground

A dummy used for dynamic analysis is placed on the driver's seat as shown in Figure 9 to calculate the change in head acceleration. Data used in the configuration of the dummy is from a 50 percentile hybrid, which can be used only for comparison due to its limited reliability.



a) front view b) side view

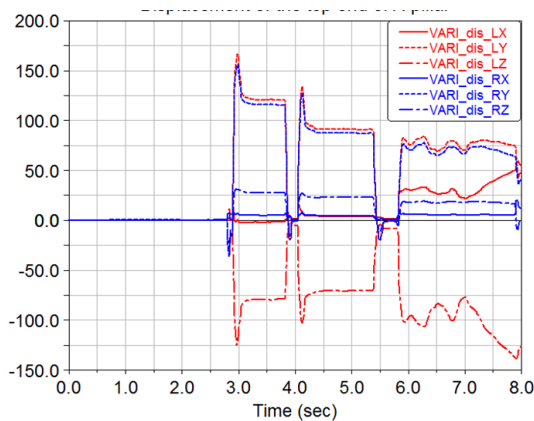
Fig. 9 View of dummy model for simulation

4.2 Simulation results

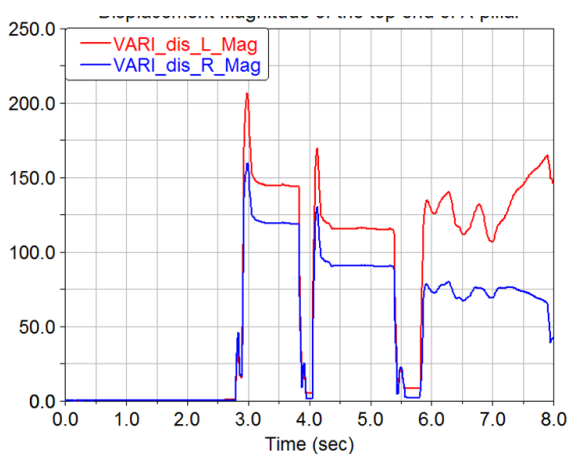
A simulation is conducted where SWR was increased to determine whether vehicles with a good roof-crush resistance prove to be safe in a dynamic rollover test. In order to determine the correlation between the results from a static roof crush resistance test and the result of a dynamic CRIS test, displacement at the point where the top end of A-pillar meets the front cross bow is calculated. Results are shown in Table 2 and Figure 10. We may find that higher SWR, which translates into greater body rigidity, results in smaller displacement at the top end of A-pillar.

Table 2 Displacement of the top end of A-pillar vs. the value of SWR

Case (SWR)	Left Corner Displacement [mm]				Right Corner Displacement [mm]			
	x	y	z	Mag.	x	y	z	Mag.
1 (1.77)	11.5	227.9	-223.3	313.8	8.05	204.1	33.2	206.1
2 (2.66)	59.4	166.6	-138.7	206.7	20.4	156.5	31.1	159.5
3 (3.55)	17.9	146.3	-107.9	181.7	9.29	138.5	-40.6	141.5
4 (4.44)	18.4	134.6	-96.5	165.6	11.6	128.3	-38.3	131.1
5 (5.33)	18.6	126.9	-90.4	155.9	12.3	121.3	-25.5	124.1



a) Displacement components of the top end of A-pillar



b) Magnitude of the top end of A-pillar vs. time

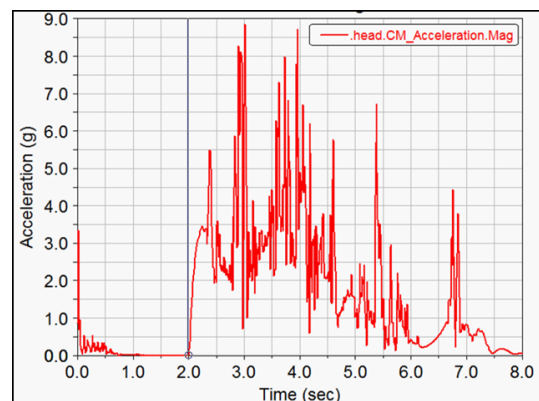
Figure 10 Displacement of the top end of left and right A-pillar for SWR=2.66.

The next factor to be considered in a CRIS simulation is head acceleration. Figure 11 shows the change in head acceleration during rollover when

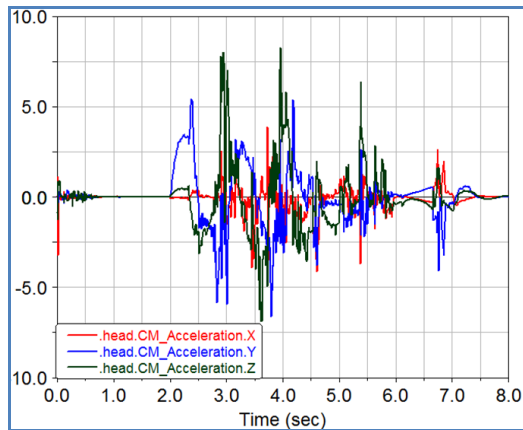
SWR is 3.55. Table 3 shows how maximum acceleration changes for different SWRs. The CRIS simulation suggests that a car can roll over two to three turns in an actual accident and that the acceleration value of the head still retains significant influence. Figure 11.b demonstrates that the acceleration component in the y direction, which causes the dummy to be ejected from the vehicle, is significant (the rollover starts at 2 sec) within 3.5 sec. Therefore this suggests that curtain airbags should retain their pressure up to this point to fully protect the head. In addition, as shown in Table 3, excessively low SWR causes the roof to deform sufficiently to come into contact with the head, producing a greater acceleration value. Higher SWR therefore prevents contact between the roof and the head, resulting in lower acceleration. Increasing the body rigidity beyond a certain point, however, results in head acceleration increasing again, as shown in Table 3. Consequently, it can be inferred that each vehicle has its own optimal rigidity.

Table 3 Maximum value of the acceleration of head vs. the value of SWR

Case (SWR)	Acceleration of head [g]				Head contact with roof
	x	y	z	Mag.	
1(1.77)	-25.7	-47.2	70.4	80.95	contact
2(2.66)	4.58	-6.16	8.73	9.47	Not
3(3.55)	-4.11	-6.62	8.25	8.85	Not
4(4.44)	-3.97	-7.15	9.52	9.82	Not
5(5.33)	6.71	-10.1	8.87	12.67	Not



a) Magnitude of the acceleration of head



b) Components of the acceleration of head

Figure 11 Acceleration of head for SWR=3.55

4. CONCLUSION

For simulating the FMVSS 216 test, the plastic behavior of each member obtained from the FEA was considered. Additionally, the effect of each member on peak load was found. For M216 condition, the stiffness of B-pillar was found to be the most effective in increasing the SWR, while second was A-pillar and center cross member (C2). The stiffness of all members was a positive factor. For 216a condition, the stiffness of roof bow members was found to be the most effective in increasing the SWR.

A correlation was found between the SWR in FMVSS 216 simulation and the displacement of A-pillar end-point in the CRIS simulation. The displacement of A-Pillar high-end was found to decrease as the value of SWR increases. Nevertheless, the acceleration of the head does not always decrease as the SWR increases. One of the reasons for this is that the head comes into contact with the ceiling due to the large deformed frame. An additional factor is the difference in the energy absorption capacity of the vehicle in question. In other words, vehicles with a high SWR can absorb reduced impact energy compared to those with lower SWR.

Consequently, there exists an appropriate modulus of members for decreasing the maximum acceleration of head, and the pressure of a curtain airbag needs to be sustained about 3.5 sec in order to prevent the ejection of crash-test dummies.

REFERENCES

1. Grzebieta R.H.1, McIntosh A.S.2, Bambach M.1, Young D.P., "Dynamic Test Protocol to Assess Rollover Crashworthiness", 2010 Australasian Road Safety Research, Policing and Education Conference, 31 August - 3 September 2010, Canberra, Australian Capital Territory
2. Friedman D. and Grzebieta R.H., (2009). A Proposed Rollover and Comprehensive Rating System, Proc. 21st International Technical Conference on the Enhanced Safety of Vehicles, Stuttgart, Germany, Paper Number 09-0515, June.
3. Tahan F.J., Digges K.H., Mohan P. (2010). Sensitivity Study of Vehicle Rollovers to Various Initial Conditions - Finite Element Model Based Analysis, Proc. 7th Int. Crashworthiness Conf. ICRASH 2010, ed. Chirwa E.C. and S. Kan, Washington DC, September.
4. Fressmann D., Munz T., Graf O. and Schweizerhof, (2007). FE Human Modelling In Crash – Aspects Of The Numerical Modelling And Current Applications In The Automotive Industry, LSDYNA Conference 2007,
5. Young D., Grzebieta R.H., McIntosh A., Bambach A. & Frechede B. Diving vs Roof Intrusion: A Review of Rollover Injury Causation, International Journal of Crashworthiness, Vol. 12 No. 6, pp. 609–628, Dec. 2007.
6. Grzebieta R.H., Bambach M., McIntosh A.S., How Stronger Roofs Prevent Diving Injuries In Rollover Crashes, Proc. 7th Int. Crashworthiness Conf. ICRASH 2010, ed. Chirwa E.C. and S. Kan, Washington DC, September 2010.

RESEARCH ON THE AE-MDB CAE ANALYSIS FOR THE IMPROVED EURO NCAP SIDE IMPACT TEST PROCEDURE

Kim Bumjin
Kim Hyunwoo
Park Dongho
 Hyundai Motor Company
 Korea
 Paper No. 13-0275

ABSTRACT

According to the EURO NCAP side impact test procedures for 2015, the European Enhanced Vehicle Safety Committee (EEVC) Working Group 13 (WG13) has made a proposal for an improved side impact barrier: Advanced European Mobile Deformable Barrier (AE-MDB), which subjects test vehicles to more severe conditions compared to the current ECE R.95 MDB in many factors, including higher strength, increased weight and lengthened width. In this paper, development study of AE-MDB Finite Element (FE) model was performed preferentially in order to cope with the enhanced EURO NCAP side impact test procedures. In the second place, analysis and study for AE-MDB side impact were carried out to evaluate its crash severity for compact and midsize vehicles.

INTRODUCTION

Increased traffic intensity, growing concern of the public and new stringent regulations have made vehicle safety one of the major research areas in the automotive industry. In the automotive industry, the goal of engineering efforts in the field of crash and safety is to satisfy, or, to the extent possible, exceed the safety requirements mandated or administered by the various legislations such as FMVSS, NHTSA, EURO NCAP, IIHS and etc. In case of EURO NCAP, the EEVC WG13 has made a proposal for an improved side impact barrier, AE-MDB [1-4] which provides more severe conditions compared to the current ECE R.95 MDB (EU-MDB), including higher strength, increased weight and lengthened width. The detailed configuration of AE-MDB is shown in Figure 1. It is considered that the frontal shape of AE-MDB is more similar to that of a real vehicle compared to the current EU-MDB. The width and weight of the AE-MDB are increased by 200mm and 350kg respectively as compared to the current EU-MDB. The centerline of the MDB is perpendicular to that of the target vehicle and is aligned 250mm aft of the target vehicle's R-point. In addition to above alterations, the Euro SID II 50th percentile dummy is changed to World SID 50th

percentile dummy. However, the EU-MDB's 300mm ground clearance and initial velocity of 50km/h remain the same. Therefore, it can easily be shown that the initial kinetic energy of AE-MDB is increased by about 36.8% compared to EU-MDB. (Figure 2.)

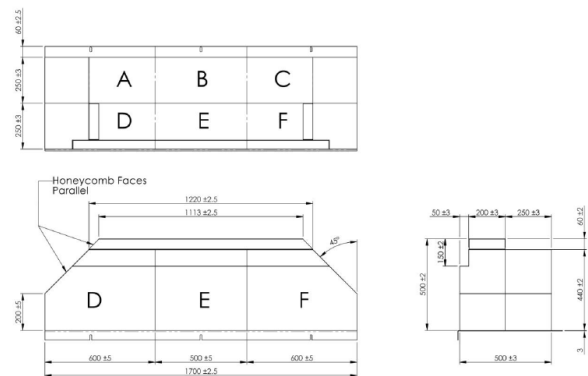


Figure 1. Configuration of AE-MDB [1]

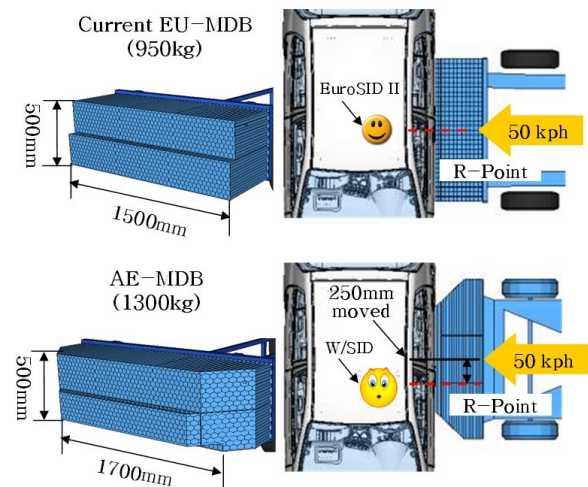
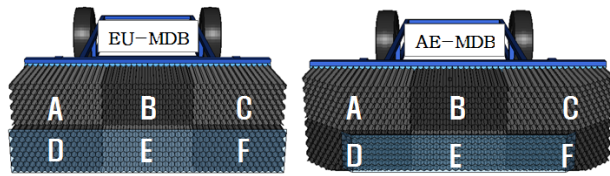


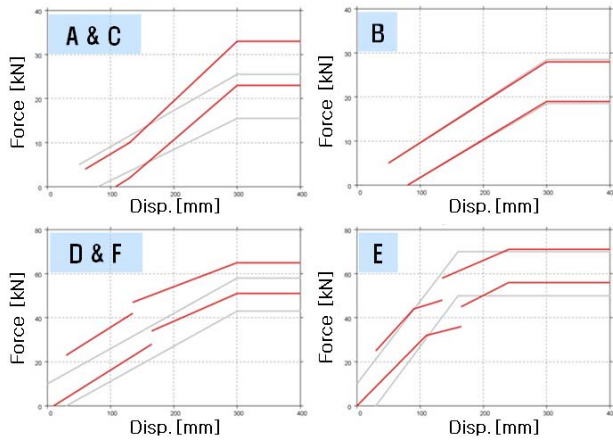
Figure 2. New EURO NCAP side impact test procedures for 2015

The dynamic corridor plots of EU-MDB and AE-MDB are shown in Figure 3 to check the stiffness and strength of deformable barrier itself. It can be

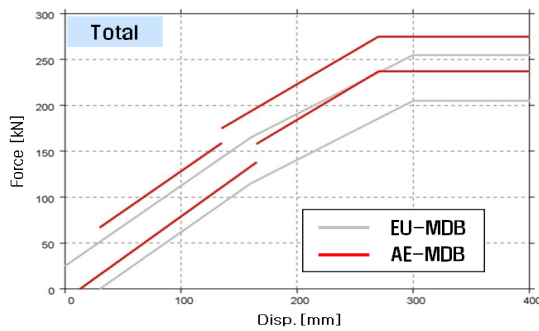
considered that the block B and E of EU-MDB and AE-MDB have similar stiffness and strength on the basis of similar slope and magnitude between the two corridors. On the other hand, the pairs of block A/C and D/F of AE-MDB showed increase in force level, about 26% and 16% respectively compared to EU-MDB. Finally, the total dynamic corridor of AE-MDB showed 11.3% increase in force level compared to EU-MDB. It is assumed that the AE-MDB has been updated to reflect the recent vehicle frontal structures, such as frontal bumper back beam, side member and apron which have increased stiffness and strength compared to the past vehicle structures.



(a) MDB block division



(b) Dynamic corridor of each MDB block



(c) Dynamic corridor of total MDB blocks

Figure 3. Comparison of dynamic corridor

In this paper, development study of AE-MDB FE

model was performed preferentially in order to cope with the enhanced EURO NCAP side impact test procedure. To verify the reliability of the AE-MDB FE model, the following steps were taken: First, collapse test and simulation of honeycomb specimen were performed. Second, single component test of AE_MDB and simulation of 100% full overlap and offset crash tests against the rigid wall were carried out. Lastly, EURO NCAP side impact test and simulation of vehicle using AE-MDB were conducted to evaluate its crash severity for the compact and midsize vehicles.

DEVELOPMENT OF THE AE-MDB FE MODEL

The FE model of AE-MDB has been developed by Hyundai Motor Company(HMC) based on the AE-MDB version 3.9 in 2012, to study preventively with the 2015 EURO NCAP side impact test procedure in regard. The development process of AE-MDB FE model is shown in Figure 4.

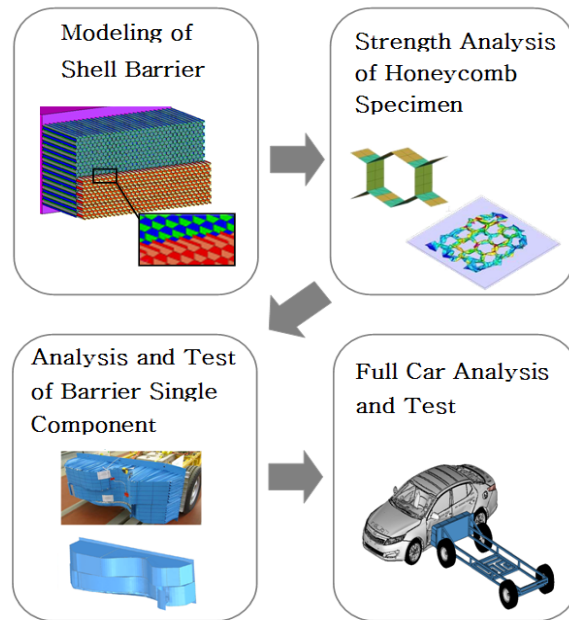


Figure 4. Development process of AE-MDB FE model

Firstly, the FE model is made with consideration of honeycomb fracture and separation between plate and block. This FE model is mainly composed of shell elements which have average of 3mm mesh size. Total number of elements is 2,229,681. Secondly, the axial collapse analysis of honeycomb sample specimen was performed to check the strength requirement. Thirdly, several types of AE-MDB single component analysis were conducted to check the force level compared to the corridor range. Lastly, the side impact analysis of

vehicles was performed with the developed AE-MDB FE model. Debugging work was done when the requirements of AE-MDB conditions were not satisfied in each process.

Strength Analysis of Honeycomb Specimen

As reported previously, the axial collapse analysis of honeycomb sample specimen was performed to evaluate the strength requirement of AE-MDB. As shown in Figure 5, quasi static analysis was performed with loading in axial direction on the honeycomb sample specimen that is 165mmX162mm square type with 25mm height. As a result, this model satisfied the strength curve requirement range; 1.587~1.793MPa.

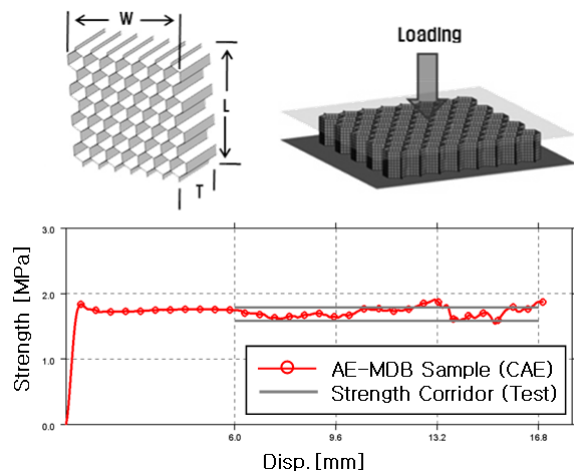


Figure 5. Result of strength analysis

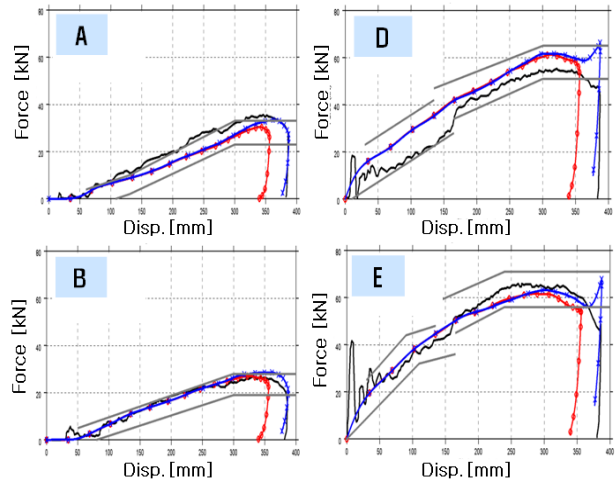
Crash Analysis of Planar Rigid Wall

After inspection of strength analysis result of the honeycomb sample specimen, the AE-MDB single component crash analysis against the planar rigid wall was performed to check the force level of each AE-MDB block compared to the each corridor range. The test condition is that the AE-MDB crash into the planar rigid wall with velocity of 35km/h. The test and analysis result are shown in Figure 6, which shows good correlation in the corridors. It is thought that the difference of 30~40mm displacement could be from the 200kg increased MDB weight.

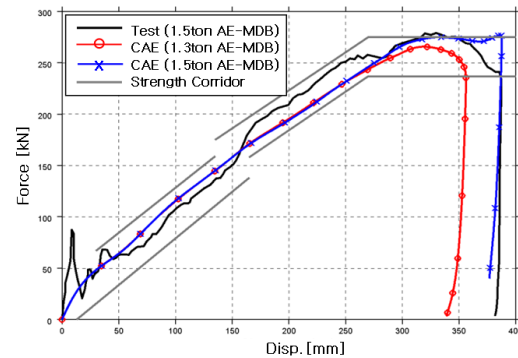
Crash Analysis of Rigid Pole

The AE-MDB single component crash analysis against the rigid pole was performed to check the force level and deformed shape of AE-MDB under local loading condition. The test condition is that the AE-MDB crash into the 30% offset rigid pole which has 350mm diameter with velocity of 20km/h. The test and analysis results are shown in Figure 7. Mostly, the force level of the FE model showed similar curve with the test result. However, the FE model of AE-MDB showed higher

level of force, with maximum of 30% in the 80~240mm displacement range compared to the test result. On the other hand, FE model of AE-MDB showed similar deformed shape on the border between MDB blocks and separation phenomena on the back plate.

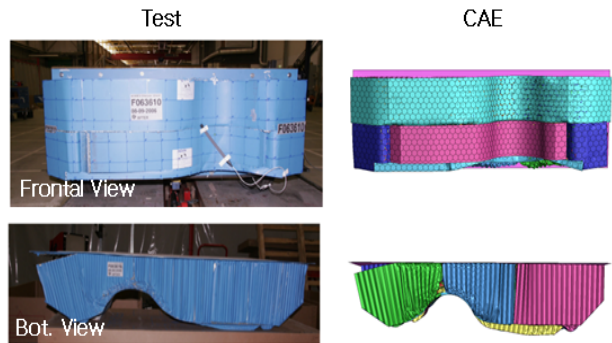


(a) Response results of each MDB block

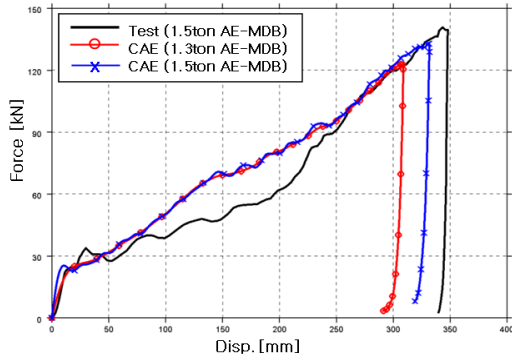


(b) Response results of total MDB block

Figure 6. Result of planar rigid wall crash analysis



(a) Comparison of deformed shape



(b) Response results of total MDB block

Figure 7. Result of rigid pole crash analysis

SIDE IMPACT ANALYSIS UNDER NEW EURO NCAP TEST PROCEDURE

After the analysis and verification of AE-MDB single component FE model, the vehicle side impact analysis and test were performed to compare and analyze the change of crash performances as compared with the results which were done by the current EURO NCAP side impact test procedures. The side impact performance indices that were used for comparison are crash energy absorption, structural displacement, and intrusion velocity. The compact and midsize vehicles utilized for side impact test and analysis are shown in Figure 8.

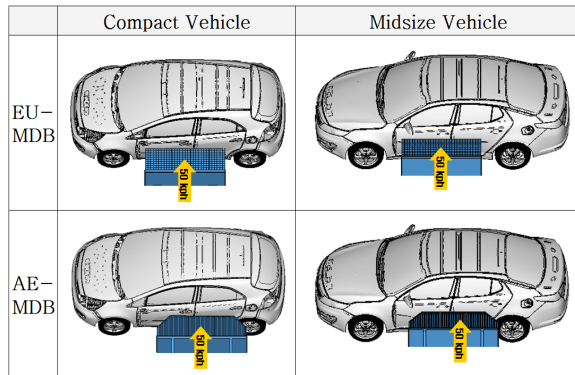
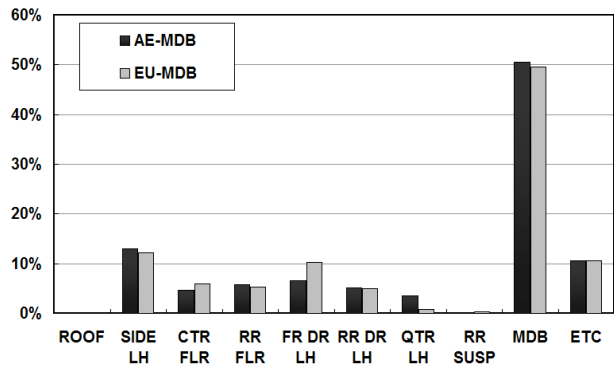


Figure 8. Condition of side impact analysis and test

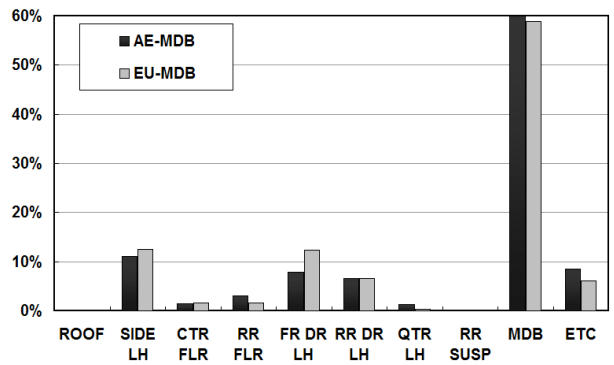
Comparison of Absorbed Energy

The side impact analysis of the compact and midsize vehicle using FE models were conducted based on the conditions shown in Figure 8. The results of energy absorption quantity of structural parts which mainly absorb the energy under side impact conditions with EU-MDB and AE-MDB are shown in Figure 9. The results showed that the absorbed energy of rear floor,

rear door, quarter LH and some other parts increased in both compact and midsize vehicles when the AE-MDB was used for side impact analysis. With the compact vehicle in particular, the AE-MDB target area was extended to wheel arch and rear quarter panel, so the energy of quarter LH, center & rear floor parts increased more compared to the midsize vehicle. The main reason is that the wheelbase of the compact vehicle is relatively shorter than midsize vehicle.



(a) Compact vehicle



(b) Midsize vehicle

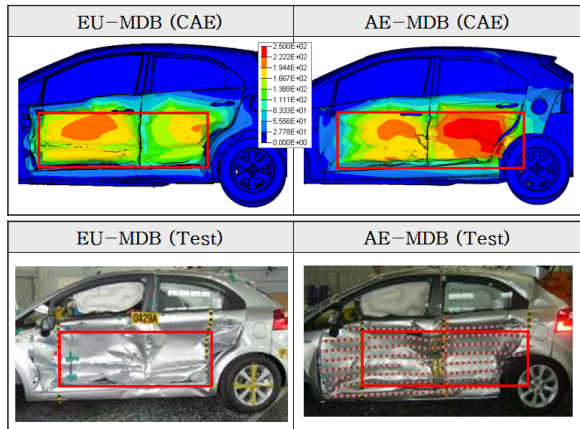
Figure 9. Comparison of energy

Comparison of Structural Displacement and Intrusion Velocity

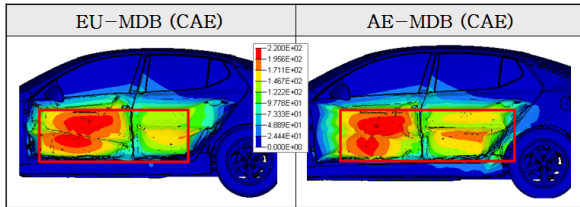
The results of intrusion contour view of compact and midsize vehicle's exteriors are shown in Figure 10. The rectangular shape with bold line shows configuration of EU-MDB and AE-MDB respectively. As the target area moved rearward, the intrusion contour color extended from rear door to quarter panel. The contour view of AE-MDB results also showed that intrusion of rear door was increased compared to EU-MDB results.

The door intrusion velocity presented in Figure 11 shows that the level of rear door intrusion velocity was higher than that of the front door in both compact and midsize vehicles. In case of the compact vehicle, the level of intrusion velocity of front and rear door showed 3% and 10% increase respectively when the AE-MDB was utilized. In case of the midsize vehicle,

the level of intrusion velocity of front and rear door showed 8% and 29% increase respectively when the AE-MDB was utilized. Therefore, it is expected that the injury of rear dummy will be increased if the same rear dummies are used for side impact test on the basis of above results. According to recent EURO NCAP test procedures, it is noted that the Q10 and Q6 dummies will be seated on the rear seat. However, the injury criteria and limit of rear dummies are not fixed yet, so it is currently unclear to conclude regarding the rear dummy injuries.

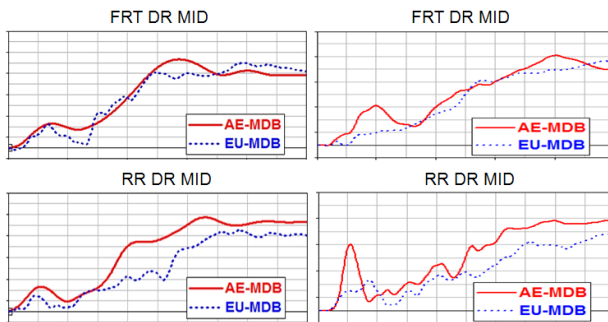


(a) Compact vehicle



(b) Midsize vehicle

Figure 10. Result of intrusion contour



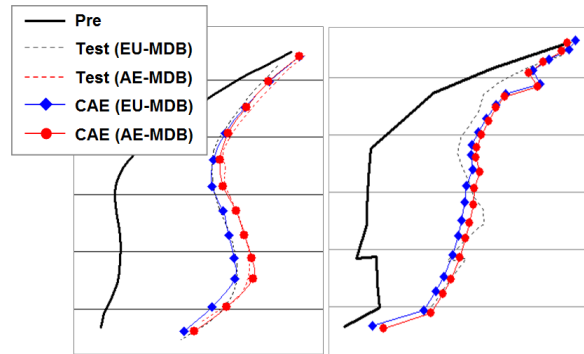
(a) Compact vehicle

(b) Midsize vehicle

Figure 11. Result of door intrusion velocity

The B-pillar profiles according to types of MDB are shown in Figure 12. The displacement of B-pillar was a little bit increased when the AE-MDB was utilized for

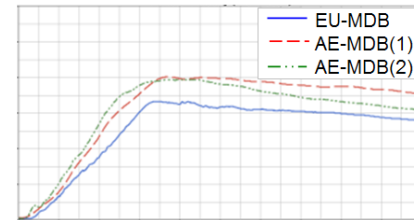
side impact analysis and test. Thus, the safety zone of the compact and midsize vehicles decreased 4.5% and 2% respectively. The safety zone means the distance between the center line of front seat and maximum deformed point of inner B-pillar. The curves of lateral velocity and the top view of the compact vehicle while impacting with EU-MDB and AE-MDB are shown in Figure 13. Due to the increased kinetic energy of the AE-MDB, the maximum lateral velocity of the compact vehicle increased by about 21.2% compared to the EU-MDB result, and the rotation angle increased as well. The left photo of Figure 13(b) is the EU-MDB result and the other is AE-MDB result. It is thought that the differences of velocity and angle result from the increased yaw moment as the AE-MDB target point moved 250mm rearward.



(a) Compact vehicle

(b) Midsize vehicle

Figure 12. Result of B-pillar profiles



(a) Lateral velocity of compact vehicle



(b) Top view of compact vehicle

Figure 13. Result of velocity and top view of test

Comparison of AE-MDB Deformation

The AE-MDB deformed shape and intrusion data of the compact vehicle are shown in Figure 14 and 15. The

result of FE model of AE-MDB showed valid correlation of deformed shapes. The most deformed B/E blocks in particular, which impacted the B-pillar, shows similar shapes with the test result. The FE model of AE-MDB also showed good correlation of deformed shape with the test result regarding fracture and face detachment on the D/F blocks. Above reported contents can be verified with the intrusion results of AE-MDB as shown in Figure 15. On the whole, the displacement curves of AE-MDB upper and lower blocks showed good fidelity between the test and CAE results. As a result, it is thought that the FE model of AE-MDB shows high degree of accuracy and fidelity as compared with test results.

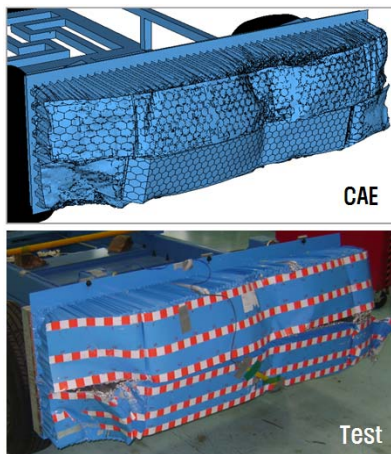


Figure 14. Comparison of deformed shape of AE-MDB between test and CAE results

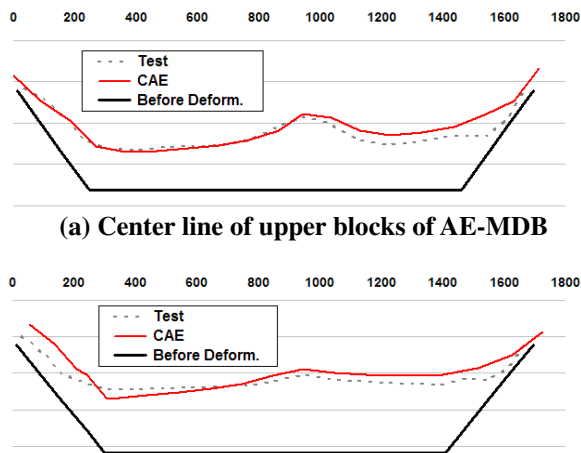


Figure 15. Comparison of displacement of AE-MDB between test and CAE results

Comparison of Dummy Injury

As of now, the exact assessment criteria and ratings of the World SID 50th percentile and Q10 and Q6

dummies are unclear. The injury assessment criteria and threshold of those dummies have not been decided yet according to recent test procedures with AE-MDB. Although it is difficult to calculate the ratings accurately, it is possible to compute and compare the results of normalized data based on the current regulation criteria of World SID 50th percentile dummy injuries as shown in Figure 16. In case of the compact vehicle, all the items except the pelvis resultant acceleration showed stable level, having normalized values lower than 50%. Meanwhile, the midsize vehicle showed that all the items except the pubic force have stable level, having normalized values lower than 50%. Consequently, it is expected that the equal ratings can be computed when the current level of assessment criteria is applied. However, if severe injury assessment criteria and threshold are enacted regarding the World SID 50th percentile and Q10 and Q6 dummies, the assessment results and ratings can be deteriorated. Thus, we are monitoring the modification of the injury assessment criteria and threshold closely.

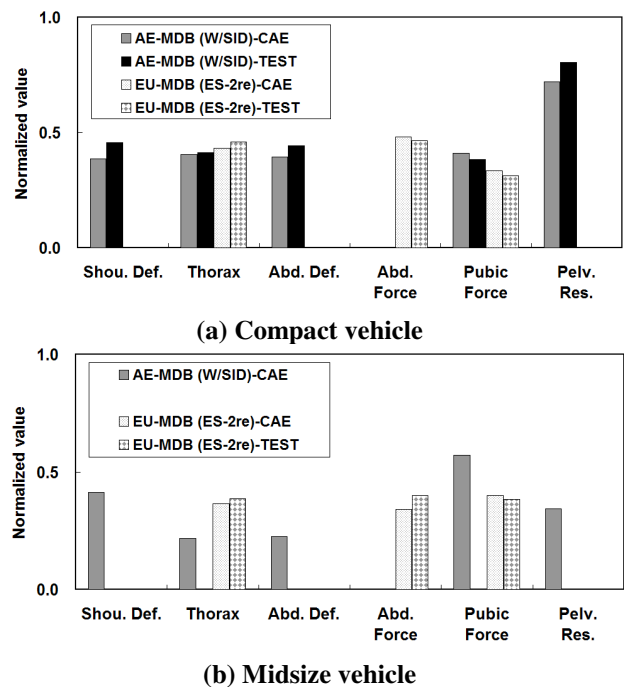


Figure 16. Comparison of dummy injury

CASE STUDY OF STRUCTURAL ENHACEMENT

In this section, a case study regarding the application of structural reinforcement concept was performed to retain larger safety zone and to diminish injuries of dummies. In this case study, the optimization process for weight reduction was not considered while enhancing the structural stiffness and strength. In Figure 17, the reinforcements on the B-pillar, door impact beam, rear floor and side sill were taken into

consideration to enhance the structural stiffness and strength with reducing the intrusions of vehicle structure. There are several ways to enhance the structural stiffness and strength such as increase of the thickness, exchanging of materials, modification of cross-sectional shape and installation of reinforcement, etc. In this case study, several items for enhancement were chosen from above methods. As a result, the weight of compact and midsize vehicle increased 3.9kg and 0.9kg respectively, for improved structure.

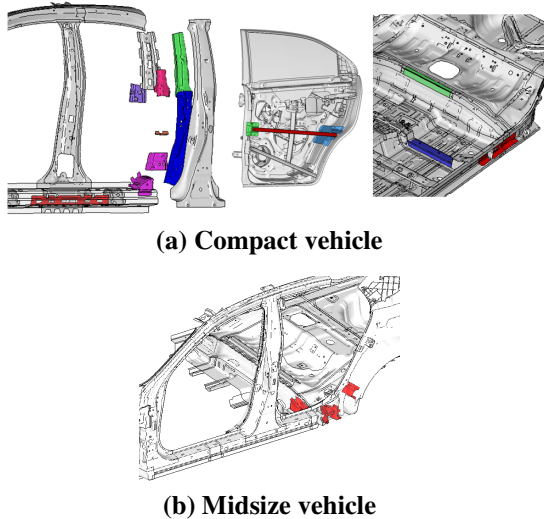


Figure 17. Concept of structural enhancement

The results of the case study are shown in Figure 18. As expected, the intrusion contour view of compact and midsize vehicle's exteriors are changed to somewhat lighter color compared to the baseline model. The structural safety zones of the compact and midsize vehicle also increased by 6% and 2.2% respectively.

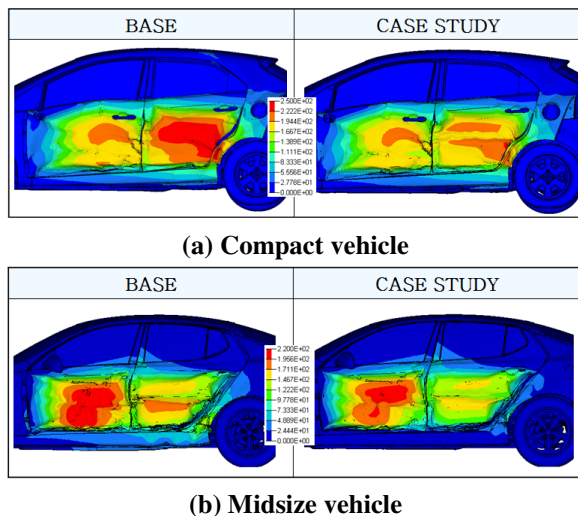


Figure 18. Result of intrusion contour of case study

The front and rear door intrusion velocity of the

compact vehicle decreased by 3.6% and 3.4% respectively and that of the midsize vehicle decreased 0% and 1.4% respectively. The normalized injury values based on the current regulation criteria of the World SID 50th percentile showed 0~10% decrease.

CONCLUSIONS

In this paper, advanced research of the AE-MDB was performed to cope with the enhanced EURO NCAP side impact test procedure which will be implemented after the year 2015. The summarized studies are as follows.

- (1) The detailed shell FE model of AE-MDB that satisfied all requirements of the test specifications was developed in order to use in the vehicle development process considering the EURO NCAP AE-MDB side impact test and simulation.
- (2) The structural safety zone of compact and midsize vehicles decreased by 4.5% and 2% respectively, and the rear door intrusion velocity increased by 10% and 29% respectively, when the AE-MDB was applied for simulation.
- (3) The case study showed that the reinforcements on the B-pillar, door impact beam, rear floor and side sill were effective in reducing the displacements of vehicle body and dummy injuries.
- (4) Further study of dummy injuries and restraint systems, paired with structural optimization should be going on after confirmation of the injury assessment criteria and threshold to enhance the ratings of EURO NCAP.

REFERENCES

- [1] "The Trend of Crashworthiness Regulation", Hyundai Motor Company Internal Report, 2012.
- [2] M. Edwards, D. Hynd, J. Carroll and A. Thompson, "Assessment of High Speed AE-MDB Test WorldSID with RIBEYE", ESV, 2011.
- [3] J. Ellway, "The Development of an AE-MDB Face", ESV, 2005.
- [4] Kim Bumjin, Kim Hyunwoo and Park Dongho, "The Development of AE-MDB CAE model", Hyundai Motor Group Conference, 2012.

ASSESSMENT OF A DYNAMIC TEST DEVICE TO EVALUATE VEHICLE ROLLOVER SAFETY

Fadi Tahan

Shai Cohen

Kennerly Digges

Cing-Dao (Steve) Kan

National Crash Analysis Center /The George Washington University

United States

Paper Number 13-0398

ABSTRACT

The objective of the Guided Rollover Propensity (GRP) test device is to subject vehicles and occupants to dynamic rollover accident conditions and to assess the performance of some of the active and the majority of the passive safety systems. The purpose of this study is to determine the characteristics of the rollovers produced by the GRP test device.

This study uses computer models to evaluate the GRP device's performance. The GRP device attempts to subject vehicles to repeatable initial conditions using a guided maneuver of a forward motion followed by a gradually increasing curvature sufficient to roll most vehicles. The decreasing radius of turn causes a gradual increase in lateral acceleration to a point where the vehicle rolls over. This motion is similar to a J-turn induced rollover with the exception of the increase of the turn curvature angle. The test vehicle is carried on a cart with a tripping edge to eliminate the possibility of the vehicle slipping off and to remove the influence of vehicle and road characteristics such as tire properties or road-surface friction during rollover initiation. The cart follows a guided track. The vehicle is subjected to its own roll characteristics that define the dynamics and consequently the roof-to-ground contact.

Finite element (FE) simulation results for different vehicles, subjected to GRP induced motion, show promising dynamic responses and rollover initiation consistency. The passive safety systems, such as roof structure and occupant containment systems (including airbag deployments), and vehicle mechanical systems, such as the vehicle suspension, were assessed under dynamic rollover loading. The dummies were subjected to rollover kinematics similar to a J-Turn and were used to assess injury protection and ejection mitigation during the dynamic rollover test. The study results

indicate that the test device is practicable and offers reasonable rollover conditions.

BACKGROUND

Rollover accidents make up only 2.4% of all vehicle crashes, but account for a disproportionate 33% of passenger vehicle occupant fatalities [1]. The Crashworthiness Data System (CDS), a database of the National Automotive Sampling System (NASS), years 1995 through 2005, shows that for belted front seat occupants, 33% of injuries scoring 3 or higher on the maximum abbreviated injury scale, including fatalities (MAIS3+F) occur in single vehicle rollovers without planar impact, while the remaining 67% occur in rollovers with a minor or moderate planar impact [2]. The data shows that the percentage of MAIS3+F injuries by body region with severe damage from planar impacts excluded is 33% to the Head, Face, Neck and Spine, 37% to the Chest and Abdomen, and 30% to the Pelvic, Upper and Lower Extremities [2]. Additionally, rollover data taken from the Crash Injury Research Engineering Network (CIREN) database over 10 years suggests that rollovers need to be disaggregated based on number of crash events in order to understand how to describe the scenario that led to the injury [3]. Thoracic injury, not just head and neck injury, and cervical spine injury mechanisms need to be considered in order to understand the injury causation during multiple event rollover crashes [3]. More recent data from years 2000 to 2009 of NASS-CDS for belted occupants in pure rollover crash accidents reveals serious injuries by Abbreviated Injury Scale (AIS) body region as follows: 36% to the spine, 23% to the thorax, 20% to the head, and the remaining to the upper and lower extremities, abdomen, face, and neck [4].

This injury list highlights that the roof crush is not solely responsible for all the injury mechanisms in a rollover; therefore a traditional dynamic rollover test device might not solve this complicated phenomena. Protection in a rollover should be a priority even if rollover is not the most frequent crash type since rollover injuries are so diverse and occupant

protection would benefit in other crash modes that are not included in the common planar tests (front, offset, oblique, and side impacts).

Existing Dynamic Rollover Test Devices

The National Highway Traffic Safety Administration (NHTSA) considers the development of a dynamic rollover test to be a priority [5]. Recent research has focused on understanding rollover accidents and their resulting occupant injuries. To date no dynamic rollover test method has been adopted to evaluate rollover safety and rollover occupant protection either in government safety standards or in consumer ratings. However, several dynamic rollover test devices have been used to address this topic. The most popular dynamic tests that have been widely used are: Federal Motor Vehicle Safety Standard (FMVSS) No. 208 Dolly Rollover test, Decelerated Rollover Sled (DRS) test, NHTSA Fishhook test, Corkscrew test, Inverted Vehicle Drop test, Controlled Rollover Impact System (CRIS) test, and Jordan Rollover System (JRS) test. Selected dynamic test systems are briefly mentioned herein with their operational details along with NHTSA observations on each one.

The FMVSS No. 208 dolly rollover test rolls a vehicle laterally off a moving inclined platform at 23 degrees. This test has been used extensively by the automotive industry. NHTSA mentioned that this test was originally developed only as an occupant containment test and not to evaluate the loads on specified vehicle roof components [5]. Additionally, after conducting many tests, NHTSA determined that the test conditions were so severe that it was difficult to identify which vehicles had better performing roofs [5]. The Decelerated Rollover Sled (DRS) test is another variation of the FMVSS No. 208 where the vehicle is placed horizontally on a cart, which decelerates it laterally to a specific pulse. The DRS can generate repeatable test conditions but the responses are highly sensitive to variations in the test conditions [6].

Other dynamic rollover systems closely examine the roof-to-ground event. The Controlled Rollover Impact System (CRIS) suspends a vehicle and rotates it laterally from the back of a semi-trailer equipped with a hanging fixture travelling at a fixed speed. CRIS was developed to produce repeatable vehicle and occupant kinematics for the initial vehicle-to-ground contact. Additional evaluation to the test procedure and further assessment of the repeatability following the initial contact are needed [5].

Other promising dynamic rollover test devices are being evaluated in the United States [7, 8] and Australia [9] based on the Jordan Rollover System (JRS) concept. The JRS mounts a vehicle on an axis that permits it to roll as it is dropped. The constraints with this mounting are in the longitudinal and lateral directions. As the vehicle is rotated, a roadway segment runs underneath so that the vehicle's roof strikes the road as it would in an actual rollover. After both sides of the roof have struck the roadway, the vehicle is caught so that it will sustain no further damage. The JRS is a versatile and repeatable rollover test system developed to evaluate the performance of roof structure and occupant restraint system during rollover. The CRIS and JRS test devices primarily control the roof crush in a dynamic way.

NHTSA believes that there is a large number of unresolved technical issues related to the JRS as performed by the Center for Injury Research. These issues are with respect to whether it would be suitable as a potential test procedure to replicate real-world crash damage patterns for a safety standard evaluating vehicle roof crush structural integrity. These issues include lack of real-world data to feed into the test parameters and dummies biofidelity [5].

NHTSA has initiated research toward achieving a dynamic test standard that provides a sufficiently repeatable test environment [5, 8]. NHTSA's principal research contractor for developing a dynamic rollover test is the University of Virginia. A Dynamic Rollover Test Device (DRoTS) as described by Kerrigan [10] has been installed and is now being operated by NHTSA's research contractor. This rollover test device employs concepts that were patented in the Jordan Rollover System (JRS) [11]. Additionally, the Australian government is funding the Dynamic Rollover Occupant Protection (DROP) project that uses an updated version of the initial JRS test device [9]. These two test devices are being evaluated. Some of the current research is focused on identifying the test parameters: initial roll rate, roll angle, drop height, road surface speed, and a test dummy to replicate some real world injuries.

NHTSA has also performed dynamic rollover tests based on selected maneuvers. NHTSA experimentally examined on-road untripped light vehicle rollovers [12]. These were vehicle characterization maneuvers (Pulse Steer, Sinusoidal Sweep, Slowly Increasing Steer, and Slowly Increasing Speed) and rollover propensity maneuvers (J-Turn, J-Turn with Pulse Braking, Fishhook # 1 and

2, and Resonant Steer). The repeatability of the steering controller handwheel inputs were found to be good for all maneuvers studied. Other measurements were also analyzed in this study [12].

Need for a New Rollover Test Device

Recognizing the shortcomings of the existing methods of testing occupant protection in a realistic dynamic rollover situation, this study combines the concepts addressed above and proposes a Guided Rollover Propensity (GRP) test device. The GRP test device enables a test vehicle to behave in a fashion similar to a real-life rollover, exposing the (dummy) occupant to realistic kinematics, loading the roof structure dynamically, and assessing the full- and partial-ejection and injuries of the occupants.

The GRP device consists of a railed track that is maneuvered similar to a specific forward J-turn with a carrying cart. The carrying cart has a tripping edge that eliminates the possibility of the vehicle slipping off prematurely. The GRP device removes the influence of any contaminating factors in the rollover, like vehicle and road characteristics such as tire properties or road-surface friction. As a result, the test will involve only rollover specific properties of the vehicles – for example, center of gravity, inertias, and suspension design – while subjecting all vehicles to similar rollover initial conditions. Therefore, the GRP device assesses the following parameters: vehicle rollover propensity, dynamic roof structure loading, occupant safety restraint systems, ejection epidemic, and dummy injuries.

METHOD

Vehicle Dynamic Analysis (VDA) software was used to evaluate variations in rollover initiation among different vehicles. Different vehicles follow different tracks and roll at different times and locations. The vehicle's suspension and inertia characteristics affect rollover initiation. The GRP test device was based on vehicle dynamic analysis and assessments. Then, a finite element (FE) model of the GRP test device was created, followed by a sensitivity study and an evaluation of three vehicle FE models.

The test development concept is addressed in this section. A dynamic vehicle handling simulation was performed using VDA software, the Human Vehicle Environment (HVE) by Engineering Dynamics Corporation. Several passenger vehicles were randomly selected and were subjected to the same speed and steering inputs (a linear acceleration

followed by an increasing turn radius with respect to time). The results showed that each vehicle traced a different curvature. The findings are not surprising since each vehicle has a unique weight, center of gravity (CG), inertia, tire characteristics, steering-rack ratio, suspension geometry, and design that influence the vehicle dynamics motion. HVE is capable of showing the tires' traces on the ground surface. The different traces' curvatures are shown in Figure 1. The vehicles with low CG heights, small wheel bases, and well designed suspensions had small curvatures while the vehicles with higher CG heights and longer wheel bases had larger curvatures.

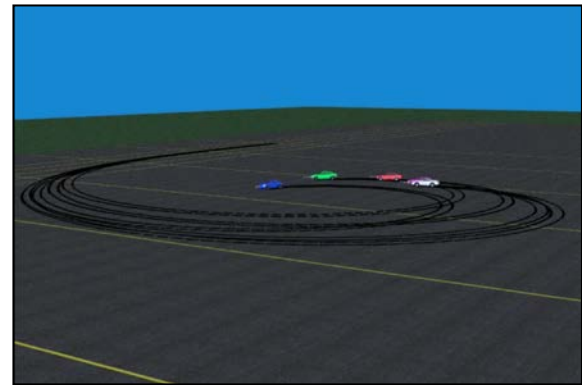


Figure 1. Multiple vehicles with different characteristics do not follow similar curvatures when subjected to motion similar to a J-turn maneuver.

The vehicle motion is similar to a J-Turn and the different traces shown in Figure 1 were expected. Two comparable vehicles were needed in order to achieve a similar path. The two vehicles selected from the HVE database were the Audi TT and the Mercedes-Benz C230. The TT and C230 models have similar weights, 1321.3 kg (2913 lbs) and 1416.6 kg (3123 lbs), and CG heights, 562 mm (22.16 in) and 572 mm (22.54 in), respectively. The same speed and steering input maneuver were performed and the tires' traces were tracked. Figure 2 shows the trace curvatures for each vehicle. Both curvatures are similar. It is observed that the C230 rolled sooner than the TT. The vehicle characteristics played a crucial part in determining when each vehicle rolled from the similar paths.

Therefore, if different vehicles were positioned on a carrying cart with an imposed track path, then the vehicles are subjected to the same input and the vehicles' abilities to resist rolling (i.e. leaving the track) and to protect the occupants can be tested. The GRP test device concept is shown in Figure 3. The

carrying cart subjects each vehicle to the same initial conditions. The track path has a gradually increasing curvature that is sufficient to roll most vehicles.

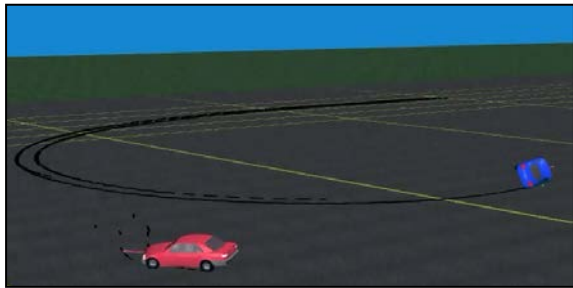


Figure2. Audi TT and Mercedes-Benz C230 have similar weight and CG height, follow similar curvature, but one rolls before the other.

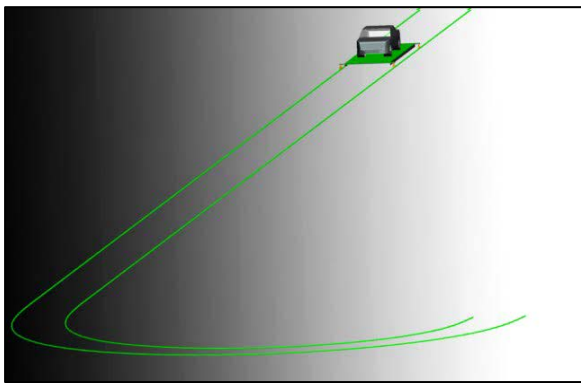


Figure3. GRP test device concept: track and cart design.

DISCUSSION

In order to evaluate the concept, FE analysis was performed. The commercial LS-DYNA software by Livermore Software Technology Corporation (LSTC) was used. The GRP test device concept was modeled initially with a simplified generic vehicle. Then three full scale FE models were analyzed. Finally, a Hybrid III dummy was incorporated in one of the full scale models.

Concept Simulation

The track curvature was taken from the HVE output based on similar vehicle characteristic simulation traces. The track is made of 3 sections. The first is a straight section, which allows the cart and the vehicle to accelerate and reach the designed test speed as the dummies remain seated in a natural position. The second section is a gradually increasing curvature.

The third is a straight section sufficient to allow cart braking after the vehicle rolls off it.

The cart is a simple platform, big enough to carry common passenger vehicles and Sport Utility Vehicles (SUV). The cart wheels follow the track curvature. The cart has a tripping edge, which has two benefits. First, it prevents the vehicle from falling off the cart during the acceleration phase of the test. Second, it prevents the vehicle from skidding off the cart while turning begins, reducing contaminating motions prior to the rollover of the vehicle, and improving the test device repeatability.

The simplified vehicle shown is based on a generic vehicle shape and property. The baseline model weighs 2392 kg (5273 lbs) and has a 2900 mm (114 in) wheel base, a 1550 mm (61 in) track width, and a 623 mm (24.5 in) CG height. The tires are made of elastic material and were rigidly connected to the vehicle body in order to eliminate suspension effects on the roll initiation. Figure 4 shows the FE assembly of the simplified vehicle, cart and the straight section of track. Figure 5 shows the FE assembly of the cart on the track alone. The cart assembly can be designed and installed at ground level to simulate a vehicle losing control on a horizontal plane or above ground level to simulate a vehicle losing control and rolling over in a ditch. The GRP test device parameters (the decreasing radius of curvature, cart height, and other specifications) will be addressed in future work to correlate to real-world crashes [13].

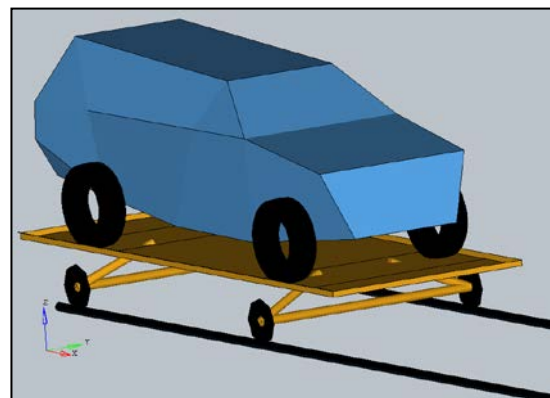


Figure4. GRP test device with a simplified vehicle.

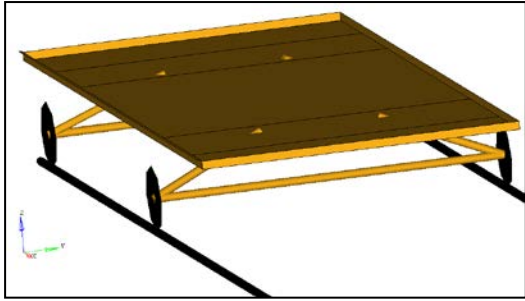


Figure 5. GRP cart with the wheels following the straight section of the track.

The cart is 203.4 mm (8 in) above the ground. The cart and vehicle were given an initial velocity of 20.1 m/s (45 mph, 72.42 km/h). The system starts to accelerate along the straight section of the rails until the initial speed is reached (only constant speed is simulated in FE). Thereafter, the system starts to travel on the curved rail section. The system longitudinal velocity starts to decrease while the lateral velocity starts to increase. Since the cart is only allowed to follow the prescribed track rails, the cart does not experience any vertical separation from the rails and its initial total speed is maintained throughout its motion. Since the vehicle is not attached to the cart, it starts to experience different kinematics. Additional to the longitudinal and lateral velocity changes, the vehicle starts to have an angular velocity component that eventually allows it to roll over the tripping edge of the cart. The vehicle and cart motions at different positions and times are shown in Figure 6. The simplified vehicle model starts to gain some lift off the cart starting at 1.5 seconds. At around 2 seconds, the vehicle completely separates from the cart and is in a free rollover motion.

Sensitivity Simulation

In order to illustrate the GRP test device sensitivity, the vehicle CG characteristics were changed from the simplified vehicle model used in the concept simulation. The CG height variations should affect the position on the curved section of the track at which the vehicle departs the cart. This location of departure is indicative of the vehicle's rollover propensity as it would be expected in real life. Two variations of CG heights were addressed by computer simulations. The first variation has a 152.3 mm (6 in) CG height lower than the original height position. The second variation has a 152.4 mm (6 in) CG height higher than the original height position.

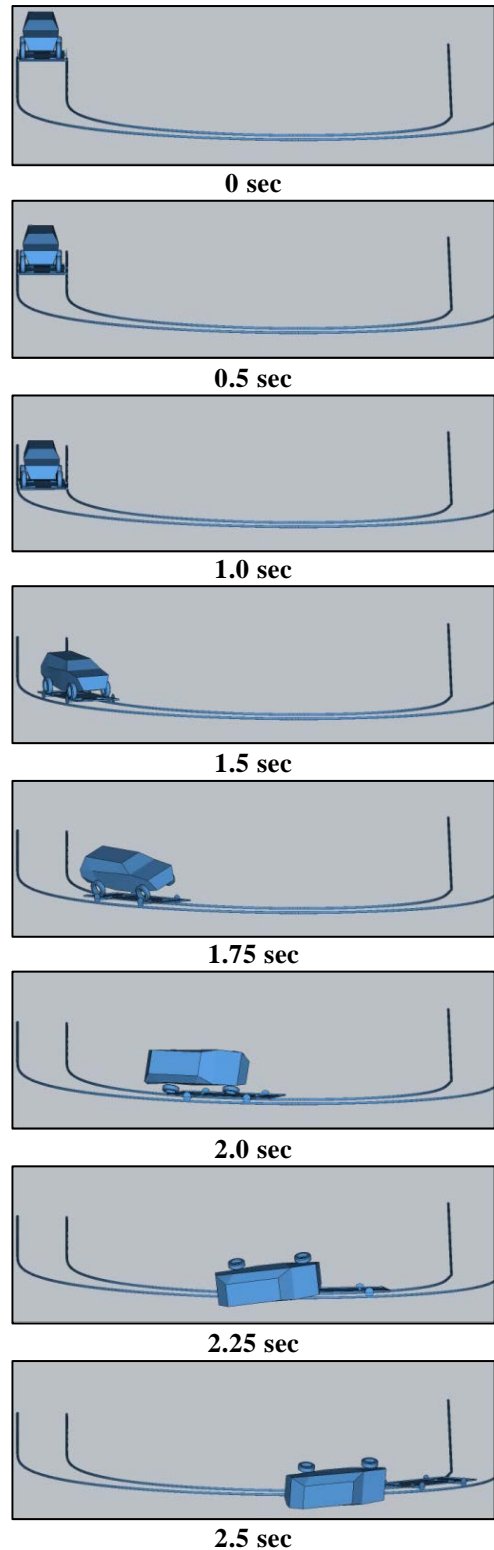


Figure 6. Simplified vehicle motion subjected to the GRP test device conditions up to 2.5 sec (note the additional pictures at the critical time between 1.5 seconds and 2.5 seconds).

The three models were given the same initial conditions as prescribed in the previous section. The models are overlaid and shown in red, blue, and green for the higher, the original, and the lower CG height positions respectively, as shown in Figures 7 and 8.

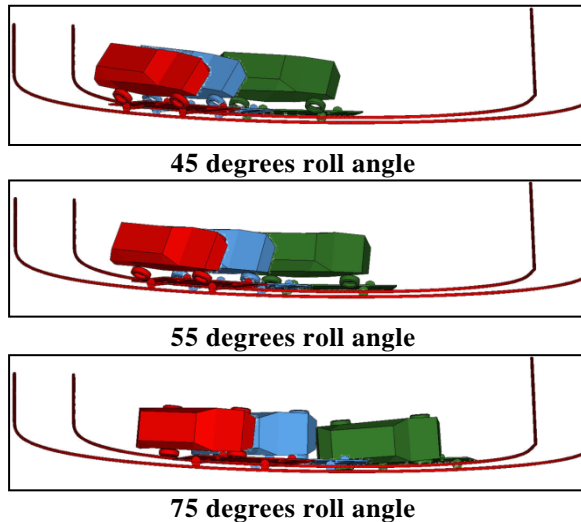


Figure 7. Selected simplified vehicle positions overlay horizontal view at vehicle roll angles of 45°, 55°, and 75°.

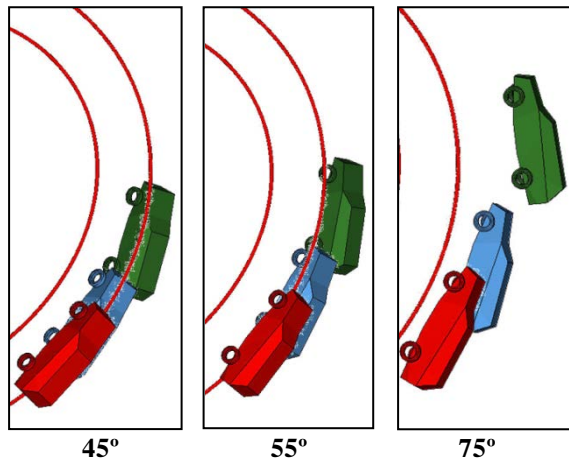


Figure 8. Selected simplified vehicle positions overlay top view at vehicle roll angles of 45°, 55° and 75°.

These figures show the models leaving the cart at the curvature section of the track with horizontal and top views. Three different roll angles are shown in order to distinguish the important vehicle positions. The first roll angle is 45° in, which shows the pre-roll position. The second roll angle is 55°, which shows that the CG position of the

original model is vertically above the near side tripping point. The third roll angle is 75°, which shows the models rolling over. The results shown in Figures 7 and 8 are based on roll angles rather than time since the 3 different vehicles have different CG heights and the roll angle is a good rollover prediction.

The different CG height models clearly show a distinction when each model leaves the cart. The longer the vehicle model stays on the cart, the better the stability performance is for the vehicle.

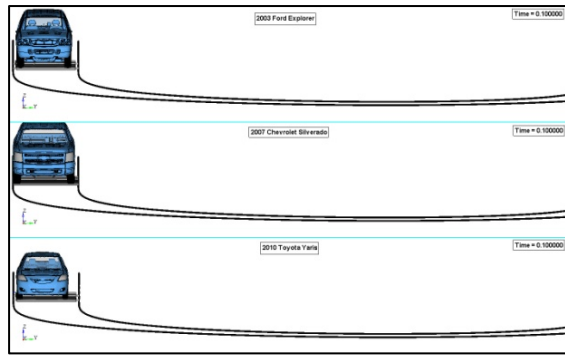
Full-Scale Simulation

The same test setup was used to perform the rollover analysis using full-scale FE vehicle models. Three models were selected: a 2003 Ford Explorer, a 2007 Chevrolet Silverado, and a 2010 Toyota Yaris. These models were developed for the Federal Highway Administration (FHWA) and the National Highway Traffic Safety Administration (NHTSA) by the National Crash Analysis Center (NCAC), the George Washington University. The models are available publicly on the NCAC website [14].

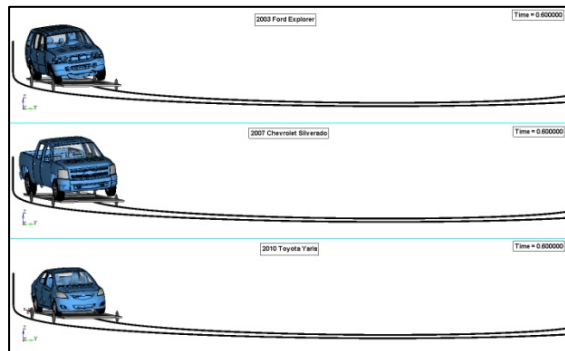
Since these models were validated to multiple planar crashes with rigid barriers, deformable barriers, movable deformable barriers, and roadside hardware barriers, the vehicle behaviors were assumed adequate for the GRP test conditions.

The three models are compared at the same time in Figure 9. The top section of each figure shows the Explorer model, the middle section shows the Silverado model and the lower section shows the Yaris model. Different timing was considered in Figure 9 in order to highlight the far side lift off from the cart, the vehicles completely leaving the cart, and several roof contact conditions.

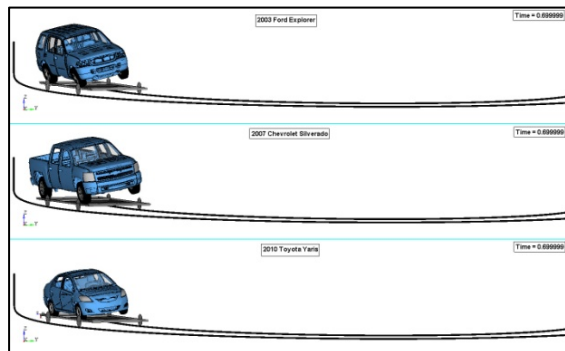
An interesting observation is seen in Figure 9 at 1.3 seconds. The three different vehicles have their own rollover characteristics that initiated the roll and that affected each model contact with the ground. The Explorer model contacts the ground at a low positive pitch angle while the other two models contact the ground at negative pitch angles. This observation is seen in some NASS-CDS cases in pure rollovers where vehicles have extended rear roof damage [15].



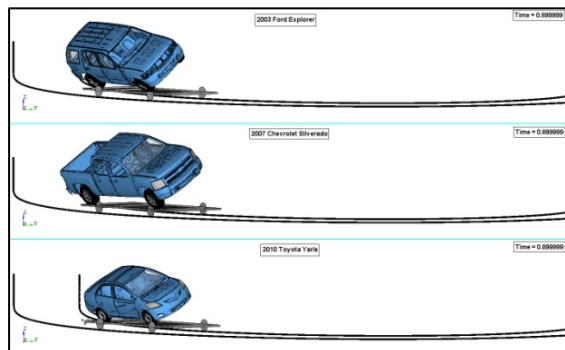
0.10 sec



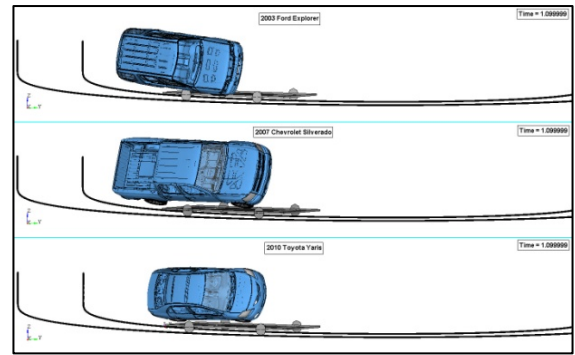
0.60 sec



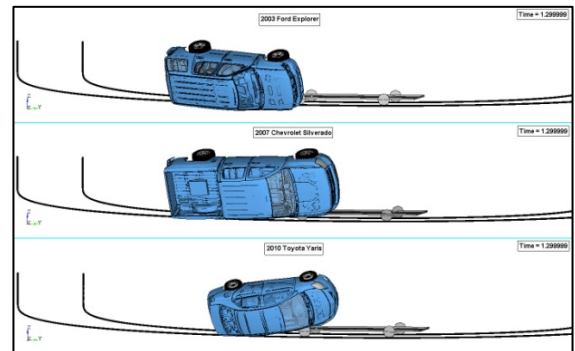
0.70 sec



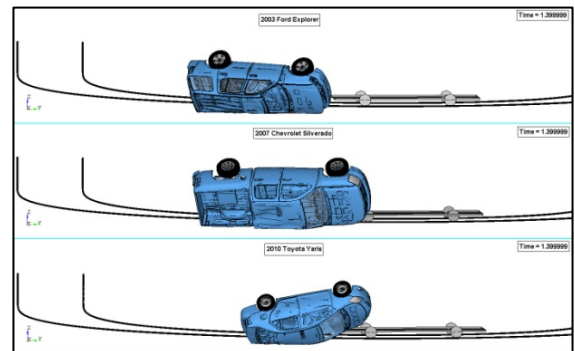
0.90 sec



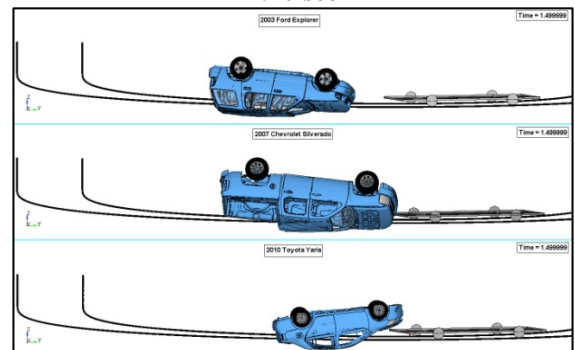
1.10 sec



1.30 sec



1.40 sec



1.50 sec

Figure9. Selected GRP simulations of a 2003 Ford Explorer, 2007 Chevrolet Silverado, and 2010 Toyota Yaris between 0.1 -0.9 sec.

Figure9. Selected GRP simulations of a 2003 Ford Explorer, 2007 Chevrolet Silverado, and 2010 Toyota Yaris between 1.1 -1.5 sec. (Cont.).

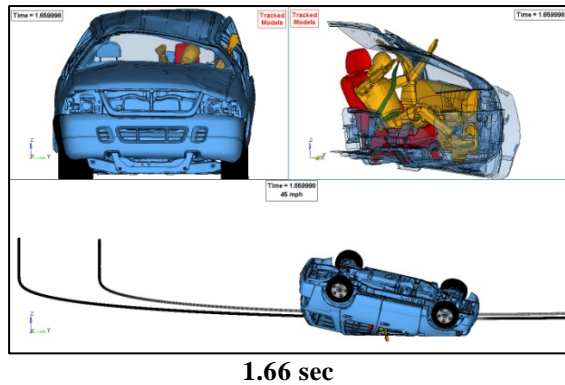


Figure 10. GRP simulation of a 2003 Ford Explorer with a Hybrid III Dummy at 1.66 sec. (cont.).

The dummy at 0.7 seconds, as shown in Figure 10, moves inboard inside the vehicle when the far side of the vehicle starts to lift off the cart. At 1.1 seconds, the dummy moves upward off the seat and outboard into the B-pillar. When the vehicle contacts the ground at its near side at 1.42 seconds, the dummy is at its highest position with respect to the driver seat. When the vehicle continues its roll and contacts the ground at its far side at 1.66 seconds, the dummy slams into the back of the seat. The dummy motion and impacts with the vehicle interiors correspond to real rollover accidents. This simulation demonstrates multiple injury potentials during rollovers.

Potential Rating System

The GRP test device can be used to produce a rollover rating score for vehicles similar to the Static Stability Factor (SSF) that is currently used by the New Car Assessment Program (NCAP) rollover star rating and the roof crush rating by the Insurance Institute for Highway Safety (IIHS). The GRP can produce a similar rating to the SSF. Figure 11 suggests that a vehicle should be rated based on the position that it leaves the track.

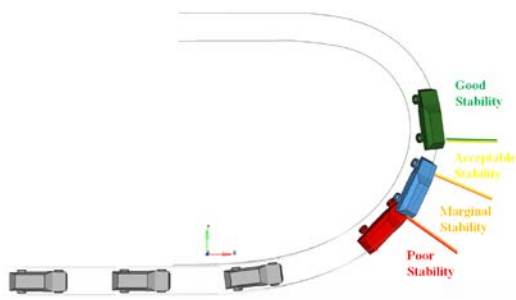


Figure 11. GRP test device rating proposal.

A rating system similar to the rating system used by the IIHS is recommended. Poor, Marginal, Acceptable, and Good stabilities are proposed based on when the vehicle leaves the cart and track system. In order to distinguish between SUV and passenger cars, two GRP rating systems should be created since the vehicles belong to different categories. Additionally, dummy injuries and ejection mitigation can also be assessed dynamically and rated. Finally, a comprehensive rollover rating can be based on all the ratings listed above in order to create an easy vehicle comparison score rating. Such a rating system should be thoroughly assessed in future work.

CONCLUSIONS

The Guided Rollover Propensity (GRP) test device subjects the vehicle to a forward motion followed by a gradually increasing curvature on a guided track that is sufficient to roll most vehicles. The forward motion is similar to pre-roll conditions in real world rollovers. The vehicle is positioned on a cart that follows the track and the vehicle is free to roll based on its roll inertial and other design properties. Computer simulations show that the initial conditions for rollover from the test cart are repeatable and the GRP test device is designed to eliminate conditions that would bias the rollover outcome.

Finite element methods used in this paper simulate the test device and the results show repeatable tests and promising rollover behavior of both vehicles and occupant kinematics.

Since pure rollover injuries are divided into three main categories (injury to the head and neck, to the spine, and to the thorax), rollover assessment should not only be based on roof strength (static or dynamic). Dynamic rollover assessment should be a comprehensive approach of the restraint system with the vehicle interiors during a realistic one full roll scenario additional to the dynamic roof crush. The proposed rating is an evaluation of multiple rollover characteristics in order to give a score to each vehicle.

The main limitation of the GRP test device is assessing the performance of the Electronic Stability Control (ESC). ESC is a notable rollover risk-reducer that can only be evaluated by driving maneuvers. Nevertheless, the GRP device may encourage manufacturers to produce better handling vehicles regardless of ESC.

The GRP test device has the advantage over several dynamic rollover test devices. It is a research tool that assesses the vehicle roof structure and occupant injuries at the same time in a dynamic rollover scenario. The GRP device can be used to evaluate all passive safety systems. An overall rating system is suggested.

ACKNOWLEDGEMENT

The authors would like to thank the Livermore Software Technology Corporation (LSTC) for providing the technical assistance in developing the guided cart motion. The authors would also like to thank the National Crash Analysis Center, at the George Washington University for providing the funds to carry out this research.

REFERENCES

[1] Strashny, A., "An Analysis of Motor Vehicle Rollover Crashes and Injury Outcomes," 2007, DOT HS 810 741.

[2] Digges, K. and Eigen, A.M., "Injuries in Rollovers by Crash Severities" in proceedings of the 20th International Technical Conference on Experimental Safety Vehicles, Lyon, France, 2007, Paper No. 07-0236.

[3] Ridella, S.A., Eigen, A.M., "Biomechanical Investigation of Injury Mechanisms in Rollover Crashes From the CIREN Database," in proceedings of the 2008 International IRCOBI Conference, Bern, Switzerland.

[4] Bambach, M.R., Grzebieta, R.H., and McIntosh, A.H., "Thoracic Injuries to Contained and Restrained Occupants in Single-Vehicle Pure Rollover Crashes," 2012, Accident Analysis and Prevention Journal, Volume 50, 2013, Pages 115–121.

[5] Office of the Federal Register. 2009. Federal Register, vol. 74, no. 90, pp. 22348-22393. (May 12, 2009) National Highway Traffic Safety Administration – Final rule. Docket no. NHTSA-2009-0093, RIN 2127-AG51; 49 CFR Part 571 – Federal Motor Vehicle Safety Standards, Roof Crush Resistance. Washington, DC: National Archives and Records Administration.

[6] Kerrigan, JR, Dennis, NJ, Parent, DP, Purtsezov, S, Ash, JH, Crandall, JR, and Stein, D. "Test System, Vehicle, and Occupant response Repeatability Evaluation in Rollover Crash Tests: The Deceleration Rollover Sled Test," 2011 International Journal of Crashworthiness, Vol. 16, Issue 6.

[7] Maddox, J., "United States Government Status Report," in the proceedings of the 2011, 22nd Enhanced Safety of Vehicles Conference, Washington, DC. Paper No. 11-465.

[8] U.S. DOT, NHTSA Cooperative agreement with University of Virginia - Center for Applied Biomechanics, Title: "Discretionary Cooperative Agreement to Support Biomechanical Research."

[9] Grzebieta, R., "Dynamic Rollover Occupant Protection" (DROP) Nov. 5, 2010, Australian Research Council, (LP110100069).

[10] Kerrigan, JR, Jordan, A, Parent, DP, Zhang, Q, Funk, J, Dennis, NJ, Overby, B, Bolton, JR, and Crandall, JR. "Design of a dynamic rollover test system," 2011, SAE Technical Paper 2011-01-1116.

[11] Friedman, K., and Hutchinson, J., "Review of Existing Repeatable Vehicle Rollover Dynamic Physical Testing Methods," in proceedings of the ASME 2008 International Mechanical Engineering Congress & Exposition. Paper No. IMECE2008-68751.

[12] Garrot WR, Howe JG, Forkenbrock G, "An Experimental Examination of Selected Maneuvers that may Induce On-Road Untripped, Light Vehicle Rollover – Phase II of NHTSA's 1997-1998 Vehicle Rollover Research Program." July 1999, DOT HS NRD-22, VRTC-86-0421.

[13] Shai, C., Tahan, F., Digges, K., Marzougui, D., Kan, C.D., "Design and Evaluation of a Guided Dynamic Rollover Test Device," in proceedings of the ASME 2013 International Mechanical Engineering Congress & Exposition, San Diego, CA. Paper No. IMECE2013-66170,

[14] National Crash Analysis Center, The George Washington University, 2003 Ford Explorer, 2007 Chevrolet Silverado, 2010 Toyota Yaris FE models. 2012, <http://www.ncac.gwu.edu/vml/models.html>

[15] Digges, K., Tahan, F., Grzebieta, R.H., Bambach M.R., Mattos, G.A., McIntosh, A.S., "Crash Damage Patterns Associated With Chest Injuries In Far-Side Rollovers", in the proceedings of the 2013, 23rd Enhanced Safety of Vehicles Conference, Seoul, South Korea. Paper No. 13-0066

[16] Tahan, F.J., Yan, L., Digges, K., "Selective Sensitivity Study of the Jordan Rollover System - Comparison with Un-Constrained Model," 2012 Transportation Research Board journal, TRB12-3779

[17] Tahan, F.J., Digges, K., "An Effect of the Initial Roll Angle on Vehicle Rollovers for Similar Drop Height," in proceedings of the 2012, International Crashworthiness Conference, Milan, Italy, Paper No. 2012-092.

INJURY RISK FOR CHILDREN AND ADOLESCENTS INVOLVED IN ROLLOVER CRASHES

Aditya Belwadi

Caitlin Locey

Matthew R. Maltese

Kristy B. Arbogast

The Center for Injury Research and Prevention, The Children's Hospital of Philadelphia
Philadelphia, USA

Rachel Hammond

Westat Biostatistics and Data Management Core, The Children's Hospital of Philadelphia
Philadelphia, USA
Paper Number 13-0408

ABSTRACT

Rollover crashes account for more than 33% of all motor vehicle related fatalities and have the highest fatality risk at 1.37% in the U.S. There is increased awareness of the high fatality rate associated with this crash type, but there is very limited pediatric-specific data related to rollover crashes in the United States. Previous studies based on data almost twenty years old have revealed that nearly ten percent of all children involved in motor vehicle crashes are in rollover crashes, with the risk of fatality and injury for children in rollovers being nearly twice that of non-rollover crashes. Recent focus on rollover mitigation has resulted in implementation of countermeasures, making it important to evaluate rollover risk for child occupants with a more current data set.

Thus, to provide a contemporary analysis of rollover crashes involving young people, we queried the National Automotive Sampling System's Crashworthiness Data System (NASS-CDS) from 1998-2011. Rollover crashes for passenger vehicles of model year 1998 or newer with at least one restrained occupant between 0 and 19 years of age were included. Occupant frequency was examined with number of quarter turns, vehicle type, vehicle specific rollover event, rollover type and direction, airbag deployment and Electronic Stability Control availability. Further, occupant age, restraint type, seating position, occupant role, and proximity to the roll direction were analyzed. Univariate and multivariate logistic regression models of MAIS 2+ and MAIS 3+ injury were built to establish the relationship between the key factors and the injury outcomes.

The study cohort consisted of 1560 occupants weighted to represent 515,470 occupants. Results indicate that children restrained in FFCSR or booster seats were less likely to sustain an MAIS 2+ injury than lap/shoulder restrained occupants in a rollover

crash. The abdomen was the most commonly injured body region at the AIS 2+ level while the head was most common at the AIS 3+ level, followed by the thorax and spine (for weighted data). However, for unweighted data, the head was the most commonly injured body region followed by the spine at the AIS 2+ level while the head was most common at the AIS 3+ level, followed by the thorax and upper extremities. The variations between the weighted and unweighted distributions points out some of the challenges with conducting child-specific analyses with NASS-CDS, as some cases have extremely high sample weights. Averages of 2.8-quarter turns were associated with an MAIS 2+ injury. Because there were limited cases with rollover mitigation technologies (ESC and airbags), their protective benefits in rollover crashes could not be ascertained.

INTRODUCTION AND BACKGROUND

Motor vehicle crashes (MVC) are the leading cause of unintentional injury deaths among ages 5-24 years in the U.S. (Centers for Disease Control, 2010). In 2010 alone, motor vehicle crashes killed 32,885 individuals (Traffic Safety Facts, 2012) and injured over 2.2 million others (NHTSA). Of these fatalities, 4,400 were occupants 0-19 years of age (WISQARS Fatal Injury Reports query, February 2013). Additionally, pediatric risk of exposure to motor vehicle crashes is significant because children and adolescents travel nearly as much as adults. Prevention of fatalities, injury, and disability associated with MVC must be a priority for ensuring our children's overall health.

Attention has been placed on understanding injury and fatality risk in rollovers for adult occupants due to the large percentage of fatalities attributed to this crash type. Although the number of rollover fatalities have decreased from 10,200 in 2005 to 7,600 in 2010 due to overall reduction in miles travelled combined with the adoption of mitigation technologies, the percentage of fatalities due to rollovers has increased

from 30.9% in 2000 to 34.5% in 2010 (NHTSA Traffic Safety Facts, 2012).

Research in the 1990's and early 2000's examined rollover risk for child occupants. Rivara et al. (2003) utilized NASS-CDS and Fatality Analysis Reporting System (FARS) datasets (data from 1993-1998) and found that nearly ten percent of all children in crashes experience a rollover, with the risk of fatality and injury for children in rollovers being nearly twice that of non-rollover crashes. In this analysis, when the data set was restricted to SUVs, there were more child occupants involved in rollovers (60%) than in non-rollover crashes because SUVs were 11 times more likely to be in a rollover than a passenger car (Rivara et al., 2003). A review of the FARS database (data from 1996-2006) by Viano and Parenteau (2008) identified rollovers as the most common crash type resulting in fatality (20.3%) for the 0-7 year-old. Data reviewed from the Partners for Child Passenger Safety dataset (data from 1998-2005) showed the risk of injury to occupants 0 to 15 years of age was more than 6 times higher in rollover crashes compared to other crash modes (Kallan et al., 2006). Daly et al. (2006) studied child occupants in SUVs and passenger cars in all types of crashes (data from 2000-2003) and found an equivalent risk of injury for children in the two vehicle types. The authors suggested that despite a seeming advantage for SUVs due to being on average more than 1,300 pounds heavier, this advantage was offset by several factors--primarily a rollover risk nearly two and a half times higher compared to that of passenger cars.

Vehicle manufacturers and restraint suppliers have responded to the heightened awareness of increased fatality and injury risk associated with rollover crashes. They have introduced improved technology such as Electronic Stability Control (ESC), Roll Stability Control (RSC), as well as the improvement of advanced restraints such as frontal and side airbags. In addition, in 2003 NHTSA began evaluating rollover resistance in its NCAP program, spurring design changes by vehicle manufacturers in order to improve their NCAP evaluations. With these vehicle specific changes, there is a need to examine more recent data to understand the risk of injury (both overall and body region specific) in rollover crashes for children 0-19 years of age.

The objective of this project was to estimate AIS 2+ and AIS 3+ risk of injury for children and adolescents 0 to 19 years of age involved in a rollover crash using the NASS-CDS dataset from 1998 through 2011.

METHODS

The National Automotive Sampling System's Crashworthiness Data System (NASS-CDS) was the primary data source for this study. The NASS-CDS dataset provides detailed information for a random sample of motor vehicle crashes ranging in severity from minor to fatal. Approximately 5,000 cases per year are collected from Primary Sampling Units (PSU's) across the United States. A trained crash investigation team gathers information about the crash by visiting the impact location and inspecting and photographing the involved vehicles. Restraint usage and occupant contact locations are determined from a close examination of the vehicle interior. Occupant characteristics such as age, anthropometry, and injury are ascertained by interviewing the crash victims and reviewing police and emergency medical service reports and medical records. Individual cases are weighted (based on the NASS-CDS weighing factors) to represent the entire U.S. population.

To create the study cohort, cases were gathered from the NASS-CDS dataset using the following inclusion and exclusion criteria:

Inclusion Criteria:

- Passenger vehicle or light truck (GVWR <10,000 lbs /4536 kg)
- Model year 1998 or newer
- Vehicle involved in a rollover event (number of quarter turns ≥ 1 or end-over-end)
- Occupant age 0-19 years

Exclusion Criteria:

- Occupant unrestrained or unknown if restrained

MAIS 2+ and MAIS 3+ Injury risks were examined overall and stratified by the following vehicle-based and occupant-based variables (Table 1 and Table 2):

Table 1: Stratification– Vehicle Based

Variable of Interest	Values
Quarter Turns	1 through 16, End-Over-End
Vehicle Type	Minivan/van, Passenger Car, Pickup/Light Truck, SUV
Vehicle Specific Event Number	1 (Single Vehicle Single Event) and >1
Rollover Type and Direction	Longitudinal (Left Sided, Right Sided), End-Over-End
Airbag Deployment	Deployed During Crash, Deployed (Details Unknown), No Deployment
ESC Availability	Standard, Not Available, Optional, Unknown

Primary vs. Principal Rollover Event-- A “Vehicle Specific Event Number” variable was derived from the NASS-CDS “event” table. Because crashes are often complicated and may involve several vehicles in addition to the case vehicle, the event count can include events in which the case vehicle was not involved. Thus, “Vehicle Specific Event Number” is the rollover event number when only events in which the case vehicle was involved were counted. If vehicles had more than one rollover event, the first rollover event number was used. For cases with Vehicle Specific Event Numbers equaling one, the rollover is considered the “primary” event. It is important to note that a “primary” rollover is not necessarily a single-vehicle/single-event type crash as subsequent events may happen after rollover.

Within the NASS-CDS “VE” (Vehicle Exterior) table, crash events are ranked by severity using delta-V and damage extent. For crashes in which the most harmful event (i.e. “event of greatest delta V”) was a non- collision rollover with the object contacted indicated as “overturn – rollover (excludes end-over-end)” or “rollover – end-over-end”, the rollover is considered to be the “principal” event; that is, the rollover is the most severe event in the crash. For crashes where rollover is the primary event, it is also possible that the rollover is the principal event.

Airbag-- The availability and deployment of any airbag by occupant seating position is summarized by the variables “Air Bag Availability” and “Air Bag Deployment”. However, while these variables give an overview of airbag for the case occupants they do not provide information regarding type of airbag or deployment event. Beginning in 2000, NASS-CDS incorporated an expanded dataset of detailed airbag information, found in the “airbag” and “bagseat” tables. Specific availability and deployment details were gathered for each airbag location (e.g., steering wheel hub, top instrument panel, roof side rail, seat back), rather than combining all airbag information by seating position. Use of this data allows investigators to capture whether multiple airbags were available for each occupant, what type, and whether all or some of these deployed. This detailed airbag information was included in this analysis for case years 2000-2010.

ESC -- Electronic Stability Control (ESC) availability was determined for vehicles of model year 2005 and newer using information released by NHTSA’s [safercar.gov](http://www.safercar.gov) website (<http://www.safercar.gov/Vehicle+Shoppers/Resources/Vehicles+with+ESC>). Vehicle year, make, and model fields were matched to the NASS-CDS data,

and vehicles were assigned an ESC availability of “standard”, “optional”, or “not available”. Vehicles with model year prior to 2005 or vehicles that did not have an exact match between the datasets were given an ESC availability of “unknown”.

Table 2: Stratification– Occupant/Restraint Based

Variable of Interest	Values
Age Group (years)	0-2, 3-5, 6-8, 9-15, 16-19
Restraint Type	Rear Facing Child Restraint System (RFCRS), Forward Facing Child Restraint System (FFCRS), Booster Seat, Lap Belt only, Lap-Shoulder Belt
Seating Position	Front (Left, Center, Right), Row 2 (L, C, R), Row 3 (L, C, R), Row 4 (R)
Occupant Role	Driver, Passenger
Side of Seating Position vs. Roll Direction (Sidedness)	Center, Far side, Nearside, End-Over-End

Occupant Variables-- Occupants were assigned to an age group by age in years. Restraint type was determined by combining the expanded “childseat” dataset and the manual and automatic belt use variables. Seating position was summarized by side of the vehicle (left, center, right), and row number, with row 1 considered the “front row” and rows 2-4 considered as the “rear rows”. Sidedness, or side of seating position vs. roll direction, examined the relationship between seating position side and direction of longitudinal roll. For example, an occupant seated in the rear left in a left sided rollover was considered nearside. Center-seated occupants in any row were classified as “center” regardless of roll direction.

Statistical Analysis -- Results of logistic regression modeling were expressed as adjusted/unadjusted odds ratios with corresponding 95% CI. Because injury is a relatively rare event, the odds ratio can be interpreted as a good estimate of relative risk. Summary statistics were calculated using sampling weights available from the NASS-CDS database using the survey functions in SAS, version 9.2 (SAS Institute, Cary, NC). All analyses were conducted using weighted data and variance estimates were calculated to account for the complex sampling methodology. Univariate logistic regression models were created to determine the association between variables of interest and MAIS 2+ and MAIS 3+ outcomes. A multivariable model was fit to include the covariates determined to be significant with a p-value <0.10 in the univariate models. A final model

consisted of all factors that were associated with the outcome in the multivariable model with a p-value <0.05. Bivariate analyses were employed to examine the relationship between study variables, where we chose to include only one covariate in the multivariable model if any bivariate relationships were statistically significant. The weighted estimates were calculated as either means or proportions, with the associated 95% confidence intervals (CI) and standard errors (SE).

RESULTS AND DISCUSSION

Analysis of Rollover Events – Vehicle Based

2407 occupants aged 0-19 years in a passenger vehicle of model year 1998 or newer in a rollover collision were identified. 847 of these occupants had a restraint status of “unrestrained” or “unknown if restrained” and were subsequently excluded from the dataset. 1560 occupants met the inclusion and exclusion criteria, equating to 515,470 occupants when weighted.

Of the 1560 occupants, 8.0% involved minivans or large vans, 38.7% involved passenger cars, 16.6% involved pick-up and light trucks, and 36.8% involved SUV’s (Table 3). It was interesting to observe an almost equal distribution between passenger cars and SUV’s.

Table 3: Distribution by Vehicle Type

Vehicle Type	Unweighted Occupants	Weighted Occupants	Weighted Percent (%)	SE of %
Minivan/Van	146	41,047	8.0	3.7
Passenger Car	544	199,240	38.7	6.4
Pickup/Light Truck	214	85,578	16.6	5.0
SUV	656	189,605	36.8	8.5

Prior to 1997, NASS reported the extent of the rollover by partitioning the number of quarter-turns into five categories - 1, 2, 3, 4+ and end-over-end. After 1997, a larger number of categories have been recorded. To aid comparison with the literature, Table 4 summarizes cases up to 16-quarter turns along with end-over-end cases (which occur about the horizontal axis of the vehicle). However, in the injury risk analysis, end-over-end cases were not included as data was analyzed continuously for quarter turns 1 through 16.

26.2% of cases had only one-quarter turn while 33.7% had at least one complete roll (4 quarter turns).

73.6% of the cases had at least two-quarter turns. End-over-end rollovers were rare, accounting for only 0.2% (9 cases unweighted) of the distribution. Bedewi et al. (2004) and Hu et al. (2008) hypothesized that two or more quarter turns may expose the roof to ground contact and thereby the occupant to roof contact.

Table 4: Distribution by Quarter Turns

Quarter Turns	Unweighted Occupants	Weighted Occupants	Weighted Percent (%)
1	295	135,239	26.2
2	419	155,704	30.2
3	104	49,219	9.5
4	381	120,401	23.4
5	66	11,473	2.2
6	161	27,186	5.3
7	22	2,411	0.5
8	60	9,368	1.8
9	12	561	0.1
10	18	1,713	0.3
11	3	195	0.0
12	8	630	0.1
16	2	40	0.0
End-Over-End	9	1,203	0.2

26.2% of cases had only one-quarter turn while 33.7% had at least one complete roll (4 quarter turns). 73.6% of the cases had at least two-quarter turns. End-over-end rollovers were rare, accounting for only 0.2% (9 cases unweighted) of the distribution. Bedewi et al. (2004) and Hu et al. (2008) hypothesized that two or more quarter turns may expose the roof to ground contact and thereby the occupant to roof contact.

In 70.1% of the cases, the rollover was not the first event in the crash (Table 5). Of the 564 cases (unweighted) in which the vehicle specific event number was equal to one, 475 cases had rollover as the most severe event. Note: 411 were single vehicle single event rollover crashes, i.e., pure rollovers (Bose et al. 2011, Crandall et al. 2011). The other 153 cases were those which had subsequent planar events after the initial rollover. Of the 996 crashes (unweighted) in which vehicle specific event number was greater than one, 456 cases had the rollover event as the event of greatest severity.

Table 5: Distribution by Vehicle Specific Event Number

Vehicle Specific Event Number	Unweighted Occupants	Weighted Occupants	Weighted Percent (%)	SE of %
1	564	153,886	29.9	7.1
>1	996	361,584	70.1	7.1

The distribution of occupants by occupant role is given in Table 6. Rolls towards the driver's side accounted for 60.4% of overall rollover crashes, while rolls towards the passenger side occurred in 39.3%. Further, when the occupant seating position was compared to the roll direction, the distribution was 55.9% nearside to roll while 30.9% were far sided. In contrast, for adult drivers, roll direction was evenly divided between left and right (Bedewi et al. 2004, Hu et al. 2008).

Table 6: Distribution by Rollover Type, Direction, Occupant Role with Sidedness

	Unweighted Occupants	Weighted Occupants	Weighted Percent (%)	SE of %
Rollover Type and Direction				
End-Over-End	9	1203	0.2	0.1
Longitudinal	1551	514,267	99.7	0.1
Left-Sided	850	311,299	60.4	2.9
Right-Sided	701	202,969	39.3	2.8
Occupant Role				
Driver	489	219,160	42.5	6.5
Passenger	1071	296,310	57.4	6.5
Sidedness				
Center	127	64,620	12.5	5.3
Far side	679	159,751	30.9	6.8
Nearside	731	288,309	55.9	3.2
Other/Unknown	14	1,587	0.3	0.21
End Over End	9	1,203	0.2	0.15

Table 7 describes the availability and deployment conditions for airbags in included cases. 61.0% of occupants had at least one airbag available in their seating position. This included both frontal airbags as well as side and curtain airbags typically thought to be rollover countermeasures. In 52.5% of these cases, there was no deployment at any time during the crash. Only in 7.9% of crashes was there an airbag deployment. However, because delta-v is not calculated for non-horizontal rollover events, it is extremely challenging to interpret the lack of deployment in those 592 cases. Detailed airbag

information from the dataset including the type of airbag deployed (Bottom Instrument Panel, Door Panel, Mid - Instrument Panel, Roof Side Rail, Seat Back, Steering Wheel Hub, Top Instrument Panel, and Any Air Bags Deployed) for included cases falling within the 2000-2010 case years are listed in Table A1 under Appendix A.

Table 7: Distribution by Airbag Availability and Deployment

Airbag	Unweighted Occupants	Weighted Occupants	Weighted Percent (%)	SE of %
Airbag Availability				
Any Available	838	314,701	61.0	2.4
Disconnected	6	524	0.1	0.0
Not Reinstalled	1	10	0.0	0.0
Not Collected	8	1,551	0.3	0.1
Not Equipped	707	198,684	38.5	2.4
Airbag Deployment				
Deployed	233	41,204	7.9	2.5
Not Deployed	592	271,086	52.5	4.0
Deployed, details unknown	4	1,183	0.2	0.2
Unknown	9	1,228	0.2	0.1

In order to have a better understanding whether rollover was indeed the principal event, Table 8 lists the events of highest and second highest delta-v. 73.2% of the cases had rollover as the event of highest delta-v.

Table 8: Distribution by Rollover as the Principal Event

	Unweighted Occupants	Weighted Occupants	Weighted Percent (%)	SE of %
Rollover is Event of Highest Delta V	843	377,336	73.2	4.1
Rollover is Event of 2nd Highest Delta V	467	89,872	17.4	3.1
Other Event is Event of Highest Delta V	170	35,745	6.9	1.5
Rollover Severity Unknown	80	12,517	2.4	0.3

With the proliferation of ESC in the vehicle fleet, (all model year 2012+ vehicles under 10,000 lbs gross vehicle weights are equipped with ESC), Table 9 lists

the availability of ESC as standard equipment in the NASS-CDS dataset reviewed. Prior to vehicle model year 2005, a comprehensive list of vehicles with ESC was not available. 302 cases (unweighted) out of the 1560 rollover cases reviewed (vehicle model year 2005 onwards) could be linked to the safecar.gov list of vehicles with ESC. 23.8% (unweighted) of those 302 cases had ESC as standard equipment while 54.9% did not have them. 21.2% of the cases had ESC listed as “optional” for the corresponding vehicle make, model, and year; however, there was no data available within the NASS-CDS dataset to ascertain whether ESC was installed or used for these vehicles.

Table 9: Distribution by ESC Availability

ESC Availability	Unweighted Occupants	Weighted Occupants	Weighted Percent (%)	SE of %
Standard	72	14,484	2.8	1.5
Not Available	166	30,653	5.9	1.2
Optional	64	10,434	2.0	0.7
Unknown	1258	459,898	89.2	2.7

Analysis of Rollover Events – Occupant and Restraint Based

Of the cases examined, 53.4% were occupants 16-19 years of age. Nearly 20% of the cases were occupants 9-15 years of age, followed closely by occupants 6-8 years of age (15.6%). Table 10 shows the complete distribution by age range.

Table 10: Distribution by Age

Age (years)	Unweighted Occupants	Weighted Occupants	Weighted Percent (%)	SE of %
0-2	150	27,929	5.4	0.8
3-5	146	29,079	5.6	1.1
6-8	115	80,501	15.6	4.8
9-15	328	102,585	19.9	6.7
16-19	821	275,376	53.4	5.0

Despite approximately 27% of the occupants being less than 9 years of age and likely of the size for which a child restraint system (CRS) is required, only 14.1% were restrained in some type of CRS (including RFCRS, FFCRS, or booster seats) (Table 11). The lap shoulder belt was the most common form of restraint (81.9%).

Table 11: Distribution by Restraint Type

Restraint Type	Unweighted Occupants	Weighted Occupants	Weighted Percent (%)	SE of %
RFCRS	33	5672	1.1	0.3
FFCRS	120	21,458	4.2	1.5
Booster Seat	56	45,549	8.8	5.7
Lap Belt	60	7,075	1.4	0.6
Lap/shoulder Belt	1220	422,062	81.9	4.6
Unknown/Other CRS	61	11,945	2.3	0.4
Unknown/Other Belt	10	1,708	0.3	0.1

With respect to occupant seating position (Table 12), front left/driver (42.5%) and front right (18.9%) were the most common locations while all seating positions in the rear rows had a similar frequency (approximately 12%).

Table 12: Distribution by Seating Position

Seat Position	Unweighted Occupants	Weighted Occupants	Weighted Percent (%)	SE of %
Front Left (driver)	489	219,160	42.5	6.5
Front Middle	12	854.087	0.2	0.0
Front Right	364	97,626	18.9	5.1
Rear Rows Left	269	66,631	12.9	3.8
Rear Rows Middle	115	63,766	12.4	5.3
Rear Rows Right	297	65,847	12.8	3.7
Other/Unknown	14	1,587	0.3	0.2

*Note: Rear rows are a combination of the second, third and fourth rows

Injury Analysis

Injury risk was investigated using the Abbreviated Injury Scale (AIS, AAAM, IL) maximum score (MAIS) of 2+ and 3+ as outcomes. 1027 of the included 1560 occupants (unweighted) sustained at least one injury scoring AIS 1-7 (AIS 7 indicates injured, unknown severity); 4005 unique injuries (unweighted) were sustained. For all included case occupants, the odds of an MAIS 2+ injury was 5.5%, and the odds of an MAIS 3+ injury was 2.0% in rollover crashes.

Univariate logistic regression models were created to determine the association between variables of interest and MAIS 2+ and MAIS 3+ outcomes. Tables 13 through 16 list only those variables, which have a significant association with the outcomes.

The remainder of the variables (Vehicle Type, Rollover Direction and Sidedness) had no significant outcomes.

Table 13 lists the odds ratio for MAIS 2+ and MAIS 3+ injury for restraint type based on a univariate logistic regression model. Lap/shoulder belt was used as the reference group. For MAIS2+ injury risk, those in booster seats and FFCS had a significantly lower risk of the injury compared to those in lap shoulder belts while those in lap belts were 4.5 times more likely to be injured. For MAIS 3+ injury, only the elevated risk in lap belts remained.

Table 13: Odds ratio for MAIS 2+ and MAIS 3+ Injury for Restraint Type

Restraint Type	Outcome	Odds Ratio	LCL	UCL	P-Value
Booster Seat	MAIS 2+	0.14	0.02	0.93	0.042
	MAIS 3+	0.32	0.04	2.64	0.288
FFCRS	MAIS 2+	0.32	0.19	0.55	<.0001
	MAIS 3+	0.78	0.43	1.42	0.412
Lap Belt	MAIS 2+	4.55	1.94	10.66	0.001
	MAIS 3+	8.23	1.89	35.80	0.005
RFCRS	MAIS 2+	0.71	0.11	4.66	0.724
	MAIS 3+	1.03	0.11	9.30	0.979
Lap/shoulder Belt	MAIS 2+	1.00	--	--	--
	MAIS 3+				

*LCL = Lower Confidence Limit; UCL=Upper Confidence Limit

Examining age group, those occupants aged 0-2 and 6-8 years had a significantly lower risk of MAIS 2+ injury compared to the 16-19 year olds (Table 14). None of the MAIS3+ results for age was statistically significant.

Table 14: Odds ratio for MAIS 2+ and MAIS 3+ Injury for Age Group

Age Group	Outcome	Odds Ratio	LCL	UCL	P-Value
0-2 years	MAIS 2+	0.23	0.08	0.67	0.008
	MAIS 3+	0.56	0.20	1.56	0.266
3-5 years	MAIS 2+	0.77	0.34	1.75	0.536
	MAIS 3+	1.11	0.55	2.22	0.775
6-8 years	MAIS 2+	0.33	0.12	0.95	0.041
	MAIS 3+	0.24	0.04	1.49	0.125
9-15 years	MAIS 2+	0.42	0.14	1.24	0.114
	MAIS 3+	0.95	0.32	2.77	0.918
16-19 years	MAIS 2+	1.00	--	--	--
	MAIS 3+				

For occupant seating position, the front right (2.3x) and front center (4.5x) had a statistically significant increase in MAIS2+ injury risk compared to the rear row left. It was interesting to note that for the front left seating position (i.e. the driver), we could not detect a difference compared to the rear row left (Table 15).

Table 15: Odds ratio for MAIS 2+ and MAIS 3+ Injury for Seating Position

Seating Position	Outcome	Odds Ratio	LCL	UCL	P-Value
Front Left	MAIS 2+	1.99	0.88	4.54	0.100
	MAIS 3+	1.35	0.45	4.11	0.594
Front Center	MAIS 2+	4.55	1.39	14.88	0.012
	MAIS 3+	4.64	0.55	39.22	0.159
Front Right	MAIS 2+	2.29	1.15	4.57	0.018
	MAIS 3+	1.86	0.74	4.67	0.186
Rear Rows Center	MAIS 2+	0.73	0.12	4.46	0.736
	MAIS 3+	1.04	0.09	12.22	0.975
Rear Rows Right	MAIS 2+	1.45	0.69	3.07	0.328
	MAIS 3+	0.82	0.20	3.35	0.783
Rear Rows Left	MAIS 2+	1.00	--	--	--
	MAIS 3+				

For every one unit increase in quarter turns, the odds of having an MAIS 2+ injury increased by 33% (p<0.0001) (Table 16). Similar finding were seen for MAIS 3+ injuries. An average of 2.8-quarter turns (2.33-3.19), was associated with an MAIS 2+ injury.

Table 16: Odds ratio for MAIS 2+ and MAIS 3+ injury for Quarter Turns

Quarter Turns	Outcome	Odds Ratio	LCL	UCL	P-Value
	MAIS 2+	1.33	1.28	1.42	<.0001
	MAIS 3+	1.45	1.21	1.57	<.0001

For injured occupants, the distribution of injuries by body region for AIS 2+ and AIS 3+ injury severity were tabulated. From Table 17, for all AIS 2+ injuries the abdomen was the body region with the highest proportion of injuries (44.6%) followed by the head (21.6%). However, for unweighted percentages, the body region making up the highest proportion of injuries was head (44.6%) followed by the spine (17.1%) and upper extremities (12.7%).

For AIS 3+ injuries, the head was the number one body region at 37.4% of the injuries, followed by the thorax (20.7%) and spine (17.9%). For unweighted percentages, the body region making up the highest

proportion of injuries was head (48.1%) followed by the spine (20.4%) and upper extremities (9.3%).

Table 17: Distribution of Injuries by Body Region

AIS 2+ for Injured Occupants				
Body Region	Unweighted Occupants	Weighted Occupants	Unweighted Percent (%)	Weighted Percent (%)
Face	46	4,191	6.2	4.1
Head	279	21,860	37.8	21.6
Neck	1	124.12	0.1	0.1
Upper Extremity	94	10,693	12.7	10.6
Thorax	83	5,338	11.2	5.3
Abdomen	32	45,193	4.3	44.6
Spine	126	9,338	17.1	9.2
Lower Extremity	75	4,473	10.1	4.4
Unspecified	3	86.7	0.4	0.1

AIS 3+ for Injured Occupants				
Body Region	Unweighted Occupants	Weighted Occupants	Unweighted Percent (%)	Weighted Percent (%)
Face	14	1,340	4.1	6.6
Head	165	7,637	48.1	37.4
Neck	0	--	0.0	--
Upper Extremity	20	1,558	5.8	7.6
Thorax	70	4,229	20.4	20.7
Abdomen	12	584.1	3.5	2.9
Spine	32	3,646	9.3	17.9
Lower Extremity	27	1,312	7.9	6.4
Unspecified	3	86.7	0.9	0.4

Univariately, restraint type, age, seating position, and number of quarter turns were significantly associated with the odds of sustaining an MAIS 2+ injury among pediatric rollover occupants. After examining bivariate relationships among these covariates, we found that restraint type, age, and seating position were all significantly correlated. Therefore, only restraint type was included in the multivariable model with number of quarter turns. After observing these variables in a full multivariate model and then reducing the factors based on those that were not significant with a p-value <0.05, all factors were still significantly associated with MAIS 2+ injury.

Table 18 lists the odds ratio for MAIS 2+ and MAIS 3+ injury based on a multivariate model accounting for restraint type and number of quarter turns. Those

occupants in FFCRS had a lower risk of MAIS 2+ injury compared to lap/shoulder belts, while those in lap belt only restraints had an increased risk of MAIS 2+ injury. Lap belt only restrained occupants had greater risk for an MAIS 3+ injury as compared to those restrained in lap shoulder belts. For number of quarter turns, one unit increase in the number of quarter turns was associated with an odds ratio of 1.33 (p<0.001) and 1.45 (p<0.001) for MAIS2+ and MAIS 3+ respectively.

Table 18: Odds ratio for MAIS 2+ and MAIS 3+ Injury with a Multivariate Model accounting Restraint Type and Quarter Turns

	Outcome	Odds Ratio	LCL	UCL	P-Value
Restraint Type					
Booster Seat	MAIS 2+	0.22	0.04	1.28	0.092
	MAIS 3+	0.55	0.09	3.35	0.515
FFCRS	MAIS 2+	0.35	0.22	0.57	<.0001
	MAIS 3+	0.88	0.50	1.56	0.655
Lap Belt	MAIS 2+	4.35	1.50	12.62	0.007
	MAIS 3+	7.77	1.27	47.40	0.026
RFCRS	MAIS 2+	0.81	0.11	5.93	0.832
	MAIS 3+	1.19	0.12	11.97	0.882
Lap/shoulder Belt	MAIS 2+	1.00	--	--	--
	MAIS 3+				
Quarter Turns					
Quarter Turns	MAIS 2+	1.32	1.25	1.39	<.0001
	MAIS 3+	1.36	1.22	1.51	<.0001

CONCLUSIONS

An unweighted 1560 cases (weighted n=515,470) meeting the inclusion and exclusion criteria (restrained occupants aged 0-19 years in a rollover crash-involved passenger vehicle of model year 1998 or newer) were identified from NASS-CDS. Results indicate that:

- The most commonly involved age group was 16-19 year olds, making up 53.4% of the weighted population, followed by 9-15 years olds comprising 20%.
- The lap shoulder belt was the most common form of restraint (82%). Univariate analysis showed that children restrained in FFCRS or booster seats were less likely to sustain an MAIS 2+ injury than lap/shoulder belt restrained occupants. Lap belt restrained occupants were much more likely to be injured. Multivariate analysis again showed that FFCRS odds ratio for MAIS 2+ injury (Odds Ratio=0.35, p<0.0001)

was significantly lower than the lap/shoulder belt reference value, while lap belt MAIS 2+ odds ratio (OR=4.35, p=0.007) was significantly higher. The protective benefit of proper restraint in rollover crashes is apparent.

- Occupants were most likely to be drivers (42.5%), then front right passengers (18.9%), with rear rows left (12.9%), center (12.4%), and right (12.8%) showing very similar occupant distributions. Front right (OR=2.29, p=0.018) and front center (OR=4.55, p=0.012) seating positions showed a higher likelihood of MAIS 2+ injury than the rear left seating position.
- The included rollover crashes experienced up to 16-quarter turns; 2-quarter turn crashes were most common (30.2%), followed by 1 quarter turn (26.2%) and 4 quarter turns (23.4%). Most rollover crashes consisted of at least 2-quarter turns. Multivariate analysis shows that number of quarter turns is a significant predictor of both MAIS 2+ and MAIS 3+ injury risk, with odds ratios of 1.32 (p<0.001) and 1.36 (p<0.001) respectively for each additional quarter turn. An average of 2.8-quarter turns (2.33-3.19) was associated with an MAIS 2+ injury.
- For individual AIS 2+ injuries, the abdomen was the body region with the highest weighted proportion of injuries: 44.6%; followed by the head at 21.6%. However, for unweighted percentages, the body region making up the highest proportion of injuries was head (44.6%) followed by the spine (17.1%) and upper extremities (12.7%). For AIS 3+ injuries, the head was the most injured body region at 37.4% of injuries, followed by the thorax (20.7%) and spine (17.9%). For unweighted percentages, the body region making up the highest proportion of injuries was head (48.1%) followed by the spine (20.4%) and upper extremities (9.3%). The variations between the weighted and unweighted distributions points out some of the challenges with conducting child-specific analyses with NASS-CDS, as some cases have extremely high sample weights.
- The protective benefit of air bags and rollover mitigation technologies such as ESC could not be evaluated due to limited cases for which that data is available. However, ESC was standard for 2.8% of the included case vehicles, and optional in an additional 2.0%.
- More complex multivariate modeling is needed to study the combined effect of significant factors such as restraint system, age, vehicle type, crash severity and countermeasures such as airbags and ESC on the injury outcomes. In addition, understanding which constellation of

factors result in injuries to which specific body regions is of interest to further injury mitigation.

ACKNOWLEDGEMENTS

The authors would like to acknowledge the National Science Foundation (NSF) Center for Child Injury Prevention Studies at The Children's Hospital of Philadelphia (CHOP) and The Ohio State University (OSU) for sponsoring this study and its Industry Advisory Board (IAB) for their support, valuable input and advice. The views presented are those of the authors and not necessarily the views of CHOP, OSU, the NSF or the IAB members.

REFERENCES

1. Bedewi, P.G., Godrick, D.A., Digges, K.H., Bahouth, G.T. (2004) "An investigation of occupant injury in rollover: NASS-CDS analysis of injury severity and source by rollover attributes." *Progress in Technology* 101 (2004): 437-451.
2. Bose, D., Kerrigan, J. R., Foster, J. B., Crandall, J. R., and Tobaru, S. (2011). Planar impacts in rollover crashes: significance, distribution and injury epidemiology. *Association for the Advancement of Automotive Medicine*, 55 (October), 243-52.
3. Crandall, J., Bose, D., Shaw G., Lockerby, J., Bollapragada, V. Kerrigan J., Mutter, K. (2011) "Single Vehicle Multiple Event Rollover Crashes: NASS and CIREN Analysis Rollover fatality", CIREN Center Presentation.
4. Daly L, Kallan MJ, Arbogast KB, Durbin DR. (2006) "Risk of injury to child passengers in sport utility vehicles", *Pediatrics*. 2006 Jan; 117(1):9-14.
5. Hu, J, Lee, J.B., Yang, K.H., King, A.I. (2005) "Injury patterns and sources of non-ejected occupants in trip-over crashes: a survey of NASS-CDS database from 1997 to 2002." *Annual Proceedings/Association for the Advancement of Automotive Medicine*. Vol. 49. Association for the Advancement of Automotive Medicine, 2005.
6. Kallan, M. J., Arbogast, K. B., and Durbin, D. R. (2006). Effect of model year and vehicle type on rollover crashes and associated injuries to children. *Association for the Advancement of Automotive Medicine*, 50, 171-84.

7. Rivara, F. P., Cummings, P., and Mock, C. (2003). Injuries and death of children in rollover motor vehicle crashes in the United States. *Injury prevention : journal of the International Society for Child and Adolescent Injury Prevention*, 9(1), 76-80.
8. Rollover Data Special Study Final Report. Distribution, (January 2011), NHTSA, DOT HS 811 435
9. Viano DC, Parenteau CS., (2008) "Fatalities of children 0-7 years old in the second row", *Traffic Injury Prevention*, 2008; 9(3):231-7.

APPENDIX A

Table A1: Distribution by Airbag Type and Deployment

Bottom Instrument Panel				
Bottom Instrument Panel	Unweighted Occupants	Weighted Occupants	Weighted Percent (%)	SE of %
Available - Not Deployed	1	1,266	0.2	0.2
Available - Deployed, Unknown Event	2	63,814	0.0	0.0
Not Available/Unknown If Available	1442	490,661	95.2	1.7
Detailed Air Bag Information Not Available	115	23,479	4.6	1.5
Door Panel				
Door Panel	Unweighted Occupants	Weighted Occupants	Weighted Percent (%)	SE of %
Available - Not Deployed	3	451,465	0.1	0.1
Available - Deployed After Rollover	2	208.95	0.0	0.0
Not Available/Unknown If Available	1440	491,330	95.3	1.6
Detailed Air Bag Information Not Available	115	23,479	4.6	1.5
Mid - Instrument Panel				
Mid - Instrument Panel	Unweighted Occupants	Weighted Occupants	Weighted Percent (%)	SE of %
Available - Not Deployed	138	53,574	10.4	2.6
Available - Deployed During Rollover	3	661.334	0.1	0.1
Available - Deployed Prior To Rollover	20	2,009	0.4	0.1
Available - Deployed, Unknown Event	8	413.248	0.1	0.0
Not Available/Unknown If Available	1276	435,334	84.5	3.6
Detailed Air Bag Information Not Available	115	23,479	4.6	1.5
Roof Side Rail				
Roof Side Rail	Unweighted Occupants	Weighted Occupants	Weighted Percent (%)	SE of %
Available - Not Deployed	50	12,060	2.3	0.9
Available - Deployed After Rollover	3	276.862	0.1	0.1
Available - Deployed During Rollover	37	6,134	1.2	0.4
Available - Deployed Prior To Rollover	7	749.802	0.1	0.1
Available - Deployed, Unknown Event	9	1,055	0.2	0.1
Not Available/Unknown If Available	1339	471,715	91.5	2.7
Detailed Air Bag Information Not Available	115	23,479	4.6	1.5
Seat Back				
Seat Back	Unweighted Occupants	Weighted Occupants	Weighted Percent (%)	SE of %
Available - Not Deployed	110	23,569	4.6	1.2
Available - Deployed After Rollover	2	87.703	0.0	0.0
Available - Deployed During Rollover	4	1,109	0.2	0.1
Available - Deployed Prior To Rollover	7	799.597	0.2	0.1
Available - Deployed, Unknown Event	16	2,648	0.5	0.4
Not Available/Unknown If Available	1306	46,3777	90.0	2.9
Detailed Air Bag Information Not Available	115	23,479	4.6	1.5

Steering Wheel Hub				
Steering Wheel Hub	Unweighted Occupants	Weighted Occupants	Weighted Percent (%)	SE of %
Available - Not Deployed	314	183,149	35.5	8.0
Available - Deployed After Rollover	4	321.216	0.1	0.0
Available - Deployed During Rollover	11	921.9844	0.2	0.1
Available - Deployed Prior To Rollover	84	21,176	4.1	1.9
Available - Deployed, Unknown Event	29	5,386	1.0	0.3
Not Available/Unknown If Available	1003	28,1035	54.5	5.2
Detailed Air Bag Information Not Available	115	23,479	4.6	1.5
Top Instrument Panel				
Top Instrument Panel	Unweighted Occupants	Weighted Occupants	Weighted Percent (%)	SE of %
Available - Not Deployed	102	24,793	4.8	1.7
Available - Deployed After Rollover	3	332.441	0.1	0.1
Available - Deployed During Rollover	3	183.868	0.0	0.0
Available - Deployed Prior To Rollover	34	5,498	1.1	0.4
Available - Deployed, Unknown Event	14	1,427	0.3	0.1
Not Available/Unknown If Available	1289	459,756	89.2	3.6
Detailed Air Bag Information Not Available	115	23,479	4.6	1.5
Any Air Bags Deployed				
Any Air Bags Deployed	Unweighted Occupants	Weighted Occupants	Weighted Percent (%)	SE of %
Available - Non Deployed	550	262,527	50.93	4.59
Deployed as a Result of Rollover	57	8,922	1.73	0.42
Deployed, Other Event	216	39,241	7.61	3.08
Not Available/Unknown if Available	737	204,780	39.73	2.55

POLE IMPACT TEST: STUDY OF THE TWO CURRENT CANDIDATES IN TERMS OF COST AND BENEFITS FOR FRANCE

Olivier Billot,
Mickael Coulot,
Richard Zeitouni,
Céline Adalian
PSA Peugeot Citroën
France

Cyril Chauvel
LAB PSA Peugeot Citroën Renault, France
France
Paper number 13-0440

ABSTRACT

Regulatory and consumerism discussions currently take place on the definition of a pole impact that could be representative of car accidents in order to better protect the occupants.

Two main test protocols are in competition: the FMVSS 214 one and the current Euro NCAP one. France, taking part of the discussion in WP29 GRSP, provided accident data as well as cost benefit study.

To supply data for this debate, PSA Peugeot Citroën carried out physical tests on different car platforms with the two types of impact:

- pole test 75° 32 km/h, also called “oblique pole test”
- pole test 90° 29 km/h

With the results of these tests, numerical models were improved to get correlated models.

Then, the correlated models were used to define the optimized technical solutions needed on the 75°/32 km/h test to get back to the same intrusion level as the 90°/29 km/h.

It is therefore possible to quantify the cost of this test if it becomes mandatory for Europe or for another country (eg. China).

In addition, accident data analysis assesses the possible benefits for the European roads.

This paper presents these data as well as the detailed analysis made by PSA Peugeot Citroën to establish the additional cost (in terms of Euros but also of kilograms) if the discussion ends to the selection of the FMVSS214 compared to the selection of the Euro NCAP test protocol.

The overall conclusion is that there is no justification of such a test for Europe when comparing the costs with the benefits.

INTRODUCTION - AIM OF THE STUDY

Pole impact test is not yet mandatory worldwide. USA [1] defined an oblique pole impact test several years ago and it is now required via FMVSS n°214. In Europe, a pole test 90° is applicable in consumer testing [2] but it is not mandatory. The main purpose of Euro NCAP when they introduced this test, in the early 2000's, was to incite the car manufacturers to fit a head protection on the first row (curtain airbag is usually the protection device used to answer this request). Korea and Australia consumer organisations are also using the same test protocol [3]. But here again, this is not a mandatory / regulatory requirement.

And for the other countries in the world, no requirement exists so far for a pole test.

But things are changing since a couple of years. At the request of USA, an informal working group on Pole Side Impact (PSI) was set up in WP29/GRSP to derive a GTR (Global Technical Regulation) on Pole impact for the coming years [4]. With this informal group creation, started the discussion on test configuration (mainly on angle, impact speed and dummy model).

A regulatory test configuration should be pertinent in terms of real world accident statistics and should also be assessed via a cost benefits analysis to check the improvements worth the money. This is where the debate could start since the oblique pole test would require additional structures (and mass) to control intrusion. And some members questioned if the additional efficiency in terms of occupant protection with respect to a 90° pole impact test was really there. In parallel, the cost for society in terms of CO₂ additional emission is put forward when oblique pole test is compared to the 90° one.

In order to bring some data to this discussion, this paper presents the application of the two pole tests protocols on current cars. This allows the comparison of the protocols and their consequences

on the car structures. It allow us to reckon the cost and weight needed to go from a car designed from a 90° pole test to a design for an oblique pole test. This data is then used to assess a cost/benefit study applied to the European roads.

PRESENTATION OF BOTH TYPES OF POLE IMPACT

Two types of pole impacts are applied throughout the world as described in Figure 1:

- 254mm diameter pole impact on a 75° oriented car, travelling at 32 km/h, also called “oblique pole test”. The test configuration is defined in FMVSS 214 regulation. But, here we took into account the proposal made to the PSI informal group, i.e. using a WorldSID-50th dummy,
- 254mm diameter pole impact on a 90° oriented car, travelling at 29 km/h. It is applied in Euro NCAP, KNCAP and ANCAP. It uses an ES-2 50th dummy.

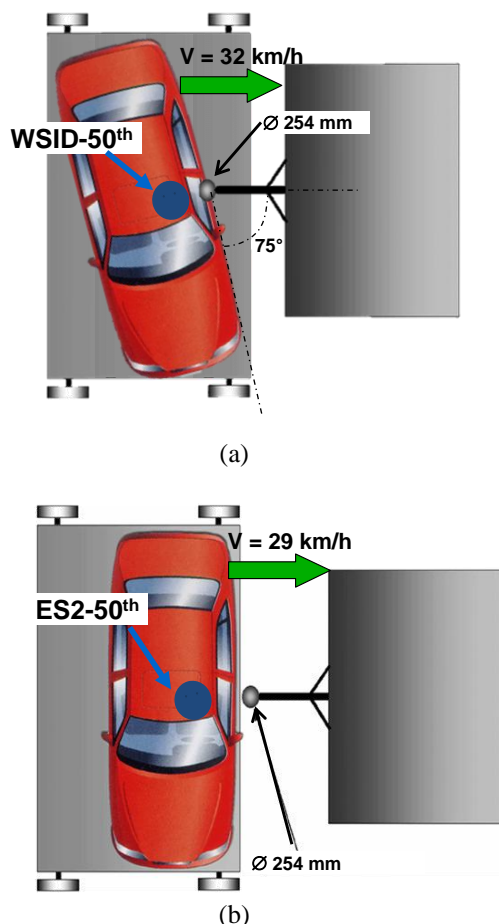


Figure 1. Illustration of pole tests procedures – (a) 75°-pole test and (b) 90°-pole test

It has to be highlighted that if we consider the Euro NCAP protocol and the current discussion in the PSI informal working group, the crash test

dummies are not the same between 75°-pole and 90°-pole (respectively WorldSID 50th and EuroSID-2 50th), as well as their seating position. For this reason and because the pole test is designed to be the worst case and therefore requires impacting the centre of gravity of the dummy, the two impact locations on the car structure may differ.

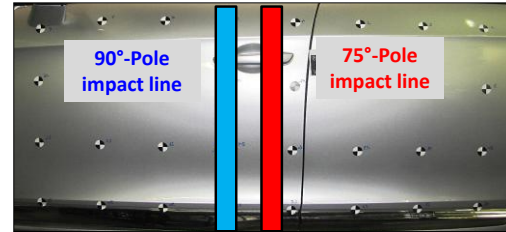


Figure 2. Example of difference in pole impact line between the two tests procedures due to the dummy used

In terms of impact energy, because of the velocity is higher in the oblique pole test, the increase is of 22%. For example, for a 1,500 kg vehicle the crash energy for the 90°-pole test is 63kJ and 77kJ for the 75°-pole test.

Final general remark, the difference in the impact angle (15°) adds an X-component to the force applied to the vehicle, which could destabilize the reinforcements based on Y-direction.

METHOD

This study is based on the analysis of physical and numerical tests performed with the two test protocols on vehicles of different sizes and built on different platforms. We can split the study into three phases:

- The first phase was to make an initial picture of consequences of the two tests on current cars in terms of intrusion and to derive correlated numerical models
- The second phase was to use numerical models to design the reinforcements needed to get the same intrusion level in the 75°-pole impact test as in the initial 90°-pole test.
- The third phase was to assess these reinforcements in physical tests to check if they were effective.

Thanks to this study, we could calculate the cost of reinforcements, in term of mass and price.

In parallel to this analysis, a real world accident data analysis was carried out to identify the relevance of the two test protocols.

A cost/benefit study can be derived from the combination of the two studies to assess the social consequences of adopting one or the other protocol on European roads.

COMPARATIVE TESTS AND STUDIES ON VEHICLES STRUCTURE

Numerical and physical tests were carried out on several platforms:

- small vehicle,
- family vehicle,
- large family vehicle.

Both test protocols were performed on each platform and the differences were identified.

Comparison of the two Pole Test protocols on structural behaviour

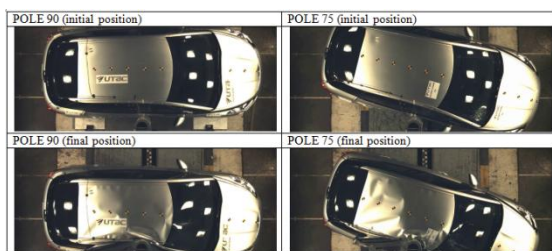


Figure 3. Large Family Car during Pole Tests

Due to dummy availabilities and also because we wanted to have a direct comparison between tests, we decided to use ES2 dummy in all the tests. But in order to be representative of the exact 75°-pole test, we applied the WorldSID seating position in the oblique test even if an ES2 was used. Therefore, the pole impact lines as described in Figure 2 were representative of each of the test protocol.

On the three vehicles, intrusions were measured on the external limit of the underbody and compared.

The first comparison is made on the first phase of the crash. Indeed the beginning-of-crash intrusions are essential to guarantee a good airbag deployment. The results are presented in Figure 4

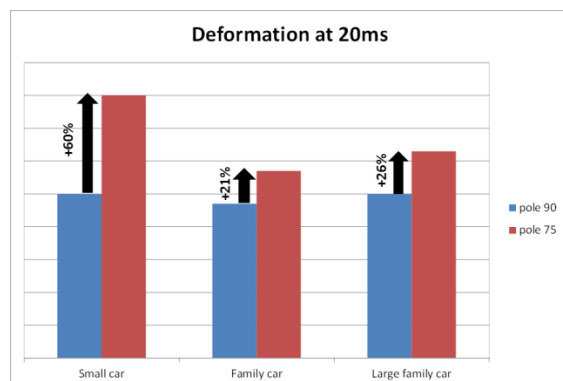


Figure 4. Comparison of the beginning-of-crash deformation between the two pole test protocols and for the three vehicle categories under study.

If the 90°-pole test gives almost the same magnitude of intrusion on the three car families, it is not the case for the 75°-pole test. Intrusions are always higher in the beginning of crash in the oblique test and the increase varies from 21 to 60%.

Concerning the end-of-crash intrusions, which have to be controlled to maintain enough space for the occupant (especially in the pelvis zone when the car is equipped with a high centre console), the results are presented in Figure 5.

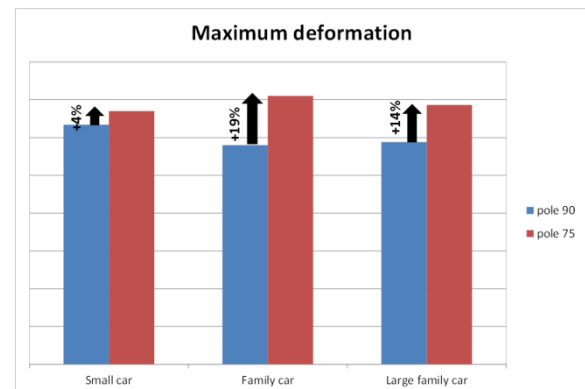


Figure 5. Comparison of the end-of-crash deformation between the two pole test protocols and for the three vehicle categories under study.

Here, the 90°-pole test does not give the same magnitude of maximum intrusion on the three car families. But they are always lower than for the 75°-pole test. In the end-of-crash phase, the oblique test gives an increase of 4 to 19% in intrusion.

We clearly see here that the change of protocol from 90° to 75° has a negative impact on the global behaviour of the structure via an increase of intrusion.

To come back to a level of intrusion equivalent to the 90°-pole test, there is a need to design specific reinforcements for the cars if tested with the oblique pole test.

To design these reinforcements (called structural add-ons), numerical models were used. These models were correlated on the 90° and on the 75°-pole tests.

Design of underbody reinforcements

According to the 75°-pole test scenario, the highest potential for reinforcement is on the underbody. This part of the vehicle presents the most interesting potential stiffness, necessary to guarantee enough vehicle deceleration during the crash and therefore prevent excessive intrusions, even if it will not be the unique part to upgrade.

The principles of such reinforcements are presented in Figure 6.

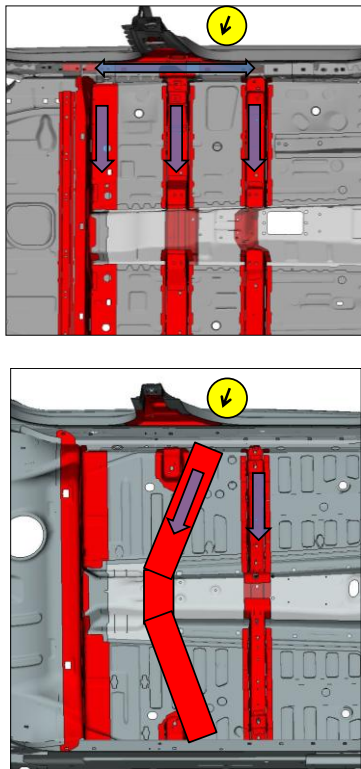


Figure 6. Two examples of underbody reinforcement principles

To give a concrete example, to counterbalance the increase of 19% in the intrusion, the add-ons represent 5 to 10 kg for the family vehicle.

Of course, to maintain a balanced performance between underbody and superstructure, similar reinforcements are necessary on the B-Pillar and in the doors, increasing as well the addition of mass.

Check of performances

For the small vehicle, studies went even further. After having performed the numerical analysis to design the reinforcements, a physical test was carried out with them. Figure 7 presents the reinforcements made on the underbody for the small vehicle.

It is interesting to notice that these simple reinforcements dedicated to the underbody represent, here, 5 kg.

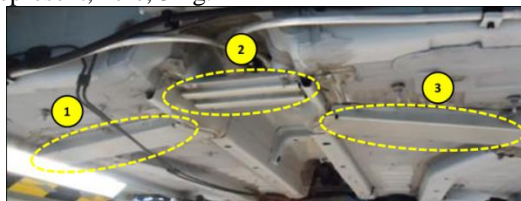


Figure 7. Reinforcements made on the small vehicle to counterbalance the excessive intrusion due to the oblique pole test

To illustrate the improvements made thanks to the add-ons designed for 75°-pole test, Figures 8 and 9 compare the beginning of crash and end of crash deformations for the small car and for the family car. Three configurations are displayed: the initial 90° pole test, the initial 75° pole test and the reinforced 75° pole test.

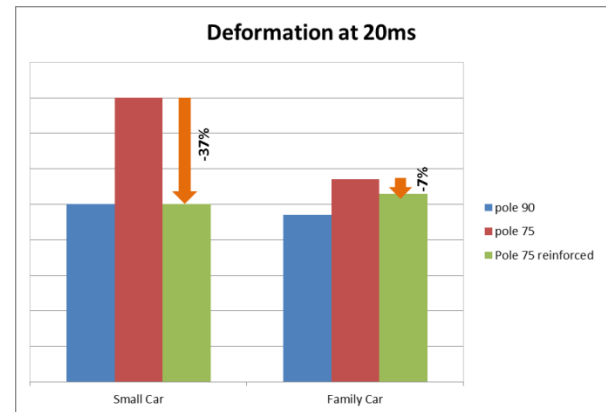


Figure 8. Beginning-of-crash deformation for the three test configurations (initial 90° pole test, initial 75° pole test and reinforced 75° pole test) for small car and family car.

In the first phase, crucial for the airbag deployment, the reinforcements helped to come back at the same level as in the initial 90° test for the small car. But for the family car, the improvement is not sufficient to reach the same level.

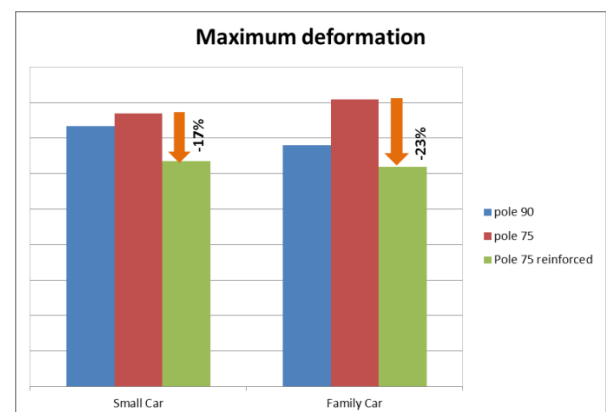


Figure 9. End-of-crash deformation for the three test configurations (initial 90° pole test, initial 75° pole test and reinforced 75° pole test) for small car and family car.

As shown above, for the small car as well as for the family car, there is a substantial gain on the end-of-crash intrusions. The level is even better than in the 90°-pole test.

DISCUSSION ON THE TEST COMPARISON IN TERMS OF STRUCTURAL BEHAVIOUR

As expected when looking at the initial test conditions, the 75°-pole impact test is more severe than the 90° one in terms of intrusion.

This severity is not only present at the end of impact but also in the first phase of deformation, when space is needed to deploy correctly the airbag.

So the first questions to ask are “what would be the consequence on the occupant protection? Will a reinforcement be enough to ensure the same protection? Or should there is a need to change the restraint system and the interaction between the structure, the door and the occupant?”

Therefore, we also investigated the biomechanical criteria between the 90°-pole test and the reinforced 75°-pole test.

Biomechanical criteria comparison

This comparison is presented in Figure 10 in terms of percentage of variation for the small car.

We remind that, for both tests, the measurements were made on the ES2-50th dummy so they can be compared without the need of a transfer function.

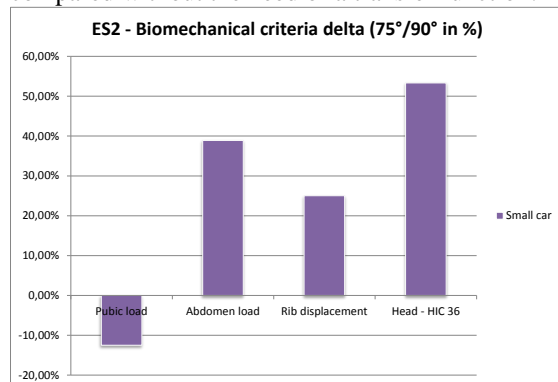


Figure 10. Biomechanical criteria variation when comparing the 75° reinforced test to the 90° one.

In this graph, a positive value means the results on the 75°-pole test is more severe than the 90°-pole test.

So we can conclude that for the small vehicle, the improvement gained with the reinforcements is significant in intrusion. But this is not enough to guarantee same protection as in 90°/29kph without changing the airbag characteristics.

In addition, it is also important to stress that WorldSID 50th is larger than ES2 50th and therefore, it will be even more difficult to ensure a good airbag deployment. This was not taken into account in our research. This means that our study is optimistic with respect to the modifications needed to fulfil a 75°-pole impact.

Therefore, to ensure a similar level of protection between the two tests configuration, there is no other possibility than adding some structural reinforcements to counterbalance this extra severity.

This will increase the mass, and so the energy to absorb and will also increase the CO₂ emission.

Moreover, a redesign of the airbag is needed to deploy earlier and in a smaller available space. This also increases the cost of vehicle.

This part of the study is somewhat “theoretical” because it just compares objectively two different test protocols. It tells us that if the 75°-pole impact is justified, we will have to take its negative effects on board. It is now time to try to answer to the following questions: is the 75°-pole impact relevant to the real life? And are the additional costs counterbalanced by the benefits that will be provided by an extra protection? And therefore, the final question would be: is the 75°-pole impact justified and needed?

For this reason, we also carried out a costs/benefits study focused on European roads.

COSTS/BENEFITS STUDY

Objectives

The aim of this study is to evaluate the cost/benefit ratio of regulation evolution for passenger cars and light commercial vehicles regarding side impacts. It was carried out to contribute to the WP29 discussion within the Pole Side Informal Working Group.

For this discussion on a regulatory topic, two evolution types have to be considered: the injury reduction in barrier side impact and the injury reduction in pole side impact.

Database used

To realize this work, we used the BAAC (Bulletin d'Analyse d'Accident Corporel) data base which is the French National database coming from the police data collection. Year 2009 was taken into account and we sampled fatalities and serious injuries distribution of passenger cars (M1 vehicles) and light commercial vehicles (N1 vehicles) involved in side impact (see Table 1).

Table 1.
Fatalities and serious injuries distribution
regarding side impact types – Year 2009

M1 vehicles	Fatalities: pole side impacts	Fatalities: barrier side impacts	Fatalities: all side impacts
ONISR year 2009	167	307	474
N1 vehicles	Fatalities: pole side impacts	Fatalities: barrier side impacts	Fatalities: all side impacts
ONISR année 2009	11	14	25
M1 vehicles	Serious injuries: pole side impacts	Serious injuries: barrier side impacts	Serious injuries: all side impacts
ONISR year 2009	312	1301	1613
N1 vehicles	Serious injuries: pole side impacts	Serious injuries: barrier side impacts	Serious injuries: all side impacts
ONISR année 2009	6	95	101

French Fleet

To be able to calculate a cost/benefit ratio regarding French vehicle evolution, we need to have some accurate data about fleet. In 2009, the M1 French fleet was about 30.85 Million of vehicles. For the same year, N1 French fleet was about 5.75 Million. Table 2 gives the gravity vs. vehicle fleet ratio for both categories. We find that ratio is much higher for M1 vehicle rather than N1. This is due to different amount and road use between M1 and N1 vehicles.

Table 2.
Ratio (fatalities + severe injuries) versus M1 and N1 French fleet

Gravity (Fatalities + severe injuries) per million vehicle	Pole side impacts	Barrier side impacts	All side impacts
M1	16	52	68
N1	3	19	22

To estimate also this cost/benefit ratio we need to know the time of fleet renewal (progressive increase of new M1 and N1 designed cars into the fleet). For France, it takes about 14 years to renew completely M1 and N1 car fleets.

French social costs

We can estimate some positive and some negative effects on social costs. For year 2009 in France, the positive effect on fatalities and serious injuries reduction is estimated to 1.2 M€ per fatality and 0.132 M€ per severe injured people. These figures are in the average of European figures.

The negative effect will be on fuel consumption and CO₂ emissions due to vehicle weight increase. Vehicles have to offer the same level of protection for a higher test velocity and a more severe configuration (see EEVC WG13 and WG21 Subgroup, Report: Analysis to estimate likely benefits and costs for the EU of modifying Regulation 95). This last assumption was not taken into account for the cost/benefit calculation due to the difficulties to estimate the CO₂ emission cost.

Technical evolutions - Technical cost and additional weight for M1 and N1 vehicles

The analysis is made with a two-step approach allowing to go from the current initial state to an intermediate state (addition of the 90°-pole test) or to a final state (use of the 75°-pole test instead of 90° one), as shown in Figure 11.

Indeed, the first step is to consider the 90°-pole test impact as the regulatory requirement in addition to the current ECE 95 requirement and in addition to the current fleet performance that could be assessed as scoring at least 13 points in Euro NCAP. We can define the car fleet that would answer this target and its cost and benefits.

And then, the second step would be to go from the car fleet defined in the first step to a car fleet answering to the 75°-pole test as already required in FMVSS 214.

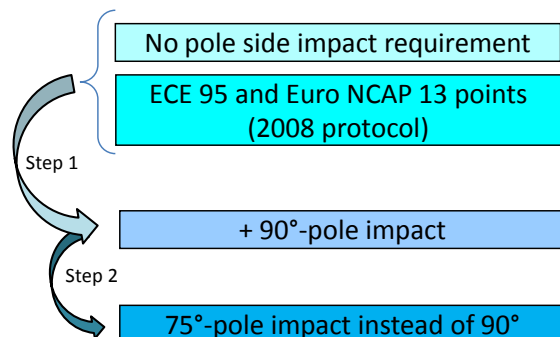


Figure 11. Assessment of side impact technical evolutions as a two-step approach.

To respect the 90°-pole test requirements in regulation, the upgrade of vehicles would require an additional cost of about 290 € to 348 € and an additional weight of about 13 to 20 kg per vehicle (source EEVC studies). This would be the cost for the first step of the approach described above.

To respect the 75°-pole side impact, the vehicle answering to the first step would need an additional update that would cost about 84 € to 223 € (source NHTSA 2004 studies) and about 50 € to 60 €/vehicle (source France) per vehicle. For this second step of upgrade, the additional weight will represent 7 to 15 kg per vehicle.

To maximize result in our study, the global cost used for calculation is 340 € to 408 €/vehicle and the total weight is 20 to 35 kg/vehicle. It takes into account the two steps presented below.

Potential reduction of Fatalities and Serious injuries

At this stage, it could be good to recall that this study was made to analyse the effect of all the types of side impact; meaning the ones due to large obstacle (eg. other car, heavy vehicle...) combined to the ones due to narrow obstacles (eg. tree, pole). This could be done by requiring what is presented as the first step in Figure 11.

Benefit evaluation of new side impact safety systems on cars (improvement of curtain airbags, and structural changes: car stiffness, side body and doors) contributes to a 34% potential efficiency gain (source: LAB studies).

Evaluation of benefits due to the 75°-pole side impact (optimized airbags, structural changes such as increased reinforcement,...) contributes to a maximum of 20% potential efficiency on fatalities and serious injuries reduction (Figure 12).

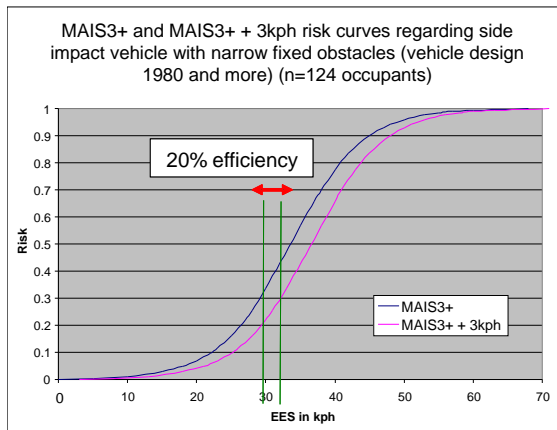


Figure 12. MAIS3+ and MAIS3+ +3kph risk curves regarding side impact vehicle with narrow fixed obstacles.

Cost / benefit ratio results

Regarding M1 vehicle, after 14 years French fleet renewal, stiffness and protection upgrade contributes to a reduction of 4,150 severe injured people and an avoidance of 1,326 fatalities. Societal benefit is 2,139 M€ and technical cost is between 10,489 M€ and 12,587 M€. Cost/benefit ratio result is between 4.9 and 5.9. It may be useful to recall that when result is >1, it means that the cost/benefit ratio is not good. Therefore, to get something economically interesting the technical cost balance should be at 69€ per vehicle.

Regarding N1 vehicle, after 14 years French fleet renewal, reduction represents 241 severe injured people and 73 fatalities avoidance. Societal benefit is 119 M€ and technical cost is between 1,955 M€ and 2,346 M€. Cost/benefit ratio result is between 16.4 and 19.6 (>1, therefore not good). Therefore, technical cost balance should be economically interesting at 21€ per vehicle (see Table 3).

Table 3. Cost/benefit ratio for M1 and N1 vehicle – standard fleet.

	Cost / benefit ratio		Balanced cost / benefit ratio in Euros
	Min	Max	
M1 vehicles	4.9	5.9	69.3
N1 vehicles	16.4	19.6	20.8

DISCUSSION ON THE COST BENEFIT ANALYSIS

This cost benefit analysis shows that the ratio is always above 1, for M1 and even more for N1 fleet. The technical cost to be economically interesting would need to be very low – 69€ for M1 and 21€ for N1, which is not realistic.

But, one critic could be to stress that the car fleet will be influenced by a new regulation that came into force not so long ago: the mandatory fitment of ESC.

Therefore, we can carry out a second analysis taking ESC into account.

Potential reduction of Fatalities and Serious injuries with ESC generalisation

Benefit evaluation of ESC (regulation in 2012) regarding pole side impact avoidance gives a 34% potential efficiency (source: EEVC).

Benefit evaluation regarding pole side impact implied by the 75°-pole side impact gives a 20% additional potential efficiency.

Cost / benefit ratio results

Regarding M1 vehicle, after 14 years French fleet renewal, stiffness and protection upgrade contributes to 4,007 severe injured people reduction and 1,249 fatalities avoidance. Societal benefit is 2,028 M€ and technical cost is between 10 489 M€ and 12,587 M€. Cost/benefit ratio result is between 5.2 and 6.2 (so >1, therefore not good). Therefore, to get something economically interesting the technical cost balance should be at 66€ per vehicle.

Regarding N1 vehicle, after 14 years French fleet renewal, reduction represents 238 severe injured people and 68 fatalities avoidance.

Societal benefit is 113 M€ and technical cost is between 1,955 M€ and 2,346 M€. Cost/benefit ratio result is between 17.3 and 20.8 (>1, therefore not good).

So, technical cost balance should be economically interesting at 20€ per vehicle (see Table 4).

Table 4. Cost/benefit ratio for M1 and N1 vehicle ESC equipped

	Cost / benefit ratio		Balanced cost / benefit ratio
	Min	Max	in Euros
M1 vehicles - ESC equipped	5.2	6.2	65.7
N1 vehicles - ESC equipped	17.3	20.8	19.6

This is even more stringent to take ESC into account for the cost benefit analysis.

CONCLUSION

Conclusion on the structural reinforcements needed for the 75°-pole test

Comparing the two test configurations, there is no discussion possible: the 75°-pole impact test is more severe than the 90° one in terms of intrusion. It is also important to stress that the severity is not only present at the end of impact but also in the first phase of deformation, when space is needed for a correct airbag deployment.

To counterbalance this additional intrusion severity, structural reinforcements are needed. These add-ons would weigh up to 10 to 15 kg. But this would not be enough to reach the target of getting the same level of occupant protection as the 90°-pole test. The restraint system would also need to be modified.

Moreover, because WorldSID 50th is larger than ES2 50th, it will be even more difficult to ensure a good airbag deployment in this limited space. This was not taken into account in our research. This means that our study is optimistic with respect to the whole set of modifications needed to fulfil a 75°-pole impact.

These modifications would increase the mass of the vehicle, and so the energy to absorb and would also increase the cost of vehicle and the CO₂ emissions.

Conclusion on the cost benefits

As a conclusion, the analysis shows a cost/benefit ratio > 1 for passenger vehicles, and a huge rate for commercial vehicles.

Without ESC, the cost/benefit ratio is estimated > 4 for M1 vehicles and > 16 for N1 vehicles. And for Europe, where ESC is mandatory since January 1st

2012, the cost/benefit ratio is estimated > 5 for M1 vehicles and > 17 for N1 vehicles.

Human benefit versus technical cost balance is then about 66 Euros per M1 vehicle and 20 Euros per N1 vehicle.

Therefore, even if the decrease of fatalities and serious injuries is important, this new possible regulation is not economically interesting for Europe.

We guess that the same conclusion would be derived for China.

ACKNOWLEDGMENTS

The authors wish to thank the different labs (the internal PSA Peugeot Citroën Crash Test Centre, UTAC, Autoliv France and Millbrook Crash Test Centre), and the PSA Peugeot Citroën research teams that were involved in this study.

REFERENCE

- [1] FMVSS No. 214, DYNAMIC SIDE IMPACT PROTECTION -Rigid Pole Side Impact Test Requirements - <http://www.nhtsa.gov/Vehicle+Safety/Test+Procedures?procedurePage=1>
- [2] Euro NCAP Pole Impact Testing Protocol - Version 5.2, Feb 2012
- [3] Safety Companion, Safety Wissen - Regulation and consumerism tests, 2013 edition
- [4] WP29/GRSP – Informal Group on Pole Side Impact - <https://www2.unece.org/wiki/pages/viewpage.action?pageId=3178630>

A CONSIDERATION ON THE AE-MDB FOR THE SIDE IMPACT TEST IN KNCAP

Jaemoon Lim

Daeduk College

Korea

Hyungjin Chang

Gyuhyun Kim

Jaewan Lee

Korea Automobile Testing & Research Institute (KATRI)

Korea

Paper Number 13-0443

ABSTRACT

The data on car to car side impacts in Korea had increased every year from 67,105 cases in 2006 to 76,556 cases in 2011 by the Police Agency in Korea. In Korea, sales of mid-sized cars, large-sized cars and SUVs have increased since 2001. The ratio of vehicles over 1,400 kg represented 56 % in 2010. The current test procedure for side impact in KNCAP uses 950 kg MDB. The current test method may not reflect the real world traffic conditions and vehicle populations in Korea.

The study for improving the side impact test in KNCAP has been carried out. This study shows the test results of three size of vehicles (compact car, mid-sized car and large-sized car) using the current KNCAP MDB, 1,300 kg AE-MDB and 1,500 kg AE-MDB. The ES-2 dummy is mounted on the driver's and front passenger's seat, and the SID-2 5 %tile female dummy is mounted on the rear left passenger's seat.

Adopting the side airbag and the curtain airbag, the injury values and the star ratings of cars were not showed a big difference according to the size of cars. The dominant factor affecting the occupant safety when using the AE-MDB was pelvis injury of the dummy in the rear seat. The deformations of vehicle side structure showed big difference depending on using the current KNCAP MDB or AE-MDB.

If the AE-MDB will be adopted in the KNCAP, the assessment method will be prepared for the enhancement of safety for the smaller occupant in rear seats.

INTRODUCTION

The Korean New Car Assessment Program (KNCAP), administered by the Ministry of Land, Transport and Maritime Affairs (MLTM), works to provide consumers with information on the car safety by evaluating the crashworthiness to reduce the occupant injuries and promote the manufacture of safer cars.

The side impact test procedure has been adopted in the KNCAP since 2003. Considering the traffic circumstances in Korea, the test procedure of the EuroNCAP was adopted. However, the impact speed

of the KNCAP is slightly higher than that of the EuroNCAP. In the KNCAP, the driver's door side of the vehicle is impacted by the moving deformable barrier (MDB) at the speed of 55 kph [1]. The adoption of the side impact test method in the KNCAP has been contributed to the improvement of the vehicle side structure and the enhancement of the occupant protection.

The data on car to car side impacts in Korea had increased every year from 67,105 cases in 2006 to 76,556 cases in 2011 by the Police Agency in Korea [2]. 855 dead and 125,327 injured by the side crash were reported in 2011 [2].

In Korea, sales of mid-sized cars, large-sized cars and SUVs have increased since 2001. The ratio of vehicles over 1,400 kg represented 56 % in 2010 [3]. The current test procedure for side impact uses 950 kg MDB. The current MDB of the KNCAP would not reflect the real world side crashes. When SUVs impact passenger cars, the safety of passenger cars are expected to be degrade.

The EEVC Working Group 13 has performed studies to improve the MDB for the side crash and developed the Advanced European Mobile Deformable Barrier (AE-MDB) [4]. The weight of originally developed AE-MDB was 1,500 kg. Recently, the 1,300 kg AE-MDB was newly developed.

The study for improving the side impact test in KNCAP has been carried out [3]. It was compared which MDB was appropriate for the current traffic conditions and vehicle populations. Also, it was investigated whether the smaller occupant in the rear seat would be secured or not under the side impact crashes.

Three size of vehicles (compact car, mid-sized car and large-sized car) were tested how to improve the side impact test of the KNCAP. The results using the current KNCAP MDB and two types of AE-MDB were represented and compared.

KNCAP SIDE IMPACT TEST METHOD

The side impact test is conducted as shown in Figure 1, where a moving barrier impacts a car containing ES-2 dummy on the driver's seat at a speed of 55kph. This is 5kph faster than the official speed of 50kph.

This test mimics a situation where a car hits the side of another car at a perpendicular angle.

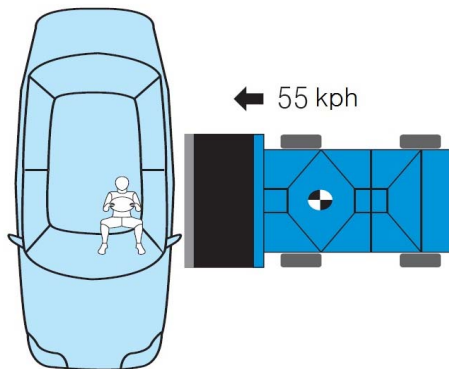


Figure 1. Schematic diagram of the side impact test.

The injury rate totals 16 points by adding injury values of the crash dummy's head, chest, abdomen and pelvis as shown Table 1. Points on each body part can be induced by interpolation from injury values. Point deduction can be made by subtracting points of back plate load F_y and chest T12 load and moments as shown in Table 2. Deduction cannot be more than 2 points. A bigger point of chest T12 load or moment will be deducted.

Table 1.
Assessment method for the side impact test.

	Injury	Criteria	Points	Injury Risk (AIS3)
Head	HIC36	650 - 1000	0 - 4	5 - 20 (%)
Chest	Compression	22 - 42 (mm)	0 - 4	5 - 30 (%)
	Viscous Criterion	0.32 - 1.0 (m/s)		5 - 50 (%)
Abdomen	Abdominal Forces	1.0 - 2.5 (kN)	0 - 4	-
Pelvis	Lateral Acceleration	3.0 - 6.0 (kN)	0 - 4	-
Injury Rating	★★★★★	13.00 - 16.00 Points		
	★★★★	9.00 - 12.99 Points		
	★★★	5.00 - 8.99 Points		
	★★	2.00 - 4.99 Points		
	★	0.00 - 1.99 Points		

Table 2.
Side-impact modifiers

	Injury	Criteria	Points
Backplate	F_y	1.0 - 4.0kN	0 - 2
T12	F_y	1.5 - 2.0kN	0 - 2
	M_x	150 - 200Nm	0 - 2

As shown in Figure 2, the impactor consists of 6 single blocks of aluminum honeycomb, which have been processed in order to give a progressively increasing level of force with increasing deflection.

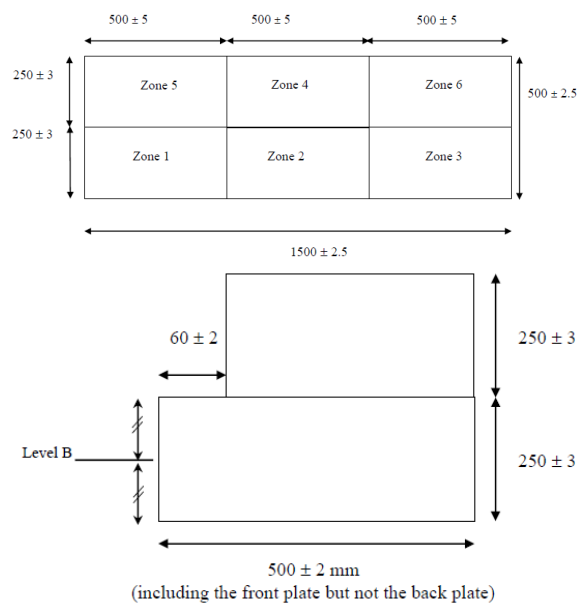


Figure 2. Features and specifications of the aluminum honeycomb of KNCAP.

SIDE IMPACT TEST METHOD USING AE-MDB

The side impact test method using the AE-MDB is represented in Figure 3. The ES-2 dummy is mounted on the driver's and front passenger's seat, and the SID-2 5 %tile female dummy is mounted on the rear left passenger's seat. The method of KNCAP was used for the assessment of the ES-2 dummy. The method of USNCAP was used for the assessment of the SID-2 dummy.

As shown in Figure 4, the impact position of the struck vehicle was moved 250 mm to the backward longitudinal direction based on the R-point of the driver's seat according to the center line of the AE-MDB.

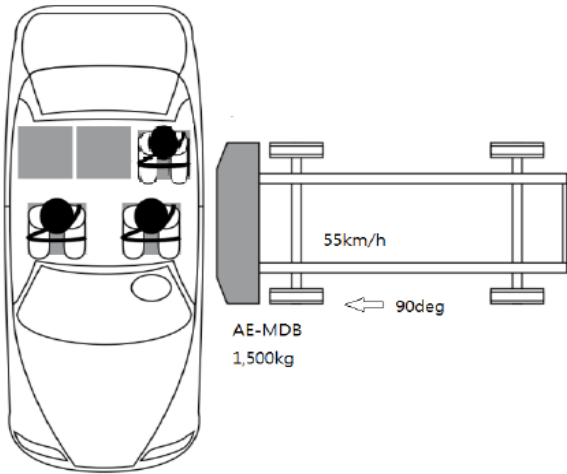


Figure 3. Schematic diagram of the side impact test using AE-MDB.

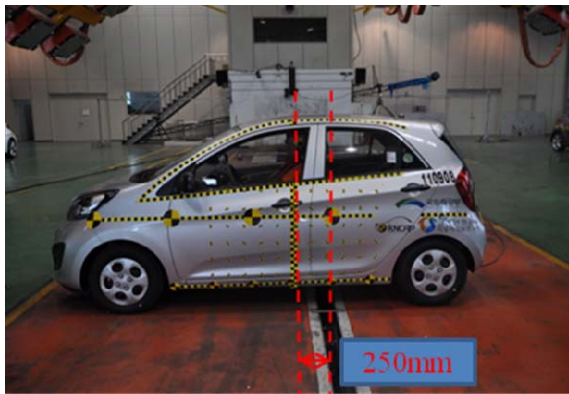


Figure 4. Impact position of struck vehicle using AE-MDB.

The features and specifications of the AE-MDB are represented in Figure 5. Two types of AE-MDB were used and the weights were 1,300 kg and 1,500 kg respectively.

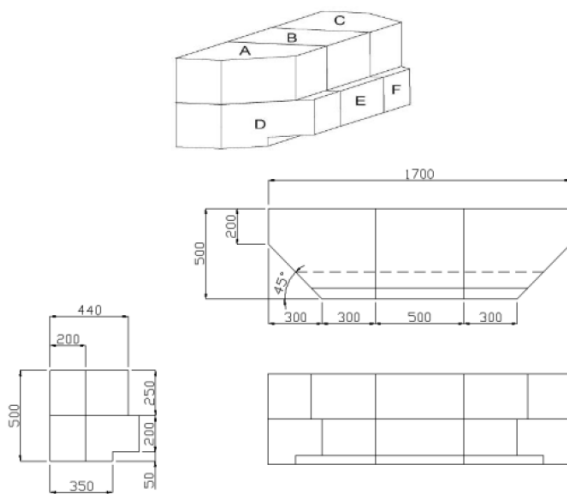


Figure 5. Features and specifications of AE-MDB.

RESULTS AND DISCUSSIONS

Results of Driver Seat Dummy

The test results and the star ratings of each vehicle are represented in Table 3 to Table 5. Side airbags and curtain airbags were mounted in all tested cars. The head injury (HIC36) increased depending on the weight of MDB. In the case of compact car, the chest compression increased depending on the weight of MDB. The trends of chest compression for the mid-sized car and large-sized car were not similar to the compact car. Increasing the weight of MDB, the safety of smaller passenger cars may decrease. Larger passenger cars may not be affected according to the increase of MDB weight. As shown in Table 3 to Table 5, all tested cars got five stars. Despite of weight increase of MDB, the good ratings reflected the effect of the side airbag and curtain airbag under side crashes. The side airbags and the curtain airbags could reduce the ES-2 dummy injuries by not contacting the dummy with the vehicle interior.

Table 3.

Test results and star ratings of compact car.

Body	Injury	Weight of MDB		
		950kg	1,300kg	1,500kg
Head	HIC36	74	238	461
Chest	Compression (mm)	15.2	21.1	23.0
	V/C (m/s)	0.12	0.19	0.26
Abdomen	Forces (kN)	0.54	0.79	0.82
Pelvis	Forces (kN)	1.55	1.62	1.69
Star Rating (Sum of points)		★★★★★ (16.0)	★★★★★ (16.0)	★★★★★ (15.8)

Table 4.

Test results and star ratings of mid-sized car.

Body	Injury	Weight of MDB		
		950kg	1,300kg	1,500kg
Head	HIC36	43	74	92
Chest	Compression (mm)	23.0	21.4	17.7
	V/C (m/s)	0.19	0.17	0.12
Abdomen	Forces (kN)	0.69	0.94	0.97
Pelvis	Forces (kN)	1.31	2.03	2.01
Star Rating (Sum of points)		★★★★★ (15.8)	★★★★★ (16.0)	★★★★★ (16.0)

Table 5.
Test results and star ratings of large-sized car.

Body	Injury	Weight of MDB		
		950kg	1,300kg	1,500kg
Head	HIC36	41	74	81
Chest	Compression (mm)	11.0	14.0	14.0
	V/C (m/s)	0.08	0.09	0.09
Abdomen	Forces (kN)	0.73	0.73	0.65
Pelvis	Forces (kN)	2.66	1.97	2.04
Star Rating (Sum of points)		★★★★★ (16.0)	★★★★★ (16.0)	★★★★★ (16.0)

Results of Rear Seat Dummy

The test results and star ratings of the SID-2 dummy are represented in Table 6 to Table 8. The assessment of the SID-2 dummy was used the method of US-NCAP because the assessment method for the SID-2 dummy does not exist in the current NCAP. The pelvis forces in SID-2 dummy were larger than that of the ES-2 dummy. This was caused by the absence of side airbags in rear seats. The dominant factor affecting the occupant safety when using the AE-MDB was pelvis injury of the dummy in the rear seat. If the AE-MDB will be adopted in the NCAP, the assessment method will be prepared for the enhancement of safety for the smaller occupant in rear seats.

Table 6.
Test results and star ratings of compact car.

Body	Injury	AE-MDB (1,300 kg)	AE-MDB (1,500 kg)
Head	HIC36	346	347
Pelvis	Force (kN)	5.73	6.36
Star Rating (Pjoint)		★★ (29.6 %)	★ (42.8 %)

Table 7.
Test results and star ratings of mid-sized car.

Body	Injury	AE-MDB (1,300 kg)	AE-MDB (1,500 kg)
Head	HIC36	228	210
Pelvis	Force (kN)	3.21	3.52
Star Rating (Pjoint)		★★★★★ (3.9 %)	★★★★★ (5.0 %)

Table 8.
Test results and star ratings of large-sized car.

Body	Injury	AE-MDB (1,300 kg)	AE-MDB (1,500 kg)
Head	HIC36	126	133
Pelvis	Force (kN)	4.53	4.35
Star Rating (Pjoint)		★★★★ (11.4 %)	★★★★★ (9.8 %)

Vehicle Body Deformation

The deformed shape of test vehicles using three types of MDB is represented in Figure 6 to Figure 8. The deformations of vehicle side structure showed big difference depending on using the current NCAP MDB or AE-MDB. There was no big difference between 1,300 kg AE-MDB and 1,500 kg AE-MDB. As shown in Figure 6 to Figure 8, the deformation of the side sill part of the vehicle using the current NCAP MDB was larger than that of the vehicle using the AE-MDBs. This is because of the height of the deformable barrier of AE-MDB.



Figure 6. Deformed shape of large-sized car using 950 kg MDB.



Figure 7. Deformed shape of large-sized car using 1,300 kg MDB.



Figure 8. Deformed shape of large-sized car using 1,500 kg MDB.

Using the AE-MDBs, around the doors of the pelvic area of ES-2 dummy and SID-2 dummy were significantly deformed. The deformed pattern of B-pillar of three types of vehicle was similar. In the case of mid-sized car, the maximum deformation of around the door of pelvic area of SID-2 dummy using the 1,500 kg AE-MDB was 28 mm larger than that of using the 1,300 kg AE-MDB.

CONCLUSIONS

Three sizes of vehicles (compact car, mid-sized car and large-sized car) were tested which MDB will be appropriate for the future KNCAP side impact test. The results of the ES-2 dummy in driver's seat and the SID-2 5 %tile female dummy in rear seat were represented. Increasing the weight of MDB, the safety of smaller passenger cars may decrease. Larger passenger cars may not be affected according to the increase of MDB weight. The side airbags and the curtain airbags could reduce the ES-2 dummy

injuries by not contacting the dummy with the vehicle interior. The dominant factor affecting the occupant safety when using the AE-MDB was pelvis injury of the dummy in the rear seat. The deformations of vehicle side structure showed big difference depending on using the current KNCAP MDB or AE-MDB. Using the AE-MDBs, around the doors of the pelvic area of ES-2 dummy and SID-2 dummy were significantly deformed. This may result the increase of the pelvis force.

Despite the increase of MDB weight, there were no big differences in the results of the ES-2 dummy in the driver's seat. This was caused by the side airbags and the curtain airbags.

If the AE-MDB will be adopted in the KNCAP, the assessment method will be prepared for the enhancement of safety for the smaller occupant in rear seats.

REFERENCES

- [1] Ministry of Land, Transport and Maritime Affairs of Korea, "Enforcement Decree on the New Car Assessment Program, 2012.
- [2] Korean National Police Agency, "Traffic Accident Statistics of 2011", 2012.
- [3] Ministry of Land, Transport and Maritime Affairs of Korea, "Research on the improvement for the KNCAP", 2012.
- [4] EEVC, "Progress on the development of the advanced European mobile deformable barrier face (AE-MDB)", 2003.

FRONT CENTER AIRBAG INFLATION INDUCED INJURY EVALUATIONS AND RESULTS

Scott Thomas

General Motors LLC
United States of America

Richard Wiik

Takata
United States of America
Paper Number 13-0495

ABSTRACT

General Motors LLC and the Takata Corporation have worked together to bring to production an industry first technology, called the Front Center Airbag, which is being implemented on General Motors' 2013 Midsize Crossover Vehicles.

The Front Center Airbag is an airbag that mounts to the inboard side of the driver front seat. It has a tubular cushion structure and it deploys between the front seating positions in far side impacts, near side impacts and rollovers, with the cushion positioning itself adjacent the driver occupant's head and torso.

This new airbag technology, which is in a different location on the vehicle than other airbags and deploys in a different manner, needed a set of demonstration tests for assessing inflation induced injury potential. This paper discusses the test setup conditions and presents the test results.

Occupants in surrounding seating positions were considered when developing the test approaches. Several of these were based on the Recommended Procedures For Evaluating Occupant Injury Risk From Deploying Side Airbags, prepared by the Side Airbag Out-of-Position Injury Technical Working Group in July 2003 for outboard mounted seat airbags [1]. Additional evaluation modes were developed through a General Motors peer review process involving internal experts. Three driver arm interaction conditions were tested, along with a driver torso in close proximity to the airbag configuration. A passenger head on console condition and infants in rear facing child seats installed in the middle seating position of the second row were also evaluated.

An example test of each approach is presented, with graphics of the test event at different points in time,

and with the anthropomorphic test device's maximum recorded injury values included.

The results presented for inflation induced injury testing of the Front Center Airbag indicate that this technology can meet inflation induced injury goals for the range of conditions evaluated.

This paper also includes a brief summary of the Front Center Airbag hardware design and in-position performance. A sister paper containing field data, a detailed hardware description, and a detailed in-position performance summary for far side impacts has been published at the 2013 SAE World Congress. [2]

INTRODUCTION – THE FRONT CENTER AIRBAG

The Front Center Airbag is an airbag that deploys from the inboard side of the driver's seat, as illustrated in the deployment sequence in Figure 1.

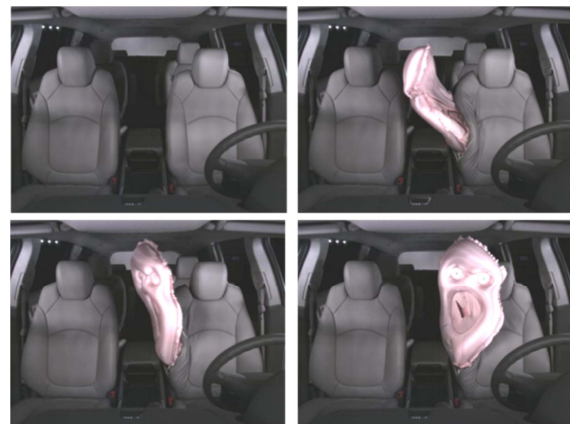


Figure 1. Front Center Airbag Deployment Sequence.

The Front Center Airbag is packaged in the side of the seat inside a pocket in the seat foam and mounts directly to the seat frame. When commanded, the airbag cushion deploys through the side trim of the seat similar to a conventional outboard seat mounted side impact airbag. The cushion is designed to initially deploy upward and forward and then to wrap around the driver occupant, providing head and torso coverage to that occupant.



Figure 2. The Cushion Design.

The cushion is a unique shape when compared to other airbags. As shown in Figure 2, the cushion has a tubular structure that has a “figure 8” shape. A tube filled with pressurized gas becomes very rigid and is difficult to bend, so the tubular structure contributes to the cushion’s lateral stiffness and resulting occupant restraint.

Two tethers are used in the cushion design to help curve it toward the driver occupant. One external tether routes from the top of the cushion to its seat anchoring location. A second, lower tether routes fore-aft on the cushion and passes through two slots in the uninflated lower region. Both tethers are shorter in length than the surrounding cushion panels and, as a result, curve the cushion toward the occupant when the cushion is under pressure. These two tethers also serve to add to the aforementioned lateral occupant restraint.

The deployment mechanization for the Front Center Airbag commands airbag deployment in near side impacts, far side impacts, and rollovers. The airbag is not deployed in frontal impacts or rear impacts so that it will be available for deployment if the vehicle is involved in a multiple impact event where a later side impact or rollover occurs.

IN-POSITION FAR SIDE IMPACT PERFORMANCE

The primary purpose of the Front Center Airbag is to provide restraint and cushioning when a front seated occupant is in a far side impact, where the impacting object is on the opposite lateral side of the vehicle from the occupant.

The Front Center Airbag was evaluated in far side impacts with both one and two front occupants present.

In-Position Demonstration Testing With A Seat Belted Single Front Occupant

A brief introduction to the Front Center Airbag’s in-position performance is provided. If more detail is desired, the SAE paper written on Front Center Airbag in-position performance should be reviewed. [3]

Figure 3 shows occupant kinematics from two far side impact, 32 kph (20 mph) oblique pole sled tests run without and with a Front Center Airbag [4]. For these technology demonstration tests, a rigid sled test buck was propelled from the passenger side to simulate an oblique pole barrier impact.

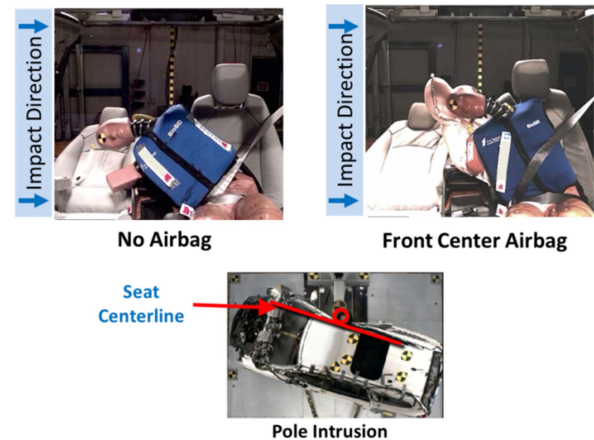


Figure 3. Single Occupant Oblique Pole Impact Without and With the Front Center Airbag.

In the sled test without the Front Center Airbag, the Anthropomorphic Test Device (ATD) pivots laterally over the center console. At maximum excursion, the top of the ATD’s head is approximately at the centerline of the adjacent seating position. This is the approximate location of the pole penetration in the 32 kph (20 mph) oblique pole test condition, as can be

seen in the overhead illustration of such a test at the bottom of Figure 3.

In the test with a single far side occupant and the Front Center Airbag, the Front Center Airbag acted as a restraint, reducing the ATD's lateral motion toward potential injury sources that would have been present in a full vehicle environment. In addition, the Front Center Airbag reduced occupant interaction with the center console and lowered rib deflections in the tested condition.

In-Position Demonstration Testing With Two Seat Belted Front Occupants

Figure 4 shows occupant kinematics from two far side impact oblique pole tests that were also run with and without a Front Center Airbag [5].

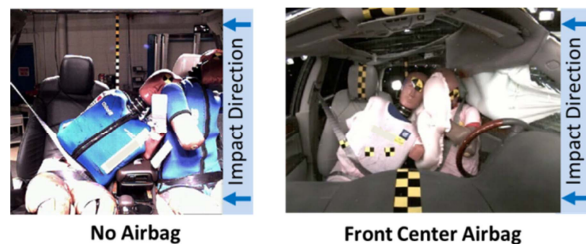


Figure 4. Two Occupant Oblique Pole Impact Without and With the Front Center Airbag.

In the demonstration test without a Front Center Airbag, conducted on a rigid sled buck, the passenger ATD's head contacts the driver ATD's shoulder region, after passing over the center console. A Head Injury Criteria (HIC) injury value of 3907 or 558 percent of the Injury Assessment Reference Value (IARV) was recorded for the passenger ATD.

The demonstration test conducted with the Front Center Airbag is shown on the right of Figure 4. In this full vehicle pole barrier test, both occupants are cushioned by the Front Center Airbag. For this test, the passenger ATD's HIC was reduced to 56 percent of the IARV and the Driver ATD's HIC was 22 percent of the IARV. For this condition with an adjacent occupant present, the Front Center Airbag acted as a cushioning element between the occupants. The passenger ATD's head did not make direct contact with the driver ATD, which reduced the magnitude of the passenger ATD's HIC value and the associated potential for head injury.

INFLATION INDUCED INJURY EVALUATIONS - METHODS AND DATA SOURCES

The Front Center Airbag is a very different restraint system from anything else in production. Because of this, several new inflation induced injury related demonstration test conditions were developed to assess the airbag's performance. Some of these conditions were based on the Recommended Procedures For Evaluating Occupant Injury Risk From Deploying Side Airbags, prepared by the Side Airbag Out-of-Position Injury Technical Working Group (TWG) for outboard mounted seat airbags [6]. Additional conditions were developed based on a General Motors internal peer review process, considering the inflation characteristics of the airbag and the potential occupant positions in close proximity to the deploying Front Center Airbag.

As a result of this work, several driver arm interaction conditions were developed for technology demonstration, along with a position where the driver torso is in close proximity to the airbag. Occupants in surrounding seating positions were also considered when developing the conditions. A position with the passenger head on the center console and a condition with infants in rear facing child seats installed in the middle seating position of the second row were included.

The setup procedures and example tests of each condition follow with images of the test events at different points in time. The anthropomorphic test device's maximum recorded injury values are also provided for each test.

ARM INTERACTION DEMONSTRATION TESTS WITH THE FRONT CENTER AIRBAG

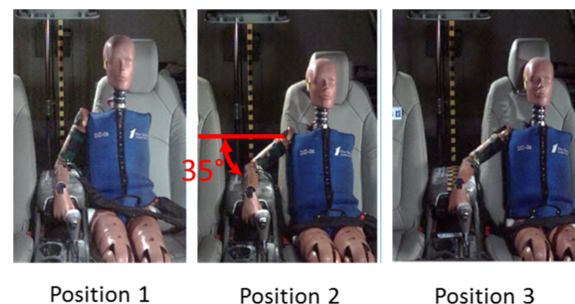


Figure 5. Arm Interaction Test Conditions.

Arm interaction was assessed in several Front Center Airbag demonstration test deployments. Three similar test conditions were developed to assess a range of arm and occupant positions using the existing Side Airbag Out-of Position Injury Technical Work Group (TWG) conditions as a basis [7]. The three positions, labeled Position 1, Position 2, and Position 3, are shown in Figure 5. A SID-II's ATD with the enhanced instrumented arm was used, the seat was set at the design seat back angle as well as the mid-fore aft location, and the center console (adjustable in the vehicle-specific test environment), was positioned in the full forward position. The front passenger seat was set in a position to mirror the driver seat. Similar to the setup procedure found in the TWG conditions for outboard seat-mounted side airbags, the arm was positioned so that the rearward surface of the elbow was tangent to the forward edge of the seat bolster with the under-side of the arm resting on a horizontal surface, that being the center console for all three conditions.

In addition for these tests, the ATD's upper arm skin was rotated so that the inner surface and the slit in the arm skin typically adjacent the torso were positioned forward on the arm, as shown in Figure 6. Tape was placed over the slit in the arm skin, as shown in Figures 6 and 7, and around the elbow, as shown in Figure 7, to prevent the deploying airbag cushion from entering an arm region at a location without skin. In earlier testing, it was noted that the deploying cushion could enter these openings in the ATD's arm skin, so these measures were adopted to create a more biofidelic interaction with the ATD's arm.



Figure 6. Rotated Upper Arm Skin And Applied Tape.



Figure 7. Tape Applied To Upper Arm Skin And Elbow Region.

For Position 1, the ATD was located with the elbow centerline at the vehicle centerline and the torso against the center console. This condition follows the intent of the TWG 3.3.3.7 position [8] for the outboard seat mounted airbag as much as possible, with the ATD being positioned with the torso vertical in the front view. The TWG specified instrumented arm and associated performance criteria (130 Nm humerus / upper arm bending moment and 44 Nm ulna / forearm bending moment) were also utilized.

Vehicles can have different width center consoles, so it was decided that an elbow centerline position at the console centerline was a reasonable approach for the test condition. In addition, the test setup procedure allows the front seat to be raised or lowered to help the ATD achieve the elbow position at the console centerline. A small block can also be positioned under a portion of the ATD's buttocks to keep it from tipping laterally.

The hand was placed at the console centerline and the console mounted shifter was placed in the drive position. The set up procedure calls for the hand to be placed on the shifter if the shifter position matches the hand position. For the results shown, these positions did not match. The arm, hand and shifter were powdered on all surfaces (including touching surfaces) with baby powder prior to deployment to achieve representative / realistic frictional characteristics on the rubber ATD skin as is typical for tests in the referenced TWG procedure [9].

Finally, the ATD's shoulder construction played a role in the setup procedure as the amount of lateral arm rotation away from the ATD's torso is limited by the SID-II's ATD's shoulder construction. In order to

keep the arm away from its lateral travel stop on very tall or very wide center consoles, a criterion was added to limit the initial arm position to a location where the arm could still be rotated (abducted) an additional 5 degrees laterally away and more upward from the torso from its initial position on the center console. If this criterion cannot be achieved, the test procedure calls for the elbow position to be modified to be closer to the ATD, so as not to limit/prevent motion of the arm in the test.

At the time of this testing, both the Hybrid III and the SID-II's ATDs were capable of using the enhanced instrumented arm. A picture of each shoulder construction follows.

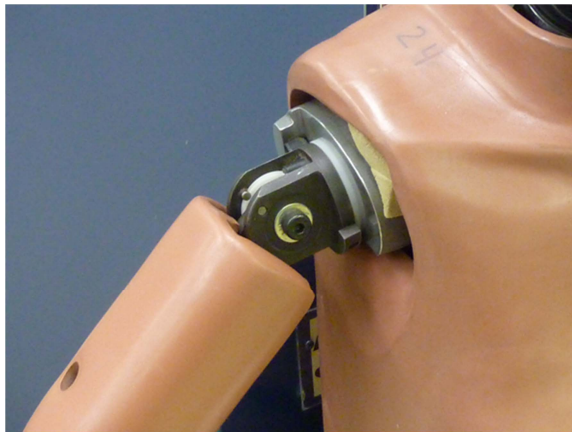


Figure 8. Hybrid III Shoulder Construction (Instrumented Arm Not Mounted In this Picture).



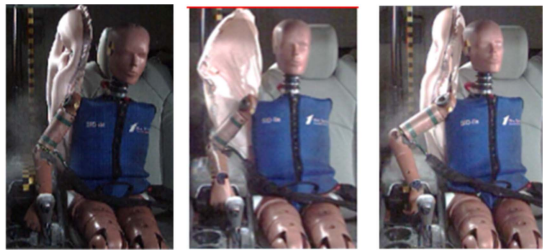
Figure 9. SID-II's Shoulder Construction (Instrumented Arm Not Mounted In This Picture).

The Hybrid III has a more rigid shoulder construction. The clevis joint and rigid torso mounting do not enable significant forward arm motion once the upper arm is rotated laterally away from the ATD's torso. The SID-II's ATD has a more compliant torso mounting via the upper metal torso ring structure and a less resistant joint torque, which together enable forward arm motion with respect to the torso when the upper arm is positioned laterally away from the torso in an abducted position. Because of this, the SID-II's was selected for testing, as an actual occupant's arm can be pushed forward relative to the torso by the deploying cushion.

Position 2 uses the same setup guidance as Position 1 with the elbow centerline at the console centerline, with the exception that the torso is positioned outboard from the center console in order to obtain an upper arm angle 35 degrees from horizontal.

Position 3 uses the same ATD setup guidance as the first two positions, but the ATD is placed at the seat centerline and the elbow centerline is positioned in a more natural location. The seat height is adjusted to laterally position the elbow centerline approximately 40 mm inboard of the console's side wall. The hand is placed at the console centerline and is also positioned on the shifter if the shifter has a location under the hand when in the drive position.

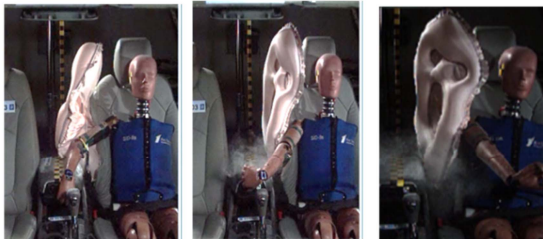
Kinematics views showing the arm performance for these three demonstration test positions are shown in Figure 10. The maximum injury value recorded for the instrumented arm was 54 percent, which is lower than the TWG research value with significant margin. In Position 1, the maximum injury value of 23 percent of upper arm moment occurs when the arm is contacted by the cushion at 14 ms. The maximum injury value of 41 percent of lower arm moment in Position 2 occurs when the wrist contacts the back of the shifter and becomes constrained behind it at 73 ms. The maximum injury value of 54 percent of lower arm moment in Position 3 occurs when the elbow reaches full extension at 75 ms.



Position 1 - Maximum IAV: 23% of Upper Arm Moment



Position 2 - Maximum IAV: 41% Lower Arm Moment



Position 3 - Maximum IAV: 54% of Lower Arm Moment

Figure 10. Arm Interaction Test Results.

OUT-OF-POSITION OCCUPANT DEMONSTRATION TESTS WITH THE FRONT CENTER AIRBAG

Two out-of-position test conditions were developed for front seat occupants to assess the Front Center Airbag's performance.

For the driver seat position Front Center Airbag demonstration test deployment, an outward facing SID-II's ATD was positioned with its back touching the center console and the rearward arm horizontal, as shown in Figure 11. This position mirrors TWG position 3.3.3.6 [10] with the seat full rear full down, seat at the design back angle, and the center console bin also in a full rear position. The associated TWG performance criteria for the SID-II's ATD were also utilized.

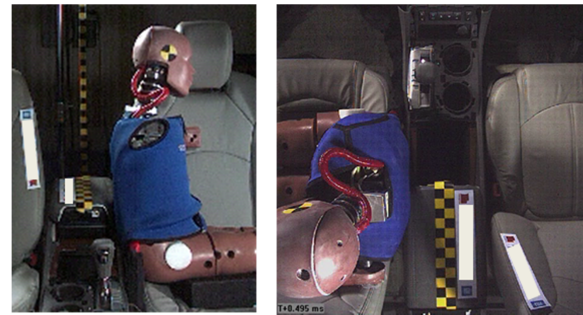
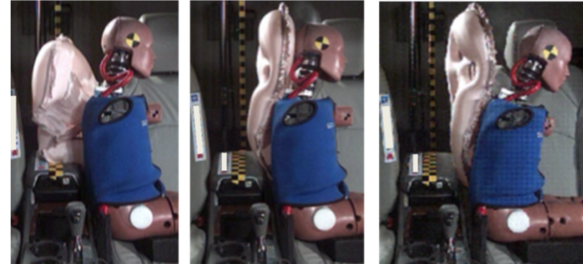


Figure 11. The Outward Facing ATD Test Condition.

The intention of the outboard seat mounted side airbag TWG 3.3.3.6. test is to maximize the head, neck and chest interactions by aligning the center of the top thoracic rib with the top edge of the seat-mounted airbag module. However, when adapting this procedure for the Front Center Airbag, it was not practical to raise the ATD to this level because this airbag package is significantly higher in the seat. In addition, the inflator nozzle is below the top of the module and better aligns with the ATD's rib cage when the ATD is not raised. For this test, the ATD was positioned with its back against the center console in an outboard-facing position, with its arm against the seatback at a 90 degree angle to its torso.



Maximum IAV: 25% of Thorax Rib Deflection

Figure 12. Outward Facing ATD Test Results.

Additional test procedure details are as follows: If needed, a block may be used under the ATD's thighs to help position its back against the console, but the presence of a block is not intended to raise the ATD. Like the TWG test, this test would typically be run with the seat in a full rear, full down position, but if the side door opening interferes with the ATD's legs, the seat can be moved forward the necessary amount to allow the legs to extend through the door opening. Finally, the back of the ATD's head is powdered before testing.

Figure 12 shows the test position and the corresponding demonstration test results which had a maximum injury value result of 25 percent of the IARV, recorded by the third thoracic rib at 17 ms when the cushion was expanding around the occupant and the lower tubular region was deflecting away from the seat bolster and the occupant torso.

For the passenger seat position, the TWG positions were adapted for this airbag application and were considered with passenger occupants. It was determined that there would not be significant airbag interaction with the ATD's head, neck, or torso. For reference, Figure 13 shows four of the adapted TWG positions.



Figure 13. Adapted TWG Positions For The Passenger Seating Position

In addition, a test was devised to represent a sleeping occupant with the head resting on the console. Pictures of several different size children are shown in Figure 14 and the overhead views of the 6 year old and 10 year old ATDs are shown in Figure 15.



Figure 14. Different Size Children With Their Head On The Console (Similar But Different Vehicle Environment).

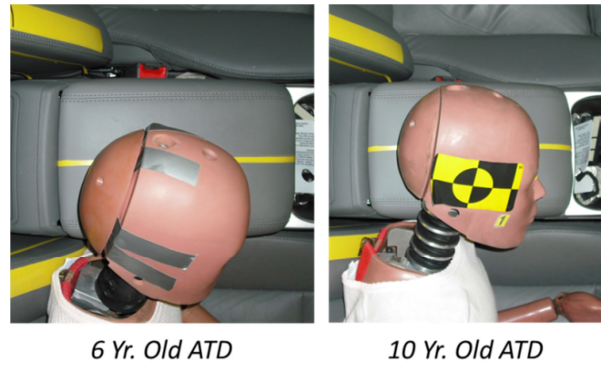


Figure 15. Overhead Views Of The 6 Yr. Old And 10 Yr Old ATDs With Their Head On The Console (Similar But Different Vehicle Environment).

Based on these pictures, a 10 year old ATD was selected because this size occupant may be more likely to interact with the Front Center Airbag than a smaller occupant, as the head and neck extend further over the console.



Figure 16. 10 Yr. Old ATD Head On Console Test Condition.

Figure 16 shows two views of the demonstration test position developed for the 10 year old ATD. The front seats are placed full rear at the design seat back angles and the driver seat is raised to a height that maximizes airbag interaction with the ATD's head. To maximize airbag interaction with the ATD, the driver seat is positioned at the lowest possible height adjustment where the bottom of the Front Center Airbag cushion deploys without significant console interaction. If there is cushion interaction with the console for the full range of vertical seat travel, the seat is positioned full up. Since the cushion shape tested had lateral interaction with the console during deployment at all seat heights, the test was run with the seat in the full up position.

The passenger seat that supports the ATD is set at the same height as the driver seat, when the passenger seat has vertical adjustment. If the console bin is adjustable, as in the cited example, it is set in the full rear position, or moved forward the minimum distance needed to support the ATD head for the test. This is done to limit the airbag escape paths and focus it on the ATD as much as possible.

The ATD is positioned with the left buttock on the seat and is tipped inboard so that the neck is positioned in a cross-vehicle orientation in the plan view. The left shoulder is touching the seat back and in some cases with wider consoles as shown in Figure 16, the side of the center console. If needed, a foam block can be placed under the left arm to support the ATD so the neck is not initially loaded and so both the head and left shoulder are in contact with the center console. The rearward, upper, top, and lower sides of the ATD's head are powdered prior to running the test. In order to prevent interference with the driver, in vehicles with laterally smaller consoles, the top of the ATD's head should not extend past the driver's side of the console top surface in the plan view into the driver's seating position.



Max. IAV: 17% of Upper Neck Bending Flexion

Figure 17. 10 Yr. Old ATD Head On Console Test Results.

Figure 17 shows the demonstration test results for this condition. The airbag cushion grazed the back of the head during deployment and the ATD's head moved forward about 100 mm in the test. The maximum injury value was 17 percent of the IARV for upper neck bending flexion at 41 ms, near the time when the cushion moved past the head.

Note that this head on console position can be viewed as an extreme condition, because a head positioned in this manner would tend to interfere with the location

of the driver's inboard arm, which could affect the driver's use of the steering wheel.

REAR FACING CHILD RESTRAINT DEMONSTRATION TESTS WITH THE FRONT CENTER AIRBAG

Rear facing child restraints (RFCRs) were evaluated in demonstration test deployments with the child restraint installed in the second row center seating position. Prior to testing, more than 40 RFCRs were evaluated to determine the models and installation configurations that appeared to have the most potential for airbag interaction. The amount of padding, top tether storage location, top tether routing configuration, and adjustable handle positions were also considered when selecting the designs and conditions that were tested. For these tests, the front seat was positioned full rear and full down at the design seat back angle and the second row seat was moved full forward to maximize the potential for airbag interaction with the selected child restraints. This arrangement positioned the RFCRs in close proximity to the inboard side of the driver seat next to the Front Center Airbag module. In these tests, the front passenger seat was positioned full rear and full down at the design seat back angle (when enabled by the RFCRs) and also evaluated in a full forward position. The adjustable center console was positioned full rear to maximize airbag interaction with the child restraint unless this location interfered with the RFCRs.

The CRABI 12 ATD was used because its height results in a head position in closer proximity to the Front Center Airbag than that of the CRABI 6 ATD. However, the injury values were evaluated against the more stringent IARVs for the smaller 6 month old ATD. Tests were run with the ATD centered in the child restraint and with the ATD leaning toward the driver seat mounted Front Center Airbag. A 50th percentile Hybrid III Male ATD was added to the centerline of the driver seat to add ballast and assess airbag deployment kinematics and positioning. In addition, a Hybrid III 3 Year Old ATD was evaluated in this test series because some RFCRs can accommodate this size occupant. The top portion of Figure 21 illustrates a setup with the CRABI 12 ATD's head leaning toward the driver seat.



37 % Of Neck Twist, 3 % Of HIC Using 6 Month Old IARVs.

Figure 21. RFCR Test Condition With Infant Leaning And Passenger Seat Full Forward – Graco My Ride.

Table 1
Selected Belted ATD Second Row RFCR Tests

RFCR	ATD	Head Orientation	Pass. Seat Location	HIC	Max. Injury Value*
Graco My Ride	12 Month	Centered	Full Forward	0%	31%
Graco My Ride	12 Month	Leaning To Driver Side	Full Forward	3%	37%
Graco My Ride	12 Month	Leaning To Driver Side	Full Rear	3%	38%
Graco My Ride	3 Yr.	Leaning To Driver Side	Full Forward	0%	9%
Graco Snug Ride 30	12 Month	Centered	Full Forward	0%	16%
Graco Snug Ride 30	12 Month	Leaning To Driver Side	Full Rear	0%	12%
Graco Comfort Sport	12 Month	Centered	Full Forward	0%	10%
Cosco Comfy Carry	12 Month	Leaning To Driver Side	Full Forward	0%	14%
Britax Boulevard	12 Month	Leaning To Driver Side	Full Forward	0%	4%
Top Tether Installed To Base Of Driver Seat					
Safety 1 st Complete Air 65	12 Month	Leaning To Driver Side	Full Forward	0	26%

**Upper neck twist was the maximum injury value for all tests. The 6 month old ATD IARV for upper neck twist is 24 Nm.*

The lower portions of Figure 21 show a deployment progression. The Front Center Airbag deployed forward and upward from its location inside the seat. While the airbag interaction resulted in some lateral motion of the child restraint in the example presented, the highest injury value measured was 37 percent of the IARV for upper neck twist (Mz moment). The peak response at 32 ms occurred as the child restraint moved laterally away from the driver seat, resulting in slight rotation of the ATD's head toward the driver side. Of all the tests

conducted, the leaning CRABI 12, with the both driver and passenger seat located full rear, produced the highest response of 38 percent neck twist (The images for this test are not shown because the full rear passenger seat obscures the view of the deploying airbag.)

Table 1 indicates the maximum injury values recorded in a selection of the RFCR demonstration tests conducted. In addition, the following general observations could be made about this testing: a) the CRABI 12 ATD produced higher responses than the Hybrid III 3 Year Old ATD, b) there was little difference in CRABI 12 response when the passenger seat position was varied and also when the CRABI 12 seating orientation was varied. c) a top-tether attached from the RFCR to the base of the driver seat did not adversely affect the deployment of the airbag, d) there was no visible damage to any of the RFCRs or the deployed airbags, e) the RFCRs did not prevent the Front Center Airbag from getting into position, and f) the RFCRs did not direct the Front Center Airbag into the driver occupant.

CONCLUSIONS

The Front Center Airbag deploys forward from the inboard side of the driver seat and provides restraint to the driver in far side impacts by reducing this occupant’s lateral motion across the vehicle toward potential intrusion, adjacent components, and the striking vehicle or object. The airbag can also provide cushioning between the driver and front passenger when present in side impacts and rollovers.

The General Motors and Takata team has spent significant engineering effort to minimize the inflation induced injury risk during Front Center Airbag deployment. As part of the development of this new technology, several out-of-position and arm interaction test conditions were conceived for technology demonstration. Some of these positions were based on existing TWG out-of-position test procedures [11] while others were developed independently. The conditions were developed with different size interior environments in mind and involve occupants in the seating positions that surround the Front Center Airbag. The Front Center Airbag has been developed and initially assessed using these conditions and has demonstrated performance that has met IARV goals with margin.

This Front Center Airbag technology is being implemented on the 2013 Buick Enclave, GMC Acadia, and Chevrolet Traverse.

REFERENCES

1. “Recommended Procedures For Evaluating Occupant Injury Risk From Deploying Side Airbags, prepared by the Side Airbag Out-of-Position Injury Technical Working Group, A joint project of Alliance, AIAM, AORC, and IIHS), Adrian K. Lund (IIHS), Chairman, First Revision – July 2003.”
2. Thomas, S. D., Wiik, R. A., and Brown, J. E. 2013. “The Front Center Airbag.” SAE 2013-01-1156
3. Ibid
4. Ibid, pgs 8, 9, 11.
5. Ibid, pgs 10 – 11.
6. “Recommended Procedures For Evaluating Occupant Injury Risk From Deploying Side Airbags, prepared by the Side Airbag Out-of-Position Injury Technical Working Group, A joint project of Alliance, AIAM, AORC, and IIHS), Adrian K. Lund (IIHS), Chairman, First Revision – July 2003.”
7. Ibid.
8. Ibid.
9. Ibid.
10. Ibid.
11. Ibid

DEFINITIONS / ABBREVIATIONS

ATD	Anthropomorphic Test Device
HIC	Head Injury Criteria
IARV	Injury Assessment Reference Value
IAV	Injury Assessment Value
kph	Kilometers per Hour
mm	Millimeters
Nm	Newton Meter
RFCR	Rear Facing Child Restraint
TWG	(Side Impact Out-of-Position Injury) Technology Work Group